

**Efficacy of Organic Nanocarriers in a 3D
Colorectal Cancer *In Vitro* Model**

By

Víctor López-Dávila

BSc MSc

Thesis submitted for the degree of

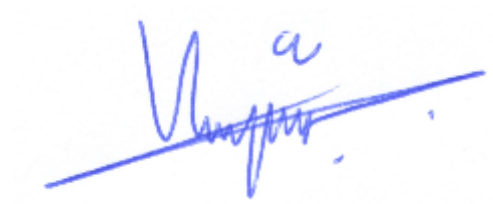
Doctor of Philosophy (PhD)

Department of Surgery and Interventional Science

University College London

2015

I certify that that I have performed and written all the work described in this thesis.
This work is original, any parts that have been conducted as part of collaboration are clearly indicated, and all external references are clearly cited.



Víctor López-Dávila

ABSTRACT

The thesis addresses two rapidly advancing fields: improvement of drug efficacy using smart targeting and nanotechnology approaches; and testing drug efficacy in clinically relevant *in vitro* models. The specific aim was to create organic nanoformulations of novel chemotherapeutic agents and test their efficacy in a 3D colorectal cancer *in vitro* model.

The first phase consisted in determining the best candidate for nanoformulations, in cell monolayers, using routine cell and molecular investigations. Different combinations of therapeutic agents were tested on colorectal cancer cells, including inhibitors of the mitogen activated protein kinase (MAPK) pathway, antagonists of the endothelin receptor A (ETAR) and short interfering RNA (siRNA) targeted against key molecules. AZD6244, an inhibitor of the MAPK pathway, produced significant inhibition of proliferation ($p < 0.05$) and was chosen for nanoformulations.

AZD6244 was encapsulated in cationic GCPQ micelles and DOPE/DC-Cholesterol liposomes using ultrasonication and extrusion methods, and tested in colorectal cancer cell monolayers. Both nanoparticles exhibited superior inhibitory effects compared to the free drug, shown by proliferation and metabolic activity assays ($p < 0.05$). Additionally, experiments with control nanoparticles and western blot analysis of target proteins suggested that the superior efficacy of the nanoformulations was mainly due to a more efficient delivery of the drug, as opposed to additional toxicity from the nanoparticles.

When the nanoformulations were tested in a collagen-based 3D model of colorectal cancer, the superior efficacy of the nanoformulations was reduced, while the efficacy of the free drug increased. Studies performed with fluorescent dye-carrying nanoparticles in these models revealed that nanoparticle efficacy was hindered by poor penetration into the tissue.

These results highlight both the potential of organic nanoformulations as therapeutic delivery systems for cancer and the need to include three-dimensional *in vitro* models in the drug testing process prior to *in vivo* work.

CONTENTS

1	Introduction and Aims	12
1.1	Colorectal cancer and therapeutics.....	12
1.1.1	MAPK pathway and its inhibitors	13
1.1.2	KRAS and BRAF mutations in colorectal cancer	15
1.1.3	The endothelin axis and cancer	16
1.1.4	Endothelin A receptor antagonism.....	17
1.1.5	Crosstalk between ETAR and the MAPK pathway and possible treatment combinations	18
1.1.6	RNA interference and cancer treatment	19
1.2	Organic nanocarriers for anticancer therapeutic delivery	20
1.2.1	Liposomes	22
1.2.2	Micelles.....	24
1.2.3	DOPE/DC-cholesterol liposomes and GCPQ micelles	24
1.3	Three-dimensional cancer models	25
1.3.1	Spheroids	26
1.3.2	Scaffolds.....	26
1.3.3	Tumouroid, a collagen-based <i>in vitro</i> model of cancer	27
1.4	Aims	28
2	General Materials and Methods.....	30
2.1	Cell maintenance	30
2.2	Proliferation and metabolic activity assays.....	30
2.2.1	Cell counting.....	31
2.2.2	3-(4,5-dimethylthiazol-2-yl)-2,5-diphenyltetrazolium bromide (MTT) assay	31
2.2.3	Total DNA assay.....	32
2.2.4	Alamar blue [®] assay.....	32
2.2.5	Aggregate area measurement.....	33
2.3	Approaches to cell molecular analysis	34
2.3.1	Protein extraction and quantification.....	34
2.3.2	Polyacrylamide gel electrophoresis (PAGE) and Western blot	34

2.3.3	RNA extraction and quantification	36
2.3.4	Conventional RT-PCR	37
2.3.5	Quantitative RT-PCR	38
2.4	Statistical Analysis	39
3	Investigations on Small Molecule Therapeutic Agents.....	42
3.1	Introduction	42
3.2	Materials and methods.....	43
3.2.1	Cell characterization	43
3.2.2	Materials.....	43
3.2.3	Cell culture and experimental protocols for therapeutic treatments	44
3.3	Results	46
3.3.1	Reference mRNA expression profiles.....	46
3.3.2	Treatment with MEK inhibitors.....	47
3.3.3	Treatment with ETAR competitive antagonists	56
3.4	Discussion.....	63
3.4.1	Inhibitors of the MAPK pathway.....	63
3.4.2	PD98059 and U0126	63
3.4.3	AZD6244 on HCT116 and HT29 cells	71
3.4.4	Treatment with ETAR competitive antagonists	74
3.4.5	Selected molecules for combination treatments	80
4	RNA Interference and Treatment Combinations	82
4.1	Introduction	82
4.2	Materials and Methods.....	83
4.2.1	Materials.....	83
4.2.2	Cell culture and siRNA evaluation	83
4.2.3	Cell culture and proliferation assays.....	84
4.3	Results	86
4.3.1	Optimization of OFA/siRNA ratio	86
4.3.2	Effect of target-specific siRNAs on mRNA expression over time.....	88
4.3.3	Effect of specific siRNAs on target proteins.....	90
4.3.4	Combination treatments.....	97
4.4	Discussion.....	101
4.4.1	ETAR silencing efficacy	102

4.4.2	MEK-1 and MEK-2 silencing efficacy.....	103
4.4.3	Combination treatments.....	104
4.4.4	Selected molecule for nanoformulations and 3D culture testing	109
5	Nanoparticle Fabrication and Characterization	112
5.1	Introduction	112
5.2	Materials and Methods.....	113
5.2.1	Fabrication of liposomes made from cholesterol and phospholipids...	113
5.2.2	Fabrication of micelles made from GCPQ	117
5.2.3	Fabrication of gold Quantum Dots	118
5.2.4	Nanoparticle characterization	119
5.3	Results	123
5.3.1	Liposome methodological development.....	123
5.3.2	Micelle methodological development.....	128
5.3.3	Characterization of optimized DOPE/DC-cholesterol and GCPQ nanoparticles	130
5.4	Discussion.....	135
5.4.1	Observations on DOPE/DC-cholesterol liposomes.....	135
5.4.2	Observations on GCPQ micelles	138
5.4.3	The influence of encapsulated molecules on the formation of nanoparticles	140
5.4.4	Organic nanoparticles for 2D and 3D experiments	141
6	Nanoparticle <i>In Vitro</i> Evaluation and Experiments on Tumouroids.....	144
6.1	Introduction	144
6.2	Materials and methods.....	144
6.2.1	Cell culture and treatment in monolayers and tumouroids.....	144
6.2.2	Protein analysis and proliferation assays.....	147
6.2.3	HCT116 metabolic standard curves in monolayers and tumouroid cultures	148
6.2.4	Preliminary penetration and uptake studies.....	148
6.2.5	Confocal microscopy imaging.....	148
6.2.6	Penetration studies.....	149
6.3	Results	150
6.3.1	Standard curves	150
6.3.2	Preliminary penetration and uptake studies.....	151

6.3.3	Toxicity assessment of control nanoparticles	153
6.3.4	Drug and nanoparticle efficacy in monolayers	155
6.3.5	Protein analysis of phosphorylated ERK.....	157
6.3.6	Drug and nanoparticle efficacy in tumouroids.....	159
6.3.7	Drug penetration studies.....	162
6.4	Discussion.....	164
6.4.1	Previous reports on nanoparticle testing in 3D models and in nanoformulations of MEK inhibitors	164
6.4.2	Standard curves and drug to cell ratios	165
6.4.3	Preliminary uptake and penetration studies.....	166
6.4.4	Nanoparticle efficacy on monolayers.....	167
6.4.5	Nanoparticle efficacy on tumouroids.....	170
6.4.6	Penetration studies.....	171
7	Conclusions and Future Directions.....	177
8	References	182

ACKNOWLEDGEMENTS

I sincerely thank **Marilena Loizidou** for her incredible support and guidance throughout these years, which came in many different forms. Her knowledge and ability to adapt to new situations has not only been invaluable for the production of this thesis, but has set our little research group on the track to accomplish great things in the years to come.

It has been an absolute pleasure to work with **Hazel Welch**, the kind of molecular biologist whose experience and expertise are difficult to put into question. Because of her passion for science, she certainly is an inspiration to work hard and enjoy the highs and lows of this formidable craft.

I also would like to thank **Miriam Dwek** and **Ijeoma Uchegbu**, both excellent researchers who did not hesitate to take me into their labs and treat me like one of their own. Many thanks go to **Bala Ramesh** for his help with confocal microscopy and kindly letting me use gold quantum dots of his own invention in my research.

I could not have survived these years without working part time in the jobs I was fortunate enough to get involved with. I owe a great deal to **Amir Gander** and **Barry Fuller**, who made my biobank technician job possible, and all of the **NORS team**: surgeons, nurses and coordinators that made my job as a transplant perfusionist such an enjoyable experience. Sincere thanks go to **Kevin Sales**, the man who makes things happen when hope is lost.

From my PhD colleagues, special thanks go to “**Ma’dawg**” **Tarig Magdeldin**. He is a brilliant scientist with a great future ahead of him and could easily have been my third supervisor. **Toke Klanrit**, the happiest man on Earth, who has shared this experience with me from the very beginning, also deserves my best wishes.

*Pero nada de esto hubiese sido posible sin **mi familia**, que me ha apoyado incondicionalmente desde que tengo memoria, y siempre me ha motivado para que persiga mis sueños. Mientras ellos estaban lejos ha sido **Paty**, el amor de mi vida, quien ha mantenido esos sueños vivos. Con ella compartiré todas las aventuras que nos esperan. Os quiero de verdad.*

ABBREVIATIONS

2D	Two-dimensional
3D	Three-dimensional
5-FU	5-Flurouracil
ABC	Accelerated blood clearance
ACM	Artificial Cancer Mass
APC	Adenomatous Polyposis Coli
BSA	Bovine Serum Albumin
CRC	Colorectal Cancer
DAG	Diacylglycerol
DC-chol	3 β -[N-(N',N'-dimethylaminoethane)-carbamoyl]cholesterol
DLS	Dynamic Light Scattering
DMEM	Dulbecco's Modified Eagles' Medium
DMSO	Dimethylsulfoxide
DNA	Deoxyribonucleic acid
DOPC	1,2-dioleoyl-sn-glycero-3-phosphocholine
DOPE	1,2-dioleoyl-sn-glycero-3-phosphoethanolamine
ECM	Extracellular matrix
EGF	Epidermal growth factor
EGFR	Epidermal growth factor receptor
EPR	Enhanced permeability and retention
ET-1	Endothelin 1
ET-2	Endothelin 2
ET-3	Endothelin 3
ETA	Endothelin receptor A
ETB	Endothelin receptor B
FAP	Familial adenomatous polyposis
FBS	Fetal bovine serum
GCPQ	Quaternary Ammonium Glycol Chitosan
HIF	Hypoxia inducible factor
HPLC	High Pressure Liquid Chromatography

HT29	Human colon adenocarcinoma cell line
IC50	Inhibitory Concentration by 50 percent
MAPK	Mitogen-activated protein kinase
MEK	Mitogen-activated protein kinase kinase
MEM	Minimal essential medium
MMP	Matrix metalloproteinase
mRNA	Messenger RNA
P/S	Penicillin/Streptomycin
PBS	Phosphate buffer saline
PC	Plastic compression
PCR	Polymer chain reaction
PDGF	Platelet derived growth factor
PEG	Polyethylene glycol
PFA	Paraformaldehyde
PGA	Polyglycolic acid
PGE ₂	Prostaglandin E ₂
PI3K	Phosphoinositide 3-kinase
PKC	Protein kinase C
PLA	Poly (lactic acid)
PLC/PLD/PLA ₂	Phospholipase C/D/A ₂
PLGA	Poly (lactic-co-glycolic acid)
QD	Quantum dot
RGD	Arginine-Glycine-Aspartic acid sequence
RIPA	Radioimmunoprecipitation assay
RISC	RNA-induced silencing complex
RNA	Ribonucleic acid
RNAi	RNA interference
RTK	Receptor tyrosine kinase
SDS-PAGE	Sodium dodecyl sulphate polyacrylamide gel electrophoresis
SiRNA	Short interfering RNA
TEM	Transmission Electron Microscope
VEGF	Vascular Endothelial Growth Factor

CHAPTER 1

Introduction & Aims

1 Introduction and Aims

The work described in this body of research consists of three well defined sections. First, the search for a therapeutic combination involving the endothelin A receptor (ETAR) and the mitogen activated protein kinase (MAPK) pathway. Second, the nanoformulation of this therapeutic combination to improve its delivery/action to the cell. And third, the evaluation of these nanoformulations in a novel, collagen-based 3D model of colorectal cancer, termed tumouroid, which mimics human tumour masses. This chapter introduces colorectal cancer, novel therapeutics against the target pathways, organic nanoformulations as therapeutic delivery systems and the use of 3D models in drug discovery.

1.1 Colorectal cancer and therapeutics

Colorectal cancer (CRC) ranks as the third most common cancer worldwide and fourth for cancer-related deaths in the world (Jemal et al. 2011). Most countries in developed regions are more vulnerable to colorectal cancer due to a high-fat and low-fibre diet and sedentary life styles (Center et al. 2010). While healthy colonic tissue is in a constant balance between apoptosis and proliferation, the initial stage of colorectal cancer pathogenesis is almost exclusively linked to the inability of epithelial cells to undergo apoptotic signalling (Deschner et al. 1988).

There are certain inheritable conditions such as Familial Adenomatous Polyposis (FAP) or Hereditary Non-Polyposis Colon Cancer (HNPCC), which predispose patients to mutations that could eventually develop into colorectal cancer. However, more than 80% of the cases are sporadic, with a variety of abnormalities in oncogenes and tumour suppressor genes, particularly in chromosomal regions such as 5q, 8p, 17p and 18q (Muleris et al. 1987). Most of the key mechanisms involved in colorectal carcinogenesis involve genes such as APC, SMAD4, p53 or KRAS (Bodmer et al. 1987; Smith et al. 1994; Fodde et al. 2001).

While early detection and surgery for therapeutic excision of the tumour are key factors in overcoming the disease, more than half of the patients develop metastases that represent the main cause of colorectal cancer mortality (O'Connell et al. 2004), and therefore require a systemic treatment. To address this problem, chemotherapy (normally constituting of 5-fluorouracil (5-FU) combined with other chemicals) is used as an adjuvant treatment after patients undergo surgery. While promising, chemotherapy is linked to significant side effects, such as immunosuppression, fatigue and severe organ damage, mostly due to its lack of specificity. For that reason, a number of novel new generation therapeutics that aim at specific signalling such as small molecule inhibitors are in constant discovery. Some of these novel therapeutics are targeted against key intracellular proteins such as the protein kinases MEK1, MEK2 or RAF or against surface receptors such as epidermal growth factor receptor (EGFR) or endothelin A receptor (ETAR). The ultimate goal is to target specific mechanisms, such as cell proliferation, apoptotic signalling or invasive potential, which are regarded as hallmarks of cancer (Hanahan & Weinberg 2011).

While the use of target-specific novel therapeutics are an improvement to some of the limitations linked to traditional chemotherapy, one of their main drawbacks is that often, only patients with a specific mutation profile derive benefit from the treatment. Such is the case of cetuximab, a humanized antibody targeted against EGFR which has no effect on tumours with certain mutations in the downstream KRAS protein (Van Cutsem et al. 2009; King & Robins 2006), due to its constitutive activation. For that reason treatment combinations must be explored to achieve an effective treatment.

1.1.1 MAPK pathway and its inhibitors

One of the most promising targets for new generation chemotherapeutic agents is the MAPK pathway, which is intrinsically activated in a number of cancers, leading to the aforementioned cancerous behaviour (Adjei & Hidalgo 2005; Dhillon et al. 2007; Hoshino et al. 1999). This pathway is not only key to cancer development and progression, but is closely involved in chemotherapy resistance in a number of cancers, including colorectal (Mueller et al. 2000).

Inhibitors against various key proteins in this pathway are constantly being developed. Its signalling consists of a phosphorylation cascade that starts with a receptor tyrosine kinase (RTK) binding to a growth factor in the surface of the cell and substituting the GDP in RAS for GTP (Bolsover et al. 2004). This signal starts a process in which a kinase is activated by phosphorylation and phosphorylates another kinase, namely RAS, RAF, MEK and ERK (Peyssonnaud & Eychène 2001; Meloche & Pouyssegur 2007; Mebratu & Tesfaigzi 2009; Crews et al. 1992; Roskoski 2010), with the latter triggering proliferative, angiogenic and anti-apoptotic signals through the activation of transcription factors (Figure 1.1). The MAPK pathway is essential for tumorigenesis in a great number of cancers (Dhillon et al. 2007; Sebolt-Leopold 2004).

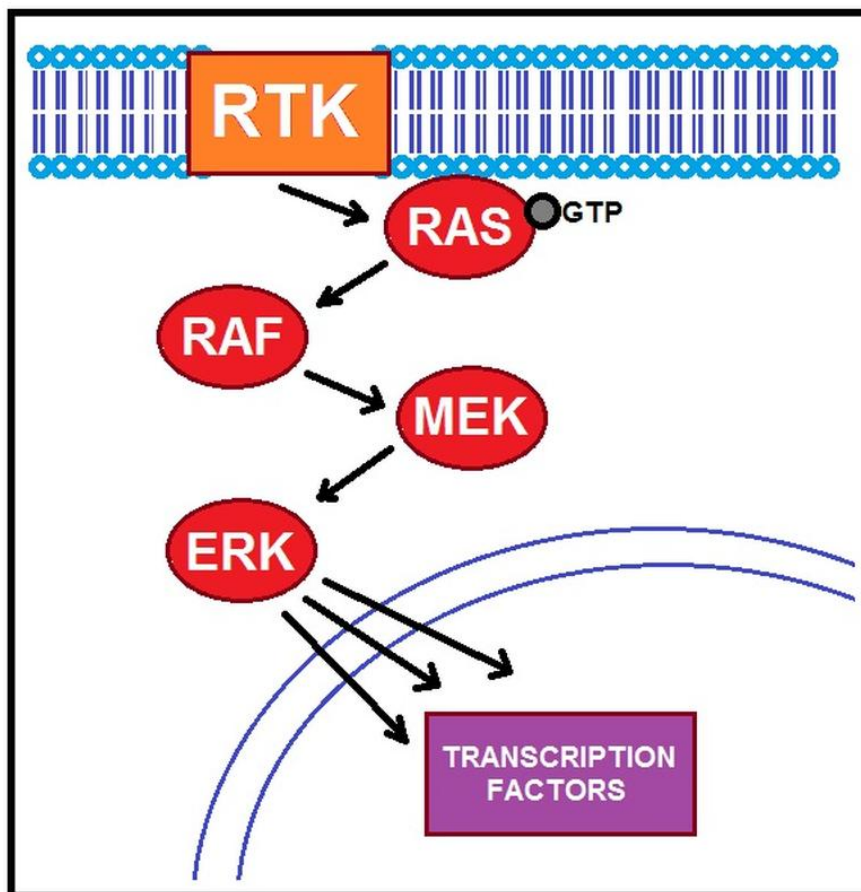


Figure 1.1 Schematic representation of the MAPK pathway phosphorylation cascade.

Since most mutations related to the constitutive activation of the MAPK pathway occur in proteins upstream of MEK1/2, these two enzymes are an excellent target for anti-cancer therapeutics. Furthermore, ERK1/2 are the only known substrates of MEK1/2 (Roskoski 2012). The specificity of these enzymes and the importance of this pathway in tumorigenesis leads to a phenomenon called “oncogenic dependency” or “oncogenic addiction” in which the survival of cancer cells relies fundamentally on this pathway (Weinstein & Joe 2008; Weinstein 2002), supporting the choice of this pathway as a therapeutic target. A number of novel chemotherapeutic agents targeted against these proteins have been developed over the last years, including small molecules such as PD98059, U0126 or AZD6244, and even interfering RNA, with promising results *in vitro*, *in vivo* and in the clinic (Santarpia et al. 2012; Balmanno et al. 2009; Gailhouste et al. 2010).

1.1.2 KRAS and BRAF mutations in colorectal cancer

The MAPK pathway is often overactive in human cancers, and in many cases the points of constitutive activation are RAS or RAF (Davies et al. 2002; Imamura et al. 2012). The fact that activating mutations in these two proteins are mutually exclusive suggests that they affect the same downstream proteins.

In CRC, KRAS is the most commonly mutated protein in the RAS family (Phipps et al. 2013), occurring in 35-45% of CRCs (Imamura et al. 2012; Normanno et al. 2009). Among these mutations, over 90% are either in codon 12 or codon 13 (Wood et al. 2007). These mutations translate into a constitutive activation of the MAPK pathway regardless of the signalling upstream of KRAS (Conlin et al. 2005). While this is extremely interesting for drug discovery and sets the basis for the development of new therapeutics, there are mixed thoughts on whether mutations in KRAS have an influence on patient's outcome (Imamura et al. 2012; Phipps et al. 2013; Ren et al. 2012; Richman et al. 2009; Roth et al. 2010).

On the other hand, BRAF mutations are found in only 5-10% of colorectal cancers (Davies et al. 2002; Yuen et al. 2002) and their presence often indicates poor patient outcome. Among all BRAF mutations, V600E represents 90% of cases (Davies et al.

2002). While mutations in KRAS are especially frequent in CRC, mutations in BRAF are more frequent in cancers such as ovarian, thyroid, and specially melanomas (Wellbrock et al. 2004; Davies et al. 2002). It is worth noting that the percentages shown here for BRAF and KRAS mutation frequencies do vary slightly among publications.

1.1.3 The endothelin axis and cancer

In the last fifteen years, the endothelins, and their cell surface receptors have gained attention as potential cancer promoters. The endothelin axis comprises two G-protein coupled receptors (ETA and ETB), which bind to ligands ET1, ET2 and ET3 with different affinities (Sakamoto et al. 1991). The binding of ET1 to these G-protein coupled receptors, triggers the activation of several proteins such as phospholipases A2, C and D or the adenylate and guanylate cyclases (Shome et al. 2000) (Figure 1.2). These result in further activations; for example phospholipases C and D activate both PI3K (which then activates RAS) and protein kinase C (PKC) (which then activates Raf1 (Blaukat et al. 2000) and increases intracellular Ca^{2+} concentration). All these mechanisms ultimately result in the activation of MAPK pathway signalling and subsequent transcription factors, which lead to cell proliferation, among other processes.

An imbalance between the signalling through these two receptors has implications in cancer cell mitogenesis, apoptosis, angiogenesis and metastatic potential. While all three endothelins bind to ETBR with similar affinity (Rubanyi & Polokoff 1994), ETAR has significantly higher affinity for ET1 compared to ETBR, which in the event of raised levels of ETAR and ET1, acts as an oncogene (Kennedy et al. 1993; Sakamoto et al. 1991), particularly through its mitogenic function (Bagnato et al. 1997; Grant et al. 2007). The expression levels of both ET1 and ETAR have been found increased in several types of cancer including colorectal, breast, prostate, stomach and glioblastoma (Kusuhara et al. 1990; Bagnato et al. 1999; Ali et al. 2000; Nelson et al. 1995; Hoosein et al. 2007; Bagnato et al. 1997). Around 80% of primary CRCs have increased levels of ET-1, not only in cancer epithelial cells themselves

but also surrounding stromal cells (Asham et al. 2001; Shankar et al. 1998), which play a central role in cancer progression.

ET1 also has implications in apoptosis, as it has been shown to counteract FasL-induced apoptotic mechanisms in rat colon carcinoma cells and ovarian cancers and has been suggested to interfere with the β -catenin pathway (Kim et al. 2005; Peduto Eberl et al. 2003). Furthermore, the binding of ET1 to ETAR has been shown to increase the production of hypoxia inducible factor 1 (HIF1), COX1, COX2, the prostaglandin PGE2 and p38 in ovarian cancer cells, which subsequently stimulate VEGF production and matrix metalloproteinase (MMP) activation, resulting in angiogenesis and invasion, respectively (Spinella et al. 2004; Spinella et al. 2002). The increased expression of angiogenic and pro-invasive proteins through ET1 stimulation was also later detected in colonic fibroblasts (Knowles et al. 2012).

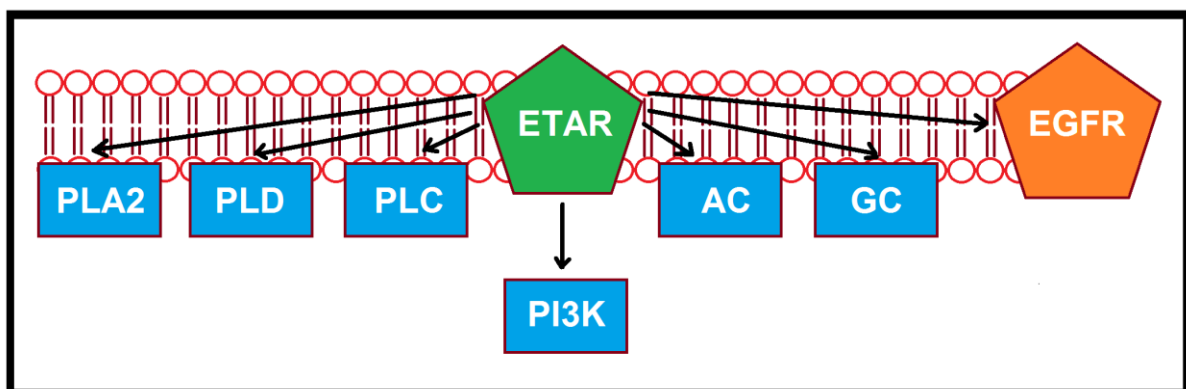


Figure 1.2 Schematic representation of the proteins activated by ETAR.

1.1.4 Endothelin A receptor antagonism

For the above reasons, the use of therapeutics targeting to impair the binding of ETAR to ET1 is a very promising approach. One of the most studied mechanisms is competitive antagonism, in which a small molecule such as ZD4054 competes with ET1 to bind to ETAR without triggering the signalling pathway, therefore acting as an antagonist. This approach has been tested in several cancers such as ovarian, in

which ETAR antagonists reduced proliferation of ovarian (Rosanò et al. 2007a) or colorectal cancer cells in which they reduced proliferation in both cancer cells and colonic fibroblasts (Ali et al. 2000; Knowles et al. 2012). This efficacy also translates to *in vivo*, where ETAR inhibition successfully inhibited liver metastasis growth (Asham et al. 2001).

ETAR is involved in several cancerous mechanisms; its inhibition has also been proven to restore apoptosis. A good example of this is the inhibition of ETAR by ETAR-specific antagonist ZD4054 (Rosanò et al. 2007a), but also dual ETAR/ETBR antagonism with bosentan (Peduto Eberl et al. 2003), both reported to promote apoptotic mechanisms. A reduction in the metastatic potential of cancers can also be achieved with ETAR antagonism. The treatment of colonic fibroblasts with ZD4054 achieved inhibition of proliferation, migration, contraction and production of MMPs, all mechanisms involved in cancer invasion and metastasis (Haque et al. 2013).

This success has driven ETAR antagonists such as ZD4054 to clinical trials, showing acceptable tolerability in a Phase II trial with prostate cancer patients (James et al. 2009) while failing, however, a number of subsequent studies. Currently ZD4054 is undergoing clinical trials in combination with the widely used FOLFIRI regime for advanced colorectal cancer patients.

1.1.5 Crosstalk between ETAR and the MAPK pathway and possible treatment combinations

Probably the most significant discovery regarding the endothelin axis, particularly with prospect of treating colorectal cancer, is the crosstalk of ETAR activation and the MAPK pathway. Being the MAPK pathway central to tumour development and progression, a combination of therapies targeted against its mainstream proteins and a closely related alternative pathway such as ETAR signalling has the potential for a synergistic cancer treatment.

As mentioned earlier, ETAR has been proven to activate the MAPK pathway through the direct activation of a number of proteins such as phospholipases and cyclases

and indirect activation of many other proteins (Shome et al. 2000; Blaukat et al. 2000; Spinella et al. 2002; Spinella et al. 2004). Furthermore, it has been reported that ETAR signalling trans-activates the epidermal growth factor receptor (EGFR), which triggers mainstream signalling of the MAPK pathway (Bagnato & Rosanò 2008; Grant et al. 2007). Similarly, ETAR activation was shown to trigger the production of platelet-derived growth factor (PDGF) on human smooth muscle cells, which interacts with other RTKs (Yang et al. 1999). The transactivation of EGFR specifically has been exploited as a combination therapy. The co-administration of gefitinib, an EGFR inhibitor, and ZD4054, an ETAR competitive antagonist, achieved tumour regression *in vivo*, as well as, a reduction in key proteins involved in angiogenesis and metastases (Rosanò et al. 2007b).

These results shed light on the possibility of a treatment combination that involves the inhibition of an intracellular MAPK pathway protein such as MEK, and the antagonism of the ETAR.

1.1.6 RNA interference and cancer treatment

Another therapeutic approach that has raised interest in the last years in cancer therapy is RNA interference (RNAi). It is a natural process occurring within the cell through the use of non-coding RNAs such as microRNA (miRNA), with functions such as gene expression regulation and defence against foreign genetic material (Hamilton & Baulcombe 1999; Wilkins et al. 2005; Huang & Zhang 2013). However, this natural process can be exploited to silence target genes through the use of short interfering RNA (siRNA) (Fire et al. 1998). These are small double stranded RNA molecules, of approximately 20 base pairs in length that have the ability to destroy target complementary mRNAs. The process involves the siRNA being processed by an enzyme called Dicer and incorporated into an RNA-induced silencing complex (RISC). The RISC containing processed siRNA then interacts with its complementary mRNA sequence to allow Argonaute, the active enzyme of the RISC to degrade the target (Hammond et al. 2000; Bernstein et al. 2001). The degradation of target mRNAs subsequently prevents the expression of the target protein. While there are not any reports on the use of siRNA as a therapeutic molecule in colorectal cancer,

some studies have shown promise such as proliferation inhibition observed in head and neck carcinoma (Ishimoto et al. 2012).

Due to its specificity and effectiveness in the reduction of target protein expression, the use of siRNA as a potential treatment in combination with small molecules such as AZD6244 or ZD4054 could potentially exploit the connection between the MAPK and ETAR pathways.

1.2 Organic nanocarriers for anticancer therapeutic delivery

Traditional chemotherapy presents a number of limitations, such as side effects and toxicity. While the development of new generation therapeutics addresses these limitations and allows the targeting of key molecules with increasing specificity, their efficacy is also hindered by their physicochemical properties. Most of these new therapeutics, while promising, are prone to degradation or have very poor solubility in an aqueous environment.

Nanotechnology is defined as the manipulation of matter in a scale ranging from 1 to 100 nm in size, at least in one of its dimensions. The emergence of nanotechnology has applications in a number of fields, from novel resistant materials and extraordinary physical properties to medical and pharmaceutical applications. A subcategory within nanotechnology is nanomedicine, which can be roughly defined as the application of nanotechnology for medical purposes. Although there are a number of correct definitions of nanomedicine, it is generally considered that it involves applications in biosensing, therapeutics, theranostics and medical devices.

While the concept of “nanoparticle” traditionally refers to structures smaller than 100nm in size, in the field of nanomedicine is stretched to several hundreds of nanometres. Nanoparticles can be divided in inorganic (such as gold nanoparticles, iron oxide magnetic nanoparticles or quantum dots) and organic nanoparticles (such as peptides, dendrimers, micelles or liposomes). While inorganic nanoparticles are significantly smaller (often a few nanometres) and generally used for their unique physical properties (such as fluorescence, magnetic properties or energy

transmission) organic nanoparticles tend to be in the range between tens of nanometres and hundreds of nanometres.

Organic nanoparticles are fundamentally made of carbon (although carbon nanotubes and fullerenes, also made of carbon, are considered inorganic nanoparticles), and are generally used as nanocarriers for therapeutic molecules such as drugs or nucleic acids, due to their larger size, biocompatibility and often ability to entrap smaller molecules.

Among the different organic nanocarriers, liposomes and micelles (Figure 1.3) offer better properties in terms of encapsulation and protection from the environment, but their most interesting quality is their larger size compared to dendrimers and easily degradable peptide-based nanoparticles. This larger size is desirable to take advantage of the enhanced permeability and retention (EPR) effect, which consists in the selective accumulation of nanocarriers of a certain size in the tumour masses as opposed to other organs, minimizing the side effects that the therapeutic molecule would elicit systemically. The rationale behind this phenomenon is that, due to the fast angiogenesis in tumours, the formation of the vasculature is aberrant and disorganized, leaving larger fenestrations in the vessel walls. This larger fenestrations tend to allow the passage of macromolecules and nanocarriers of several tens or several hundreds of nanometres in diameter, that are too big to translocate through the vessel wall in other tissues. The EPR effect also comprises the inefficient lymphatic clearance characteristic of tumour tissue, which favours the accumulation of compounds and nanoparticles in the tumour mass over time.

As opposed to active targeting, in which the surface of nanoparticles is functionalized to recognize specific molecules in the tumour cells, passive targeting only depends on the diffusion and accumulation of nanoparticles in the tumour through the EPR effect. However it must be noted that both active and passive targeting face similar limitations in terms of penetrating further into the tumour mass due to several physical barriers such as the high cell density and the tumour stroma.

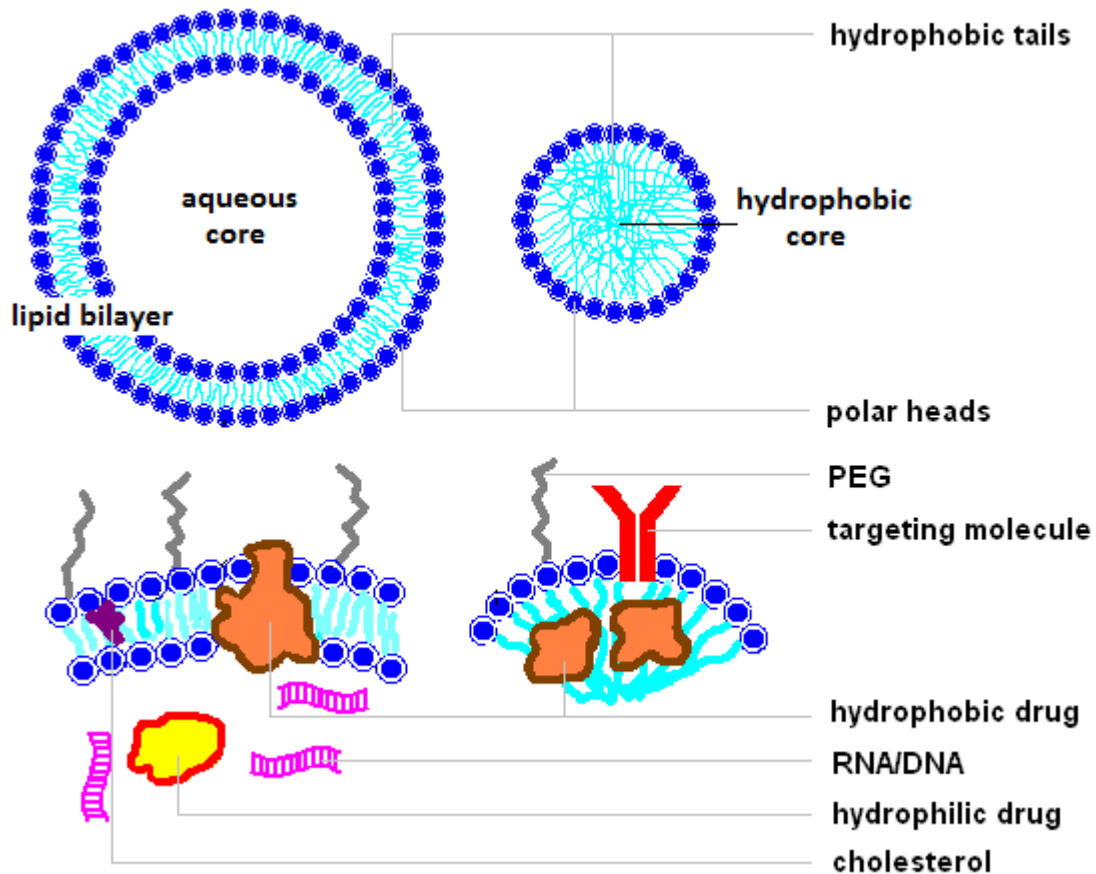


Figure 1.3 Schematic representations of a liposome (left) and a micelle (right), including examples of encapsulated molecules and surface modifications. PEG=polyethylene glycol.

1.2.1 Liposomes

Liposomes were described for the first time by Bangham and colleagues (Bangham et al. 1965), and have been the most successful nanocarrier (Mozafari 2010; Malam et al. 2009). Liposomes are formed from the interaction of the hydrophobic tails of lipid molecules forming a bilayer and exposing their polar heads to the surrounding aqueous environment (Figure 1.3). While some of the molecules shown in the image are encapsulated, others such as cholesterol or PEG have stabilization or accelerated blood clearance (ABC) avoidance purposes. The main advantage of liposomes over micelles is that, due to their hydrophobic membrane and aqueous core, they can encapsulate both hydrophilic and hydrophobic molecules. This has led to the use of liposomes to encapsulate nucleic acids such as siRNA, with

successful results knocking down targeted gene expression *in vivo* (Gao et al. 2012; Gao et al. 2011). The dual different affinity of the liposome membrane and core for hydrophobic and hydrophilic molecules has also been exploited for combination therapies. For example, the combination of Mcl1-targeted siRNA and the MEK inhibitor PD0325901 in a cationic liposome achieved proliferation inhibition and increased apoptosis *in vivo* (Kang et al. 2011). However, the stability of liposomes is often compromised by the encapsulation of a hydrophobic drug such as rhodamine compared to a hydrophilic molecule such as fluorescein (Khan et al. 2008), although certain hydrophobic compounds may elicit the opposite effect (Moribe et al. 1998). Often, cholesterol is used to increase the stability of the liposomal membrane, regardless of the nature of the biological compounds.

Name	Nanoformulation	Drug	Cancer
Doxil	Liposomal	Doxorubicin	Breast and ovarian cancer, Kaposi's sarcoma
Myocet	Liposomal*	Doxorubicin	Breast
DaunoXome	Liposomal	Daunorubicin	Kaposi's sarcoma
Depocyt	Liposomal	Citarabine	Lymphomatus meningitis**
Genexol-PM	Micellar	Paclitaxel	Breast, lung and ovarian***

Table 1.1 Clinically approved vesicular nanoformulations: * Non-PEGylated, ** In phase II clinical trials for leukemia and phase I-II for glioblastoma ***Only approved in Korea.

Liposomes are far more advanced in clinical use than any other nanoparticle (Table 1.1) (Lammers et al. 2012). The most known example is Doxil, also known as Caelyx, a liposomal formulation of doxorubicin, which surface has been functionalized with polyethylene glycol (PEG) to avoid recognition by the immune system and ABC. Doxil is widely used in the treatment of breast cancer and has been proven to reduce neutropenia and cardiotoxicity among other side effects,

compared to free doxorubicin, as well as, vinorelbine or mitomycin C combined with vinblastine (Keller et al. 2004; O'Brien et al. 2004). Apart from those already approved liposomes, a number of them are currently in clinical trials, such as the liposomal formulation of floxuridine and irinotecan under the name of CPX-1, which is in clinical trials for colorectal cancer (Batist et al. 2009).

1.2.2 Micelles

Most micelles are especially effective in solubilizing hydrophobic molecules, due to the spacious core created by the hydrophobic tails of amphiphiles (Figure 1.3). They tend to be around tens of nanometres in diameter, and this makes them generally smaller than the liposomes. This has implications in the ABC, as they less often need to undergo surface functionalization with molecules such as PEG to avoid it (Koide et al. 2008). However, the greatest advantage of micelles over liposomes is their ability to solubilize hydrophobic drugs, preventing them from aggregating in aqueous solution and creating emboli *in vivo* (Torchilin et al. 2003).

Only one micellar formulation of paclitaxel (Genexol-PM) has reached clinical approval in Korea for breast, lung and ovarian cancers (Table 1.1), although it is undergoing clinical trials in other countries (Lammers et al. 2012). Many other micellar formulations are currently undergoing clinical trials, such as a formulation of cisplatin (NC-6004), which significantly reduced the renal toxicity commonly linked to other cisplatin formulations (Plummer et al. 2011).

1.2.3 DOPE/DC-cholesterol liposomes and GCPQ micelles

Two of the most promising organic nanocarriers are cationic liposomes made from 3beta-[N-(N',N'-dimethylaminoethane) carbamoyl] cholesterol (DC-chol) and *dioleoylphosphatidylethanolamine* (DOPE), which have been shown to have potential as nucleic acid and drug nanocarriers (Zhang et al. 2010; Yang et al. 2012; Ciani et al. 2004), and micelles made from N-palmitoyl-N-monomethyl-N,N-dimethyl-

N,N,N-trimethyl-6-O-glycolchitosan (GCPQ) , also cationic in nature, which have been used to solubilize and orally deliver hydrophobic molecules with high efficiency (Qu et al. 2006; Siew et al. 2012; Lalatsa et al. 2012). Cationic nanoparticles have the advantage of improving internalization by interacting with the anionic cell surface (Pelaz et al. 2013; Hino et al. 2012; Dokka et al. 2000). Due to these positive results and promise, these two nanocarriers have been chosen for the present research.

1.3 Three-dimensional cancer models

Most investigations on anti-cancer therapeutic agents follow the same two steps, starting with their evaluation in a two-dimensional *in vitro* model, and then testing their efficacy in immunosuppressed animal models. Although, this workflow has yielded very valuable information over the years, the development of better cancer models is becoming increasingly urgent. On the one hand, the reductionist two-dimensional *in vitro* models overlook key mechanisms such as cell-matrix interactions and cell three-dimensional orientation, which are extremely important for cellular behaviour and response to therapy (Trédan et al. 2007; Cukierman et al. 2001). Similarly, *in vivo* studies are not only expensive but a crude approximation to real tumours, and do not consider mechanisms, which also play a key role in disease development, such as the immune system (Crompton et al. 2014).

Three-dimensional *in vitro* models are a compromise between conventional *in vitro* models and *in vivo*, (Fischbach et al. 2007) and are particularly valuable for cancer research. They provide a cellular environment closer to the real tumour mass, whilst simultaneously allowing control over a number of parameters (Talukdar et al. 2011; Lee et al. 2007). The use of 3D *in vitro* cancer models has revolutionised cancer research, allowing a more controlled environment for cancer to be studied in the laboratory. Culturing cells in 3D elicits changes in proliferation, behaviour and protein expression compared to monolayers (Magdeldin et al. 2014; Trédan et al. 2007; Mikhail et al. 2013), which have an influence on cell fate. In addition, 3D cancer models allow for drug penetration factors to be investigated (Hickman et al. 2014; Huang et al. 2012).

One of the keys to this improvement is the presence of an extracellular matrix (ECM), composed of proteins, polysaccharides and proteoglycans (Cukierman et al. 2001). The interaction of these components with both cell membrane and intracellular proteins creates focal adhesion points that trigger mechanotransduction pathways and regulate the expression of a number of genes. Three-dimensional *in vitro* models can be roughly divided in two subcategories: 1) spheroids and 2) 3D scaffolds.

1.3.1 Spheroids

The use of spheroids in cancer research has revolutionized the field. They are large aggregates of cells that form without a scaffold, through methods such as gyratory rotation. Spheroids successfully mimic cellular behaviour *in vivo* and have been widely used for this reason (Pickl & Ries 2009). They also allow the development of more complex approaches, such as co-cultures of various cell types which have been successfully used to study a wide range of therapeutic approaches, such as chemotherapy, radiotherapy and immunotherapy (Santini et al. 1999). In this model, while cells in the periphery are highly proliferative, the core of the spheroid tends to contain quiescent cells due to the limited access of oxygen and nutrients (Kunz-Schughart et al. 1998). The dense structure of spheroids also has implications in the penetration of therapeutic agents, providing an accurate representation of tumour mass density *in vivo*, in which density remains a physical barrier. The downside is that the absence of an extracellular matrix limits cell motility and arguably limits the potential of spheroids as models of invasion and metastases.

1.3.2 Scaffolds

While spheroids are invaluable systems for drug testing and the study of cell behaviour to a certain extent, more sophisticated approaches involve the use of scaffolds, which allow the study of cell-matrix interactions and mechanisms such as cell migration and invasion. These scaffolds can be natural or synthetic.

Natural scaffolds are composed of ECM proteins such as collagen, laminin or hyaluronic acid (Holliday et al. 2009; Suri & Schmidt 2010; Gurski et al. 2009). The presence of ECM proteins not only facilitates cell-matrix interactions, but makes the environment susceptible to degradation and remodelling by cells through the secretion of metalloproteinases (MMPs) and migration. A good example of a natural scaffold that has been widely used for this properties is Matrigel (Shekhar et al. 2001), which consists of a mixture of ECM proteins.

On the other hand, synthetic scaffolds are made of polymers such as polyglycolic acid (PGA) or polylactide (PL). These scaffolds are stiffer and more representative of the ECM mechanical properties (Mooney et al. 2006; Place et al. 2009), but require modifications such as the addition of RGD to allow for cell adhesion (Villanueva et al. 2009). Due to the interest of our group in cell behaviour as opposed to matrix mechanical properties, our research involves the use of natural scaffolds, fundamentally collagen type I hydrogels.

1.3.3 Tumouroid, a collagen-based *in vitro* model of cancer

While the use of collagen type I hydrogels mimic the ECM and is a promising approach, their main limitation is their high water content (Szot et al. 2011). In this research, we use a plastic compression technique to create tumouroids, 3D *in vitro* models of colorectal cancer, by removing the excess water from collagen type I hydrogels. This model mimics the mechanical properties of real tissue better than uncompressed collagen hydrogels (Ricketts et al. 2014; Nyga et al. 2013; Magdeldin et al. 2014).

1.4 Aims

The overall aim of this thesis was to create organic nanoformulations, of a suitable anticancer therapy and test their efficacy on a collagen-based 3D model of colorectal cancer. This is based on the great promise of both approaches, as described in this chapter. The purpose behind that aim is to merge three of the most significant advances in cancer research: novel targeted therapeutic molecules (e.g. AZD6244), the use of nanotechnology as a drug delivery platform (e.g. liposomes and micelles), and the inclusion of complex *in vitro* approaches to study both cancer behaviour and anti-cancer drug development (e.g. 3D models of cancer).

By combining therapy, nanotechnology and tissue engineering this work intends to shed light on the need to integrate these technologies as they must evolve together with the process of drug discovery. The specific objectives include:

- I) Find suitable candidates for a combination of treatments involving the ETAR and MAPK pathways that achieve an additive or synergistic inhibitory effect on cancer proliferation, including small molecules and siRNAs as therapeutic agents.
- II) Create nanoformulations of the chosen treatments using DOPE/DC-cholesterol liposomes and GCPQ micelles.
- III) Test the efficacy of said nanoformulations in both conventional monolayer cultures and collagen-based three-dimensional *in vitro* models of colorectal cancer (tumouroids).

CHAPTER 2

General Materials & Methods

2 General Materials and Methods

This chapter describes general techniques that are routinely used throughout this research. Further details are included in the Materials and Methods sections of specific chapters as needed.

2.1 Cell maintenance

Cell lines HT29 (human colorectal adenocarcinoma) and HCT116 (human colorectal carcinoma) were obtained from the European Collection of Animal Cell Cultures (ECACC, Sigma Aldrich, Gillingham, Dorset, UK). All experiments were performed using cells between the 9th and the 40th passage.

Cells were cultured routinely under aseptic conditions in 75 cm² tissue culture polystyrene flasks at 37°C and in a 5% CO₂ / 95% humidified air atmosphere, using McCoy's 5A (Lonza, Castleford, UK) supplemented with 10% foetal bovine serum (FBS) and 1% penicillin/streptomycin (P/S) as culture medium, unless stated otherwise. When 80-90% confluence was reached, cells were washed with phosphate buffered saline (PBS), detached from the flask with 1mg/mL trypsin in PBS and passaged to a new flask at 1:5 to 1:10 fold dilution after neutralizing the enzyme activity, using medium supplemented with FBS (approximately every 72 h). When cells did not undergo passage, they were fed with fresh medium supplemented with FBS every 48 hours.

2.2 Proliferation and metabolic activity assays

Two types of techniques were used to determine basal or changing proliferation levels in these cell lines. One of the techniques is more directly related with the amount of cells present (e.g. cell counting, total DNA assay), and the other indirectly measures the relative amount of cells present by measuring their metabolic activity (e.g. alamar blue assay, MTT assay) or aggregate size.

Specific cell culture protocols from cell seeding to the proliferation and metabolic activity assays are described in the corresponding chapters, while the protocol for the assay itself is described in the following sections.

2.2.1 Cell counting

This technique directly measures the number of cells in a population, and hence is an indicator of proliferation. As the gold standard for measuring cell proliferation, cell counting was used to validate MTT as an indirect indicator of cell proliferation, and to seed known concentrations of cells in every experiment that required so.

Cells were trypsinized and neutralized, counted in a haemocytometer, and calculations were made to determine the required cell dilutions. To use the haemocytometer, 10 μL of cell suspension were added on each side of the haemocytometer and the cells entrapped in 8 squares out of the total 18 were counted. The total value was divided by 8 and multiplied by 10^4 to obtain the total number of cells in 1 mL. The total number of cells in the suspension were determined, multiplying this value by the total volume of the suspension.

2.2.2 3-(4,5-dimethylthiazol-2-yl)-2,5-diphenyltetrazolium bromide (MTT) assay

Metabolic activity in conventional 2D *in vitro* cultures was determined through MTT assay. The NAD(P)H-dependent oxidoreductases present in cells are capable of reducing this tetrazolium compound into formazan, which forms insoluble blue crystals. Therefore, the amount of formazan crystals formed is proportional to the metabolic activity of cells. MTT solution (3-(4,5-dimethylthiazol-2-yl)-2,5-diphenyltetrazolium bromide) was prepared dissolving 200mg of powder (Sigma Aldrich M2128) in a mixture of 5 mL of 100% v/v molecular grade ethanol (Sigma Aldrich E7023) and 5 mL of milli-Q water, making it 40 times more concentrated than the active concentration for cellular assays. Then 12.5 μL (24-well plate) or 25 μL (12-well plate) of this solution were added to the pre-existing 500 μL (24-well plate) or 1 mL (12-well plate), hence diluting it to its active concentration. 20 mins later,

when blue crystals formed (and a colour change from yellow to blue was observed), medium was aspirated, wells washed with PBS, and crystals dissolved in 400 μ L of dimethyl sulfoxide (DMSO) (Sigma Aldrich D5879). 100 μ L of the resulting blue liquid were transferred to a 96-well plate and absorbance was read at 570 nm in a colorimetric plate reader (Anthos 2010 Standard, Biochrom) (n=12).

2.2.3 Total DNA assay

Proliferation in conventional 2D *in vitro* cultures was determined by total DNA assay, using the Hoechst stain total DNA kit (Sigma Aldrich, DNAQF). Hoechst 33298 is a water-soluble bis-benzimide that binds to double stranded DNA. This binding shifts its fluorescence emission from a 510-540 nm range to a maximum 461 nm . A 1:1000 dilution Hoechst 33298 dye solution and a 10 μ g/mL DNA standard solution were prepared following the conventional protocol. A DNA concentration standard curve of dilutions from 0 to 10 μ g/mL was prepared to extrapolate the concentration of DNA (μ g of DNA per mL) from the fluorescence emitted from known concentrations of calf thymus DNA reacting with the dye. 100 μ L of sample or standard were added to 100 μ L of dye previously loaded in a black 96-well plate. Fluorescence was read immediately after (excitation=350 nm, emission=460 nm) in a Fluoroskan Ascent FL (Thermo LabSystems) (n=12).

2.2.4 Alamar blue[®] assay

Metabolic activity in 3D *in vitro* models was determined using Alamar Blue[®] assay (Invitrogen, Paisley, UK). The blue compound 7-hydroxy-3h-phenoxazin-3-one-10-oxide, also known as resazurin shows a weak fluorescence, but when reduced by cell metabolism to resorufin, it changes to a pink colour with a strong red fluorescence. Concentrated Alamar Blue was diluted 1:10 in Phenol Red-free medium and protected from photodegradation using tin foil. Then wells were washed, medium was substituted by an equal volume of the diluted Alamar Blue, covered in tin foil, and incubated for four h in a 37⁰C, 5%CO₂/air humidified

atmosphere, rocking occasionally. After observing a colour change from blue to pink, 100 μ L of the resulting solution were transferred to a black 96-well plate and fluorescence was read (excitation=530 nm, emission=620 nm) in a Fluoroskan Ascent FL (Thermo Labsystems) (n=12)

2.2.5 Aggregate area measurement

Another technique to measure proliferation in a 3D *in vitro* model involves calculating the areas of cell aggregates. Images of tumoroids were taken using an Olympus CKX31 microscope (x200 magnification) with a Panasonic camera (x0.5 magnification). Aggregate areas were measured using the Image J software (version 1.47v, released 08/07/2013) (Figure 2.1).

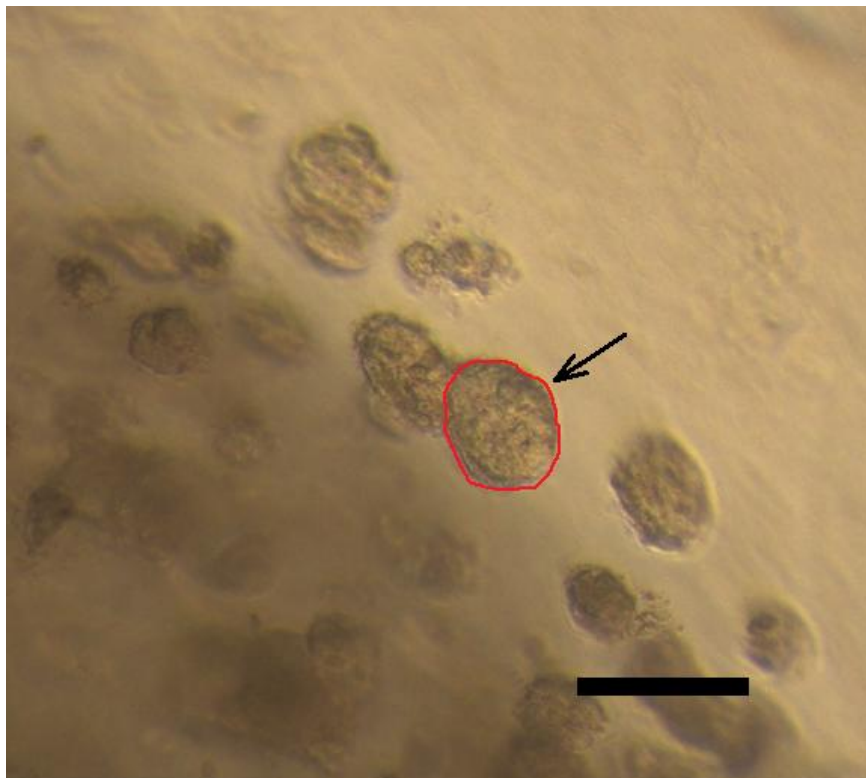


Figure 2.1 Demonstration of the use of Image J software to measure cell aggregate areas. Cell aggregates in 3D *in vitro* cultures were delineated by using the “Freehand selection” tool manually and areas were extrapolated using a graduated size scale. Scale bar = 50 μ m

2.3 Approaches to cell molecular analysis

Specific protocols involving cell culture and drug treatments prior to molecular studies will be described in subsequent chapters. The techniques explained here describe the experiments after the end point of the specific small molecule and siRNA treatment protocols.

2.3.1 Protein extraction and quantification

After washing remaining medium with PBS, plates were placed on ice and cells were lysed by adding 250 μ L of RIPA (Radio-Immunoprecipitation Assay) buffer (Sigma-Aldrich R0278) supplemented with a mixture of protease inhibitors. Lysates were centrifuged at 12,000g for 5 mins at 4 $^{\circ}$ C to precipitate large fragments of cells, and the supernatant containing the protein was stored at -20 $^{\circ}$ C.

Protein extracts were diluted in protease-free molecular grade water at a 1:5 dilution, and quantified using the Lowry assay (Thermoscientific, 23240). Absorbance was read at 750nm using a Jenway Genova Plus Spectrophotometer and protein concentrations were extrapolated from a the Lowry standard curve.

2.3.2 Polyacrylamide gel electrophoresis (PAGE) and Western blot

Total protein concentration was standardized for all samples through dilutions in RIPA buffer. After mixing the protein with a loading dye (NuPAGE $^{\circ}$ LDS Sample Buffer, Life technologies, NP0007) containing 12.5% β -Mercaptoethanol (Sigma Aldrich, M3148) to make a total of 40 μ L, samples were heated at 95 $^{\circ}$ C for five minutes to denature the protein (heating block QBT1, Grant). 34 μ L of the samples were loaded in the corresponding lane of a NuPAGE 4-12% Bis-Tris polyacrylamide gel (Invitrogen, NP0322BOX) next to a pre-stained protein ladder (SeeBlue $^{\circ}$ Prestained, Invitrogen LC5625) for molecular weight identification, covered in buffer (MES SDS running buffer, Life Technologies, NP0002) and run at 150V of voltage

(as limiting parameter), 150mA of current and 20W of power for 60-90 min in a XCell SureLock™ Electrophoresis Cell connected to a Consort EV231 powerpack.

Once proteins are separated by weight, gels are set up against PVDF membranes (Immun-Blot® PVDF membrane, Biorad, 162-0177) as indicated in Figure 2.2 to be transferred, covered in transfer buffer (NuPAGE® transfer buffer, Life technologies, NP0006-1) and run at 30V of voltage, 250mA of current, and 20W of power for 90 min in a (XCell II Blot Module, Invitrogen). Transfer was confirmed by the pre-stained protein ladder.

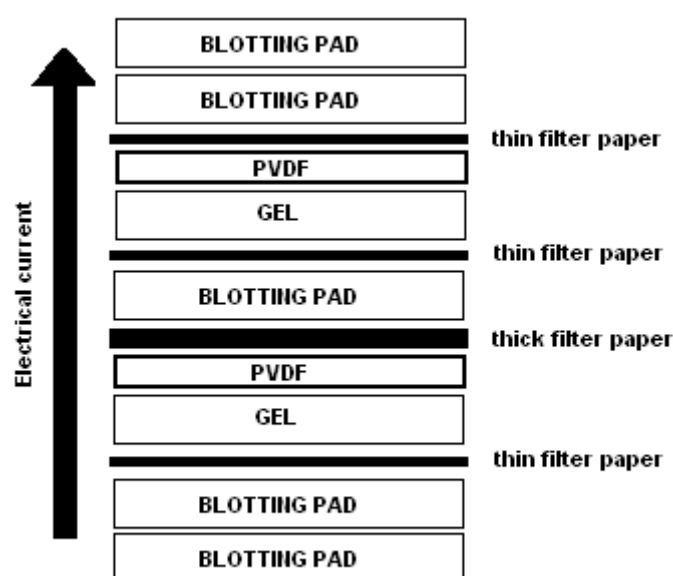


Figure 2.2 Representation of the Blot Module set up. Blotting pads and filter papers were pre-soaked in transfer buffer and layered as shown above. Bubbles were removed from every layer by rolling with a plastic cylinder.

Membranes were rinsed with PBS-tween20, blocked with a 5% milk solution (2.5% BSA for pERK detection) for 30 mins, and incubated with a specific primary antibody (diluted in 1% BSA solution) overnight at 4°C, or two hours at room temperature (details on the antibodies are shown in Table 2.1). After rinsing with PBS-tween, membranes were incubated with a secondary antibody linked to horseradish peroxidase (HRP) for 40 min, rinsed again, treated with the Bio-Rad Immuno-Star Western C developer (BioRad, 170-5070) and visualized using a BioRad Molecular Imager®, ChemiDoc™ XRS+ with ImageLab™ Software.

After visualization, bound antibodies were removed using Restore Plus Western Stripping Buffer (Thermo Scientific, 46430), re-incubated with a GAPDH antibody for 30 min, rinsed, incubated with a secondary antibody for 40 min, developed and visualized.

This two-step approach is intended to prevent the strong signal from the housekeeping gene glyceraldehyde 3-phosphate dehydrogenase (GAPDH) from eclipsing the target protein. GAPDH was used to ensure equal loading among samples and to standardize the densitometry of Western Blot images, obtained with the Image J software (version 1.47v, released 08/07/2013).

Company	Antibody	Species	Catalog code
Abcam	Anti-ET _A R	Rabbit	ab76259
Alomone Labs	Anti-ET _A R	Rabbit	AER-001
Cell Signalling	Anti-pERK1/2	Mouse	9106S
	Anti-rabbit HRP-linked	Goat	7074P2
Santa Cruz Biotechnology	MEK1/2	Rabbit	sc-436
	GAPDH	Mouse	sc-32233
	Anti-mouse HRP-linked	Goat	sc-2005

Table 2.1 Source and details of the antibodies used in this research. All antibodies were used at dilutions that range from 1:500, in the case of anti-ETAR, and 1:2000, in the case of anti-GAPDH. All antibodies are primary except for the HRP-linked antibodies raised in goat, which are secondary.

2.3.3 RNA extraction and quantification

After washing remaining medium with PBS, plates were placed on ice and cells were lysed using 350µL of RNeasy lysis buffer (RLT) buffer and passed through a 30G needle to homogenize the sample. RNA was extracted using the RNeasy mini kit (Qiagen, 74104) and quantified using a spectrophotometer (at wavelength 260 nm and 280 nm to also determine its purity) before storing them at -20°C.

2.3.4 Conventional RT-PCR

RT-PCR was performed using the OneStep RT-PCR Kit (Qiagen, 210210). Three master mixes were created separately to facilitate manipulation, and to increase accuracy by manipulating larger amounts of liquid. The first master mix contains 0.6 μ L of enzyme mix, 3 μ L of (5x) buffer and 1.4 μ L of molecular grade water per reaction. The second master mix contains 0.9 μ L of each sense and antisense primers, 0.6 μ L of deoxynucleotides-tri-phosphate (dNTP) and 2.6 μ L of molecular grade water per reaction. The last master mix contains 20ng/mL of sample RNA in molecular grade water. For all these mixtures, an extra 10% volume of every reactant was added to allow for pipetting errors.

5 μ L of each master mix were combined to make a total of 15 μ L (100ng of template RNA) and target sequences were amplified in a thermal cycler (Techne Flexigene) following a cyclic programme as indicated in Figure 2.3. PCR products were mixed with 2 μ L of 6x loading dye solution (Thermo Scientific, R0611) to facilitate handling, loaded in a 1% agarose gel containing ethidium bromide (EtBr) next to a 50bp DNA Step Ladder (Promega, G452A) and run for 20 min at 100V in a electrophoresis gel system (Midcell® Primo™ EC330, Thermo Electron), before visualizing them under UV light (100nm) using a BioRad Molecular Imager®, ChemiDoc™ XRS+ with ImageLab™ Software (n=3).

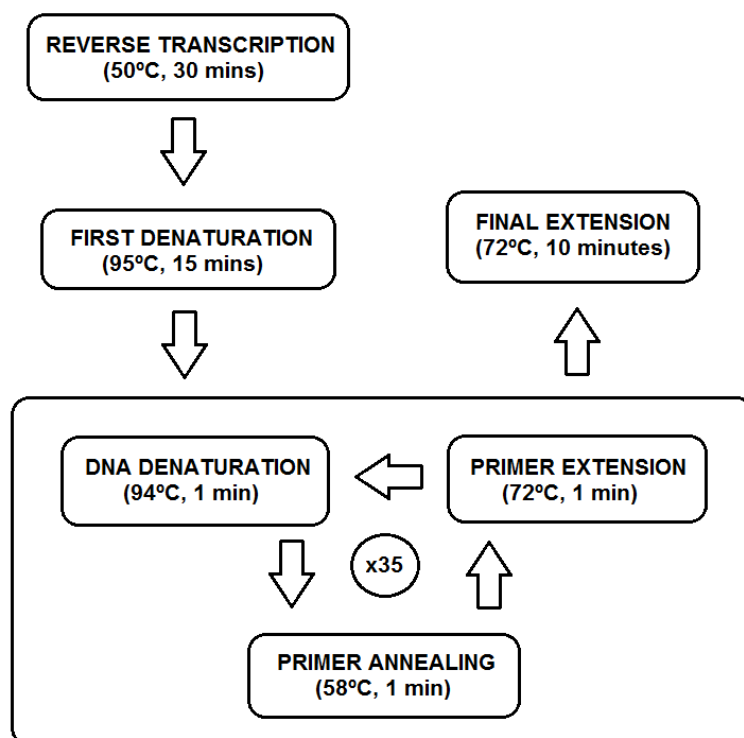


Figure 2.3 Schematic representation of RT-PCR amplification cycles. Changes in temperature allow for the DNA strands to denature, anneal and amplify the sequence for 35 cycles. The process starts with the reverse transcriptase copying the target RNA sequence into complementary DNA. The enzyme is deactivated after the first denaturation. 35 cycles of amplification by a DNA polymerase follow. A final longer extension period is allowed before samples are visualized.

2.3.5 Quantitative RT-PCR

For accurate comparative measures of mRNA copy numbers a quantitative technique is needed. Quantitative RT-PCR was performed using the QuantiTect SYBR Green RT-PCR kit (Qiagen, 204243) and the LightCycler[®] 1.5, with LightCycler[®] Software 3.5.3 (Roche). mRNA copy numbers were determined using a housekeeping gene (G6PDH), both as an internal control to standardize the samples of the same template and to extrapolate the copy number from fluorescent signals and a standard curve.

The method is similar to the conventional RT-PCR represented in Figure 2.3 with a few differences in the preparation and programme. As before, three master mixes were prepared. The first one contained 0.2µL and 9.8µL of 2x buffer per reaction, the second one contained 2µL of each primer and 1µL of molecular grade water per

reaction, and the template mix was identical to the previous section (20ng/mL) (all mixtures were prepared adding an extra 10% of every reactant to account for pipetting errors). 5 μ L of the primer mix and 5 μ L of the template dilution (100ng of sample RNA) were mixed in a reaction tube, and 10 μ L of the enzyme mix were added last, protecting the glass capillaries from the light. Each template had an internal control of G6PDH, which was also used to create a standard curve for absolute quantification. 40 cycles of amplification of 3x30 sec each were run, accumulating fluorescent signals for the quantification and recording a melting curve to assess the quality of the reaction (n=3). Details on the primers used both for conventional and quantitative RT-PCR are shown in Figure 2.4.

Primer name	Length (base pairs)	Primer sequence (5' to 3')	Melting point (°C)	GC content (%)
ET _A R sense	21	CTCAACCTCTGCGCTCTTAGT	62.6	52.3
ET _A R antisense	21	AGCCAATCGCTTCAGGAATGG	69.3	52.3
ET-1 sense	21	GCTCGTCCCTGATGGATAAAG	64.6	52.3
ET-1 antisense	19	CCATACGGAACAACGTGCT	63.6	52.6
EGFR sense	16	ATCGCAAAGGGCATGA	61.5	50
EGFR antisense	19	CCAGCCCAAATCTGTGAT	62.5	47.3
MEK-1 sense	16	CTCCACCATCGGCCTT	62.4	62.5
MEK-1 antisense	17	AAGCGACATGGCAAACC	62.4	52.9
MEK-2 sense	18	GGGCCATCCCCTACCAG	68.8	72.2
MEK-2 antisense	21	TTCTGCTGCTCGTCAAGTCC	66.8	52.3
GAPDH sense	20	AGATCATCAGCAATGCCTCC	64.2	50
GAPDH antisense	21	AGTGATGGCATGGACTGTGGT	66.8	52.3

Figure 2.4 Details and sequence of the primers used in this research. All primers were designed to have melting temperatures and GC contents as similar to their counterparts as possible. All primers were obtained from Sigma-Aldrich.

2.4 Statistical Analysis

Results are shown grouping means and standard deviations from different experiments for representation, and treatment groups were normalised in reference to their control groups for convenience. This normalisation was done by considering the control group of that experiment as a 100% value (represented as 1 from a 0 to 1 scale) and the different treatments as percentage fractions of that control (also

represented in a 0 to 1 scale). However, statistical analysis (indicated by asterisks and figure descriptions) was performed on the original data.

Comparisons between two individual data sets such as the treatment with ET-1 versus the control were analysed using the Student's t-test. Drug concentration ranges and analyses involving more than two treatment groups were analysed using one-way ANOVA followed by post hoc analysis using Dunnett's test or Bonferroni's test. Differences were considered significant with p values equal or less than 0.05.

Parametric tests were used since data can be considered to follow a normal distribution. Individual samples were considered independent (random sampling from defined populations) and standard deviations between treatment groups were similar, with n=12 for drug treatments. Parametric tests intrinsically have more statistical power and are designed to calculate differences between means as opposed to medians.

All data analysis and graphical representations were done using the GraphPad Prism software (v5.01, 07/08/2007).

CHAPTER 3

Investigations on Small Molecule Therapeutic Agents

3 Investigations on Small Molecule Therapeutic Agents

3.1 Introduction

This chapter reports on the response of two colorectal cancer (CRC) cell lines to different therapeutic molecules currently in clinical trials. Three of them were chemotherapeutic molecules directed against the MAP kinase pathway, but a competitive antagonist of the ETAR receptor was also explored as a possible treatment combination.

The therapeutic targets of interest have been widely reported to contribute to tumour growth and progression. These are the mitogen activated protein kinase kinases 1 and 2 (MEK1 and MEK2), and the endothelin A receptor (ETAR), whose activation triggers a phosphorylation cascade that also cross talks with the MAP kinase pathway. The expression levels of these molecules, as well as, ETAR natural ligand endothelin-1 (ET-1) and a membrane receptor associated to the MAPK pathway, the epidermal growth factor receptor (EGFR) were also studied, as they influence MAPK and ETAR signalling.

The colorectal cancer cell lines used in this study, HCT116 and HT29, have known mutational status, both in terms of expression of these targets and natural ligands, but also in terms of other molecules within the pathways of interest, such as KRAS or BRAF, which are mutated in HCT116 and HT29, respectively (Little et al. 2011).

The aim of these experiments is to define the most efficacious therapeutics to take forward into combination treatments, targeting both pathways simultaneously in cancer cells with known, relevant mutations; hypothesising that a treatment combination would be more effective than monotherapies. In the process of determining the most suitable therapeutic molecules or combinations for nanoformulations (described in this and the next chapter), a variety of unexpected and interesting results were found, which are subject to discussion.

3.2 Materials and methods

3.2.1 Cell characterization

The morphologies of HCT116 and HT29 colorectal cancer cell lines (ECACC, Sigma-Aldrich, UK) are easily distinguishable. While HCT116 cells have visible, strongly defined pseudopodia giving them a barbed aspect, HT29 cells tend to form aggregates with round edges, mimicking the glandular epithelial tissue they arise from, therefore, these cells are more differentiated than HCT116. Both HCT116 and HT29 are small, fast-proliferating cells (HCT116 more than HT29) with abundant dark granules in their cytoplasm.

3.2.2 Materials

A number of small therapeutic molecules were tested *in vitro*, both alone and in combination with appropriate growth factors. This is in line with widely accepted experimental protocols where the efficacy of therapeutic drug against a receptor/target is tested in the presence of the natural ligand, such as the growth factors EGF and ET-1, that binds directly or upstream of the receptor/target, to promote activation. Chemical representations of the key small molecules are shown in Figure 3.1. PD98059 was obtained from Enzo Life Sciences (EI-360-0005, UK), U0126-EtOH and AZD6244 (Selumetinib) were obtained from Selleckchem (S1102 and S1008, Germany). ZD4054 (Zibotentan, ETAR antagonist) was purchased from Selleckchem (S1456), and BQ123 (ETAR antagonist; not shown in figure 1; used for comparison) was acquired from Sigma-Aldrich (B150). For the growth factors, all three batches of Endothelin-1 (ET-1) were acquired from Bachem (H6995) and Epidermal Growth Factor (EGF) from Sigma-Aldrich (E9644).

All inhibitor treatments were performed over a range of concentrations, while the growth factors EGF and ET-1 were used at 10 ng/mL and 10 nM, respectively, according to previous work in this department and the literature (Davenport 2002; Haque et al. 2013).

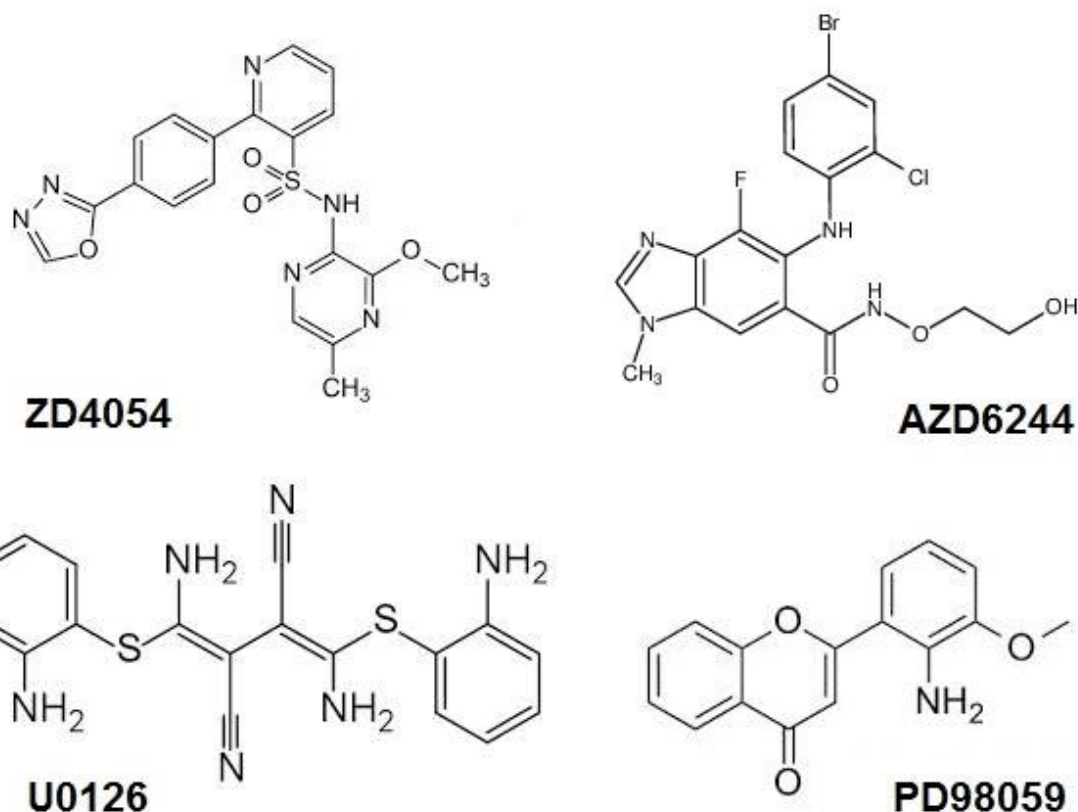


Figure 3.1 Schematics of therapeutic small molecules. MEK inhibitors PD98059, U0126 and AZD6244, and ETAR-specific antagonist ZD4054.

3.2.3 Cell culture and experimental protocols for therapeutic treatments

Colorectal cancer cell lines HCT116 and HT29 were specifically selected for their different mutation profile regarding the MAPK pathway. All cell culture relative to this chapter was carried out without antibiotics.

For drug testing, experiments cells were seeded in 24-well plates (3.2×10^4 cells/well for HT29s and 3×10^4 cells/well for HCT116) in 500 μ L of McCoy's 5A medium supplemented with 10% fetal bovine serum (FBS). Serum was removed after 24 h to prevent possible drug-serum interactions and to semi-synchronize cell cycles (at G₀). 24 h later, small molecules were diluted into serum-free medium at a range of concentrations and used to treat cells for 48 h. At this end point, proliferation and metabolic activity assays were performed to measure inhibition (see chapter 2 (pg. 30)). Ligands were added 1 hour after the start of inhibitor treatment for studies

investigating pathway activation with EGF (10ng/mL) or ligand competitive binding with ET-1 (10nM).

Specifically for AZD6244, a set of experiments were carried out to attempt to duplicate published outcomes (Troiani et al. 2012); therefore, the protocol followed mirrored that of Troiani and colleagues. Here cells were seeded in 24 well plates and left to grow in serum containing media for 48 h, prior to treatment. Inhibitor concentrations and time of exposure were exactly the same, but medium was substituted by DMEM.

The following molecular investigations were carried out. For mRNA reference level analysis of target genes, 1 million cells were seeded in a Petri dish, and lysed using RLT buffer at 60% confluence.

For protein studies, to determine the effect on MEK inhibition, cells were seeded in 6-well plates (2.5×10^5 cells/well for HT29 and 2×10^5 cells/well for HCT116), following the same serum removal and treatments as for the proliferation assays described above. After one hour of treatment, 10ng/mL of EGF was added to the treated cells for 10 min to activate the MAPK pathway. Cells were then lysed using RIPA buffer supplemented with protease inhibitors. RNA and protein extraction, quantification and analysis were performed as described in section 2.3 (pg.34).

3.3 Results

3.3.1 Reference mRNA expression profiles

Before any treatment with growth factors or therapeutic molecules was carried out, quantitative RT-PCR of the target molecules was performed to determine if they were expressed by the two cell lines at significant levels

Molecules investigated include the direct targets for the drugs used; MEK-1 (one of the targets of PD98059, U0126 and AZD6244), and ETAR being (the target of ZD4054 and BQ123). Also, EGFR was included as a common initiator of the MAPK pathway and as a known subject of transactivation through ETAR signalling and ET-1 was included as the natural ligand for ETAR. Results show detectable levels of all target molecules (Figure 3.2), with average MEK-1 (~100-fold) and EGFR (~40-fold) levels much higher than the endothelin axis molecules.

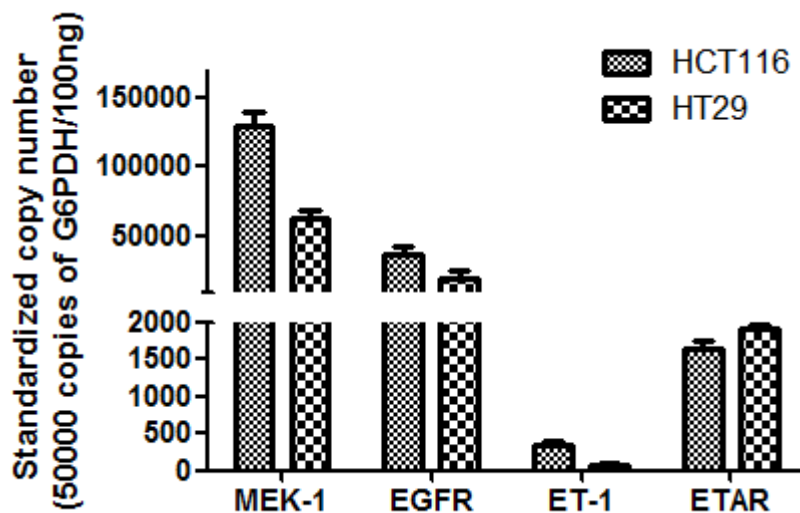


Figure 3.2 mRNA expression levels of target genes in HT29 and HCT116 colorectal cancer cells. 1,000,000 cells were seeded in Petri dishes, lysed at 60% confluence and processed for quantitative PCR. The relative expression levels in 100 ng of total RNA were determined using known standards of the housekeeping gene h-G6PDH (3261883001, Roche) and normalized accordingly. Statistical analyses were not performed.

3.3.2 Treatment with MEK inhibitors

All three inhibitors of MEK-1/2 (AZD6244, PD98059 and U0126) showed significant effects on both cell lines, HCT116 and HT29, although there were clear differences among molecules and cells as delineated below.

The principle indicator of proliferation was the total DNA assay, and was supported by the MTT assay, which measures metabolic activity and is validated later in this chapter (see Response to ET-1).

The approximate range of concentrations for each drug was obtained from the literature and previous studies from the group (Troiani et al. 2012; Davies et al. 2007; Dokladda et al. 2005; Yamaguchi et al. 2002; Tentler et al. 2010; Little et al. 2011; Favata et al. 1998; Haque et al. 2013); according to these PD98059 should be used at much higher concentrations than U0126 or AZD6244.

3.3.2.1 PD98059

When treated with PD98059, HT29s appeared to respond more readily than HCT116s, showing more proliferation inhibition especially at high concentrations of the drug. Cell proliferation was determined by measuring the total amount of DNA present in the sample culture and supported by a measurement of metabolic activity determined via MTT. The two assays showed similar trends to each other.

HCT116 cells showed a drop in proliferation of less than 30% which appeared constant over 10-50 μ M, followed by a further response to treatment at 100 μ M resulting in a final proliferation inhibition of 45% and metabolic activity inhibition of 29%, which reached significance of $p < 0.05$ and $p < 0.01$, respectively (Figure 3.3). HT29 cells showed a constant reduction in proliferation and metabolic activity with increasing concentrations of this inhibitor (Figure 3.4), reaching a 50% proliferation inhibition and a 75% metabolic activity inhibition at the maximum tested dose of 100 μ M.

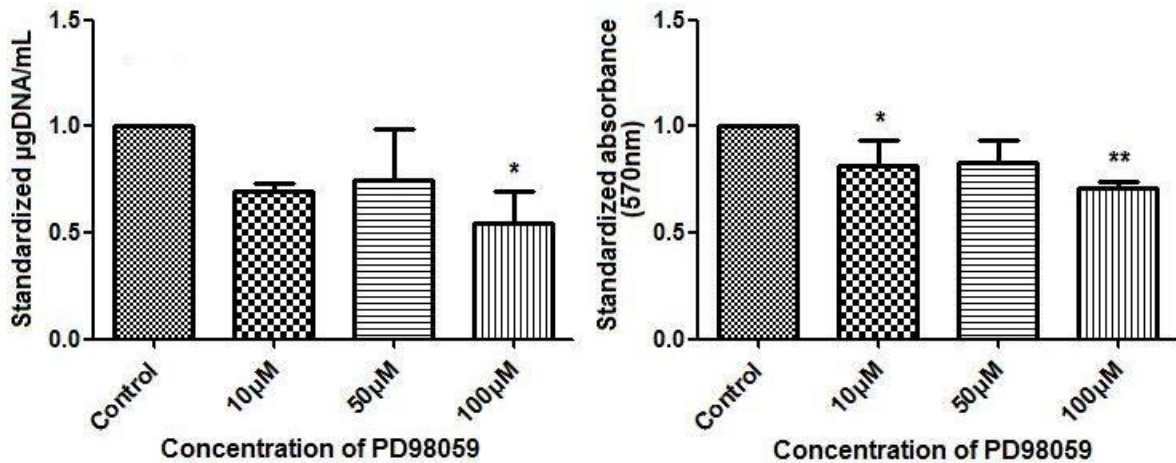


Figure 3.3 Effect of the MEK inhibitor PD98059 on HCT116 cells. Cells were treated with different concentrations of the drug for 48 h before total DNA assay (left) and MTT assay (right) were performed. Significance (compared to control): * $p < 0.05$, ** $p < 0.01$.

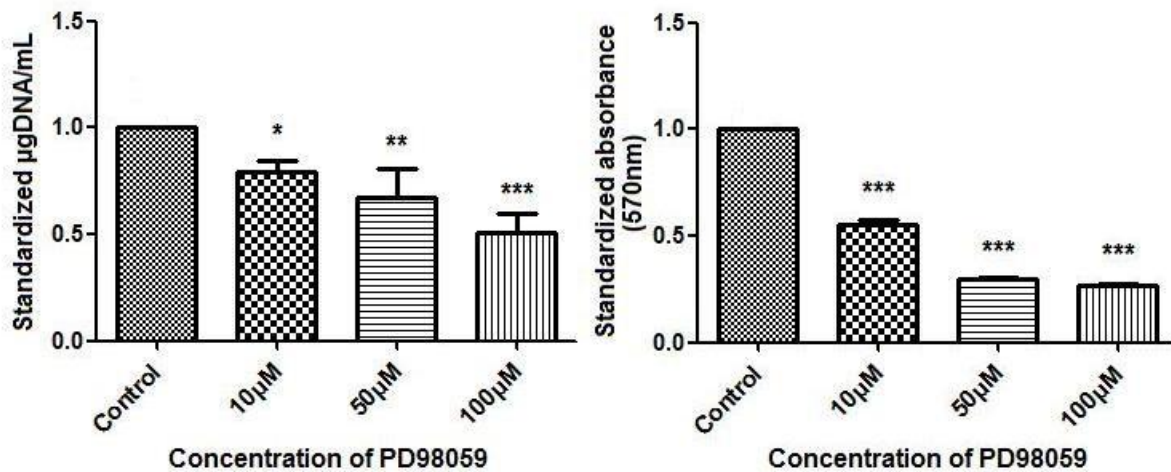


Figure 3.4 Effect of the MEK inhibitor PD98059 on HT29 cells. Cells were treated with different concentrations of the drug for 48 h before total DNA assay (left) and MTT assay (right) were performed. Significance (compared to control): * $p < 0.05$, ** $p < 0.01$, *** $p < 0.001$.

In order to further explore the apparent plateau of response (from 10-50 µM) in HCT116 cells and the more significant and stepwise inhibition in HT29 cells, these experiments were repeated including an extra step: 10ng/mL of EGF was added 10 min after the inhibitor, in order to activate the MAPK pathway and see differences which may be driven by the different mutation profiles of these cell lines.

Results were exciting. PD98059 changed the response profile of HCT116 cells, resulting in a more step-wise response and an overall greater response, with 50% proliferation inhibition (total DNA) and 27% metabolic activity inhibition (MTT) at the greatest concentration tested, 100 μ M ($p < 0.01$ and $p < 0.001$, respectively, Figure 3.5). For HT29 cells, the inhibition of proliferation that resulted from treatment with PD98059 (Figure 3.4) was abolished in the presence of EGF. Furthermore, the overall effect of PD98059 and EGF on these cells was one of significant proliferation increase (2-fold, $p < 0.05$). Surprisingly, only a small reduction in metabolic activity of 7% was observed at the highest PD98059 concentration ($p < 0.05$, Figure 3.6)

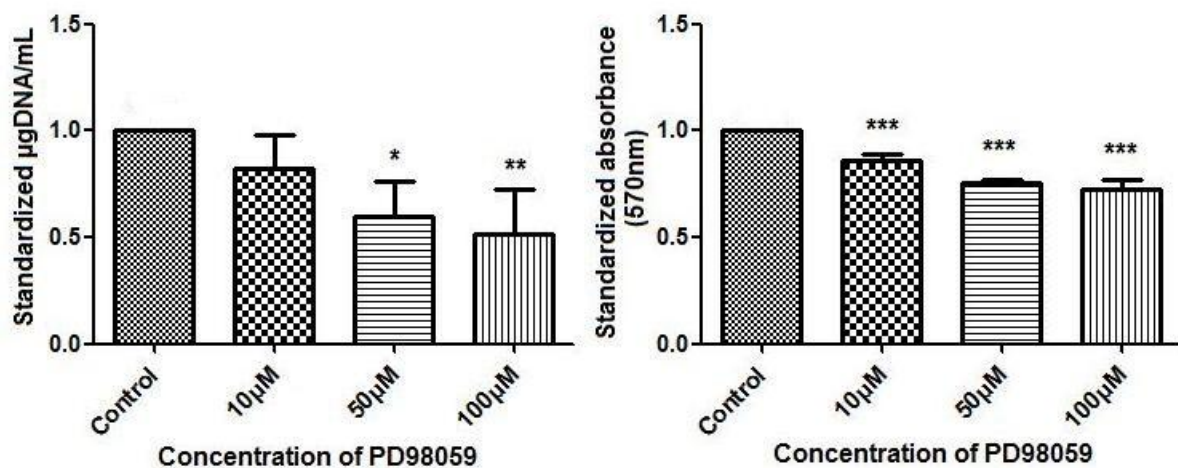


Figure 3.5 Effect of the MEK inhibitor PD98059 in the presence of EGF on HCT116 cells. Cells were treated with different concentrations of the drug for 1 hour. Following this, 10ng/mL of EGF was added to all treatment groups including the control in order to activate the MAPK pathway. 48 h after the treatment total DNA assay (left) and MTT assay (right) were performed. Significance (compared to control): * $p < 0.05$, ** $p < 0.01$, *** $p < 0.001$.

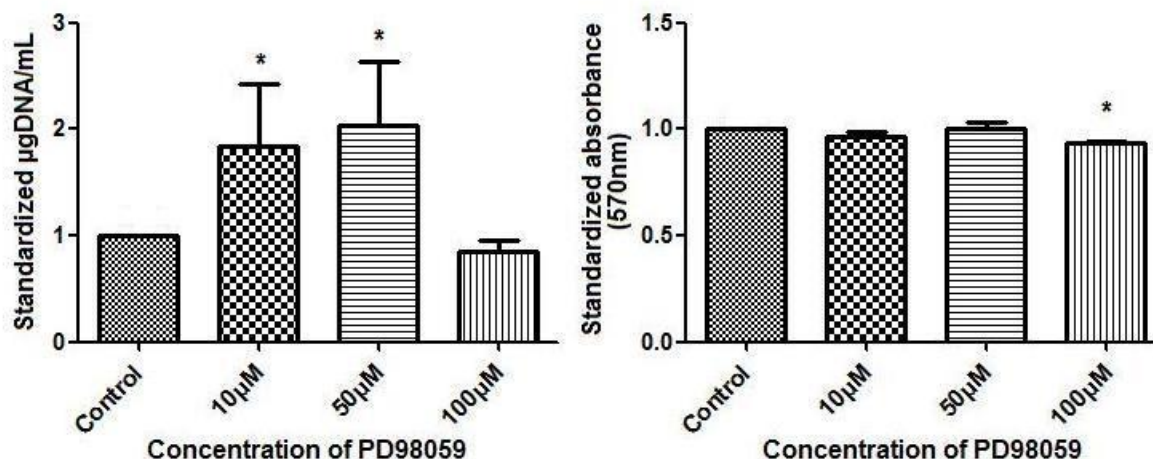


Figure 3.6 Effect of the MEK inhibitor PD98059 in the presence of EGF on HT29 cells. Cells were treated with different concentrations of the drug for 1 hour. Following this, 10ng/mL of EGF were added to all treatment groups including the control in order to activate the MAPK pathway. 48 h after the treatment total DNA assay (left) and MTT assay (right) were performed. Significance (compared to control): * $p < 0.05$.

3.3.2.2 U0126

Similar to PD98059, U0126 treatment resulted in generally inhibitory responses when tested in HCT116 and HT29 colorectal cancer cells, with a major exception.

In the case of HCT116 cells, proliferation inhibition (total DNA) appeared dose dependent with a maximum response of 29% at the highest concentration of 1 μM ($p < 0.001$), while the effect on metabolic activity (MTT) was slightly uneven (specifically for 100nM) reaching its maximum inhibition of 35% also at the highest concentration ($p < 0.001$, Figure 3.7). However, the response of HT29 cells to this drug was totally different: the effect on proliferation was a typical case of paradoxical activation, often reported with anti-cancer drugs (Wang et al. 2008). Over all concentrations tested, proliferation as measured by total DNA, increased almost reaching a two-fold enhancement at the highest point (100nM, $p < 0.001$), while metabolic activity remained unchanged apart from a significant drop at the highest concentration of 1 μM ($p < 0.001$, Figure 3.8).

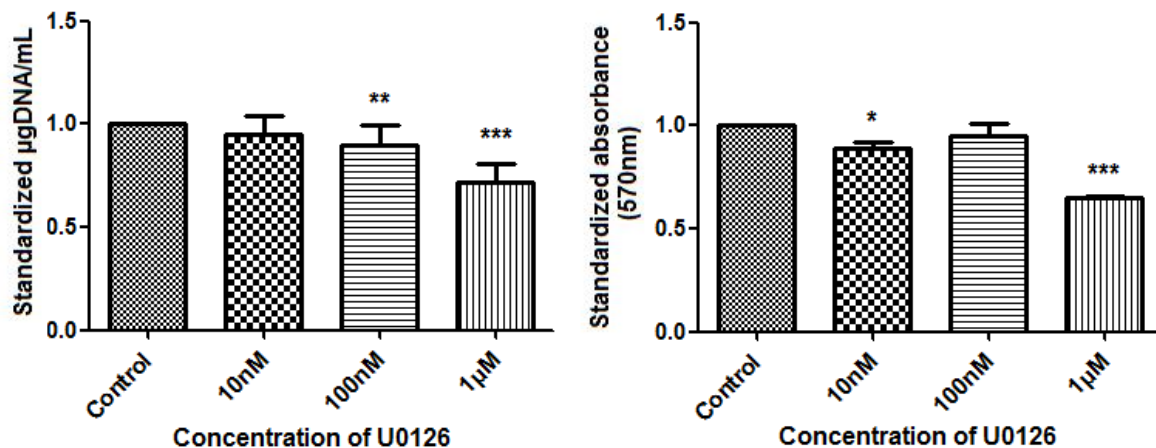


Figure 3.7 Effect of the MEK inhibitor U0126 on HCT116 cells. Cells were treated with different concentrations of the drug for 48 h before total DNA assay (left) and MTT assay (right) were performed. Significance (compared to control): * $p < 0.05$, ** $p < 0.01$, *** $p < 0.001$.

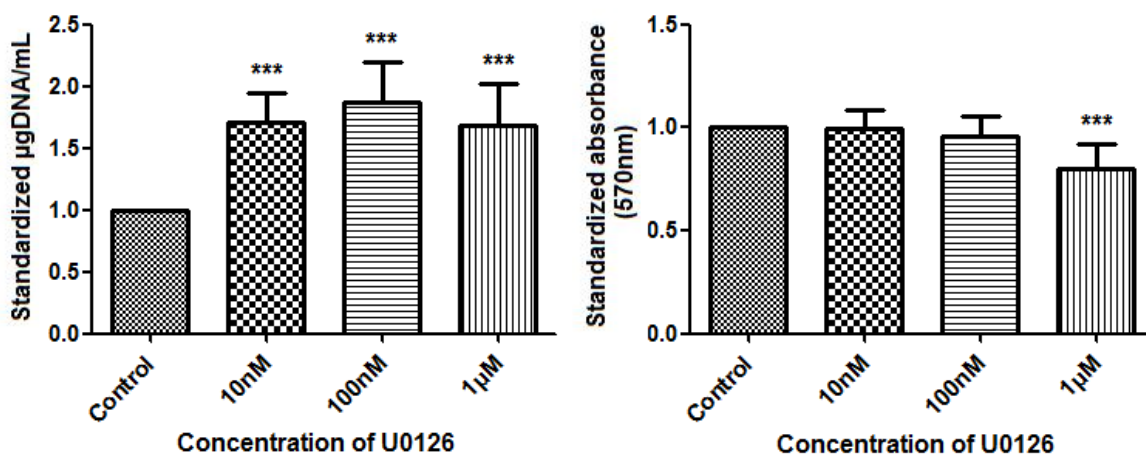


Figure 3.8 Effect of the MEK inhibitor U0126 on HT29 cells. Cells were treated with different concentrations of the drug for 48 h before total DNA assay (left) and MTT assay (right) were performed. Significance (compared to control): *** $p < 0.001$.

As for PD98059, experiments were repeated in the presence of exogenous EGF. HCT116 responded to this treatment in a similar way to the treatment with U0126 alone, with a 33% proliferation inhibition (total DNA, $p < 0.001$) and 14% metabolic activity inhibition (MTT, $p < 0.05$) at the maximum concentration of U0126 (1 μM). The reduction in proliferation was slightly less pronounced at 100 nM, although still significant ($p < 0.01$) (Figure 3.9). The addition of EGF to the treatment significantly changed cell response for HT29 cells: the proliferation enhancement observed with

the drug alone was abolished. Furthermore, the combination of U0126 and EGF had no overall effect on the cells with no statistically significant changes observed either in proliferation (total DNA) or metabolic activity (MTT) (Figure 3.10). This could be due to a positive feedback on alternative pathways caused by the inhibitor that is counteracted by the external activation of the pathway.

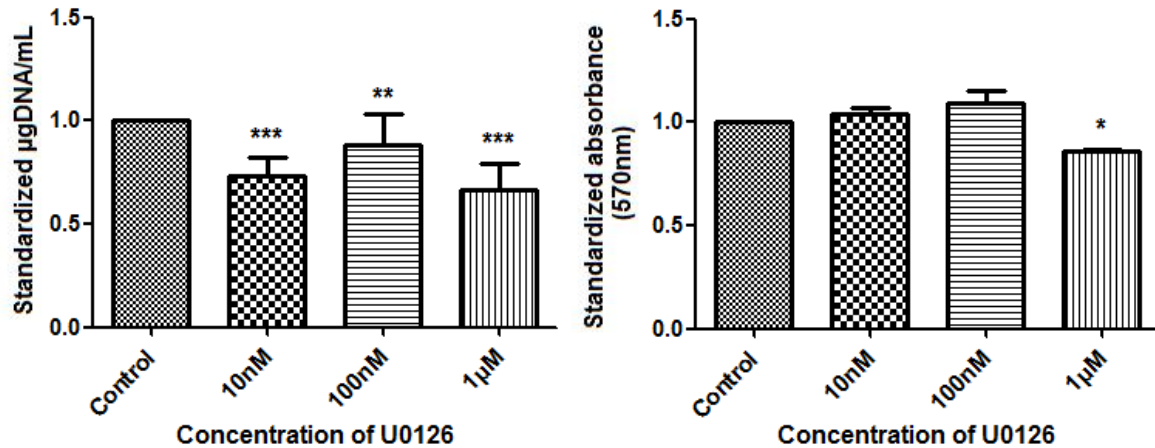


Figure 3.9 Effect of the MEK inhibitor U0126 in the presence of EGF on HCT116 cells. Cells were treated with different concentrations of the drug for 1 hour. Following this, 10ng/mL of EGF were added to all treatment groups including control in order to activate the MAPK pathway. 48 h after the treatment total DNA assay (left) and MTT assay (right) were performed. Significance (compared to control): * $p < 0.05$, ** $p < 0.01$, *** $p < 0.001$.

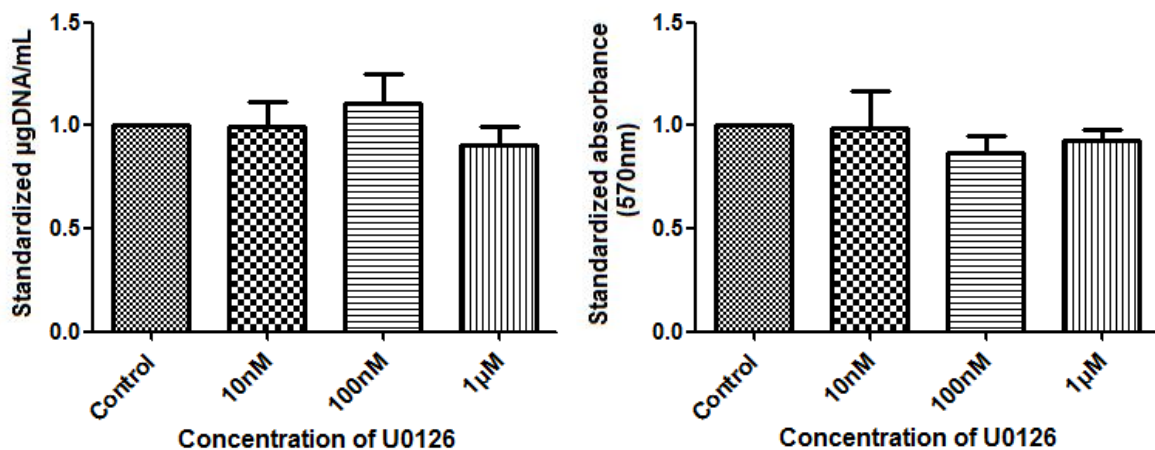


Figure 3.10 Effect of the MEK inhibitor U0126 in the presence of EGF on HT29 cells. Cells were treated with different concentrations of the drug for 1 hour. Following this, 10ng/mL of EGF were added to all treatment groups including control in order to activate the MAPK pathway. 48 h after the treatment total DNA assay (left) and MTT assay (right) were performed. No result was statistically significant.

Western blot assay was performed in order to confirm that the paradoxical increase in HT29 proliferation caused by U0126 in the absence of EGF corresponded with activation of the MAPK pathway (Figure 3.11). Since the function of MEK is adding a phosphate group to the ERK protein, its downstream target in the MAP kinase pathway, by detecting the amount of phosphorylated ERK (pERK, its activated form) we would get a direct indication of the activity (or inhibition of activity) of MEK. The levels of pERK in HT29 cells treated with U0126 correlated to the increase in proliferation.

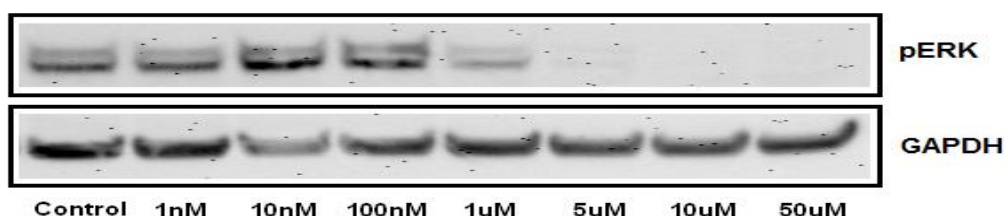


Figure 3.11 Effect of the MEK inhibitor U0126 on expression of phosphorylated ERK, in HT29 cells. Cells were treated with increasing concentrations of U0126 for 60 min and then the pathway was activated with EGF at 10ng/mL for 10 min. Western blot shows that protein levels of pERK, the protein activated downstream of MEK, are reduced with increasing concentrations of U0126, suggesting that the activity of MEK has been impaired. Control: no U0126 treatment. Top row: phosphorylated ERK. Bottom row: GAPDH (housekeeping gene).

3.3.2.3 AZD6244

This inhibitor was specifically designed for cancers bearing mutations in RAS and RAF, present in cell lines HCT116 and HT29, respectively. For experiments with AZD6244, a wider range of concentrations is shown here, since it was chosen among the MEK inhibitors as the most suitable therapeutic molecule.

Treatment with AZD6244 resulted generally in inhibition of proliferation in both cell lines used. Results were quite similar for HT29 and HCT116, with an inhibitory effect becoming evident at 100nM and higher doses, and responses appeared stepwise. In HCT116 cells, AZD6244 inhibited proliferation (total DNA) 22% at 1 μ M and 43% at 10 μ M ($p < 0.001$), and metabolic activity (MTT) 18% at 1 μ M and 32% at 10 μ M

($p < 0.001$, Figure 3.12). In HT29 cells, AZD6244 inhibited proliferation 26% at 1 μM and 48% at 10 μM ($p < 0.001$), and metabolic activity 14% at 1 μM ($p < 0.01$) and 24% at 10 μM ($p < 0.001$) (Figure 3.13). Overall, results from AZD6244 treatments are more similar to PD98059 than U0126.

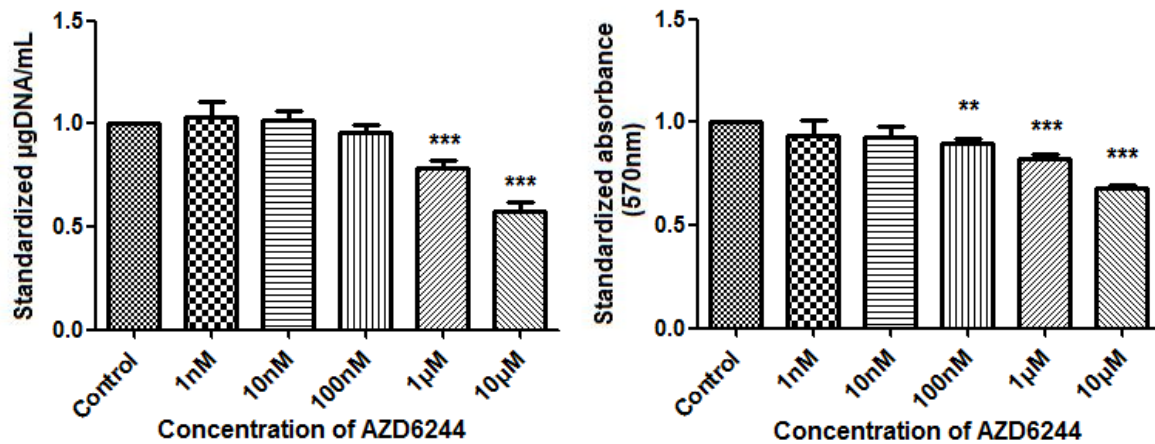


Figure 3.12 Effect of the MEK inhibitor AZD6244 on HCT116 cells. Cells were treated with different concentrations of the drug for 48 h before total DNA assay (left) and MTT assay (right) were performed. Significance: ** $p < 0.01$, *** $p < 0.001$.

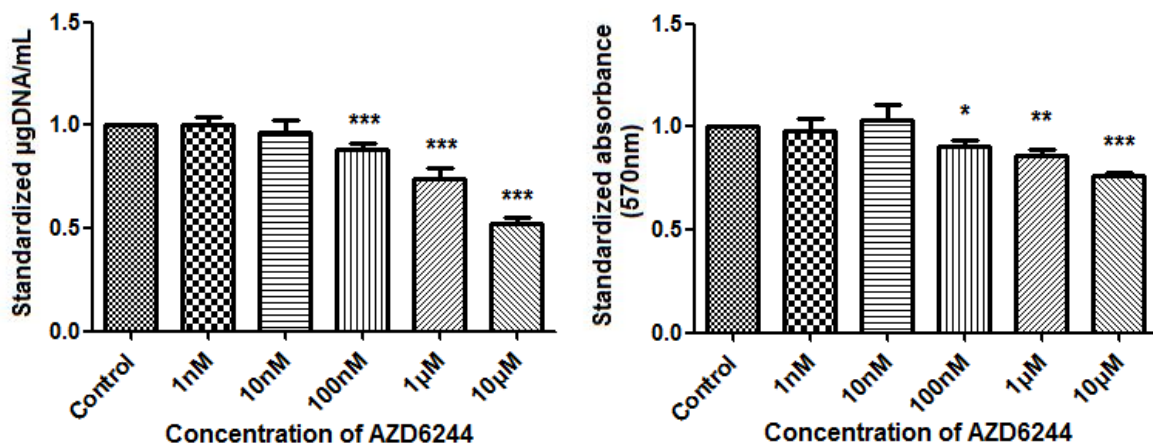


Figure 3.13 Effect of the MEK inhibitor AZD6244 on HT29 cells. Cells were treated with different concentrations of the drug for 48 h before total DNA assay (left) and MTT assay (right) were performed. Significance: * $p < 0.05$, ** $p < 0.01$, *** $p < 0.001$.

The reduction in pERK protein levels presented below following treatment with AZD6244 mimics the inhibition of proliferation and metabolic activity observed in both cell lines, resulting in apparent total abolition of protein at the highest AZD6244 concentration (10 μ M). This suggests that proliferation inhibition happens through the impairment of MEK kinase activity on ERK, caused by the inhibitor (Figure 3.14).

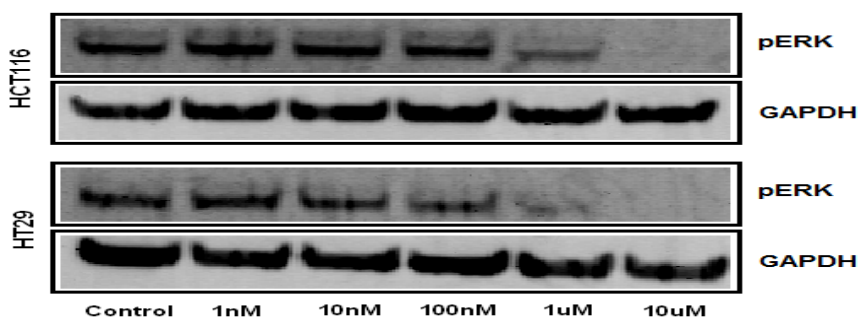


Figure 3.14 Western blot of phosphorylated ERK, activated downstream protein of MEK, after treatment with AZD6244. The levels of pERK are reduced with increasing concentrations of AZD6244, suggesting that the activity of MEK has been impaired. HCT116 cells were seeded at 200000cells/well and HT29 cells at 250000cells/well, after 24 h serum was withdrawn for another 24 h, cells were treated with increasing concentrations of AZD6244 for 60 min and then the pathway was activated with EGF at 10ng/mL for 10 min. Cells were lysed, protein was extracted, quantified and analysed by PAGE and Western Blotting.

Considering the above results for all three MEK inhibitors, AZD6244 was considered the best option for further work. In spite of AZD6244 showing the best results in metabolic activity and proliferation inhibition, the active concentrations of the drug shown here were much higher than those reported in the literature. For that reason, another experiment was designed to mimic the exact conditions and follow the same methods of one of the publications (Troiani et al. 2012) measuring AZD6244 efficacy by MTT. The most fundamental change in the protocol was not to starve the cells (not removing serum prior to the treatment). Under these conditions, HCT116 showed paradoxical activation of metabolic activity at the highest AZD6244 concentrations, 1 μ M (14% inhibition, $p < 0.05$) and 10 μ M (18% inhibition, $p < 0.01$), while HT29 only showed significant metabolic activity inhibition at 10 μ M (20%, $p < 0.001$) (Figure 3.15). These paradoxical results are consistent with the presence of growth factors in the serum that may interact with therapeutic molecules.

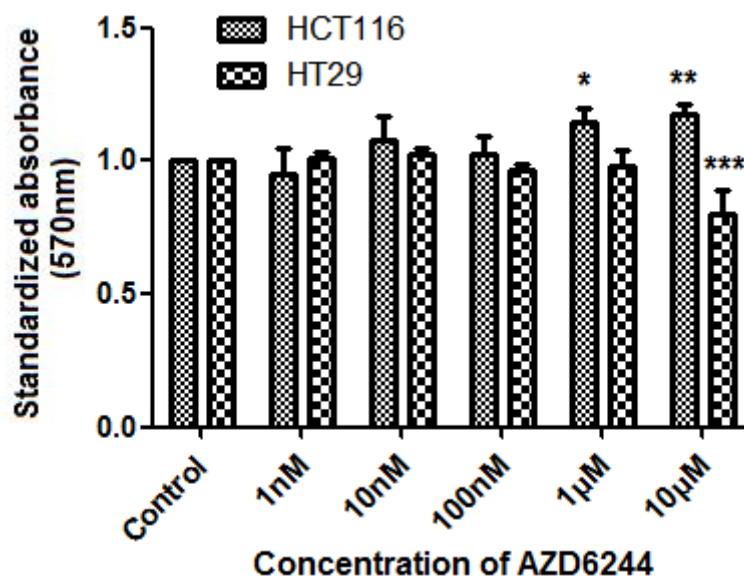


Figure 3.15 Effect of AZD6244 on metabolic activity mimicking a protocol in the literature. Cells were cultured in DMEM supplemented with 10% FBS and 1% P/S for 48h before treatment, instead of removing growth factors (present in the serum). Significance (compared to control): * $p < 0.05$, ** $p < 0.01$, *** $p < 0.001$.

Based on the results on the efficacy of the three MEK inhibitors, AZD6244 was deemed the most suitable and selected for combination treatments and nanoformulations. Also, due to the clear dose-dependent inhibitory response elicited by AZD6244 and its correlation with a reduction in target MEK1/2 activity, a comparative experiment involving EGF stimulation was not necessary in this case.

3.3.3 Treatment with ETAR competitive antagonists

3.3.3.1 Response to ET-1

The pathways of interest naturally respond to growth factors such as EGF and ET-1. While EGF is a well-known activator of the MAPK pathway (Mebratu & Tesfaigzi 2009; Gao et al. 2005) there is much less work carried out involving ET-1 (Grant et al. 2007; Haque et al. 2013). Cells responded to EGF as expected, with a maximum increase in proliferation at 10mg/mL and no differences in ERK phosphorylation between 1, 2 and 3 h of exposure to EGF (data not shown).

In the initial experiments exploring the effect of ET-1 (10nM) on HT29 and HCT116 cells, the ligand increased metabolic activity between 1.5- and 2-fold ($p < 0.01$ and $p < 0.001$ after 48- and 80-hour treatments. This experiment was carried out in 24-well plates at two different seeding cell densities (25000 and 50000 cells/well). While the lower seeding density was affected by the treatment, the higher seeding density showed no response, probably due to a plateau in cell metabolism as a result of over confluence (Figure 3.16).

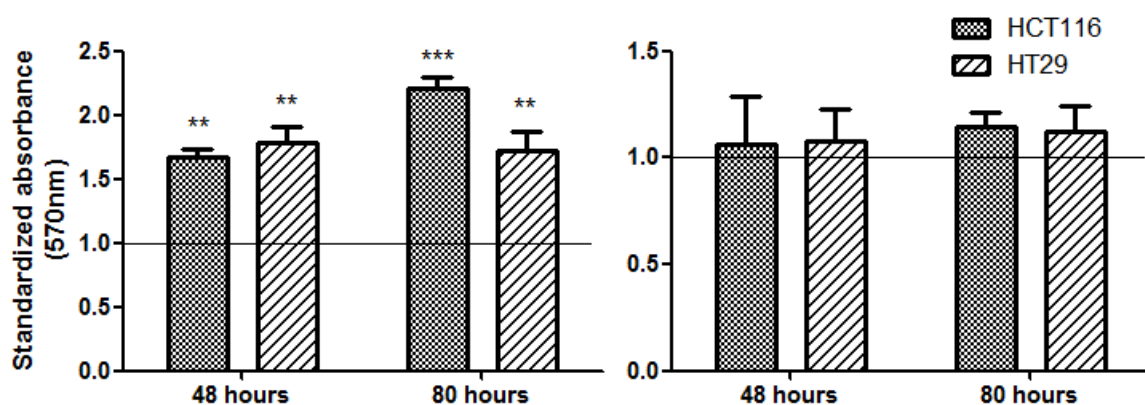


Figure 3.16 Effect of endothelin-1 (ET-1) on colorectal cancer cells (metabolic activity). 48 h after seeding 25000 cells (left) and 50000 cells (right), 10nM ET-1 was added to the medium and left for 48 h before MTT assay was performed. Control: horizontal line. Significance (compared to control): ** $p < 0.01$, *** $p < 0.001$.

Cell counting was used as an alternative proliferation measurement for ET-1 activation. Significant differences were observed between the two techniques, since for cell counting the 48-hour treatment showed no increase compared to the control in the lower seeding density, and a significant increase was observed in the highest seeding density for both time points (Figure 3.17). Generally, HCT116 cells seemed to be more responsive to the proliferative effect of ET-1 than HT29 cells.

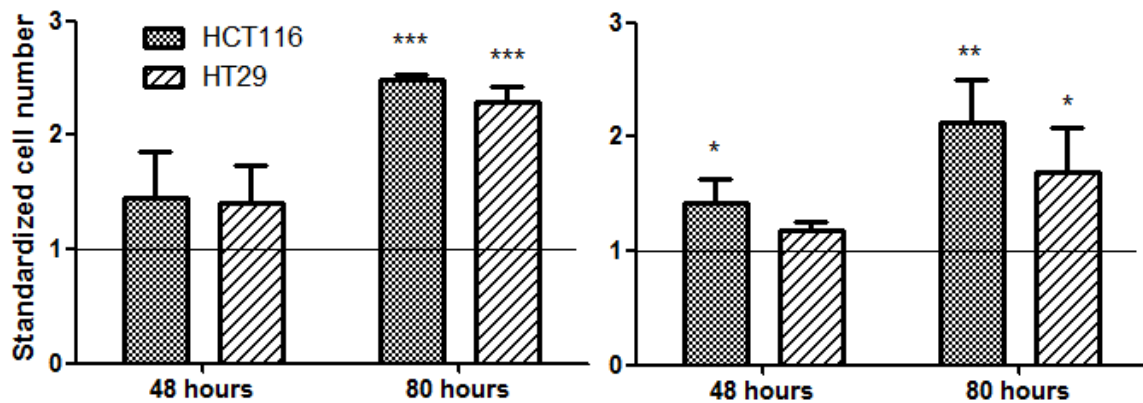


Figure 3.17 Effect of endothelin-1 (ET-1) on colorectal cancer cells (cell counting). 48 h after seeding 25000 cells (left) and 50000 cells (right), 10nM ET-1 was added to the medium and left for 48 h before cells were counted using a haemocytometer assay was performed. Control: horizontal line. Significance (compared to control): * $p < 0.05$, ** $p < 0.01$, *** $p < 0.001$.

Unfortunately shortly after demonstrating the activity of ET-1 the two new batches purchased resulted in no increase in proliferation on these cell lines. This has important consequences on the course of this research. Due to the unpredictable efficacy of ET-1 in these experiments, it was impossible to know in which treatment groups ET-1 would enhance, inhibit or not effect proliferation at all (preliminary data not shown). For that reason, experiments with ETAR antagonists were treated as a blinded study (ET-1 treated controls were not compared to untreated controls, but standardized), hoping to draw general conclusions from repetition of similar experiments.

3.3.3.2 BQ123

The ETAR-specific antagonist BQ123 is commonly used to study the endothelin pathway as the gold standard for receptor inhibition studies (Ali et al. 2000; Haque et al. 2013). Figure 3.18 shows the results of MTT assay after 48 h of BQ123 treatment with or without the addition of ET-1. The inhibitor on its own elicited no change in proliferation in either HCT116 or HT29, while the addition of ET-1 promoted proliferation at 100 nM and 1 μ M (10% and 9%, $p < 0.01$) in HT29 cells.

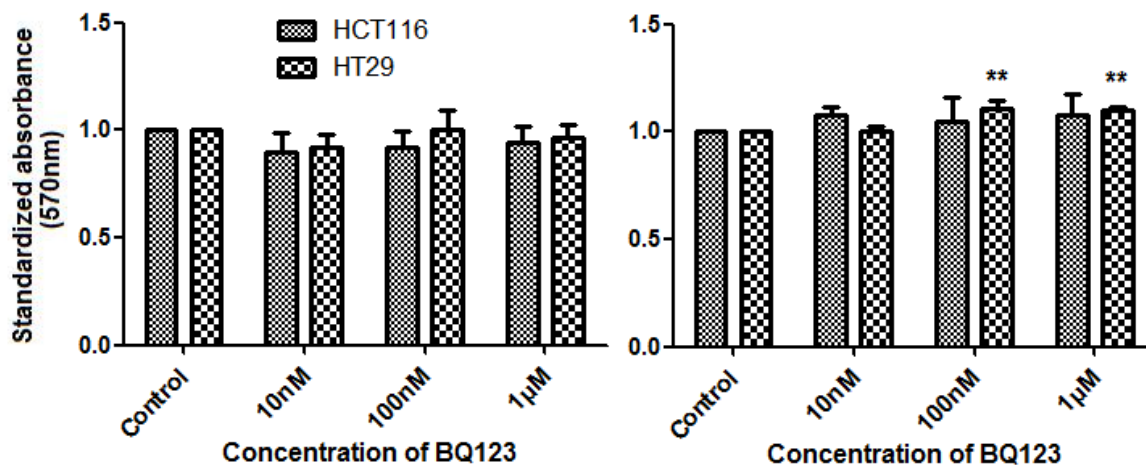


Figure 3.18 Effect of the ETAR-specific antagonist BQ123 on colorectal cancer cells. Cells were treated with different concentrations of the drug (followed by ET-1) for 48 h before MTT assay was performed. On the left, cells were only treated with the drug, on the right, all treatment groups including the control are in the presence of 10nM ET-1. Significance (compared to control): ** $p < 0.01$.

3.3.3.3 ZD4054

Similar to BQ123, previous work (Haque et al. 2013) demonstrated the anti-proliferative and pro-apoptotic effect of ZD4054 in the presence of ET-1. For experiments performed during the present research, as explained above ET-1 did not cause a consistent proliferative effect, and therefore the inhibition caused by the competitive binding of the antagonist could not be measured optimally. To compound the problem, different batches of ZD4054 also produced inconsistent effects on cells. However, overall patterns of inhibition were observed for both cell lines used, as described below.

Treatment with ZD4054 on its own led to significant inhibition of HCT116 cell proliferation (total DNA) with increasing drug concentrations (37% inhibition at the highest concentration (1 µM), $p < 0.001$) (Figure 3.19), while HT29 cells remained unresponsive (Figure 3.20). Metabolic activity responses were more modest (less sensitive) with only the highest concentration of the antagonist (1 µM) eliciting an inhibitory response in both cell lines (19% for HCT116 and 28% for HT29, $p < 0.001$).

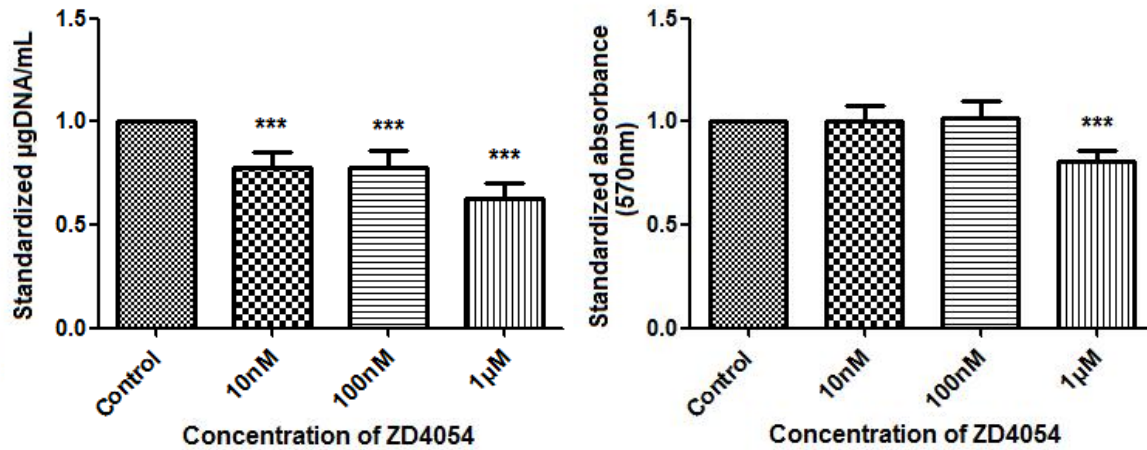


Figure 3.19 Effect of the ETAR-specific antagonist ZD4054 on HCT116 cells. Cells were treated with different concentrations of the drug for 48 h before DNA assay (left) and MTT assay (right) were performed. Significance (compared to control): *** $p < 0.001$.

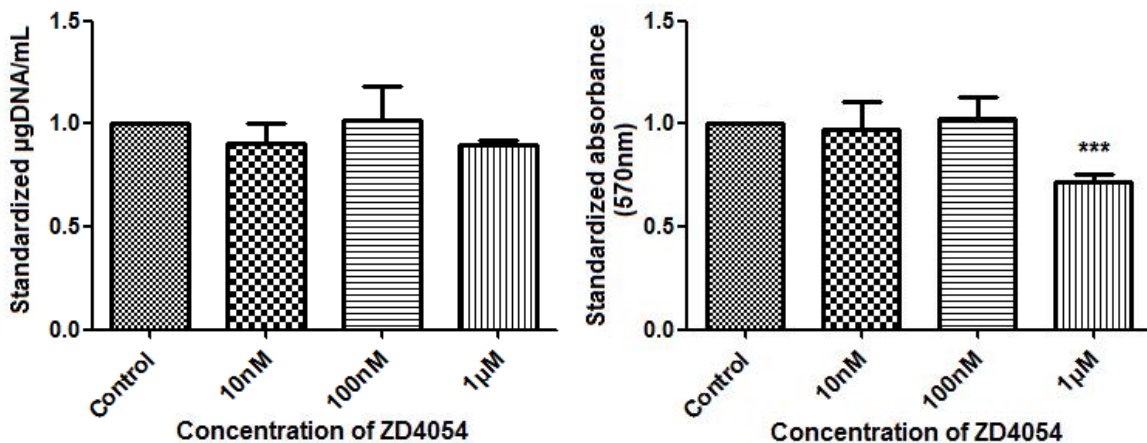


Figure 3.20 Effect of the ETAR-specific antagonist ZD4054 on HT29 cells. Cells were treated with different concentrations of the drug for 48 h before DNA assay (left) and MTT assay (right) were performed. Significance (compared to control): *** $p < 0.001$.

The addition of ET-1 to the treatment resulted in confusing results, with total DNA and MTT responses often disconnected. For example proliferation inhibition (total DNA) in HCT116 cells caused by ZD4054 is attenuated in the presence of ET-1 (Figure 3.21). A similar effect was observed for metabolic activity on HT29 cells, where ET-1 seems to enhance proliferation in the presence of 10nM (16%, $p < 0.001$) and 100nM (21%, $p < 0.001$) of ZD4054. Contrarily, on HT29 cells, ZD4054 is much more effective in the presence of ET-1 at the proliferation level (26% at 1 µM,

p<0.001) (Figure 3.22). In HCT116, metabolic activity remains unchanged in the presence or absence of ET-1, compared to ZD4054 alone.

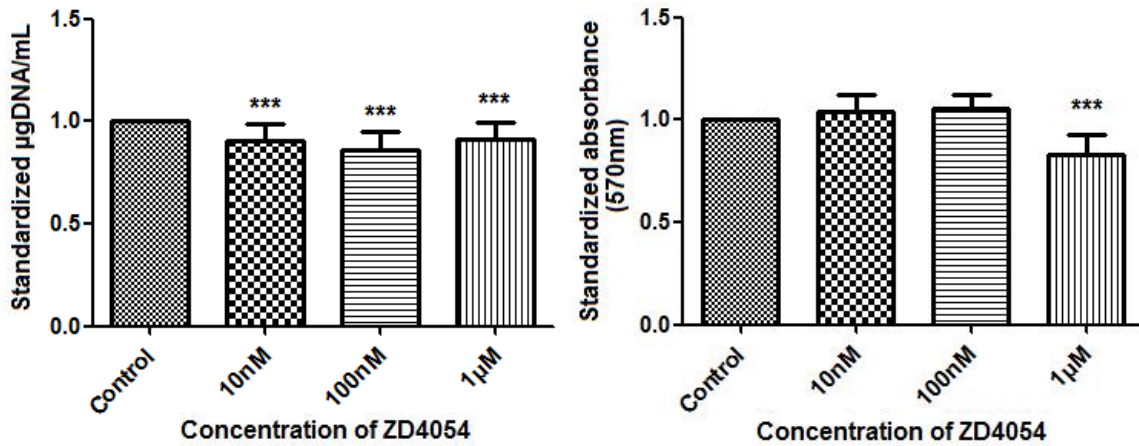


Figure 3.21 Effect of the ETAR-specific antagonist ZD4054 in the presence of ET-1 on HCT116 cells. Cells were treated with different concentrations of the drug. All treatment groups including the control are in presence of ET-1 at 10nM. 48 h after the treatment total DNA assay (left) and MTT assay (right) were performed. Significance (compared to control): ***p<0.001.

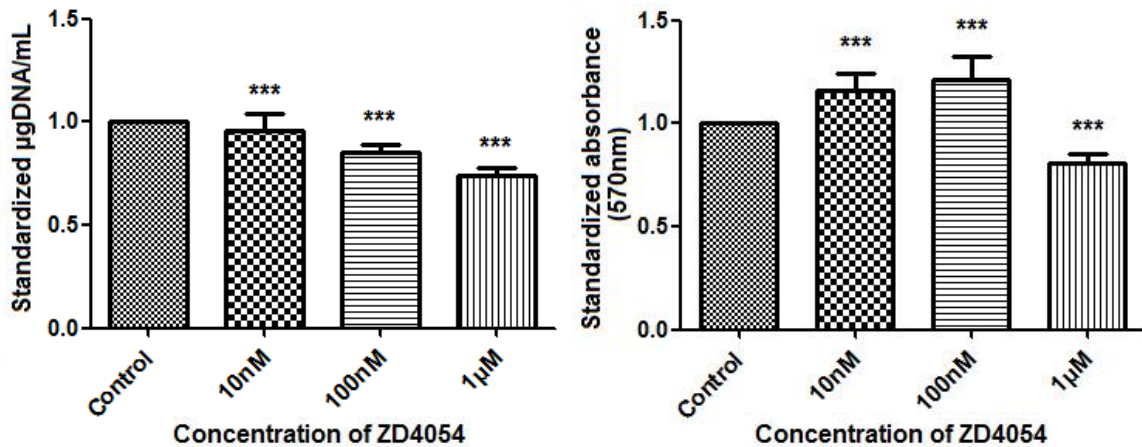


Figure 3.22 Effect of the ETAR-specific antagonist ZD4054 in the presence of ET-1 on HT29 cells. Cells were treated with different concentrations of the drug. All treatment groups including the control are in presence of ET-1 at 10nM. 48 h after the treatment total DNA assay (left) and MTT assay (right) were performed. Significance (compared to control): ***p<0.001.

In spite of partial positive conclusions that were drawn from these results and are further developed in the discussion, the effect of ET-1, BQ123 and ZD4054 is far from optimal (Figure 3.23). Figure 3.23 shows some results with a defective batch of ET-1 and two potentially defective batches of ZD4054 as proof of the many inexplicable effects these molecules caused on cells. Due to these inconsistencies, alternative treatments were explored and are described in the next chapter.

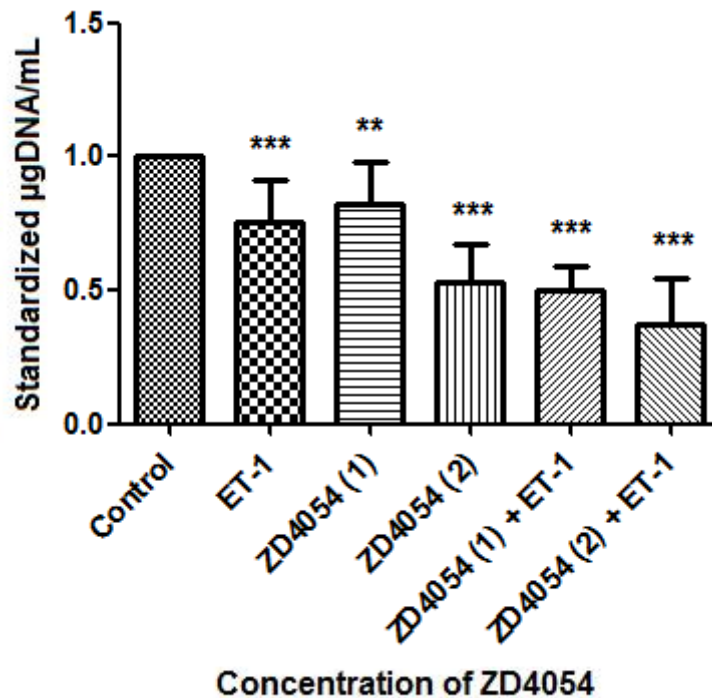


Figure 3.23 Example of the inconsistent effect on proliferation elicited by potentially defective ET-1 and ZD4054 batches. HCT116 where treated with an ineffective batch of ET-1 and two different batches of ZD4054. Total DNA assay was performed after 48 h treatment. The control group is untreated. Significance (compared to control): ** $p < 0.01$, *** $p < 0.001$.

3.4 Discussion

3.4.1 Inhibitors of the MAPK pathway

There is considerable evidence that MEK inhibition is a promising approach as a cancer treatment, particularly directed against KRAS and BRAF mutant cells, at *in vitro*, *in vivo*, and clinical levels (Yeh et al. 2009; Chapman & Miner 2011). BRAF mutants however, tend to respond better to this type of therapy (Solit et al. 2006; Engelman et al. 2008).

A number of studies have recently suggested that different mutations in the upstream molecules of the MAPK pathway lead to different mechanisms of activation of MEK1/2 (Blasco et al. 2011; Davies et al. 2002; Hatzivassiliou et al. 2013). The two most common mutations in CRC relevant to this pathway are K-RAS and B-RAF. Their different effects on MEK1/2 over-activation should be considered, since they greatly influence the efficacy of MEK inhibitors (Gilmartin et al. 2011; Hoeflich et al. 2012; Friday et al. 2008).

Here, the different mutational status regarding RAS and RAF is the core reference point for the discussion that follows.

3.4.2 PD98059 and U0126

Both the MEK inhibitors U0126 and PD98059 have been used experimentally for many years to investigate the MAPK pathway, not only in cancer but within normal physiological systems and other pathological conditions (Cuenda & Alessi 2000; Alessi et al. 1995; Davies et al. 2000).

It is worth noting that some of the MEK inhibitors are often considered MEK-1-specific as opposed to MEK-1/2-specific, with controversial reports on this matter (Davies et al. 2000). Although the three inhibitors used for the current body of work have slightly different reported affinities for these two molecules (MEKs), for this

discussion, all three MEK inhibitors are considered as MEK-1/2-specific, in line with most reported evidence (Favata et al. 1998; Dudley et al. 1995).

3.4.2.1 PD98059 and U0126 in a K-RAS mutated cell line (HCT116)

K-ras mutations are activating mutations that result in a potentiated signal with a number of growth and motility promoting cellular events. Importantly a substantial percentage of patients with colorectal cancer have such mutations (reports range from 25% to 50%, depending on studies and reported disease progression).

Hatzivassiliou and colleagues suggested that MEK inhibitors that achieved higher efficacy on K-RAS mutated colorectal cancer cell lines (such as GDC-0623 and G-573) did so by creating a strong hydrogen-bond with a Serine residue (S212) in the MEK molecule (Hatzivassiliou et al. 2013). This resulted in blocking this region of the protein which in turn prevented wild type BRAF from phosphorylating MEK as a feedback response to MAPK pathway inhibition, a well-known phenomenon in KRAS mutant cells (Friday et al. 2008; Pratilas et al. 2009). Being KRAS activation majorly mediated by wild type BRAF-CRAF heterodimers (Downward 2003), both GDC-0623 and G-573 inhibited this signalling by forming stable BRAF-MEK complexes and therefore, preventing BRAF-CRAF interaction.

Conversely, the phase III clinical trial MEK inhibitor cobimetinib, which acts by impairing the kinase activity of the already phosphorylated MEK, showed a much lower efficacy in KRAS than in BRAF mutated cell lines. These findings were transferred to *in vivo* studies in three xenografts of mutant K-RAS, in which inhibition by cobimetinib resulted in accumulation of phosphorylated MEK and a superior activation of ERK compared to the other two inhibitors. Following these results, other MEK inhibitors that prevent BRAF feedback phosphorylation of MEK (Gilmartin et al. 2011; Alessi et al. 1995) could also show more efficacy in KRAS mutant cell lines.

The MEK-1/2 specific non-ATP-competitive inhibitor PD98059 has been shown to inhibit growth and proliferation in colorectal cancer cells very effectively (Lu et al. 2007; Fang & Richardson 2005).

HCT116 cells, used in this study, bear the p.G13D mutation in KRAS and the p.H1047R mutation in PI3K (Troiani et al. 2012). Opposite to what was previously thought, the specific type of KRAS mutation present in HCT116 (codon 13) has recently been identified as a biomarker for poor outcome both in metastatic and non-metastatic colorectal cancer (Salerno et al. 2002; Yoon et al. 2014).

After EGF addition, in terms of proliferation measurements (total DNA) HCT116 cells showed a dose-dependent inhibitory curve similar to that of HT29 cells when treated only with PD98059, reaching 50% at the highest concentration used (100 μ M). This was different to the response of HCT116 cells to PD98059 alone, where the response appeared to plateau at the middle range of drug concentrations (10-50 μ M) and then reached 45% maximum inhibition at 100 μ M. This suggests the slowing down of response was partially due to pathways alternative to MAPK, activated by the mutated KRAS. This possibility has been previously suggested (Church et al. 2012). With EGF further fostering proliferation through the MAPK pathway, the inhibitory effect of PD98059 might have been more noticeable. However, this hypothesis is speculative.

U0126 is also a very specific non-ATP-competitive MEK inhibitor. Its progression to the clinic has been hampered by pharmacological limitations, but it is widely used *in vitro* to study the MAPK pathway (Sebolt-Leopold et al. 1999).

Although HCT116 cells responded to U0126 in a dose dependent manner the measurements of inhibition and the reduction resulting from each dose, in terms of total DNA and metabolic activity did not correspond step by step. For example, responses were step-wise reduction as measured by total DNA, but appeared to plateau by MTT. The converse was true when EGF was added to the system, where both proliferation and metabolic activity plateaued. This is indicative of the inherent limitations of assays (e.g. what do they measure exactly, what are the sensitivity limits, are the measurements subject to a lag effect), which is often not taken into account when reporting effects of drugs. A large number of studies depend only on metabolic assays, such as MTT to report drug efficacy, which is insufficient. Furthermore, for these cells, the addition of EGF resulted in less metabolic activity inhibition. Maximum inhibition values at the highest concentration were 35%

($p < 0.001$) for U0126 alone and 14% ($p < 0.05$) in the presence of EGF (Figure 3.7 and Figure 3.9).

The results are consistent with reports that KRAS signalling occurs through alternative pathways as well as the MAPK pathway, and this signalling could have been activated through EGFR via ligand binding. One example of these alternative pathways is the activation of the PI3K/AKT pathway by KRAS (Downward 2003), which is also mutated in this cell line. This abundance of alternative paths, which can be controlled or activated by proteins in the MAPK pathway seems logical, since the MAPK pathway is one of the pillar signalling systems that mediate proliferation and growth. Such redundancy in the system makes complete inhibition almost impossible and could be related to the common problems that EGFR inhibition platforms face with KRAS mutant tumours (Magdeldin et al. 2014); or perhaps off-target effects such as ERK-5 inhibition could play a role (Shields et al. 2000). In fact, the MAPK pathway is generally regarded as a non-linear pathway, with numerous regulatory proteins involved (Chang & Karin 2001; Dhanasekaran et al. 2007).

U0126 and PD98059 inhibit MEK activity in a similar manner, through impairment of its kinase activity and not by preventing its activation (Dudley et al. 1995; Favata et al. 1998). According to Hatzivassiliou et al., these inhibitors should be ineffective against KRAS mutant cells, or at least less effective than against BRAF mutant cells (Hatzivassiliou et al. 2013). With the exception of U0126-induced paradoxical activation in HT29 cells, discussed below, the present data is consistent with this hypothesis. Firstly, BRAF mutant HT29 cells are more sensitive to PD98059 than KRAS mutant HCT116 cells (dose dependent strong response vs. plateau at 100nM, Figure 3.3 and Figure 3.4). Secondly, HCT116 were much less sensitive to U0126 (~30% inhibition at 1 μ M) than to PD98059 (~50% inhibition at 1 μ M), despite U0126 having a much higher specificity and affinity for both MEK-1 and MEK-2 (IC₅₀ of 72nM and 58nM respectively for U0126, compared to IC₅₀ values of 10 μ M for both in the case of PD98059) (Favata et al. 1998; Dudley et al. 1995). Furthermore, the protein levels of MEK-2 protein were much higher than MEK-1 protein in both cell lines (data not shown), suggesting that the higher affinity of U0126 to MEK-2 would contribute to superior efficacy. However, this was not demonstrated for HCT116 cells, which are less sensitive to U0126 instead. This tendency to equalize the

efficacy of PD98059 and U0126 suggests a lower efficacy of these inhibitors in KRAS mutants and supports Hatzivassiliou's hypothesis.

There are several possible explanations for this KRAS-mutant-mediated resistance to MEK inhibition. For example, MEK-independent BRAF signalling, BRAF-independent MEK signalling and RAF-independent RAS signalling have all been suggested (Bromberg-white et al. 2012; Lim et al. 2005; Yip-Schneider et al. 1999), and the idea that alternative KRAS-activated effector pathways contribute to this resistance has been indicated in a variety of studies, including in HT29 and HCT116 cell lines (Little et al. 2011)

Signalling through the PI3K/Akt/mTOR system is commonly upregulated in cancer. In a natural state, mTOR is activated in response to nutrient availability and is positively regulated by the core survival pathway PI3K/Akt (Hay & Sonenberg 2004; Bjornsti & Houghton 2004). There is evidence of this pathway being activated as a result of MEK inhibition, by inhibiting the feedback loop that attenuates phosphorylation of Akt, and hence conferring resistance to MEK inhibition (Faber et al. 2009; Turke et al. 2012; Hoeflich et al. 2009; Mirzoeva et al. 2009; Yoon et al. 2009), there is also evidence of opposite regulation, i.e. inhibition of the PI3K/Akt/Mtor pathway activates the MAPK pathway, or even Akt survival signalling (Wang et al. 2008; Ebi et al. 2013; Carracedo et al. 2008; Serra et al. 2011). Combinations of inhibitors targeted at these two pathways are currently being explored (Tentori et al. 2013; Shimizu et al. 2012; Wang et al. 2008), including in HT29 and HCT116 cell models (Zhang et al. 2009).

Another pathway that might be involved in the resistance to MEK inhibitors is the Wnt pathway. In the case of CRC, mutations in the APC protein are especially abundant and can constitute the first tumorigenic step. A recent study analysed 224 CRC samples and found over 90% of them had a mutation in the Wnt pathway (Cancer & Atlas 2012). Generally though, alternative resistance suggested include over-activation, up-regulation or over-expression of surface receptors, and other RAS or RAF subtypes (Villanueva et al. 2011; Nazarian et al. 2010; Montagut et al. 2008).

Other proteins involved in MEK inhibitor resistance are less studied, or exhibit contradictory results. A recent study by Mazur et al. discovered that the kinase

MAP3K2 is methylated by the methyltransferase SMYD3, causing the former to dissociate from its negative regulator and activate the MAPK pathway in KRAS-mutant cancers (Mazur et al. 2014). DUSP4, a phosphatase known to dephosphorylate ERK, has been shown to both inhibit the MAPK pathway in BRAF V600E and KRAS G12V-mutated cells (Cagnol & Rivard 2012) and increase proliferation in HCT116 (Gröschl et al. 2013).

3.4.2.2 PD98059 and U0126 in a B-RAF mutated cell line (HT29)

It has been demonstrated that the activation of MEK by RAF is significantly different between the non-tumorigenic BRAF/CRAF wild type system and an aberrant BRAF V600E (Garnett et al. 2005; Röring et al. 2012). Contrarily to KRAS mutant cells, which are more effectively inhibited by drugs that bind to the S212 residue in MEK, BRAF mutated cell lines respond better to the strong blockage of phosphorylated MEK (i.e. by cobimetinib). This is due to the very high basal levels of MEK phosphorylation in BRAF mutant tumours (Pratilas et al. 2009), as proven by higher phosphorylated ERK levels in HT29 cell lines compared to HCT116 (data not shown). In fact, it has been demonstrated that the phenomenon of “oncogenic dependency” is more pronounced in BRAF mutant cells than KRAS mutant or KRAS/BRAF wild type cells (Solit et al. 2006), therefore sensitizing BRAF-mutants to MEK inhibition (Sebolt-Leopold et al. 1999). Feedback phosphorylation by wild type BRAF does not occur significantly in this case, since wild type BRAF levels are low in BRAF mutated cells (Pratilas et al. 2009). Conversely, evidence on a correlation between KRAS status and ERK activation is controversial and still being explored (Lim et al. 2005; Yip-Schneider et al. 1999; Schmitz et al. 2007; Yip-Schneider et al. 2001).

The present results are partly, but not wholly consistent with the above reports. PD98059 activity is through inhibiting the kinase activity of MEK on ERK. That confers it higher efficacy on BRAF-mutated cell lines. HT29 cells showed a significant reduction in both metabolic activity and proliferation levels from 10 μ M PD98059 and reach ~50% and ~80% inhibition in proliferation and metabolic activity respectively at 100 μ M. On the other hand the KRAS mutant cell line HCT116

reaches a plateau between 10 and 50 μ M at the proliferation level and only 50% inhibition at 100 μ M at the metabolic activity level.

Despite the ability of PD98059 to inhibit mutant BRAF activation of the pathway, the addition of EGF to activate the pathway triggers an almost two-fold increase in proliferation. This could be easily explained through natural wild type KRAS activation through EGFR signalling. In spite of the low levels of wild type BRAF to transmit KRAS signalling (Pratilas et al. 2009), a number of studies suggest that KRAS signalling also occurs through alternative pathways (Lim et al. 2005; Yip-Schneider et al. 1999).

Conversely, in the BRAF-mutant cell line U0126 triggers a typical response of paradoxical activation at the proliferation level, fostering proliferation almost two-fold at 100 μ M. Interestingly, metabolic activity remains impaired except at the highest concentration, in which it confers significant inhibition. The molecular mechanisms behind this paradoxical activation are not fully understood, but in this case feedback activation of BRAF is unlikely due to the low levels of wild type BRAF in BRAF-mutated cell lines (Pratilas et al. 2009). There is a significant difference in the basal pERK levels of these two cell lines, probably in part due to their differential expression of the DUSP4 phosphatase. HCT116 shows a much higher expression of DUSP4 than HT29 (Gröschl et al. 2013), in accordance to its KRAS mutant status. Higher basal levels of pERK in HT29 cells could have contributed to the paradoxical activation by U0126.

Activation of the MAPK pathway in CRC cell lines after drug treatment has also been observed with other families of drugs such as paclitaxel (Xu et al. 2009) or rapamycin (Wang et al. 2008), and it is a very common phenomenon. This surprising effect has also been observed as a side effect in a systemic manner upon treatment with BRAF inhibitors, which might lead to the development of secondary malignancies by activating the MAPK pathway in other tissues (Heidorn et al. 2010; Poulikakos et al. 2010; Arnault et al. 2012).

When EGF was added to HT29 cells after treatment with U0126, paradoxical activation was reversed. As hypothesized in the results section, the reason could be that the exogenous activation of wild type KRAS, and hence its alternative signalling

pathways, increased proliferation in the untreated cells and brought them to the same level than cells treated with U0126.

Despite it has been recently suggested that levels of phosphorylated ERK might not always be a good indicator of successful MEK inhibition (Yeh et al. 2009), this approach has been generally used for that purpose. Levels of pERK in HT29s after treatment with U0126 correlated very tightly to the increase in proliferation. However, protein was extracted after 10 min of exposure to EGF to activate the MAPK pathway. The fact that levels of pERK follows the same pattern as non-EGF-treated HT29 proliferation, as opposed to EGF-treated proliferation, suggests that the reversal of U0126-mediated proliferation increase caused by EGF addition might be mediated by a complex interaction of regulatory proteins in alternative pathways.

Opposite to the reversal of paradoxical activation, is the evidence that exposure to RTK ligands can revert drug sensitivity to MAPK pathway inhibitors (Wilson et al. 2012). These results support the significant effect of surface receptor activation on MAPK-targeted drug treatments. As indicated before, there are numerous regulatory mechanisms related to the MAPK pathway, and that not only affects KRAS-mutated but also BRAF-mutated cells. For example, the inhibition of BRAF has been associated with MEK and ERK activation (Johannessen et al. 2010; Nazarian et al. 2010), suggesting alternative pathways involved. In the light of these findings, BRAF and MEK inhibitors are being studied as a possible treatment combination, with very promising results (Flaherty et al. 2012).

It is worth noting that a number of controversial results have been reported with these two inhibitors. For example, a study by Dang et al. suggests that these two inhibitors have different effects on adipogenesis and osteogenesis in osteoprogenitor cells, and that those effects are not just through inhibition of the MAPK pathway (Dang & Lowik 2004). Furthermore, Dokladda et al reported that U0126 and PD98059 cause an elevation of ADP and AMP and activate the AMPK in a non-MAPK-mediated manner (Dokladda et al. 2005); while Harmon et al. suggested that both inhibitors reduce 2-deoxyglucose uptake in adipocytes upon insulin stimulation (Harmon et al. 2004), presumably also through AMPK activation. Both studies suggest that PD98059 and U0126 cross-react with other pathways, and experiments using these inhibitors should be interpreted with care

Furthermore, both PD98059 and U0126 at concentrations normally used for MEK1/2 inhibition *in vitro*, attenuate the apoptotic mechanism triggered by p45-JNK activation as a response to oxidative stress and, in the case of PD98059, interleukin-1. In fact, PD98059 has been shown to fade apoptosis in several occasions (Jiménez et al. 1997; Bhat & Zhang 1999), and it is known to inhibit MEK5 apart from MEK1 and MEK2, contributing to the hypothesis of cross-reactions (Kamakura et al. 1999) .

In the light of these and previously published controversial results with these two MEK inhibitors, neither of them was taken to the next phase of study, and the novel effective inhibitor AZD6244, currently in clinical trials, was explored for potential combination treatments and nanoformulations.

3.4.3 AZD6244 on HCT116 and HT29 cells

AZD6244 is a strong orally bioavailable specific inhibitor of MEK-1 and MEK-2, and it is specially designed for BRAF and KRAS mutant cell lines (Adjei et al. 2008; Yeh et al. 2007; Board et al. 2009). Its mechanism of action is also non-ATP competitive. It has reached phase I and II clinical trials with a variety of positive (Farley et al. 2013; Ho et al. 2013) and negative (Hayes et al. 2012; O'Neil et al. 2011; Kirkwood et al. 2012) results, being NCT01278615 and NCT01752569 for Diffuse large B-cell lymphoma and Kaposi's sarcoma, respectively, currently ongoing (reviewed in (Martin-Liberal et al. 2014)). Most of the failed clinical trials for AZD6244 were not successful because there was no RAS/RAF mutant selection. However, some studies without this selection showed promising results (Farley et al. 2013; Ho et al. 2013).

Contrary to the previous MEK inhibitors, there is very little difference between the effect of AZD6244 in HCT116 and HT29 cells. Both cell lines showed a smooth dose dependent response both at the metabolic activity and proliferation levels, suggesting that this small molecule is the best option for further combination treatments and nanoformulations. Davies et al. classify both HT29 and HCT116 cell lines are sensitive to AZD6244 (Davies et al. 2007).

This observation is consistent with the general hypothesis that there is not a statistically significant difference between the inhibitory effect of AZD6244 in KRAS and BRAF mutant cells, among other gene mutations (Tentler et al. 2010; Troiani et al. 2012). Said work was conducted both *in vitro* and *in vivo* showing similar results, and also classifies cell lines as resistant or sensitive to AZD6244 and states that all sensitive cell lines were mutant in either BRAF or KRAS.

The kinase inhibitory effect of AZD6244 was not dependent on the reference levels of phosphorylated ERK (found to be very different among CRC cell lines). In fact, it inhibits basal levels, as well as, newly induced phosphorylation in CRC, among other cancers. In this work, HCT116 shows moderate resistance to AZD6244, reaching its IC⁵⁰ at ~1µM after a 72-h treatment. This result is quite similar to what was found in this work, with an IC⁵⁰ of ~10µM after a 48-h treatment. On the other hand, HT29 is found as an extremely sensitive cell line, with an IC50 of less than 0.1µM after a 72-h treatment, which is non-consistent with our data.

It is worth noting that there is some controversy about the validity of pERK levels as an indicator of AZD6244 efficacy in CRC cell lines. Contrary to the hypothesis that it is not a suitable predictor (Tentler et al. 2010; Balmano et al. 2009), Davies et al. performed experiments in human tumour xenografts and suggested that it is a robust indicator (Davies et al. 2007).

One of the possible explanations for HCT116 cells partial resistance is a feedback activation of an alternative pathway that corrects the proliferation inhibition through the MAPK pathway. When the expression of Frizzled homolog 2 (FDZ2) was knockdown, HCT116 became more sensitive to AZD6244 treatment, suggesting that a feedback activation of the WNT5/FDZ pathway was involved in the partial resistance of HCT116 (Tentler et al. 2010). This of course offers new possibilities for combination treatments that aim to inhibit both pathways in pursuit of a synergistic inhibitory effect.

Oppositely, Troiani et al. also classifies a number of CRC cell lines as resistant or sensitive to AZD6244, but shows a much superior inhibitory effect on HCT116, with an IC⁵⁰ of approximately 0.25µM after 48 h treatment (compared to the ~10µM obtained in this work), but shows no results on HT29 cells (Troiani et al. 2012).

These differences could be explained through some acquired resistance or change in the proliferation profile caused by differences in the culture conditions.

For that reason, a drug treatment mimicking the experimental conditions in that publication was conducted for both HT29 and HCT116. Figure 3.15 shows that not only this protocol promotes less inhibitory effect on both cell lines, but the drug exhibits paradoxical activation in HCT116 at the highest concentrations. This is probably due to the fact that in this culture conditions cell cycle is not synchronized prior to drug treatment, making the effect of the drug less accurate and conclusions confusing. For example, MEK-1, but not MEK-2, can be strongly activated by serum (Xu et al. 1997), one of the main differences between the two cell culture protocols. The differential levels of MEK-1 and MEK-2 in these cell lines, as well as, the different affinities of this small molecule to each of them, can significantly affect the outcome of the experiments. These differences are more noticeable at the metabolic activity level, since its correlation to proliferation is much more unpredictable.

In regard to KRAS/BRAF status and the fact that different inhibitors are needed for different activation mechanisms, the BRAF-mutated HT29 cells could be expected to respond more effectively to AZD6244 inhibition, as reported in Tentler et al. 2010. The mechanism of action of AZD6244 is proposed to disrupt signalling at the catalytic stage of its kinase activity, after allowing MEK-1/2 phosphorylation, and not at the activation of MEK1/2 itself (Yeh et al. 2007). As mentioned earlier, these types of inhibitors tend to be more effective in counteracting the strong MAPK pathway activation characteristic of BRAF mutants, and not the additional alternative pathway activation characteristic of KRAS mutants.

A number of cases of AZD6244 resistance have been reported, and alternative pathway activations have been suggested (Tentler et al. 2010; Troiani et al. 2012). One possible mechanism of resistance to AZD6244 is the activation of protein kinase A. KRAS activation as also been proposed as a resistance mechanism against MEK inhibition in murine CRC. The up-regulation of MAPK pathway genes such as BRAF- or KRAS-mutants by intrachromosomal amplification in HCT116 and HT29 cells has also been suggested as a mechanism of resistance against AZD6244 upon treatment with the inhibitor (Troiani et al. 2012; Wang et al. 2005). It can be

hypothesised that this resistance could have been conferred along a 48 hour treatment, affecting the final proliferation count.

Despite the efficacy of AZD6244 on HT29 and HCT116 cells being lower than previously reported, and a moderate degree of resistance being present, this MEK inhibitor is the most suitable option for combination treatments and nanoformulations studies. For that reason, AZD6244 was explored in combination with the ETAR-specific antagonist ZD4054 (see chapter 4 (pg. 82)).

3.4.4 Treatment with ETAR competitive antagonists

The discussion in this section interprets a set of results regarding ET-1, ZD4054 and BQ123, and has a much stronger component of speculation than those regarding inhibitor of the MAPK pathway. The reason for this is unexpected inefficacy in the treatment with these compounds. Several batches of these molecules often elicited paradoxical or inconsistent effects on cell proliferation and metabolic activity, so the discussion and partial conclusions drawn in this section are interpreted with care.

Fundamentally, batch production is controlled by testing on endothelial models. These produce and respond at fold differences higher than cancer cells. Therefore, any loss of sensitivity or subtle changes would not be easily detected by gross testing in endothelial models. Also, to exclude operator error, independent use of all the endothelin axis molecules and determination of their effect on colorectal cancer cell lines were carried out by another researcher in the group. The same inconsistent outcomes were reported.

However, Due to the large body of work carried out with these molecules (great part of it not included in the thesis) and previous reported success within this research group, abstract patterns in cellular response, however misleading, are worth discussing. Moreover, these studies inform experiments in subsequent chapters of this document.

3.4.4.1 Response to ET-1

Experiments performed to evaluate the efficacy of ET-1 are included in this section, together with ETAR receptor antagonists.

The initial response of HCT116 and HT29 cells to ET-1 was very encouraging. MTT assay showed no significant differences in metabolic activity after 48- or 80-hour treatments in the high seeding density group (50000cells/well) (Figure 3.16), cells having reached a visible state of confluence. The fact that all treatment groups equalized to the control indicates a reduction in metabolic activity due to nutrient competition. Conversely, the superior increase in cell number after 80 h of ET-1 treatment on the same seeding density (Figure 3.17) is consistent with a commonly known characteristic of cancer, lack of cell contact inhibition (Hanahan 2000).

Results are much clearer in the low seeding density group (25000cells/well). ET-1 elicits a proliferation increase in both cell lines, following a very similar pattern for both cell counting and MTT assay, and validating the later as an indirect measure of proliferation. This correlation however, is subject to ambiguity since molecules or other factors affecting cell behaviour might trigger significant changes in the metabolic state of the cell, without necessarily affecting cell division. For that reason results of the MTT assay were interpreted as a secondary supporting technique rather than conclusive data (particularly in the event of no correlation).

All experiments that showed significant differences in the effect of ET-1 (i.e. cell counting and MTT assay at the low seeding density, as well as, cell counting at the high seeding density) indicate that HCT116 has a prevalent response to ET-1. This is surprising, since the expression levels of ETAR in HCT116 cells are slightly lower than in HT29 cells. Furthermore, the expression levels of endogenous ET-1 are slightly higher, suggesting that we could expect a lower increase in proliferation by the addition of exogenous ET-1. On the other hand, as discussed earlier, Zhang et al. suggested that mRNA expression levels are not necessarily a good indicator of protein levels (Zhang et al. 2014), and this is probably more significant with such small differences in expression.

The activation of ETAR by its natural ligand ET-1 triggers a phosphorylation cascade that converges with the MAPK pathway at the RAF level. While HT29 cells bare the V600E mutation in BRAF, and that confers low levels of wild type BRAF (Pratilas et al. 2009), the levels of wild type BRAF in HCT116 cells remain normal, making this cell line more susceptible to ETAR-mediated MAPK pathway activation and justifying a higher proliferation increase.

While promising, these results following ET-1 treatment were limited to the initial studies. Further experiments involving ETAR antagonists in the presence of ET-1 were performed utilizing new batches of the ligand. A number of these experiments (mostly omitted here) failed, partly due to the inability of the new ET-1 batches to increase proliferation in these cell lines. In some cases, treatment with the molecule inhibited proliferation instead. The only explanation for such unexpected phenomenon would be the induction of cell cycle arrest by accumulation of cycline products. It has been suggested that excessive acute phosphorylation of ERK could trigger this response (Meloche & Pouysségur 2007), and this might have been caused by the further activation of the already overactive MAPK pathway by ET-1. However, this has never been reported with ET-1 treatment before and is highly unlikely. Similarly, ETAR-specific antagonists showed very different results than expected, either increasing proliferation in the presence of ET-1 or significantly inhibiting proliferation in the absence of ET-1. One of the possible explanations for ZD4054 eliciting unexpected responses is the fact that this small molecule was purchased from a different company than previously done in this department. Unfortunately, the company that kindly donated ZD4054 to our department in the past, did not support nanoformulations. Some of the contradictory results are collected in Figure 3.23.

Due to the unpredictable efficacy of newly acquired ET-1 even within the same batch and the contradiction between current results and data previously reported in this department, the discussion of results regarding ETAR antagonists in the presence of ET-1 will be significantly brief and under the assumption that ET-1 elicits a proliferative response. However, caution is advised when interpreting these conclusions, as they are in part speculative.

3.4.4.2 BQ123

Due to the antagonistic mechanism of action of BQ123, a treatment with this molecule in absence of ETAR natural ligand ET-1 should not elicit an inhibitory response. This is consistent with our data. However, in the presence of the ligand, previous reports show antagonistic efficacy, while our data concludes the opposite. Furthermore, at the highest concentrations of BQ123 and in the presence of the ligand, the antagonist significantly increases proliferation in HCT116 cells (Figure 3.18).

Despite BQ123 being a ETAR-specific antagonist, previous reports from our group have demonstrated that high concentrations of this receptor antagonist could show a degree of ETBR binding. The effect of ET-1 binding to ETBR in colorectal cancer has been shown to trigger an opposite effect to ETAR binding (unpublished data). Hence, the possible unspecific binding of BQ123 to ETBR could explain the observed proliferation increase in HT29 and HCT116 cells when treated with the antagonist.

3.4.4.3 ZD4054

There is a strong body of evidence that ET-1 mediated ETAR signalling elicits a proliferative response in several types of cancers. This is done by modulating apoptosis, angiogenesis, mitogenesis and invasion (Ali et al. 2000). ZD4054 is a highly specific ETAR antagonist, with IC₅₀ of 21nM for ETAR, and is able to prevent ET-1 binding to ETAR by competitive antagonism of the receptor (Bradbury et al. 1997; Morris et al. 2005; Rosanò et al. 2007a; Grant et al. 2007). This therapeutic molecule has been deeply studied at the clinical trial level, with some promising results.

Considering ZD4054 in absence of the ligand as a competitive antagonist of endogenously produced ET-1, HCT116 cells showed a more prominent response to ZD4054 inhibition than HT29, probably due to their already seen superior response

to the ligand. A number of CRC cell lines and cancers have been shown to produce significant endogenous ET-1 (Ali et al. 2000; Kusuhara et al. 1990).

As hypothesized earlier, one of the possible reasons for this is the constitutive activation of the MAPK pathway by V600E mutant BRAF in HT29 in contraposition to the higher levels of a wild type BRAF susceptible to ETAR-1 mediated activation in HCT116. Surprisingly, the addition of ET-1 to the ZD4054 treatment reduced the efficacy of the antagonist. This data is very controversial, since ZD4054 should only elicit significant proliferation inhibition in the presence of ET-1. However, work described in those publications doesn't involve HCT116 cells, and therefore the reasons for this behaviour in this cell line remain unknown.

Contrarily to the hypothesis that higher endogenous production of ET-1 by HCT116 cells could explain the more significant response to ZD4054 in the absence of exogenous ET-1, the expression levels of ETAR are lower in this cell lines. However, the expression levels of MEK are higher. This demonstrates that expression levels of effector proteins do not necessarily correlate to the efficacy of a drug treatment, particularly when mRNA is what is being measured. Or perhaps the addition of endogenous and exogenous ET-1 balances the rate of binding towards ET-1 instead of ZD4054. At the metabolic activity level however, the effects of ZD4054 are similar with or without the presence of ET-1.

Results obtained from HT29 treatment are more consistent with previous work. On the one hand, the constitutive high activity of V600E mutant BRAF in this cell line could be expected to soften the proliferation increase through ETAR activation. However, a significant difference between treatments with or without ET-1 can be observed, being cells activated by ET-1 more susceptible to ZD4054 inhibition, as expected from a competitive mechanism of action.

This efficacy could be explained because HT29 have less endogenous production of ET-1 compared to HCT116 so the influence of exogenous ET-1 would be clearer in HT29 cells. However, compared to HCT116 there is little wild type BRAF that could be phosphorylated by ET-1 activation. In this case, the transmission of the signalling cascade could be explained by transactivation of surface receptors such as EGFR (Vacca et al. 2000; Grant et al. 2007). In the EGFR transactivation scenario, the direct phosphorylation of scarce wild-type BRAF by ETAR-mediated signalling is

substituted by the KRAS-mediated activation of alternative pathways. This effect would sum up to the proliferation increase caused by V600E BRAF. Furthermore, ETAR activation triggers a network of complex alternative protein interactions that could also be responsible of mitogenic effects. Some of these directly or indirectly activated proteins are PI3K, PKC, PLC, PLD, PLA2, adenylate cyclase, guanylate cyclase, Raf-1, IP3, diacylglycerol (DAG), akt, mTOR, COX-1, COX-2, and prostaglandin E2 (Grant et al. 2007; Blaukat et al. 2000; Shome et al. 2000).

Considering numerous alternative pathways and surface receptor transactivation as a mechanism of increased proliferation by ETAR-mediated signalling, the superior inhibitory effect of ZD4054 on HT29 in the presence of the ligand is logical.

Results obtained from ZD4054 with or without ET-1 activation are contradictory and cannot be fully explained. In addition to the unpredictable effect of these molecules, it is worth noting that HCT116 cells occasionally secreted exosomes when treated with ZD4054, an indicator of stress (Figure 3.24).

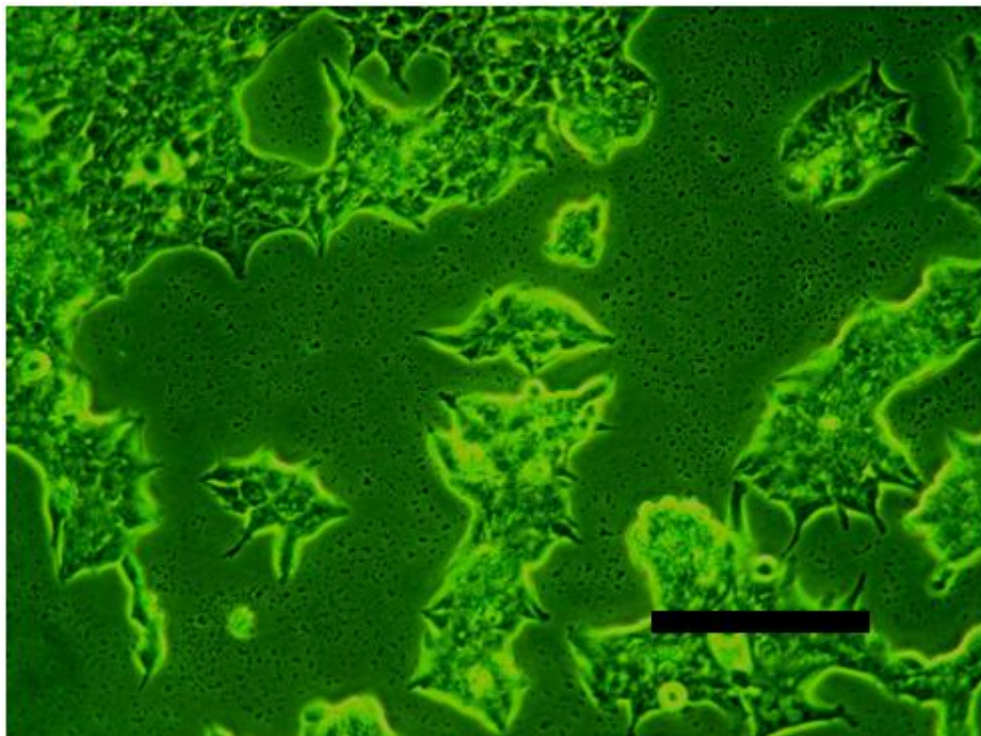


Figure 3.24 Vesicle secretion by HCT116 cells after treatment with ZD4054. Scale bar = 50 μ m

3.4.5 Selected molecules for combination treatments

While PD98059 and U0126 elicited significant proliferation inhibition consistently, there are too many controversial reports regarding these two molecules. Furthermore, efforts towards their clinical usage have been practically abandoned. Besides, U0126 exhibits paradoxical activation in one of the cell lines, and the concentrations needed to elicit any effect are far beyond previously reported doses.

Among the MEK inhibitors, AZD6244 seems the most suitable option, and combination experiments in the next chapters are carried out with this molecule. AZD6244 elicits a clear dose dependent inhibitory response, consistent with a reduction in ERK activation at the protein level. Moreover, numerous studies praise its efficacy and clinical testing has been performed and is currently ongoing.

Despite the controversial results obtained from ET-1 and the ETAR antagonists, previous work in this department has demonstrated their efficacy. It seems that the major problem regarding ZD4054 efficacy is actually due to defective ET-1. Optimally, the addition of ETAR natural ligand to receptor antagonist testing is necessary to assess their efficacy, but ZD4054 shows moderate efficacy inhibiting proliferation, presumably due to the blockage of endogenously produced ET-1 binding to the receptor, especially in HCT116 cells.

For that reason, AZD6244 and ZD4054 will be explored in combination, however in the absence of ET-1, to explore the possibility of a synergistic inhibitory effect of these two compounds. This is a very likely possibility due to the evidence on ETAR-mediated cross-activation of the MAPK pathway (Grant et al. 2007; Vacca et al. 2000). Furthermore, a similar MAPK/ETAR inhibitory combination has been attempted with very promising results. Rosanò et al. achieved significant tumour regression and reduction in biomarkers of angiogenesis in ovarian carcinoma xenografts, by administering ZD4054 and the EGFR inhibitor gefitinib (Rosanò et al. 2007a).

CHAPTER 4

RNA Interference & Treatment Combinations

4 RNA Interference and Treatment Combinations

4.1 Introduction

In the previous chapter, AZD6244 was selected as the most suitable MEK inhibitor for combination treatments. However, since the efficacy of ETAR-specific antagonists was potentially compromised by deficient ligand-binding activation, an additional combination treatment was considered.

This chapter briefly describes the therapeutic potential of ETAR- and MEK- targeted therapies in combination. Firstly, the co-administration of ZD4054 and AZD6244 was explored, with a very interesting but paradoxical outcome. For that reason, the possibility of combining AZD6244 with interfering RNA targeted against MEK-1, MEK-2 or ETAR was also considered.

4.2 Materials and Methods

In this chapter, most experiments were performed on HCT116 cells only, with the exception of the initial siRNA/OFA ratio optimization and the AZD6244/ZD4054 combination experiment, which were performed on both HCT116 and HT29 cells.

4.2.1 Materials

Details on the small molecules AZD6244 and ZD4054 are compiled in chapter 3 (pg. 42). SiRNAs targeted against specific genes (ETAR, MEK1 and MEK2) and a control (scrambled) siRNA were all part of the ON-TARGET plus SMART pool series and were purchased from (Dharmacon, Lafayette, USA). SiRNA transfections were performed using the reagent Oligofectamine (OFA) (Invitrogen).

4.2.2 Cell culture and siRNA evaluation

For the optimization experiments, cells were seeded on 6-well plates (250000cells/well for both HT29 and HCT116 cells) and left for 24 h to allow attachment and starting proliferation, before serum was removed. After 24 h of serum starvation, cells were treated with different volumes of oligofectamine (OFA) (3 or 4 μ L) and different concentrations of target-specific (ETAR, MEK1 and MEK2) siRNAs (10, 50 or 100 nM). OFA and siRNA were mixed and added to the cells as instructed (Invitrogen): OFA was allowed to interact with serum-free medium for 8 min, then siRNA was mixed with serum-free medium and both solutions were added together and left for 18 min to interact. 800 μ L of serum-free medium were added in advance to each well and the 200 μ L of the concentrated OFA/siRNA mixture were added to make a total of 1 mL. After 4 hours of transfection, 500 μ L of serum-free medium were added to give a final volume of 1.5 mL; cells were left for 24 h before RNA extraction and analysis were performed, following the protocols described in chapter 2 (pg. 30). Quantitative PCR was performed to determine which combination achieved the most efficient gene silencing.

Once the optimal ratios were chosen, a whole characterization of siRNA efficacy at the mRNA and protein levels was done on HCT116 cells (seeding at 250000 cells/well). Similar to the optimization experiments, 48 h after seeding (including a 24-hour starvation step) cells were treated with specific and scrambled siRNAs using OFA and following the same protocol. The selected OFA/siRNA ratios were: 3 μ L OFA and 50 nM siRNA (for ETAR and MEK2 siRNAs) and 3 μ L OFA and 100 nM siRNA (for MEK1 and control siRNAs). Proteins and RNAs were extracted 24, 48 and 72 h after transfection. For protein experiments involving siRNAs targeted against MEK1 and MEK2, cells were treated with EGF for 10 min before protein extraction to activate the pathway. Quantitative PCR of ETAR, MEK1, MEK2 and G6PDH and Western Blot of ETAR, MEK1, MEK2, pERK1/2 and GAPDH were performed following protocols described in section 2.3 (pg. 34 and pg. 38). Densitometry of protein bands in Western blot was achieved by isolating each band and quantifying its intensity using the Image J software. The intensity of the bands was standardized in reference to GAPDH.

4.2.3 Cell culture and proliferation assays

For proliferation experiments involving drug and siRNA treatments, protocols described in section 2.2 (pg. 30) and section 3.2.3 (pg. 44) were followed. Cells were seeded on 24-well plates (32000cells/well for HT29 and 30000cells/well for HCT116) and cultivated with 500 μ L of McCoy's 5A supplemented with 10% FBS. Serum was removed after 24 h to prevent possible drug-serum interactions and to semi-synchronize cell cycles. After a 24-hour starvation step cells were treated with either a combination of AZD6244 and ZD4054, or target-specific siRNAs (ETAR, MEK1, MEK2, control) alone or in combination with AZD6244. The use of siRNAs in these experiments was performed following the same silencing protocol described earlier, although adapted to the volumes in 24-well plates (200 μ L of medium were added to the well with an additional 50 μ L of the siRNA/OFA mixture). After 4 h, 125 μ L of either medium or AZD6244 in medium were added and cells were left for 48 h. After 48 h, proliferation and metabolic activity assays were performed to measure the effect of the treatments on proliferation. For ZD4054 and AZD6244 combination

experiments AZD6244 concentration remained at 1 μM for all treatment groups and ZD4054 concentration ranged between 0.01-1 μM . For AZD6244 and siRNA combination experiments AZD6244 concentration remained at 100 nM in all treatment groups and siRNA concentrations were those derived from the optimization experiments (50 or 100 nM) while the volume of OFA was reduced to 2 μL /well, as suggested by the manufacturer for 24-well plates.

4.3 Results

4.3.1 Optimization of OFA/siRNA ratio

Oligofectamine (OFA) is a transfection agent, widely used to introduce nucleic acids into cells. When mixed with the target nucleic acid in an aqueous solution OFA forms particles that allow its transport through the cell membrane; it has been successful in mediating siRNA transfections (Resnier et al. 2014). However, the exact molar ratio between the transfection agent and the transfected molecule can only be found through experimentation.

For this reason, different volumes of OFA and different concentrations of siRNA were tested to approximately determine which combination elicited the best silencing response. Since the efficacy of this molecule is being tested, it is crucial to find the right combination before performing more complex experiments involving time points or treatment combinations.

Table 4.1 shows the standardized quantitative RT-PCR copy numbers of the target mRNAs (ETAR, MEK-1 and MEK-2) after being treated with different combinations of OFA and target-specific siRNAs.

		ETAR		MEK-1		MEK-2	
RNA (nM)	OFA (μL)	HCT116	HT29	HCT116	HT29	HCT116	HT29
10	3	4957.301452	9391.054699	187790.3119	21600.96541	387979.9125	568774.7861
	4	4963.777837	6894.87543	106556.3087	145315.1618	423643.4109	1257360.96
50	3	2188.36886	7607.655502	73217.02875	143488.024	346868.7207	616604.4776
	4	40898.20359	7960.245758	112797.8694	232781.9957	171343.2836	949828.3098
100	3	2461.402735	9069.487294	138945.5782	201483.0508	272914.8376	293658.754
	4	32734.72593	6721.432527	96060.27094	182231.6384	306727.8287	1209831.739

Table 4.1: Silencing efficacy of different OFA/siRNA ratios. HT29 and HCT116 cells were seeded on 6-well plates and treated with target-specific siRNAs at different OFA/siRNA ratios. Results are expressed as copy number present in 100ng of RNA template and normalized to 50000 copies of G6PDH. The highlighted values show the lowest copy number for each target mRNA after treatment.

The highlighted values are the lowest copy number for each target mRNA after treatment and therefore indicate the optimal OFA/siRNA ratio for each individual target (Table 4.1). These ratios, however, are selected considering the lowest copy number of both HCT116 and HT29, to standardize the protocol between cell lines for simplification. This simplification was due to the initial plan of performing silencing experiments on both cell lines. However, due to some confusing results derived from HT29 cell experiments (such as a drop of ETAR expression after a number of passages), silencing experiments and experiments in the following chapters are limited to HCT116 from this point onwards. The selected OFA/siRNA ratios were 3 μL and 50 nM for ETAR and MEK2 siRNAs, and 3 μL and 100 nM for MEK1 and control siRNAs (100 nM were chosen for scrambled siRNA as it represents the non-target-specific damage that the transfection process may elicit on the cells and therefore was equalised to the highest concentration of siRNA present on the other treatments).

In order to further confirm the efficacy of the primers selected for qPCR experiments, conventional PCR of the genes of interest (ETAR, EGFR, MEK1, MEK2 and GAPDH (housekeeping gene)) was performed on HCT116 cells (Figure 4.1). While both techniques are performed in one step and based in the reverse transcriptase (RT), the main difference between them is that quantitative PCR detects and quantifies the amplified genes in real time, while conventional PCR is semi quantitative.

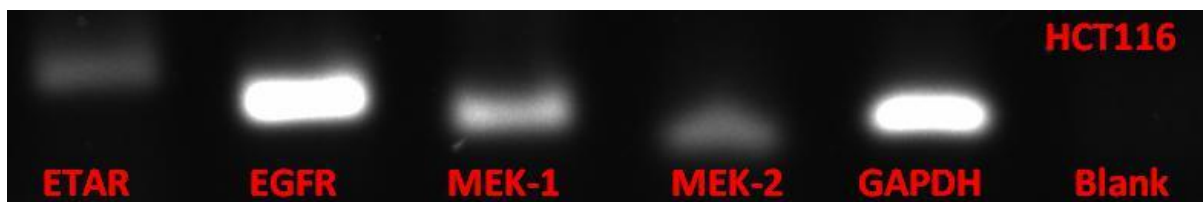


Figure 4.1: Conventional PCR of key proteins in HCT116 cells. 1000000 HCT116 cells were seeded on a Petri dish and left to proliferate until 60% confluence. RNA was extracted and purified and conventional PCR was performed following the protocol described in chapter 2 (pg. 30).

4.3.2 Effect of target-specific siRNAs on mRNA expression over time

In order to select the timepoint in which maximum silencing is achieved for each target, quantitative RT-PCR was performed 24, 48 and 72 h after silencing treatment, including a control (scrambled) siRNA. There was a maximum silencing effect at 24 h for ETAR-specific siRNA, and 48 h for MEK-1 and MEK-2-specific siRNAs, all of which started to recover to reference levels 24 h after that point (Figure 4.2).

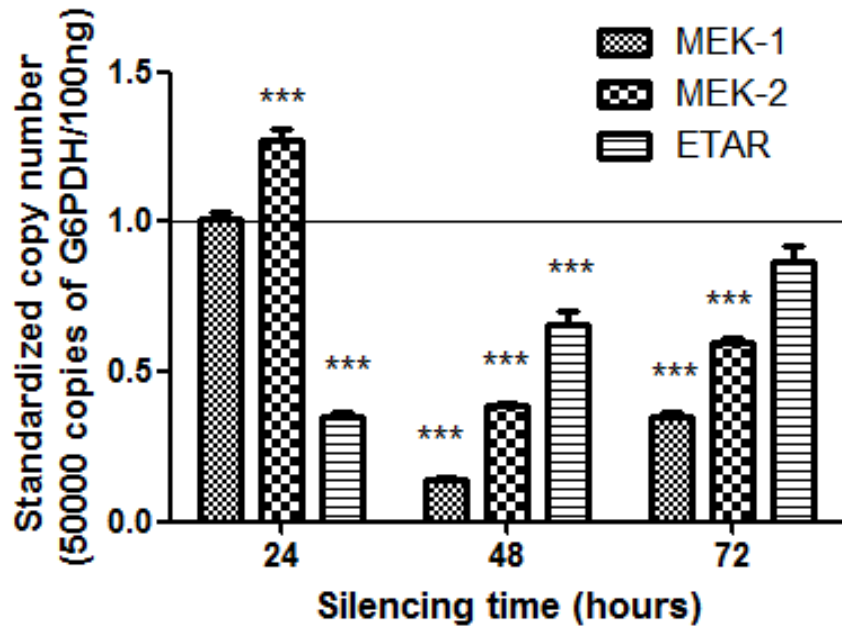


Figure 4.2 Effect of target-specific siRNA on mRNA levels. 200000 HCT116 cells were seeded in 6-well plates, starved for 24 h and treated with specific siRNAs assisted by OFA. RNA was extracted after 24, 48 and 72 hour treatments and quantitative PCR was performed for the siRNA targets. Results from quantitative PCR were standardized against a housekeeping gene (G6PDH), used both as an internal control and as a standard curve. Significance: *** $p < 0.001$ against control (thin horizontal line).

Cells treated with scrambled siRNA as the non-specific siRNA control also showed a certain reduction in the levels of the target mRNAs, probably by causing some cell damage that inhibited the expression of certain proteins in response. Results shown here compensated for that effect, as the results are normalised to the basal levels obtained from the siRNA control treatment. At the macroscale, the damage elicited by siRNA transfection in cells is also visible even for the control group (Figure 4.3), and suggests apoptotic mechanisms in response to the transfection.

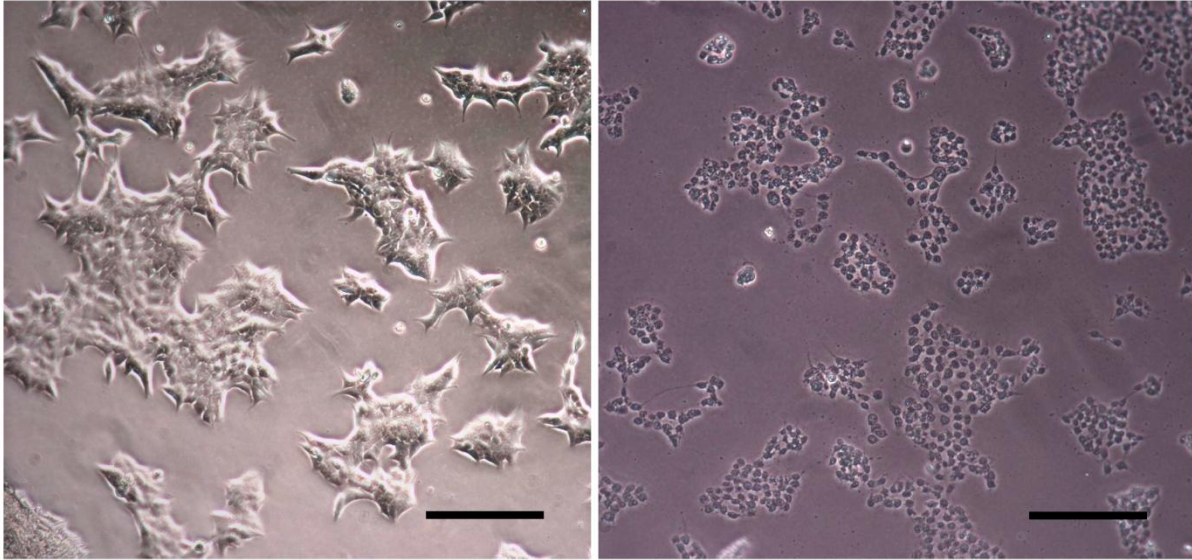


Figure 4.3 Effect of control (scrambled) siRNA on cells. A certain degree of cell damage is observed in some regions within the treated plates, including those treated with scrambled siRNA. Left: healthy HCT116 cells, right: apoptotic HCT116 cells, both images taken from different regions of the same well. Scale bars = 100 μ m.

Wells treated with siRNAs, both specific and control, present a mixture of both morphologies, which explains why differences in expression are still visible, even in the presence of abundant cell death. This is partly due to the fact that siRNA transfection is a very heterogeneous process, in which not all cells receive the same amount of the treatment or contribute equally to the visible changes in expression.

Even so, this needs to be taken into account. If the mere phenomenon of non-specific transfection is causing apoptosis, this could present non-specific side effects in a combination treatment involving siRNA.

4.3.3 Effect of specific siRNAs on target proteins

Once the mRNA silencing efficacy was proven, Western Blot was performed to determine whether knocking out target genes effectively reduced the levels of target proteins, which ultimately carry out the cellular function.

4.3.3.1 ETAR

In the case of ETAR, this task was particularly difficult. Two different anti-ETAR monoclonal antibodies were used and neither of them seemed to recognize the target protein specifically. Figure 4.4 show the whole membranes after immunoblot, with very unspecific recognition of proteins of a variety of sizes. The highlighted bands (Figure 4.4c) are potentially subunits of ETAR (isolated and magnified) with their corresponding housekeeping gene bands), based on protein size extrapolated from a ladder and suggested by the manufacturer.

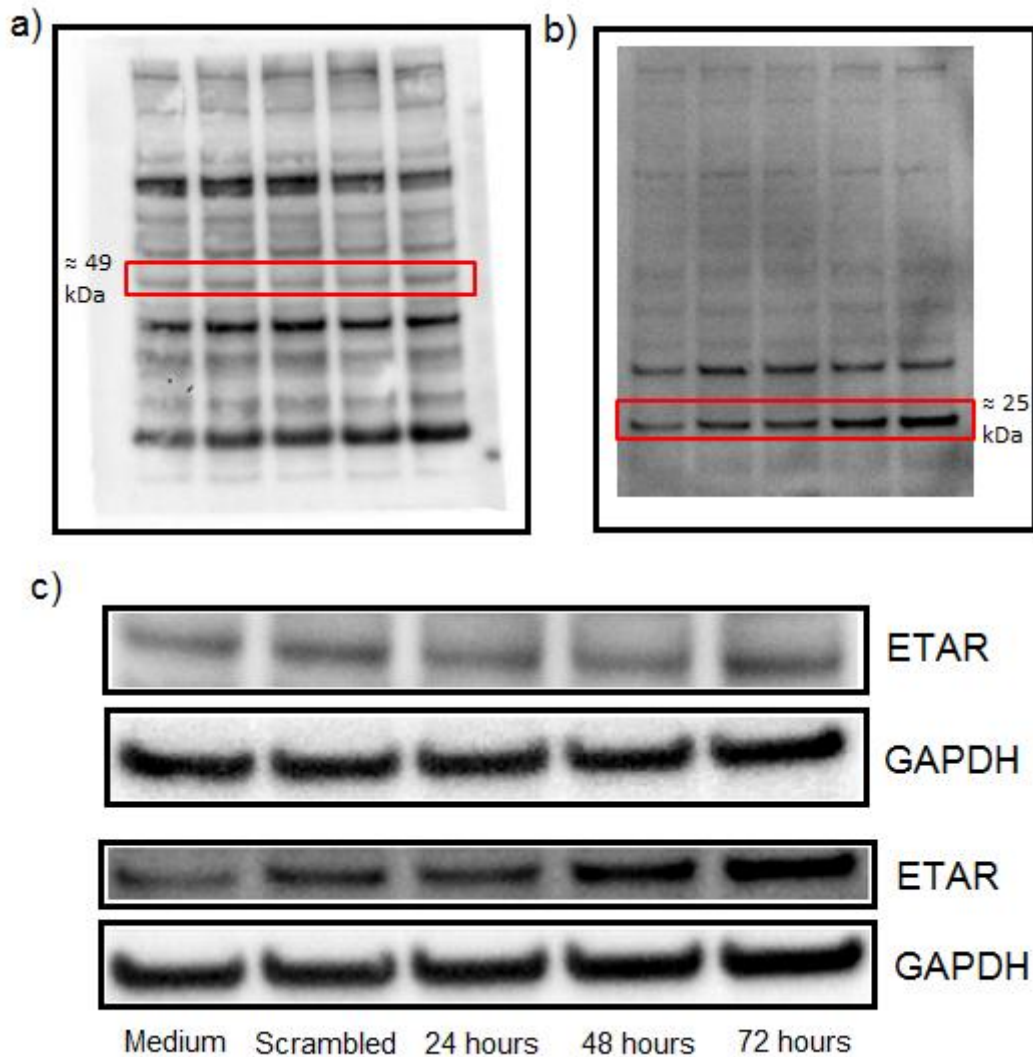


Figure 4.4 Non-specific protein recognition by two different ETAR antibodies. Following treatment with ETAR-specific siRNA, HCT116 protein extracts were run in a polyacrylamide gel, transferred to a PVDF membrane and recognized by ETAR-specific antibodies. However, results consistently showed non-specific recognition. a) whole membrane treated with Abcam ETAR antibody, b) whole membrane treated with Alomone labs ETAR antibody, c) bands presumed to represent ETAR or ETAR subunits according to their size and response to ETAR-specific siRNA next to housekeeping protein GAPDH (top: Abcam ETAR antibody, band at 49kDa, bottom: Alomone labs ETAR antibody, band at 25 kDa).

Densitometry of the selected bands (Figure 4.5) was calculated to have a graphical representation of increases or decreases of protein levels, standardized using the housekeeping gene. While the levels of one of the potential subunits recognized by the Abcam antibody are relatively stable over treatment times, the potential subunit recognized by the Alomone labs antibody shows significant increases over time, suggesting two possible explanations. On the one hand, it could be either a subunit

of ETAR that gets paradoxically overexpressed when the mRNA that codifies for it is silenced, or it could be a peptide functionally related to ETAR that gets expressed in response to a reduction in ETAR mRNA. It could also be a peptide completely unrelated to ETAR that happens to get overexpressed after a traumatic event such as transfection occurs. In any of those cases, in spite of the clear reduction in mRNA levels following its silencing, the treatment could not be proved to reduce the levels of the target protein. Nevertheless, due to the extremely unspecific binding of the antibody to proteins of many sizes, there is no evidence that the peptides or subunits analysed here are part of ETAR at all.

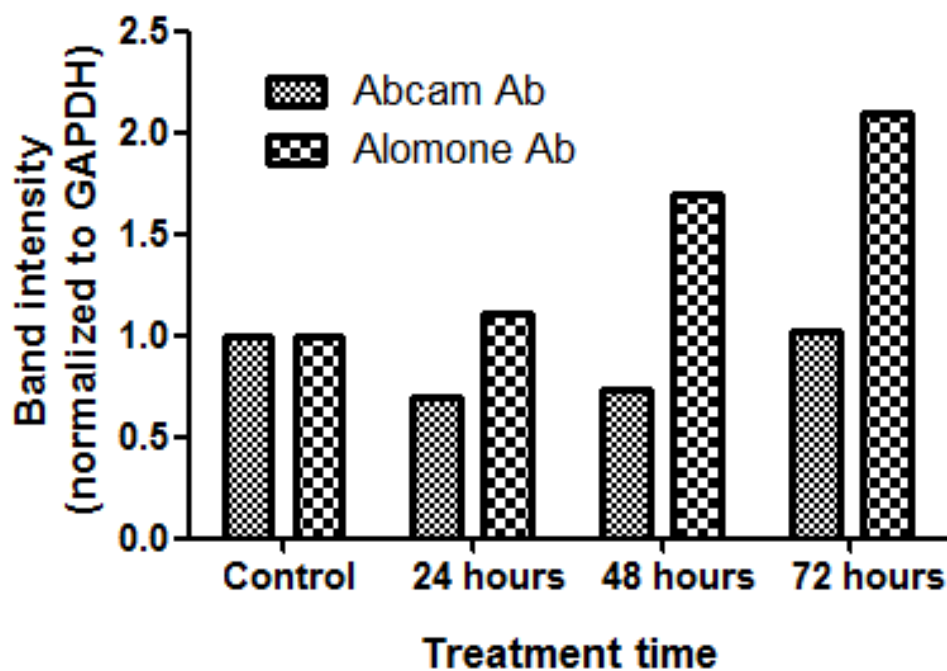


Figure 4.5: Densitometry analysis of selected ETAR bands. The bands that could potentially represent ETAR were isolated and their intensity was quantified using the Image J software and standardized to the intensity of the housekeeping protein GAPDH for each lane.

4.3.3.2 MEK-1 and MEK-2

In contrast to the difficulty demonstrating ETAR protein inhibition, silencing MEK1 and MEK2 at the mRNA level showed a clear correlation with decreases in target

protein levels. A clear reduction in the levels of both proteins is shown in (Figure 4.6 and Figure 4.7) for MEK1-specific siRNA and MEK2-specific siRNA, respectively. In these images, MEK1 and MEK 2 are represented together in the same band since they are close in size, and they are also effectively recognized by the same antibody.

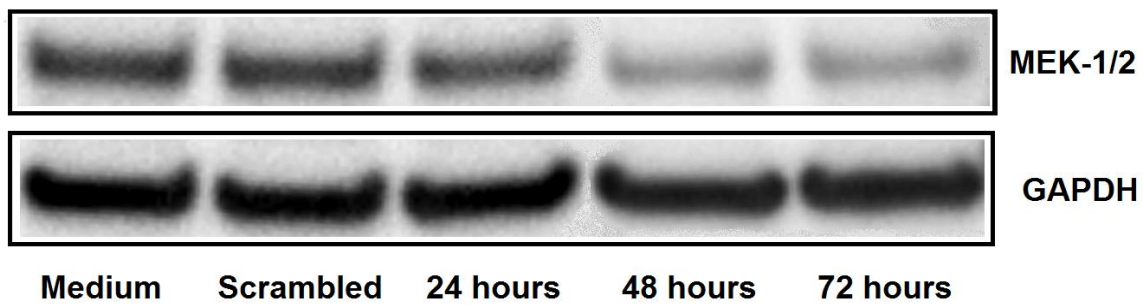


Figure 4.6: Effect of MEK1-specific siRNA on MEK-1/2 levels. Following treatment with MEK1-specific siRNA, HCT116 protein extracts were separated by PAGE, transferred to a PVDF membrane and recognized by a MEK1/2-specific antibody. MEK-1/2 is shown next to GAPDH control.

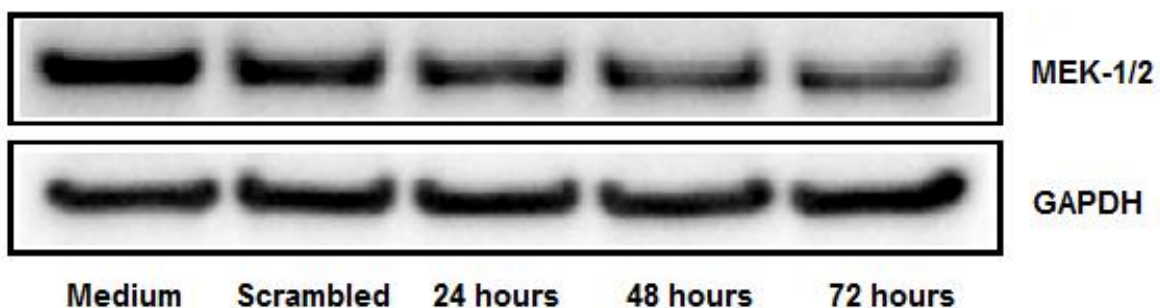


Figure 4.7: Effect of MEK2-specific siRNA on MEK1/2 levels. Following treatment with MEK2-specific siRNA, HCT116 protein extracts were separated by PAGE, transferred to a PVDF membrane and recognized by a MEK1/2-specific antibody. MEK-1/2 is shown next to GAPDH control.

Densitometry supports these findings and reveals that while both MEK1- and MEK2-specific siRNAs steadily decrease the levels of MEK1/2 with increasing treatment times, the effect of MEK-1 is more pronounced (Figure 4.8), and this is clearly visible in the membrane.

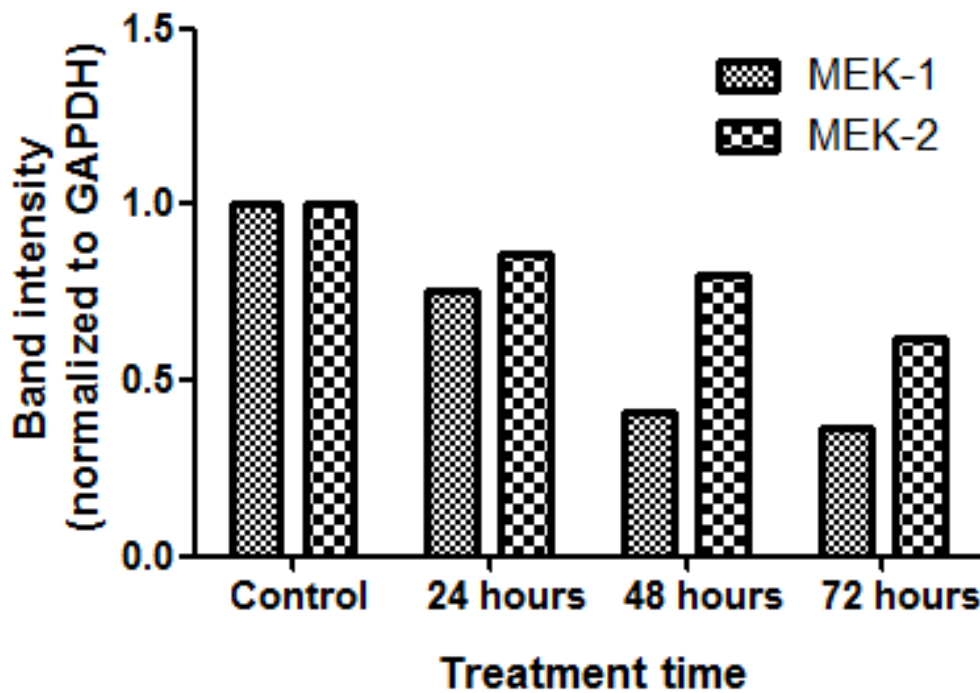


Figure 4.8: Densitometry analysis of MEK1/2 bands after treatment with MEK1- and MEK2-specific siRNAs. Bands were isolated and their intensity was quantified using the Image J software and standardized to the intensity of the housekeeping protein GAPDH for each lane.

4.3.3.3 Downstream marker pERK

The ultimate aim of reducing the levels of MEK1/2, whether it is by blocking it with a drug or by silencing its expression is reducing the activation of ERK1/2 and therefore reversing the aberrant proliferation resulting from hyper-activation of MAPK pathway signalling. An additional experiment was designed to determine the effect of MEK1- and MEK2- specific silencing as well as a combination of both on the levels of phosphorylated ERK1/2 (Figure 4.9). Densitometry results were very promising, showing that not only each of this individual siRNAs reduce both pERK1 and pERK2, but a combination of both could be even more effective, although the differences were very subtle (Figure 4.10).

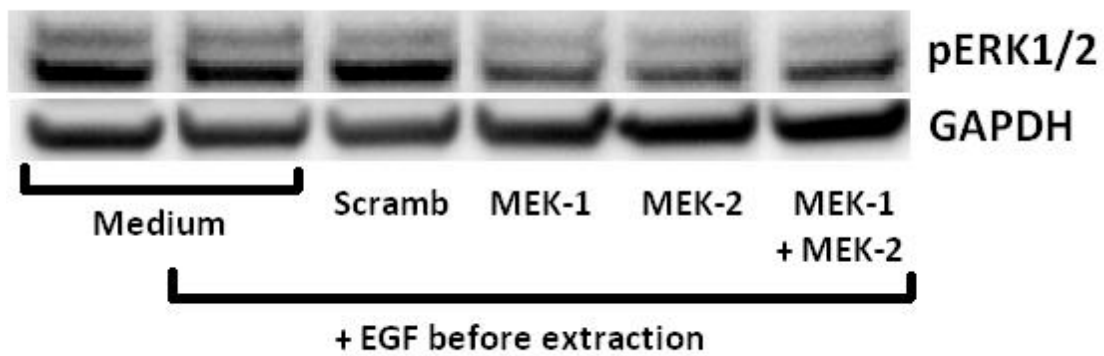


Figure 4.9: Effect of MEK1- and MEK2-specific siRNAs on the levels of phosphorylated ERK1/2. Following treatment with MEK1- and MEK2-specific siRNA, individually or in combination, HCT116 protein extracts were separated by PAGE, transferred to a PVDF membrane and recognized by a pERK1/2-specific antibody. pERK-1/2 is shown next to GAPDH control.

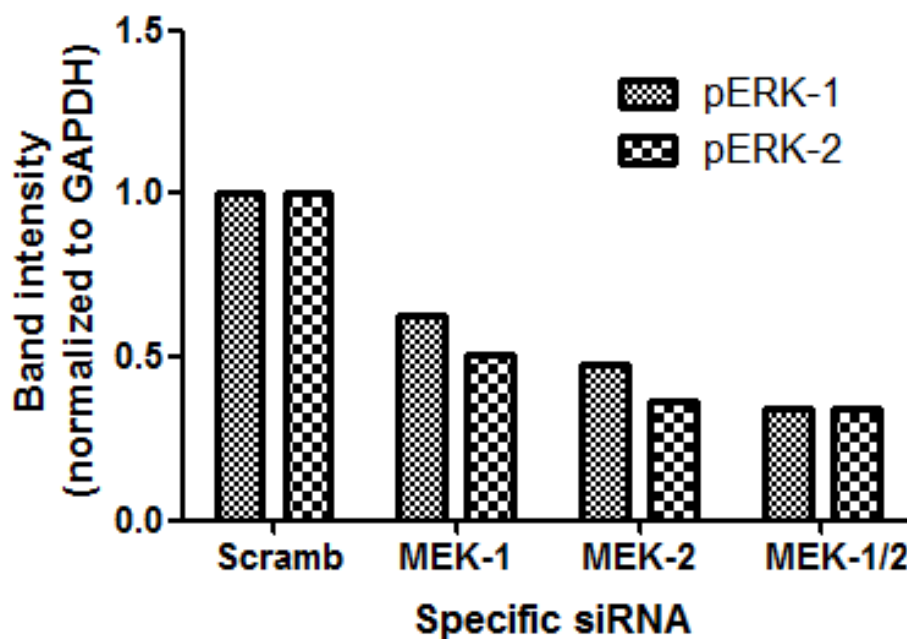


Figure 4.10: Densitometry analysis of pERK1/2 bands after treatment with MEK1 and MEK2-specific siRNAs. Bands were isolated and their intensity was quantified using the Image J software and standardized to the intensity of the housekeeping protein GAPDH for each lane.

4.3.4 Combination treatments

4.3.4.1 Combination of small molecules: AZD6244 and ZD4054

It is believed that the downstream signalling cascade derived from the activation of ETAR is cross-linked to the MAPK pathway. For that reason, one of the main objectives of this research was to find a treatment combination that interrupts proliferative signalling cascades at two different points: the ETAR at the cell surface and the intracellular MEK1/2. Due to the availability of small molecules targeted at both proteins and the previous work with the endothelin receptors that took place in this department (Asham et al. 2001; Ali et al. 2000; Haque et al. 2013), one of the combinations explored here is that of AZD6244 (MEK inhibitor) and ZD4054 (ETAR antagonist). Due to the interaction or cross-talk between pathways, it has hypothesized that these two small molecules could achieve a synergistic inhibitory effect if administered together.

To prove that hypothesis, HT29 and HCT116 cells were treated with different concentrations of AZD6244 and ZD4054 in combination. AZD6244 was chosen as the most appropriate MEK inhibitor for further experiments because of its superior status in research and clinical trials, its consistent dose-dependent effect among cell lines and its specific efficacy in RAS and RAF mutated tumours (Davies et al. 2007; Troiani et al. 2012; Tentler et al. 2010).

A number of concentrations of both AZD6244 and ZD4054 were tested in combination, however, the major conclusion can be drawn from keeping AZD6244 at its highest concentration (1 μ M) and testing it in combination with a range of ZD4054 concentrations (0.01 - 1 μ M) (Figure 4.11).

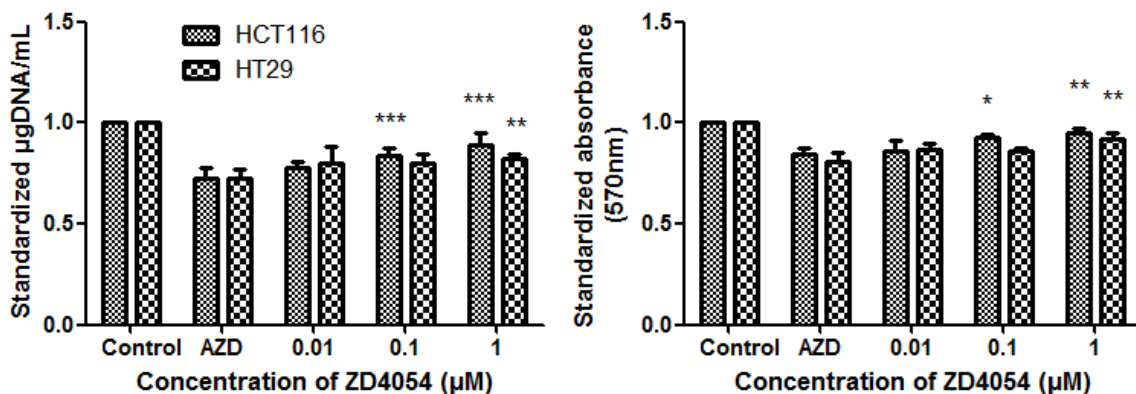


Figure 4.11: Effect of the combination of AZD6244 and ZD4054 on HCT116 cells. HCT116 cells were treated with 1 µM AZD6244 alone or with a range of ZD4054 concentrations (0.01 - 1 µM) for 48 h before total DNA assay (left) and MTT assay (right) were performed. Significance: * $p < 0.05$, ** $p < 0.01$, *** $p < 0.001$, compared to the AZD6244 treatment alone.

Results from this combination are not consistent with the hypothesis of synergism. The superior proliferation inhibition observed in the group treated with AZD6244 alone suggested that this drug was the only one producing the desired effect. Moreover, cells treated with both ZD4054 and AZD6244 presented less proliferation inhibition than cells treated with the same concentration of AZD6244 in absence of ZD5054, suggesting that ZD5054 has an antagonistic effect towards the inhibitory effect of the MEK inhibitor.

4.3.4.2 Combination of small molecule and silencing: AZD6244 and siRNAs

In view of the antagonistic effect elicited by the combination of AZD6244 and ZD4054, a new approach was designed involving the combination of AZD6244 with various target-specific siRNAs. While the effect of ETAR-specific siRNA on its protein levels could not be demonstrated, its effect at the mRNA level was very positive (Figure 4.2). On the other hand, MEK1- and MEK2-specific siRNAs showed promising results both at the RNA, protein, and kinase activity levels (Figure 4.2, Figure 4.8 and Figure 4.10). The ability of all three siRNAs to inhibit proliferation was assessed independently and in combination with AZD6244. A 48-hour treatment was

chosen since the kinase activity of MEK1/2 was significantly reduced at this point and the silencing of ETAR mRNA reaches its maximum at 24 h (and the subsequent effect on the ETAR protein if there were any would happen at the earliest after that).

Surprisingly MEK1-, MEK2- and MEK1/2-specific silencing treatments did not inhibit metabolic activity in HCT116 cells, but promoted it instead, as indicated by MTT assay (Figure 4.12). This could be an overall increase in metabolism through other pathways to compensate a reduction in MAPK pathway signalling. On the other hand, ETAR silencing did cause a slight reduction in metabolic activity, perhaps due to a milder and indirect effect on the key MAPK pathway.

The addition of 100 nM AZD6244 to the silencing treatments reversed these results completely. In the presence of AZD6244, cells treated with MEK1- and MEK2-specific siRNA and the combination of both exhibited an exact correlation between the inhibition of metabolic activity (Figure 4.12) and the previously observed inhibition of MEK1/2 activity (Figure 4.10), with the combination of both siRNAs eliciting the highest inhibitory response. The addition of AZD6244 also reversed the inhibitory effect of ETAR-specific siRNA.

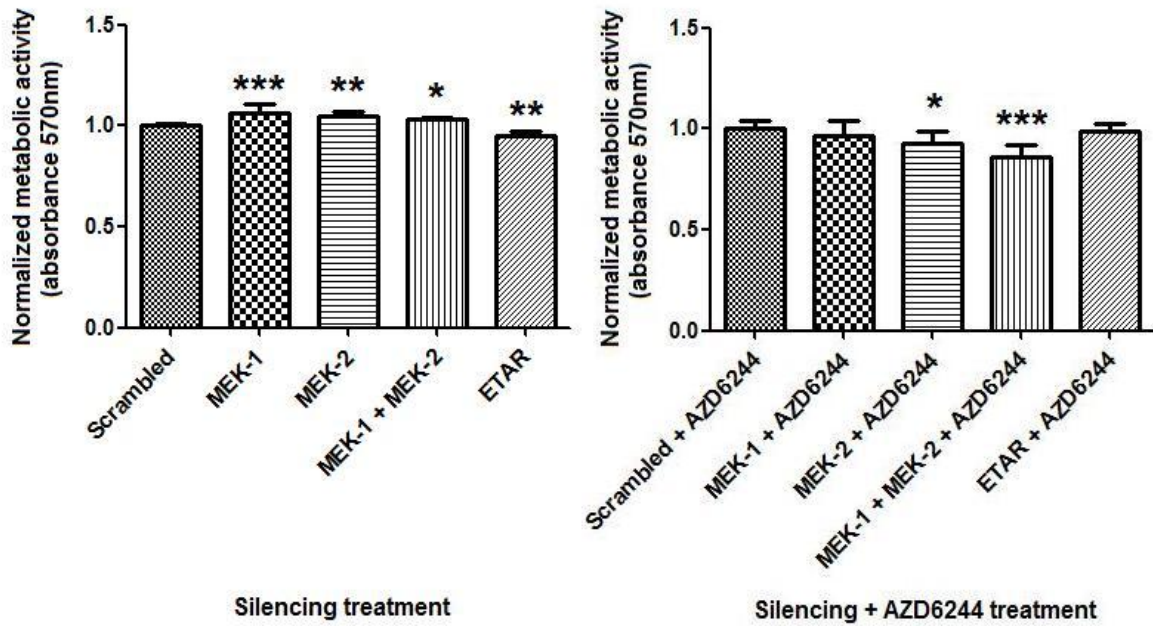


Figure 4.12: Effect of target-specific siRNAs alone and in combination with AZD6244 on HCT116 cells. Cells were treated with target-specific siRNAs, with or without AZD6244 for 48 h, before MTT assay was performed. Significance: * $p < 0.05$, ** $p < 0.01$, *** $p < 0.001$, compared to control siRNA on the left and compared to control siRNA + AZD6244 on the right.

4.4 Discussion

An initial objective in this research was finding an effective combination of two small molecules that could achieve a synergistic inhibitory effect. Interfering RNA was then used as an alternative to the second small molecule component in this combination therapy approach. Besides, even though AZD6244 doesn't show a particularly high chemical toxicity (non-target specific) compared to other inhibitors, it is a concern to take into account when using small molecules, and this makes silencing as an alternative therapy a potential candidate. Here, first the efficacy of the target-specific siRNAs and then combination treatments are discussed.

Different ratios of OFA and target-specific siRNA were tested to find the optimal ratio for each molecule. The scrambled siRNA control was not included in this step since it does not target a specific molecule and no reduction in target mRNAs should be observed after treatment with it. Even though most combinations proved effective, the maximum efficacy was achieved with 100nM siRNA + 3uL OFA in the case of MEK-1, and 50nM siRNA + 3uL OFA in the case of MEK-2 and ETAR. Initially, the combination experiments were planned for both HT29 and HCT116 cell lines, so the maximum efficacy ratio was chosen to achieve maximum response in both cell lines using the same ratio. However, due to changes in gene expression of HT29 cells over time, the efficacy of siRNA and combination experiments following the OFA/siRNA ratio optimization were assessed only on HCT116 cells.

Despite the absolute quantification of gene expression performed in this research, the levels of target mRNAs are higher than the reference expression showed in chapter 3 (pg. 42). This is due to the different conditions of the experiment; while silencing experiments were done in 6-well and 24-well plates and subject to treatments, to determine the reference levels of expression cells were grown in Petri dishes and they were not subject to any treatment or serum removal steps. For example, if a population of cells is treated with a therapeutic or silencing agent, cells might respond by overexpressing certain proteins to counteract an inhibitory effect, and that response would be very different from the reference levels even if that gene is successfully silenced relatively to the control.

4.4.1 ETAR silencing efficacy

As shown in (Figure 4.2), the silencing efficacy of the ETAR-specific siRNA peaks after 24 h. Based on this, if protein levels of ETAR were indeed reduced after ETAR-specific siRNA treatment, this would have happened at least 24 h after the treatment. Two different ETAR-specific antibodies were used to explore the reduction in protein expression, but unfortunately that hypothesis could not be demonstrated (Figure 4.5). The antibody purchased from Abcam recognized a large number of bands with different intensities and only one of the weak bands corresponded to the size that the company suggested for ETAR. Even though said band showed a slight reduction in protein levels 24 and 48 h after the ETAR-specific siRNA treatment, the lack of specificity of this antibody suggests that the band could represent another protein, or a number of different proteins other than ETAR.

The other antibody used was purchased from Alomone labs, and in this case only two bands were clearly intense. One of them did correspond to the size suggested by the company but the protein level increased considerably as the ETAR-specific siRNA treatment time increased. Considering this ETAR-specific siRNA has previously been used by this group with positive results (unpublished data), the increase in ETAR protein levels might not be a coincidence, however discouraging this result may be. On the other hand, the effect of ETAR-specific siRNA on the levels of ETAR was not examined in those previous experiments, as they were performed to study changes in the expression of other proteins, not ETAR.

Assuming the silencing of the ETAR gene was in fact related to an increase in the protein levels, this could be explained as a compensatory decrease in its turnover. After the interaction with its ligand, at least part of the ETAR is known to be recycled and returned to the cell membrane, as opposed to constantly destroyed and new receptor synthesized. A reduction in the level of ETAR mRNA could result in compensatory translation of the remaining transcripts and increased expression of the protein or reduced receptor turnover, which combined with the recycling of the existing receptor, could increase the amount of ETAR in the cell.

4.4.2 MEK-1 and MEK-2 silencing efficacy

The efficacy of MEK-specific siRNAs was much clearer than in the case of ETAR. Both subtype-specific siRNAs elicited a significant reduction of their targets at the mRNA (Figure 4.2) and protein (Figure 4.8) levels, and they successfully reduced their activity, as shown by decreased levels of pERK (Figure 4.10).

According to these experiments, in HCT116 cells the expression levels of MEK-1 were significantly higher than those of MEK-2, and so were the levels of ERK-2 compared to ERK-1. This is consistent with previous reports in the literature (Lefloch et al. 2009). At the same time, MEK-1 silencing was more efficient lowering the mRNA levels of MEK-1/2 than MEK-2 silencing, although this could be due to the higher initial levels of MEK-1 or the higher concentration of siRNA used to silence MEK-1 compared to MEK-2. On the other hand, silencing MEK-2 was more efficient reducing the levels of both pERK-1 and pERK-2 even though the basal levels of MEK-2 and the amount of siRNA to silence it were lower than MEK-1; and the levels of activated ERK-1/2 (pERKs) are the principal targets of interest. Similar findings in this area have been reported, such as the fact that MEK-1 expression alone is not enough for melanoma proliferation but MEK-2 is (Lee et al. 2011), or the fact that knocking out MEK-2 expression has a more prominent effect as a proliferation inhibitor than knocking out MEK-1 in colorectal cancer (Voisin et al. 2008). This idea is also supported by T. W. Sturgill, who suggested that MEK-2 might have a role compensating the silencing of MEK-1 (Sturgill 2008). Specifically in HCT116 cells, it has been demonstrated that silencing MEK-1 induces p21^{Cip1} and promotes G1 arrest, which appears to be compensated by MEK2 activity (Ussar & Voss 2004). These findings suggest a more important role of MEK-2 in cancer proliferation than MEK-1, but interestingly also point towards a differential function of MEK-1 and MEK-2.

A large body of work suggests that some of the roles of MEK-1 and MEK-2 are differential (Giroux et al. 1999; Bélanger et al. 2003; Scholl et al. 2009), but not all of them are in favour of MEK-2 as the most important protein. For example, it is believed that MEK-1 and MEK-2 have a different role in G1 progression, since MEK-

1 function is activated in human glioblastoma, mouse embryonic fibroblasts and Chinese hamster ovary cells by the addition of serum to culture media, and this does not happen to MEK-2 (Xu et al. 1997).

This is different in the case of ERK-1 and ERK-2, both of them believed to have a similar function in G1 progression (Lefloch et al. 2009), which then suggests that MEK-1 at least has the ability to phosphorylate both ERKs in that phase. Contrary to this theory, it has been hypothesised, although as pure speculation, that MEK-1 may preferentially act on ERK-2 (Sturgill 2008). This is because while mice knockouts of MEK-2 (Bélanger et al. 2003) and ERK-1 (Pagès et al. 1999) are viable, the equivalent for MEK-1 (Giroux et al. 1999) and ERK-2 (Hatano et al. 2003; Saba-EI-Leil et al. 2003) are embryonic lethal. However, if this hypothesis were true, it might only be significant in stages of embryonic development and not have an effect on cancer.

The efficient reduction in MEK1/2 activity elicited by MEK-specific siRNAs was surprising. HCT116 is a KRAS-mutant cell line and therefore a number of alternative signalling pathways originating upstream of MEK are expected. Furthermore, there is increasing evidence of RAF-independent MEK signalling. These results are consistent with the theory that the MAPK pathway elicits oncogenic dependency (Weinstein & Joe 2008; Weinstein 2002), since many alternative pathways lead into the MAPK pathway via MEK and other upstream kinases.

4.4.3 Combination treatments

The general aim of this chapter was finding a combination of therapeutic agents more effective than monotherapy to take forward for nanoformulations and 3D testing. In many cancers, the MAPK pathway harbours constitutively active mutations in key proteins, eliciting the phenomenon of “oncogenic dependency” or “oncogenic addiction”, in which the cancerous behaviour of the cell heavily relies on signalling through this pathway (Weinstein & Joe 2008; Weinstein 2002). Although it is highly interconnected to other pathways, the interactions between certain proteins are almost exclusive, such as MEK-1 and MEK-2 being the only known substrates of

RAF, or the ERKs being the only known substrate of the MEKs (Ahn et al. 2001). This fact, together with the oncogenic dependency, throws light on the possibility of combining therapies that are closely related to the same pathway to achieve a synergistic effect.

Two different approaches have been explored in this chapter: one combining two small molecules (AZD6244 and ZD4054), and after their unexpected antagonistic effect, another one combining AZD6244 and target-specific siRNAs.

4.4.3.1 Combination of AZD6244 with ZD4054

The initial approach was combining two small molecules that could potentially show a synergistic inhibitory effect: AZD6244, an inhibitor of MEK-1/2 and ZD4054, a competitive antagonist of ETAR. Many therapeutic molecules have been combined with MEK inhibitors as a combination therapy, some with very positive outcome. Some of these combinations were with more toxic traditional chemotherapies such as irinotecan or docetaxel (Davies et al. 2007), and others aimed for specific cancer-related pathways such as BRAF inhibitors (Flaherty et al. 2012), or inhibitors of the PI3K/Akt/mTOR axis (Shimizu et al. 2012; Tentori et al. 2013). Similarly, ZD4054 showed promising efficacy *in vivo* combined with the cytotoxic drug paclitaxel, and the EGFR inhibitor gefitinib (Rosanò et al. 2007a; Rosanò et al. 2007b).

These results combining AZD6244 and ZD4054 were not so promising. In spite of the clear dose-dependent inhibitory effect of AZD6244 and the potential of ZD4054 in absence of ET-1 in these cell lines, the administration of both seemed to elicit an antagonistic response. Both metabolic activity and proliferation assays showed that concentrations of ZD4054 equal or superior to 100 nM in combination with 1 μ M of AZD6244 reversed the inhibitory effect of the later.

The reasons for this are uncertain, since no antagonistic effect of ETAR therapeutics has been reported before, but there could be a number of explanations for this unexpected cell behaviour. Some of the alternative pathways explained in the previous chapter that could have hindered the efficacy of MEK inhibitors might also

have a role in this antagonism. The binding of ETAR to its ligand ET-1 activates wild-type BRAF, which is more abundant in HCT116 cells than HT29 cells. The blockage of this receptor could therefore affect HCT116 cells slightly more, which is what we observe in our data.

Any pathway that cross-talks with the MAPK pathway could be affected by a positive or negative feedback, in the event of ETAR and MEK signalling being impaired or reduced simultaneously. ETAR signalling has a mitogenic effect through the activation of a number of proteins, such as PI3K, PKC, PLC, PLD, PLA2, adenylate cyclase, guanylate cyclase, Raf-1, IP3, diacylglycerol (DAG), akt, mTOR, COX-1, COX-2, and prostaglandin E2 (Grant et al. 2007; Blaukat et al. 2000; Shome et al. 2000).

As considered in chapter 3 (pg. 42), the activation of the Wnt/FDZ pathway is partially responsible of the suboptimal effect of AZD6244 on HCT116 (Tentler et al. 2010). Also, the inhibition of MEK could activate the PI3K/mTOR/Akt pathway (Mirzoeva et al. 2009) and reactivation of MEK and ERK might lead to resistance to BRAF inhibitors (Johannessen et al. 2010; Nazarian et al. 2010), which at the same time could cause secondary malignancies in other tissues by fostering MAPK pathway signalling (Heidorn et al. 2010; Poulikakos et al. 2010; Arnault et al. 2012). Any of these paradoxical feedbacks could be of a similar nature to the ETAR and MEK dual blockade antagonistic effect.

The fact that a portion of the ETAR pathway signalling is upstream of KRAS indicates that more alternative pathways would be involved in both HT29 and HCT116 cells than in the case of a direct phosphorylation of BRAF. Some of these alternative pathways involve PI3K or PKC, which have been proven to be part of the ETAR signalling network (Grant et al. 2007; Asham et al. 2001), among many others.

One of the major ways by which ETAR induces proliferation is the transactivation of other surface receptors. For example, Vacca and colleagues demonstrated that ET-1 induced phosphorylation of EGFR in ovarian carcinoma cells and this is in part what triggers ET-1-mediated mitogenesis (Vacca et al. 2000). Similar data was reported by Grant and colleagues in colorectal cancer cells (Grant et al. 2007). In human smooth muscle cells, ET-1 increases the effect of PDGF, which interacts with similar

surface receptors (Yang et al. 1999). This receptor transactivation has been exploited to find successful therapeutic combinations, such as the tumour regression achieved after co-administration of ZD4054 and gefitinib on ovarian carcinoma xenografts (Rosanò et al. 2007b).

The success of ZD4054 in combination with paclitaxel and gefitinib suggests that the antagonistic effect we observed in combination with a MEK inhibitor could just be due to the lack of exogenous ET-1 or the suboptimal efficacy of ZD4054 itself.

However, human cancer cell lines, including colorectal, produce large amounts of ET-1 *in vitro* (Kusuhara et al. 1990; Sone et al. 2000) and the autocrine effect of ET-1 has been demonstrated in colorectal cancer cell lines (Ali et al. 2000), suggesting that ZD4054 should have some inhibitory effect and at least not induce proliferation. Also, the inhibitory effect of the dual surface receptor inhibition (ETAR and EGFR) observed in ovarian cancer (Rosanò et al. 2007b) could be due to the inhibition of alternative pathways that signal upstream of MEK, although most of these pathways eventually lead to MEK (Grant et al. 2007; Asham et al. 2001; Shome et al. 2000; Blaukat et al. 2000). In any case, the efficacy of this combination could change drastically if an active ET-1 that consistently triggers ETAR signalling could be included in the experiment, or if the efficacy of ZD4054 could be properly assessed as a monotherapy.

4.4.3.2 Combination of AZD6244 and target-specific siRNAs

Surprisingly, ETAR-specific siRNA did elicit an inhibitory response in the absence of AZD6244, while the addition of AZD6244 apparently reversed this inhibitory effect (Figure 4.12). Since, to my knowledge, the silencing of ETAR has never been used as a therapy, it is difficult to put these results into context. However, the fact that the inhibition of MEK cancels the inhibitory effect of ETAR silencing suggests that the effect of AZD6244 could simply be overtaking that of ETAR silencing. Note that the control for the combination of AZD6244 and ETAR silencing contains AZD6244 and scrambled siRNA (Figure 4.12). Since ETAR signalling indirectly acts through the MAPK pathway, the blocking of MEK1/2 by AZD6244 might be the limiting point regardless of a reduction in ETAR signalling.

Since MEK1/2 are widely used targets for small molecules, the use of siRNA directed against these molecules is seldom used as a therapeutic agent, while many studies have used siRNA to knock down MEK in order to study the effect of both upstream and downstream proteins of cancer pathways. To my knowledge, this is the first time a small molecule and siRNA have been targeted against the same protein as a therapeutic approach. Results were interesting, since it showed a statistically significant difference compared to the small molecule on its own.

In order to explain the results obtained from the AZD6244 and MEK silencing combination it should be pointed out that we are observing changes in metabolic activity, not proliferation *per se* (Figure 4.12).

Overall, the effect of AZD6244 as a small molecule inhibitor on metabolic activity appears to be more efficient than silencing MEK1/2. There are some pieces of evidence in favour of a stronger effect of AZD6244. First, AZD6244 inhibits both the already existing active and inactive forms of MEK1/2 in colorectal cancer while siRNA can only prevent the translation of new protein. Therefore the effects of siRNA are more likely to be compensated by the pre-existing protein. Besides, AZD6244 has been reported to induce apoptosis, suggesting that it is not only cytostatic but in fact cytotoxic (Huynh et al. 2007; Troiani et al. 2012).

As mentioned earlier, the increase in metabolic activity observed in the MEK1-, MEK2-, and MEK1/2-specific siRNA treatments could just be to compensate a reduction in MAPK signalling. In the absence of the apoptotic effect of AZD6244, this could translate in an overall increase in metabolic activity. However the silencing of MEK1/2 expression in combination with the blockage of active and inactive forms of the pre-existing protein do elicit an additive inhibitory effect, which is significant considering the difference between AZD6244 alone and the combination is statistically significant ($p < 0.001$, Figure 4.12), and so is the difference between AZD6244 and the untreated control ($p < 0.001$, Figure 3.12).

The silencing of MEK1 in the absence of AZD6244 enhanced metabolic activity more effectively than the silencing of MEK2, and in the presence of AZD6244 its inhibitory effect was also lower. This could be explained under the hypothesis that MEK2 has the ability to compensate for the absence or reduction of MEK1, including specific

data on HCT116 cells (Ussar & Voss 2004; Sturgill 2008), which also makes the former a better target for cancer therapy. This is especially surprising considering that HCT116 cells express significantly more MEK1 than MEK2 mRNA (also probably the reason why double the amount of siRNA was needed to knock-down expression levels), so it could be expected that a greater reduction in the levels of a key protein would have a greater proliferation inhibitory effect. Additionally, the higher activity of MEK2 over MEK1 could be supported by the fact that MEK2, unlike MEK1, is not activated by serum (Xu et al. 1997) and all these treatments were in fact performed in the absence of serum, potentially increasing the importance of MEK2.

4.4.4 Selected molecule for nanoformulations and 3D culture testing

The work performed in this and the previous chapter yielded both positive and negative results. While both the inhibition and silencing of MEK1/2 showed inhibitory promise at the proliferation, metabolic activity and molecular levels, studies on the endothelin axis have been challenging and mostly unfruitful from the very beginning.

The inability of ZD4054 to elicit a significant and reproducible inhibitory response, either alone or in the presence of ET-1, combined with its antagonism of AZD6244-mediated inhibition was instrumental in the decision to abandon the endothelin axis completely and focus on MEK1/2 as the only target for nanoformulations and studies using a 3D model. Due to the oncogenic dependency that the MAPK pathway elicits on these cells (Weinstein 2002; Weinstein & Joe 2008) the inhibition of MEK1/2, although not optimal, should be sufficient for further investigations.

While results from the use of MEK1- and MEK2-specific siRNAs alone and in combination with AZD6244 do suggest a potential combination therapy, there are some limitations regarding the use of siRNA as a therapeutic. First and foremost, the clear toxicity elicited by all siRNA treatments, including the non-target-specific control, supposes too much of a toxicity risk for the rest of this research. Whilst it is not clear whether it is the method of transfection or the effect of the siRNA itself, any inhibitory success derived from siRNA as a therapeutic agent would potentially be

related to this off-target toxicity. However, it must be noted that, in general terms gene silencing remains a promising anti-cancer therapeutic approach (Ryther et al. 2005; Misale et al. 2014). Secondly, however significant, the additional inhibitory potential achieved by combining AZD6244 with MEK-specific siRNA was so subtle that the creation of a dual-cargo nanoformulation of this complexity with no guarantee of success would not be worth the time and resources.

For these reasons, AZD6244 was once again selected as the only therapeutic molecule to undergo nanoformulations and 3D testing in the following chapters.

CHAPTER 5

Nanoparticle Fabrication & Characterization

5 Nanoparticle Fabrication and Characterization

5.1 Introduction

AZD6244 was chosen for nanoparticle-mediated drug delivery in 2D and 3D colorectal cancer models. This chapter contains everything related to the fabrication and characterization of nanoparticles, including micelles and liposomes loaded with AZD6244 as a therapeutic agent, Nile Red and quantum dots as fluorescent tracking agents and control nanoparticles containing only water. During fabrication, different approaches and techniques were evaluated to optimize the nanoparticles before testing them on cell monolayers and tumouroids as described in the next chapter.

5.2 Materials and Methods

5.2.1 Fabrication of liposomes made from cholesterol and phospholipids

DC-cholesterol, DOPE and DOPC (Figure 5.3) were obtained from Avanti polar lipids (Alabama, USA). Liposomes were fabricated using variations of some of the protocols described by Mozafari (Mozafari 2010). The process can be divided in two fundamental parts: 1) the formation of large vesicles by rehydrating a thin layer of lipid components attached to a glass surface, and 2) the formation of nanoliposomes derived from these vesicles. The second part of the protocol was initially achieved through ultrasonication, but it was later substituted by extrusion, during the methodological development phase.

5.2.1.1 *Thin layer rehydration method*

Equimolar concentrations (5mM) of DOPE (or DOPC) and DC-cholesterol (Avanti polar lipids) were dissolved in chloroform-methanol (2:1). This represents a relatively high amount of cholesterol, in order to provide good stability and low leakage of the content out of the nanocarrier, as well as increase the fraction of cationic moieties in the surface. If a hydrophobic molecule was to be encapsulated in the batch, 2mM of AZD6244 or Nile Red were included in the mixture at this stage. Organic solvents are essential for the dissolution of hydrophobic molecules, such as cholesterol, phospholipids, and small molecules like AZD6244 or Nile Red. The final concentration in the mixture for both the phospholipid and cholesterol components was 5mM, and the volume was 9mL. The mixture was placed in a rotaevaporator to remove the solvents and leave a thin film in the inner surface of the glass containing the lipids. To remove any trace of solvents left, the film was further dried with N₂.

Note: Nile Red is a dye that only fluoresces in a hydrophobic environment and is therefore suitable to selectively track nanoparticles with a hydrophobic regions such as liposomes and micelles.

The thin film containing the hydrophobic components was then rehydrated in 10mL of deionized water. If hydrophilic gold quantum dots were encapsulated within the aqueous core of the nanoparticle, 1 mg of these were included in the 10mL rehydration solution. A combination of 1 minute vortexing and 5 minute sonication in a water bath were used to fully detach all layers of lipids from the surface, which spontaneously formed large multilamellar vesicles (MLVs).

5.2.1.2 Ultrasonication method

For the ultrasonication method, MLVs were transferred to a beaker and left for 1 hour at room temperature to stabilise. The beaker was then placed in a water bath and calculated probe sonication steps were used to turn MLVs into nanoliposomes. Probe sonication cycles consisted of 20 sec ON/OFF at a pulsed rate at amplitude 30% for a total time of 10 min (Cole-Palmer Instruments, Illinois, USA). The suspension was then centrifuged at 12000 x g for 30 min to remove large lipid clusters, and the remaining solution was left at room temperature for 1 hour to stabilise again. Nanoliposomes were dialysed against deionised water for six cycles of two h using a 10 mm diameter, 12000 kDa cut-off membrane (Sigma Aldrich) to remove unencapsulated drug or fluorescent marker, and then stored at 4°C.

5.2.1.3 Extrusion method

For the extrusion method, MLVs were transferred to a polystyrene tube and left for 1 hour at room temperature to stabilise. The suspension was then extruded 14 times through a polycarbonate membrane (7 through 1000nm and 7 through 200nm) using a liposome extruder with 1 mL syringes (Figure 5.1) (Avanti polar lipids, Alabama, USA) and always keeping the first loading syringe separated from the last receiving syringe to minimize debris (Figure 5.2). Nanoliposomes were dialysed and stored as in the sonication protocol. This method, although more complex, was eventually chosen for liposome fabrication and cell *in vitro* testing for a number of reasons. Since the last part of the thin layer step involves detaching the lipids from the glass

using ultrasonication, the thin layer-extrusion combination does involve a small ultrasonication step and therefore some nanoliposomes do form before extrusion.



Figure 5.1 Liposome extruder and support with 1 mL air tight glass syringes (Avanti Polar Lipids). A polycarbonate membrane flanked by filter supports is placed between two teflon membrane supports and the system is locked using an outer casing and a nut. The extruder containing the membrane is then placed on a support and the syringes are introduced into the membrane supports through the sides.

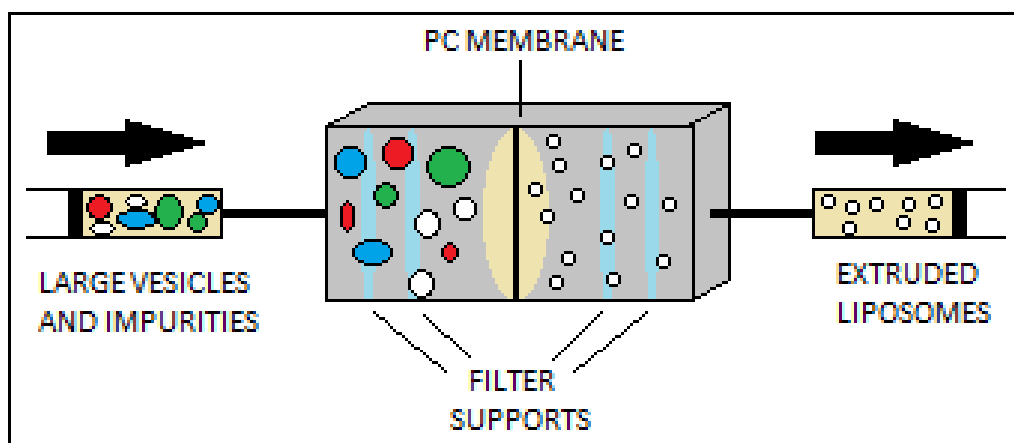


Figure 5.2 Extrusion method. A solution of large vesicles is injected into the left side of the extruder. The particles are forced through two support filters, a polycarbonate membrane and another two support filters. Nanoliposomes are collected on the right side syringe and the process is repeated back and forth between both syringes 7 times through a 1000nm polycarbonate membrane and another 7 times through a 200nm polycarbonate membrane. The last extrusion is collected on the right side syringe to remove large debris.

5.2.1.4 Liposome methodological development

Before the fabrication of AZD6244- and Nile Red-loaded liposomes for drug treatments and penetration studies, a few experiments aimed at optimizing encapsulation and liposome formation were performed. To create fluorescent liposomes at this stage, 1 mg of gold Quantum Dots was added to the rehydration phase at the final stage of the thin layer method. Upon rehydration of the lipid layer, these hydrophilic QDs were encapsulated in the liposomes aqueous core. Confocal microscopy was used to image these fluorescent nanoparticles, mostly as precipitated aggregates due to the difficulty to image a single nanoparticle in suspension. An attempt was made, however, to image single liposomes by suspending them in glycerol, with the resultant viscosity slowing down their movement.

5.2.2 Fabrication of micelles made from GCPQ

5.2.2.1 Polymer synthesis and characterization

Unlike the liposome components, which were purchased commercially, quaternary ammonium palmitoyl glycol chitosan (GCPQ) was synthesized in the laboratory prior to its use to encapsulate a hydrophobic molecule. GCPQ was fabricated following the protocol described in (Uchegbu et al. 2001), with slight modifications. The polymer was provided by Professor Uchegbu's research group (School of Pharmacy, UCL), and all experiments involving GCPQ micelles on cell monolayers and tumouroids derive from the same highly palmitoylated batch of the polymer.

5.2.2.2 GCPQ micelle fabrication

Using the previously synthesized polymer, micelles were fabricated following a modified version of the protocol described in (Qu et al. 2006). This protocol is similar to the liposome ultrasonication method, but the nature of the polymer induces the formation of micelles. 20mg of highly palmitoylated GCPQ polymer (palmitoylation=18.9%, quaternization=11.2%, MW=17,120 g/mol), were dispersed in 2 mL of deionised water. For micellar formulations encapsulating a hydrophobic molecule, either 2 mg of AZD6244 or 1.3 mg of Nile Red were added to this solution. The mixture was vortexed until it became turbid and sonicated in a water bath for one minute to assist homogenisation. The homogenised solution contained in a glass vial was placed inside an ice bath to reduce sample heating and probe-sonicated with amplitude 45% for six five-minute cycles alternated with three-minute breaks (Qsonica, Connecticut, USA). The sonicator tip was placed just below the surface of the fluid to minimize the formation of foam. The resulting GCPQ micelles were allowed to stabilize for 15 min at room temperature before filtration through a 0.45 µm filter and centrifuged at 1000 x g to remove unencapsulated drug crystals. Due to the inclusion of this step, AZD6244-loaded micelles were not dialysed to remove unencapsulated drug like in the case of liposomes, while Nile Red-loaded

micelles underwent identical dialysis steps to the liposomes. After fabrication, GCPQ micelles were also stored at 4°C.

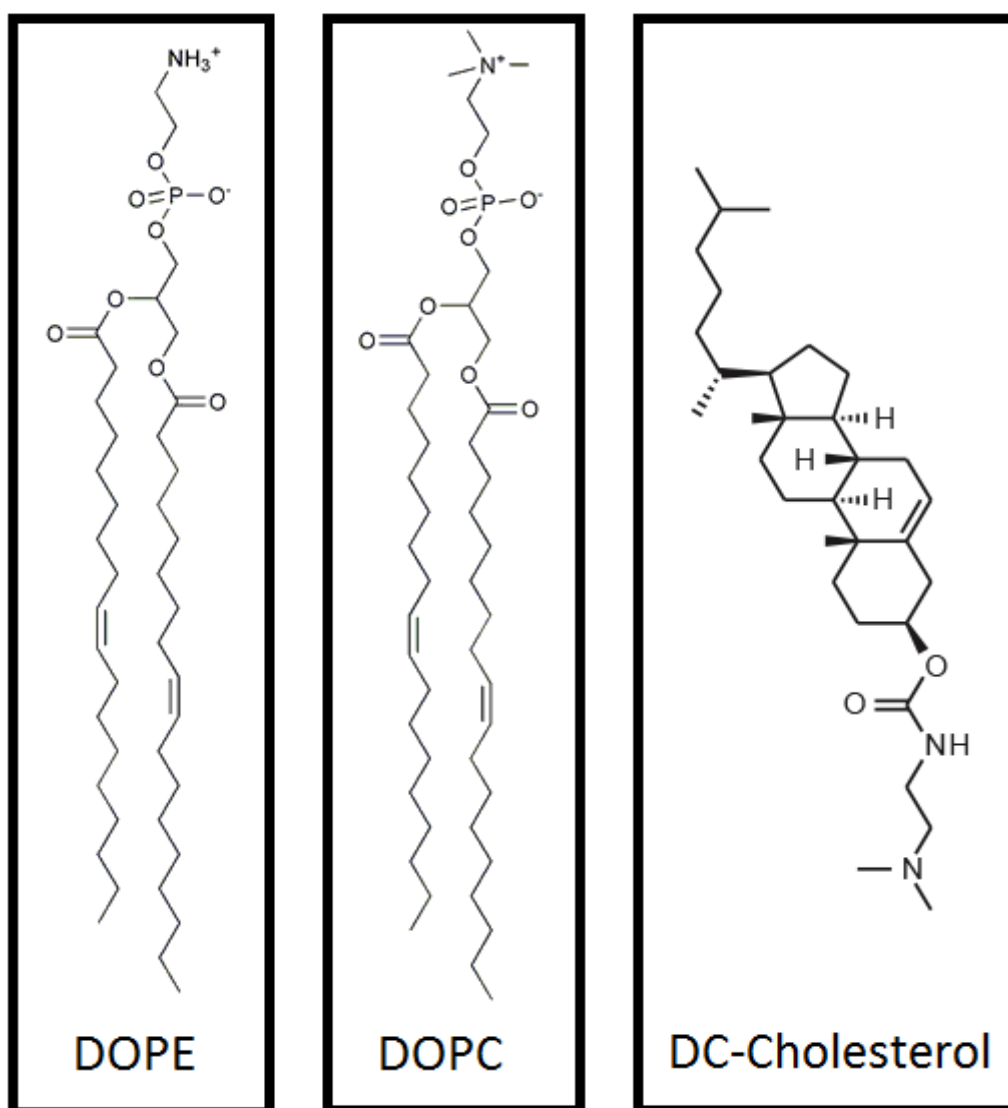


Figure 5.3 Chemical structure of liposome components. Liposomes were fabricated using equimolar ratios of DOPE and DC-cholesterol or DOPC and DC-cholesterol.

5.2.3 Fabrication of gold Quantum Dots

Gold quantum dot fabrication was undertaken by Dr. Bala Ramesh (Division of Surgery, UCL). Before fabrication, glassware was washed with chromic acid and ammonium hydroxide to remove impurities. HAuCl₄ (20mM) and MSA (20mM) were mixed in a 20mM Na₂B₄O₇ and 20mM of trisodium citrate buffer solution adjusted to

pH 7.2, and underwent vigorous stirring for 10 min before being transferred to a single neck flask attached to a condenser and refluxed at 250°C with mixing. 500 µL of DMF were then added drop by drop to the mixture as a reductant until colour change to light brown was observed after one hour, indicating the presence of gQDs. The maximum emission of gQDs is located at 800 nm wavelength in the near infrared region. All chemical used in this synthesis were purchased from Sigma-Aldrich.

5.2.4 Nanoparticle characterization

5.2.4.1 *Dynamic light scattering (DLS)*

Dynamic light scattering (DLS) was used to determine the size of nanoparticle and nanoparticle aggregates in an aqueous solution. A diluted suspension of nanoparticles was placed in a disposable cuvette and measured 3 times for 15 repeats each for size analysis in a Malvern Nanosizer ZS (Malvern, Worcestershire, UK). For the analysis, parameters were set to backscatter mode and a 1.33 dispersant refractive index. Results are shown maintaining the format of the Malvern Zetasizer software.

5.2.4.2 *Transmission electron microscopy (TEM)*

Transmission electron microscopy (TEM) was used to visualize the particles in the nanoscale, and to determine their morphology and approximate size. An aqueous suspension of nanoparticles was placed on a Formvar © / Carbon Coated Grid (F196/100 3.05 mm, Mesh 300, Tab Labs Ltd, England) and stained with a 1% w/v aqueous solution of uranyl acetate. However, no negative staining was needed to image gold QDs, as they are electron dense. TEM images were taken at a minimum of 30000 X magnification using a Philips CM120 BioTwin transmission electron microscope, (Philips, Eindhoven, The Netherlands) with a AMT 5 megapixel digital camera (AMT, UK).

5.2.4.3 Encapsulation efficiency and compound measurement (HPLC)

Drug content of both formulations was determined by HPLC against a standard curve of free AZD6244 (Figure 5.4). This standard curve was repeated before every set of measurements to minimize possible variations caused by the UV lamp losing power through usage. Samples were diluted in methanol (1:3 for micelles and 1:25 for liposomes) to break the nanoparticles open and then filtered through a 0.2 μm membrane prior to chromatography analysis. 30 μL of the sample were chromatographed over a 5 μm bead, 4.6 mm diameter, 100 mm length Luna C18 reverse phase column preceded by a Safeguard pre-column (Phenomenex, Cheshire, UK) at 25 C, using a Waters TM717 autosampler, a Waters TM515 HPLC pump and a TM486 absorbance detector set at 260nm wavelength (Waters, Hertfordshire, UK). The mobile phase was HPLC grade methanol with an isocratic flow rate of 0.8 mL/min, and AZD6244 showed a retention time of 21.5 min under these conditions. The concentration of AZD6244 contained in liposomes and micelles was extrapolated from the standard curve.

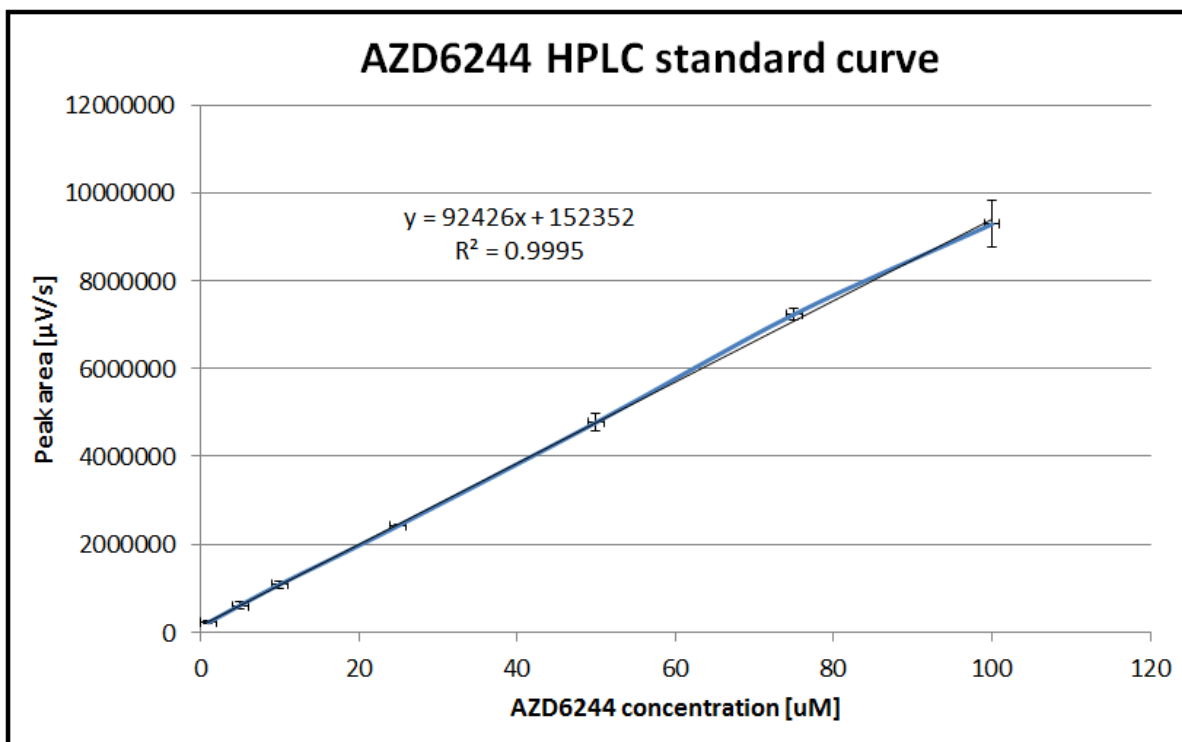


Figure 5.4 Example of AZD6244 standard curve. Different concentrations of AZD6244 were used to create a standard curve on HPLC before each set of measurements. Standard curves such as this one were used to extrapolate the drug content within the nanoparticles, after releasing the drug using methanol.

5.2.4.4 Confocal microscopy

In this chapter, confocal microscopy was used to evaluate the potential of liposomes to internalize a hydrophilic molecule. These preliminary experiments were initially designed to inform further experiments involving the encapsulation of nucleic acids such as the siRNA treatments tested in chapter 4 (pg. 82). While AZD6244 was eventually selected as the only therapeutic molecule for nanoformulations, these experiments helped determine the nature and morphology of the liposomes.

Furthermore, the penetration of quantum-dot loaded liposomes into the tumouroids and their individual aggregates established the basis for penetration studies included in section 6.3.7. (pg. 162).

500 μl of liposome solution were placed in a 24-well plate, and confocal images were taken from the precipitated aggregates at the bottom of the well or from

nanoparticles suspended in the fluid. The excitation wavelength for gold quantum dots was 488 nm and the detected wavelength was 650 nm.

5.3 Results

5.3.1 Liposome methodological development

As mentioned earlier, the protocol used here for liposome fabrication involved two steps. The first step consisted on dissolving the lipid components in organic solvents and letting them form a thin lipid layer on a glass surface after evaporation. When this layer was rehydrated with deionised water, large vesicles formed. Several attempts were undertaken to image both the large vesicles and subsequent nanoliposomes in solution, by encapsulating hydrophilic gold quantum dots into their aqueous core. However, this presented many complications since the particles tended to aggregate and precipitate and they also quickly drifted when dispersed in aqueous media (Figure 5.5).

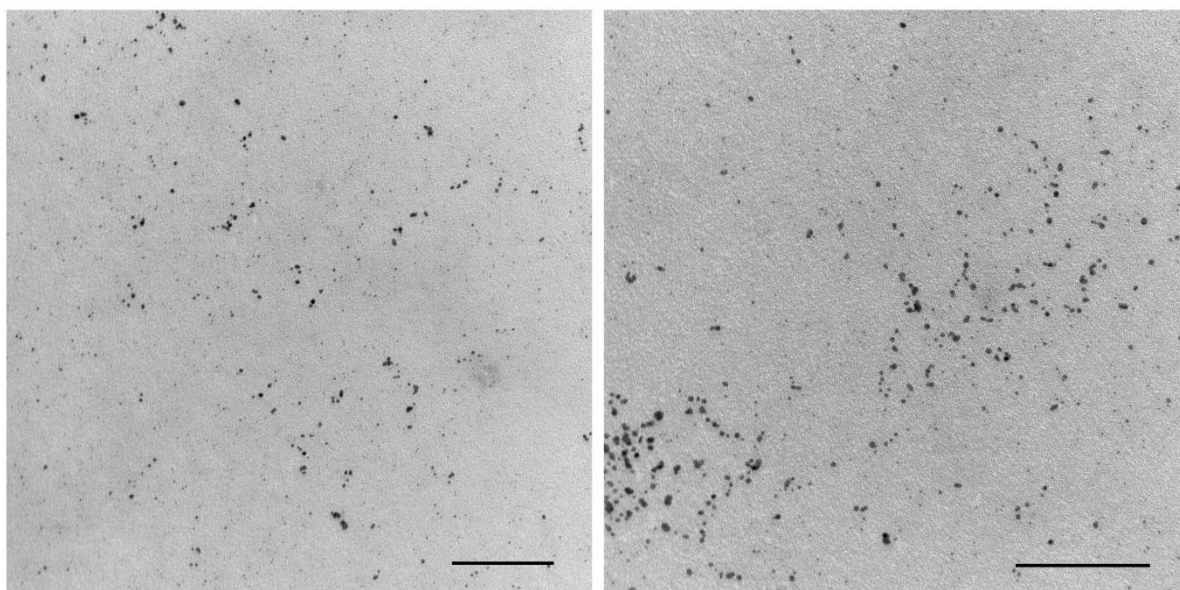


Figure 5.5 TEM images of gold quantum dots (gQD). (Left) magnification 175000X, HV=80.0kV, scale bar = 100 nm. (Right) magnification 230000X, HV=80.0kV, scale bar = 100nm. gQDs were encapsulated into liposomes for imaging purposes.

As shown, these large vesicles successfully encapsulated gold quantum dots that were added to the aqueous phase during the rehydration step. The fluorescent

signal emitted by the quantum dots co-localizes with the black and white image of the organic nanoparticles. Large vesicles formed large aggregates in the aqueous solution and this caused them to precipitate to the bottom of the 24-well plate (Figure 5.6).

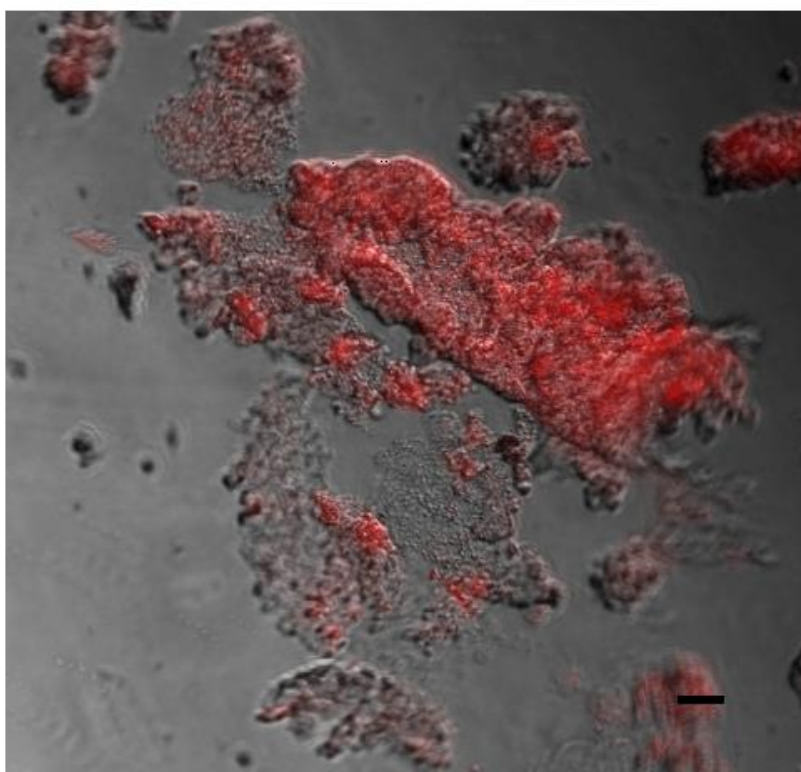


Figure 5.6 Gold quantum dot-loaded vesicles form large precipitates in aqueous solution. Large fluorescent vesicles were imaged as a precipitate at the bottom of a 24-well plate using confocal microscope. Scale bar = 20 μm .

The imaging of the large vesicles in suspension was attempted; however, their fast movement did not allow obtaining a clear image. By suspending the vesicles in glycerol instead of water, a blurred image of individual moving nanoparticles in solution could be obtained due to the high viscosity of the dispersion medium (Figure 5.7). Both fluorescent (encapsulating quantum dots) and hollow moving vesicles were visible.

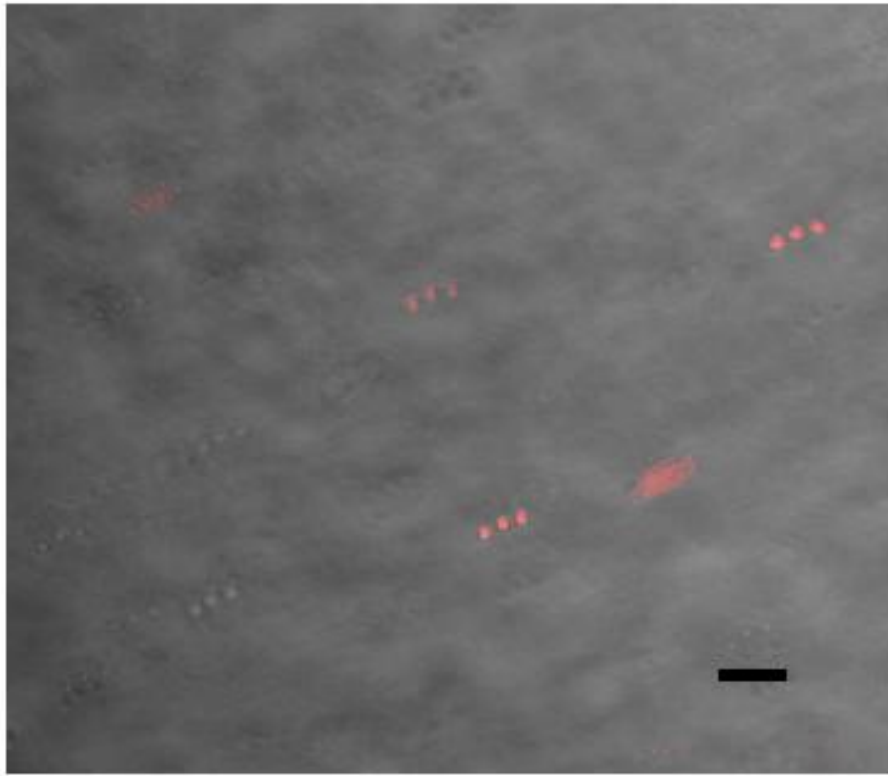


Figure 5.7 Gold quantum dot-loaded and empty large vesicles suspended in glycerol. Scale bar = 20 μ m

After the rehydration step and formation of large vesicles, two methods were explored to create nanoliposomes: ultrasonication and extrusion. (Figure 5.8) shows TEM images of after following both methods, which produced similar nanoparticle morphology and size. DLS analysis also showed similar sizes for the nanoliposomes in aqueous suspension, around 165-180 nm in diameter (Figure 5.9 and Figure 5.15a) regardless of the fabrication method.

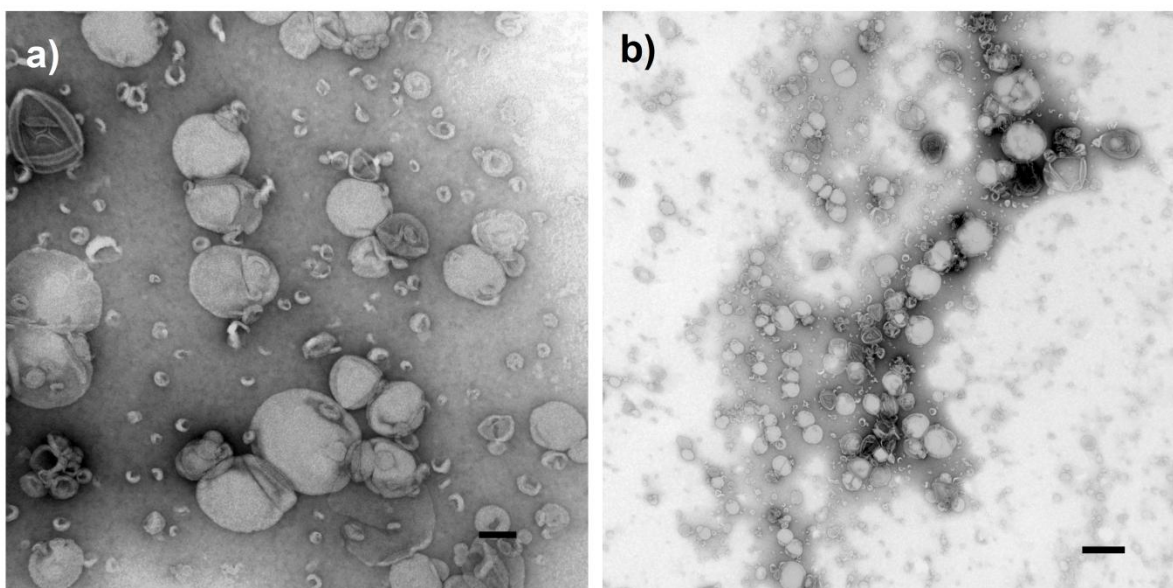


Figure 5.8 TEM images of nanoliposomes fabricated using two different methods. Ultrasonicated nanoliposomes (left, HV=80.0kV, scale bar = 100nm, magnification 66000X) and nanoliposomes extruded through 1000nm and 200nm polycarbonate membranes (right, scale bar = 500nm, HV=80.0kV, magnification 15000X) show similar morphology and size under TEM.

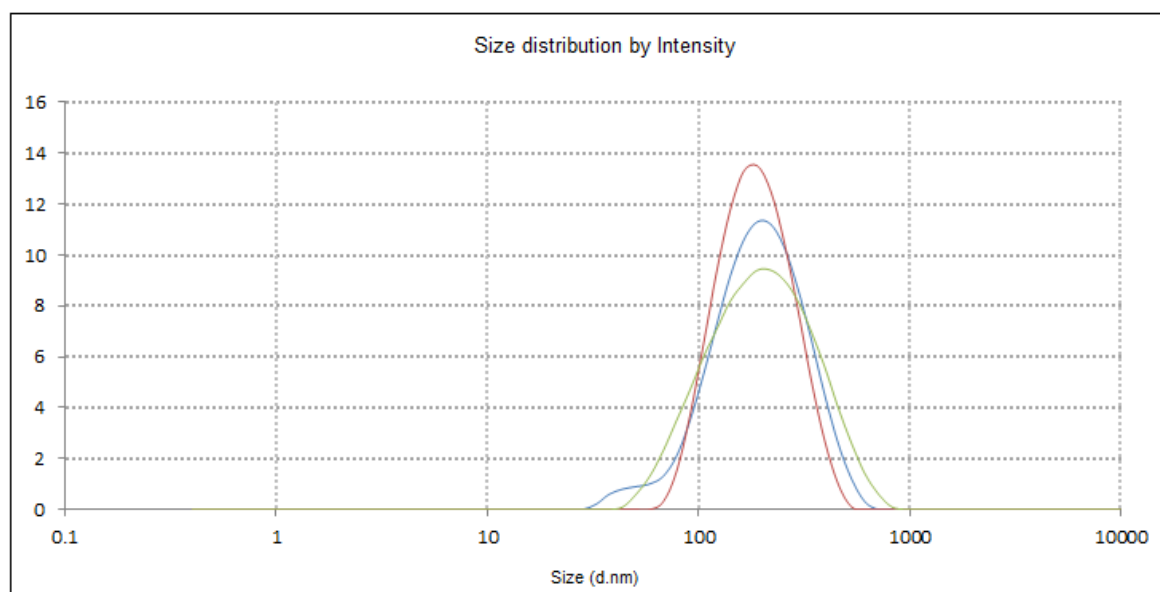


Figure 5.9 DLS analysis of ultrasonicated liposomes. Vesicles were probe sonicated for 10 min following ON/OFF pulsed cycles at 30% amplitude, allowed to stabilize for an hour and dialysed against deionised water. Each colour represents a measurement repeat. The format for this graph is slightly different from those of extruded liposomes and GCPQ micelles because it was outsourced to Malvern instrument Ltd. during the initial stages of this research.

The extrusion method was chosen over the ultrasonication method for further experiments due to its less aggressive nature and very positive reports in the literature. Thus, extrusion was used to create nanoliposomes derived from large vesicles encapsulating gold quantum dots, for similar imaging purposes. The resulting nanoliposomes were also imaged using confocal microscopy. The removal of large lipid debris and the overall reduction in particle size seemed to disperse the nanoliposomes slightly more compared to the large vesicles (Figure 5.10). Co-localization of fluorescent quantum dots and the clearly defined nanoliposomes suggests that the interaction between both nanoparticles was kept after extrusion. Both quantum dot-loaded (fluorescent) and hollow (non-fluorescent) nanoliposomes were visible. A higher magnification of these nanoliposomes revealed that the quantum dots were in fact encapsulated within the aqueous core of the nanoparticle (Figure 5.11) as opposed to adsorbed to the outer surface as it is very common with nucleic acid-nanoparticle clusters.

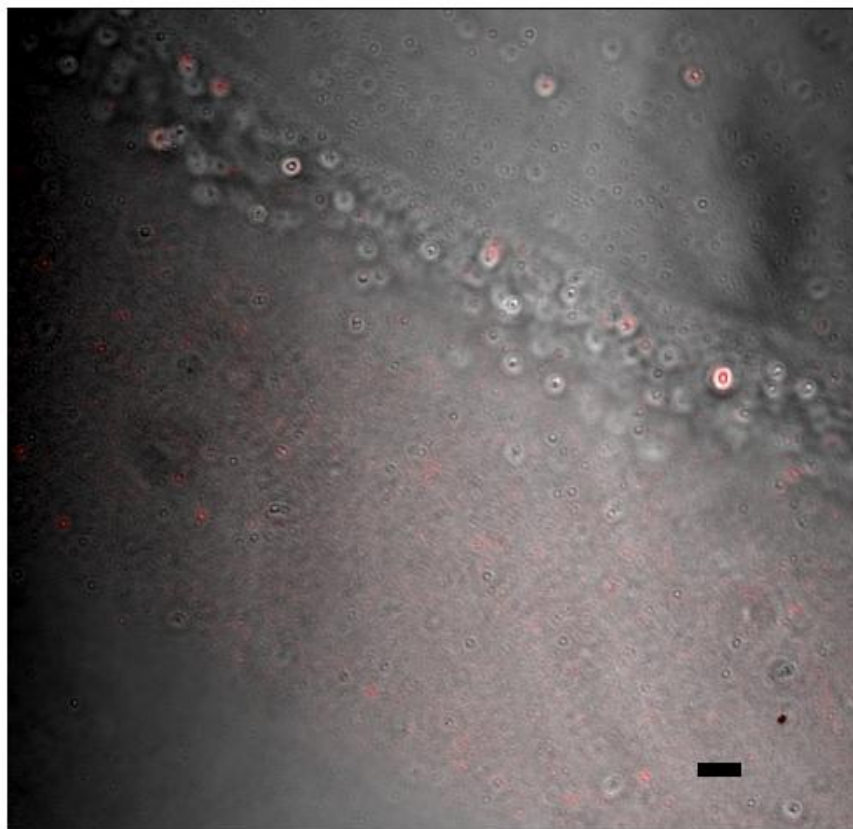


Figure 5.10 Quantum dot-loaded liposomes extruded through 1000 nm and 200 nm polycarbonate membranes. Nanoliposomes were imaged as a precipitate at the bottom of a 24-well plate using confocal microscope. Scale bar = 5 μm

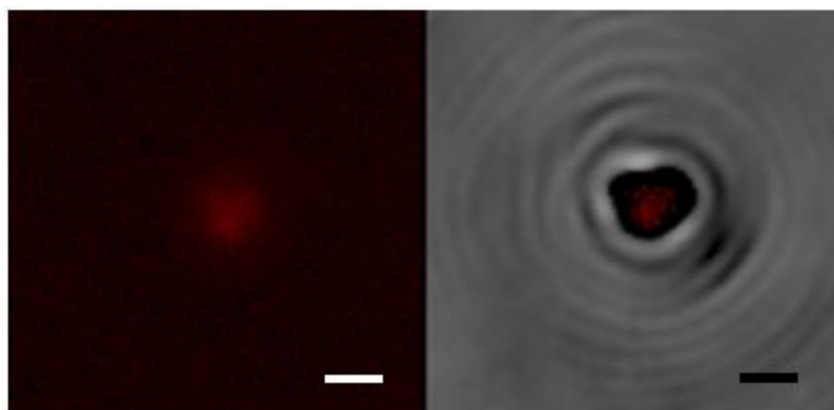


Figure 5.11 Higher magnification of a single liposome loaded with fluorescent Quantum Dots. The image reveals that the gold QDs are encapsulated in the aqueous core of the nanoparticle and not adsorbed to the surface of the membrane. Scale bar = 1 μm .

5.3.2 Micelle methodological development

While most of the methodological development regarding the GCPQ polymer and its micellar formulations was done previously by our group, it is worth including here an additional step in the micelle formation protocol that was included to solve a problem with the presence of drug crystals (Figure 5.12). Due to their large size and hydrophobic nature these crystals could be removed through simple filtration and centrifugation steps. Freshly formed micelles were allowed to stabilize for 15 min before they were forced through a 450 nm filter and centrifuged at different speeds for 15 min. Crystals were not visible in the 1000 x g and higher speed centrifugation samples. DLS analysis showed a drop in the size of micelle aggregates (and drug crystals) as centrifugation speed increased, reaching a plateau between 3000 and 4000 x g and a significant drop below 300 nm in average diameter at 2000 x g, which suggest a significant loss of usable micelles (Figure 5.13). For that reason a combination of filtration through a 450 nm filter and 15 minute centrifugation at 1000 x g were chosen as the preferred protocol to remove drug crystals with minimal loss of valid micelles.

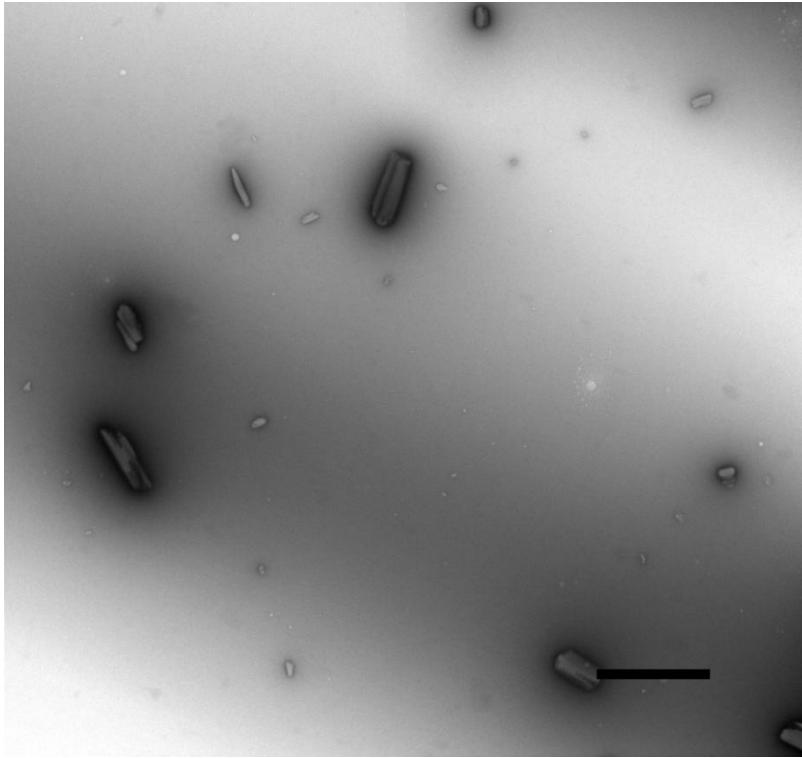


Figure 5.12: TEM image of AZD6244 crystal. Unencapsulated drug crystals were present in solution after the fabrication of AZD6244-loaded GCPQ micelles (scale bar = 2 μm , HV=120.0Kv, magnification 7400X).

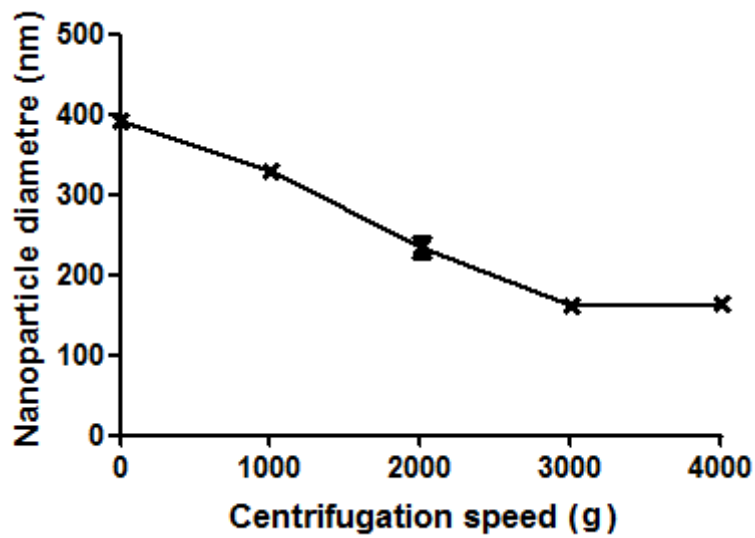


Figure 5.13: DLS analysis of size of AZD6244-loaded GCPQ micelles after different centrifugation speeds. Micelles were allowed to stabilize for 15 min before filtrated through a 450 nm filter and centrifuged at different speeds for 15 min.

5.3.3 Characterization of optimized DOPE/DC-cholesterol and GCPQ nanoparticles

After the fabrication parameters were established, these were used to create liposomes and micelles with three types of compounds (AZD6244, Nile Red and control nanoparticles) for all cell-related experiments described in chapter 6 (pgs. 155, 153, 157, 159, 162).

DOPE/DC-cholesterol liposomes were fabricated by dissolving the lipid components and hydrophobic molecules (AZD6244, Nile Red, or none) in a mixture of chloroform and methanol (2:1) and evaporating the solvents to rehydrate the remaining thin layer. The type of molecule did not influence the size or morphology of the liposomes, which remained spherical and in the same size range, as imaged by TEM (Figure 5.14a).

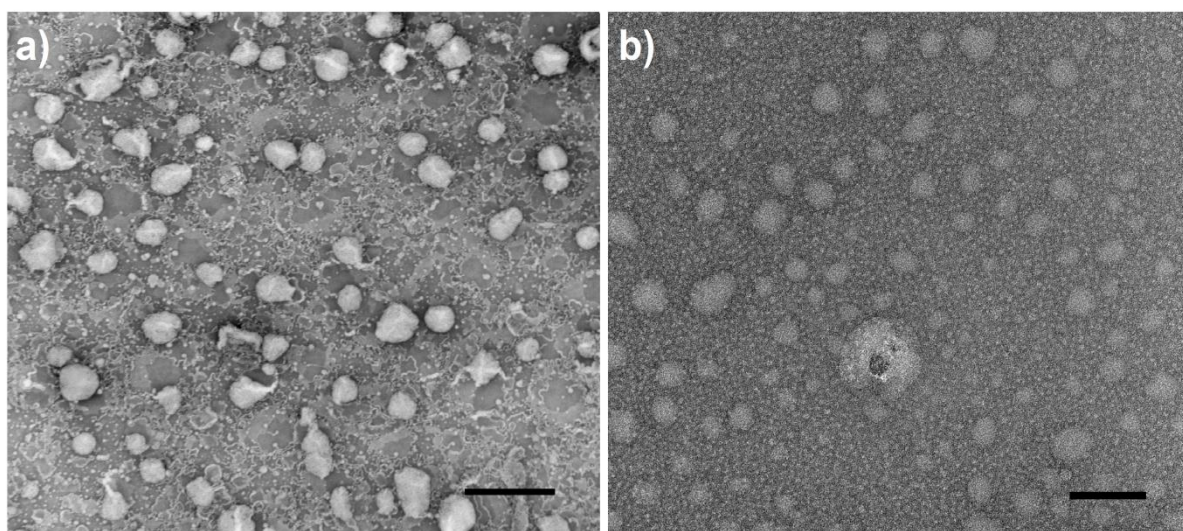


Figure 5.14: TEM images of organic nanoparticles. a) AZD6244-loaded DOPE/DC-Cholesterol liposomes (scale bar = 500 nm, magnification 31000X, 80.0 kV), b) AZD6244-loaded GCPQ micelles (scale bar = 100 nm, magnification 135000X, HV120.0 kV).

Sizes for AZD6244- or Nile Red-bearing liposomes ranged between 70 nm and 500 nm with the majority at approximately 170 nm, as shown by DLS analysis (Figure 5.15a/c). Occasionally, DLS analysis also revealed a very small peak at 3-6 μm , indicating the tendency of these nanoparticles to form aggregates in aqueous media. For control liposomes with no encapsulated molecules, the main peak at 180 nm

was very similar to that observed for the loaded nanoparticles, but with a broader size range (30 to 1100 nm) (Figure 5.17a). TEM revealed that the morphology of control liposomes was no different from those encapsulating a molecule (Figure 5.16a). A second type of liposome made of DOPC/DC-cholesterol instead of DOPE/DC-cholesterol was fabricated only for control nanoparticle testing purposes. These control liposomes showed a narrower size range very similar to the AZD6244-bearing DOPE/DC-cholesterol liposomes, in spite of not containing AZD6244 (Figure 5.17c). TEM images also showed a very similar morphology and size range to their DOPE/DC-cholesterol counterpart, with the exception of a seemingly slight less tendency to flattening on the carbon grid surface (Figure 5.16c).

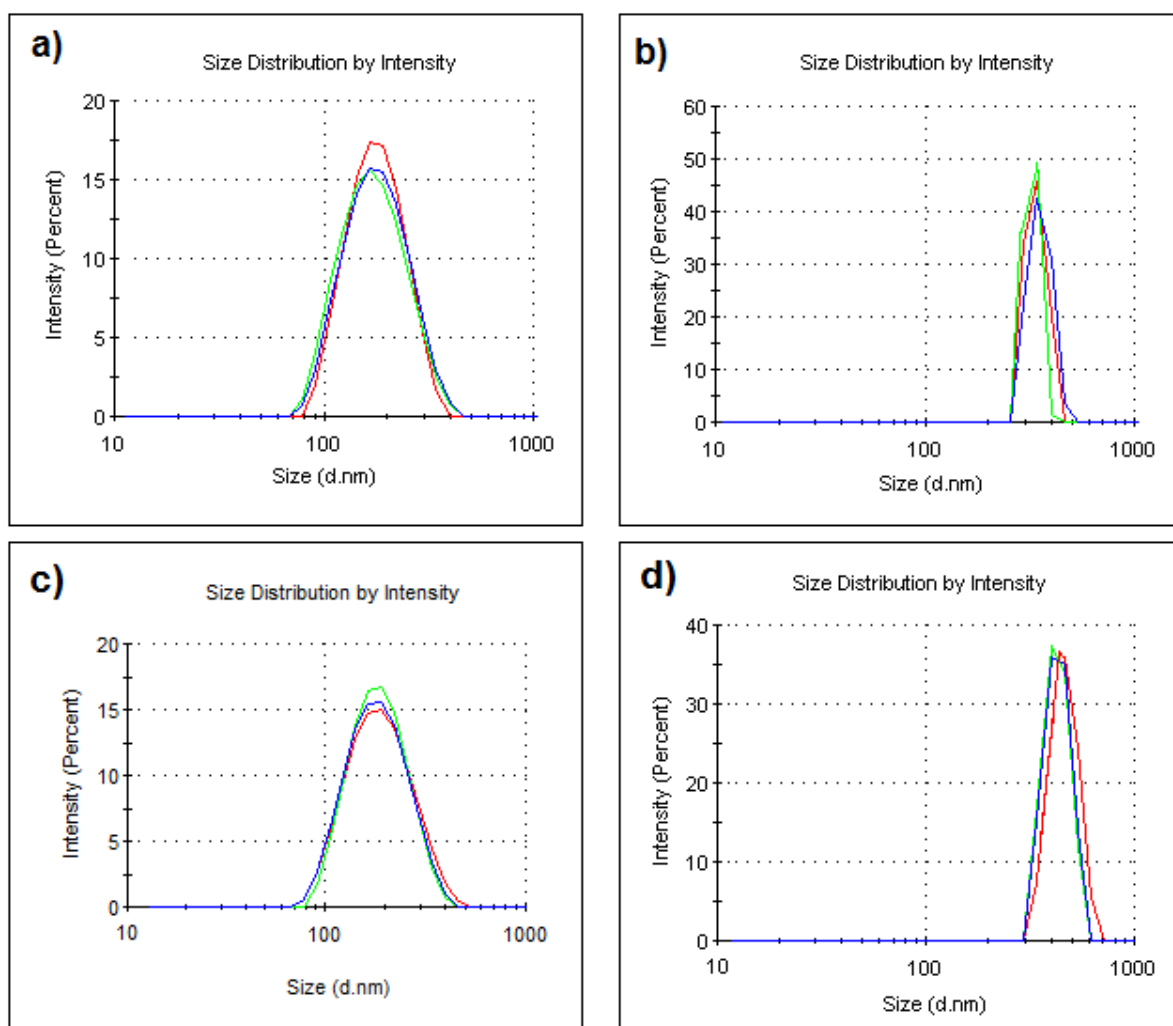


Figure 5.15: DLS analysis of organic nanoparticles. a) AZD6244-loaded DOPE/DC-cholesterol liposomes, b) AZD6244-loaded GCPQ micelles, c) Nile-red loaded DOPE/DC-cholesterol liposomes, d) Nile Red-loaded GCPQ micelles. Each colour represents a measurement repeat.

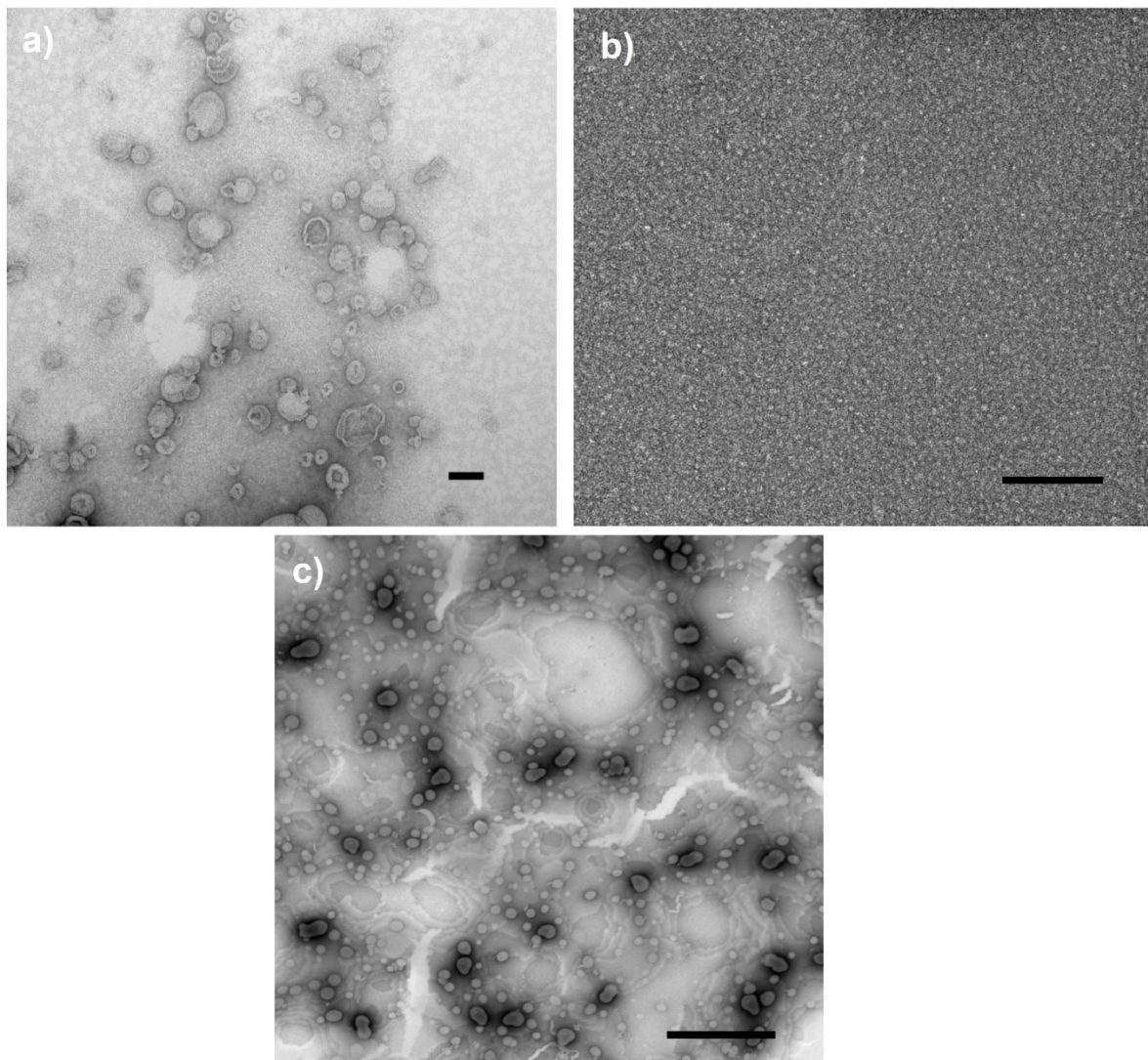


Figure 5.16 TEM images of control organic nanoparticles. a) DOPE/DC-Cholesterol liposomes with no encapsulated molecules (scale bar = 100 nm, magnification 66000X, HV=80.0kV), b) GCPQ micelles with no encapsulated molecules (scale bar = 100 nm, magnification 180000X, HV=120.0kV), c) DOPC/DC-Cholesterol

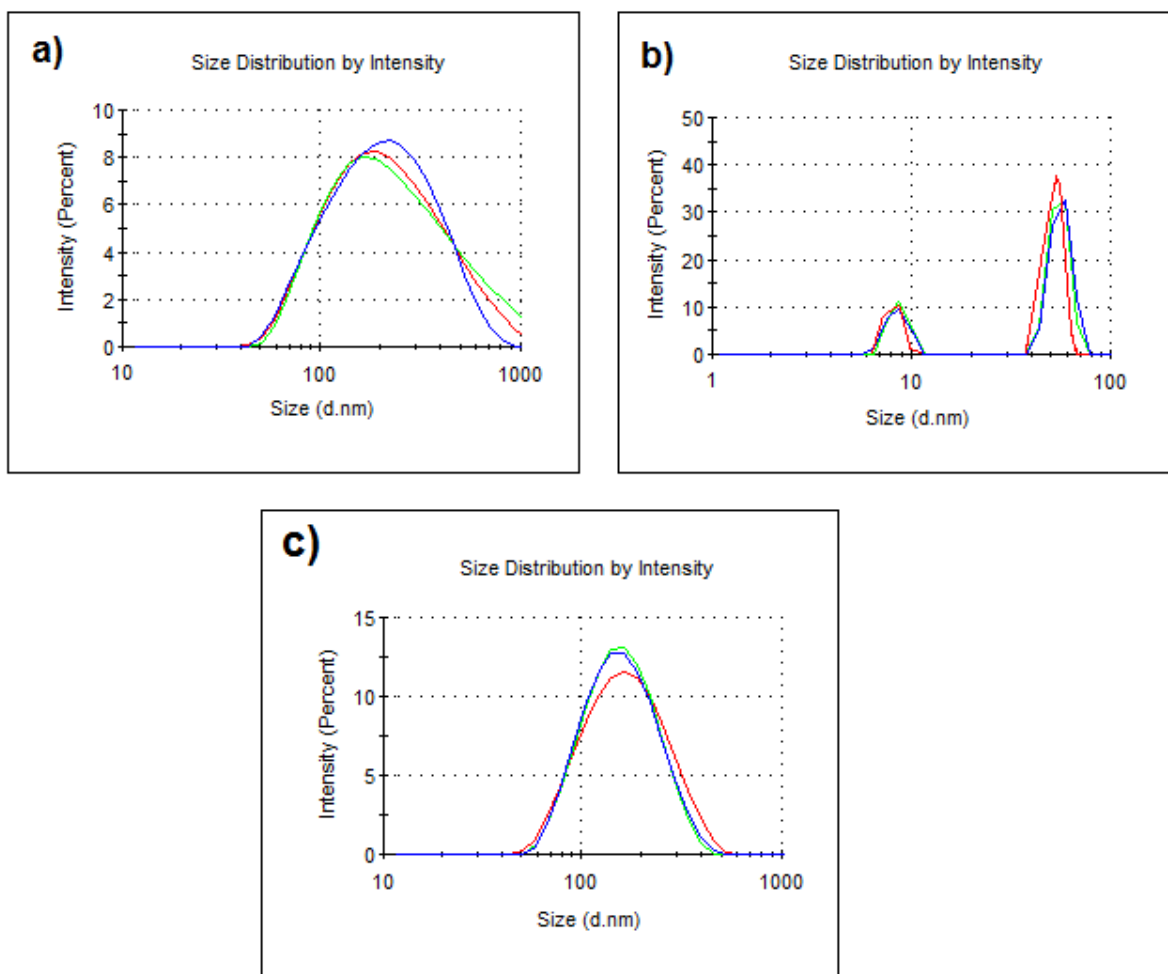


Figure 5.17 DLS analysis of control organic nanoparticles. a) DOPE/DC-Cholesterol liposomes with no encapsulated molecules, b) GCPQ micelles with no encapsulated molecules (note that b) is in a different size range from the other DLS graphs), c) DOPC/DC-cholesterol liposomes with no encapsulated molecules. Each colour represents a measurement repeat.

GCPQ micelles were fabricated using tip sonication of an aqueous solution containing GCPQ and the hydrophobic compound (AZD6244 or Nile Red), or just GCPQ for the control nanoparticles. After an additional centrifugation and filtration step to remove non-encapsulated drug, TEM analysis revealed a spherical morphology for micelles (Figure 5.14b). Similar to the liposomes, GCPQ micelle size was not influenced by the type of compound (AZD6244 or Nile Red), as shown by DLS (Figure 5.15b/d). TEM revealed that micelle diameters were on average approximately 30 nm while DLS analysis showed a distinct peak at 350 nm, ranging from 260 to 550 nm for AZD6244-loaded micelles (Figure 5.15b) and from 300 to 700 nm for Nile Red-loaded micelles (Figure 5.15d). These larger sizes were

probably due to the tendency of GCPQ micelles to form aggregates in aqueous media (Qu et al. 2006). In contrast, control micelles with no encapsulated molecules formed two different sized aggregates in solution, showing peaks at 9 and 50 nm in DLS with ranges of 5-12 nm and 40-80 nm respectively (Figure 5.17b). The smaller size of control micelles in contrast to those with encapsulated molecules was also clearly visible in TEM images (Figure 5.16b).

As part of nanoparticle characterization, HPLC analysis of AZD6244 contained within the nanoparticles was performed for every batch, and AZD6244 concentration was extrapolated from a standard curve (Figure 5.4). Both drug-loaded nanoparticles yielded AZD6244 concentrations between 0.85 and 1.15 mM, representing encapsulation efficiencies between 45% and 55%. This information was used to standardize the concentration of AZD6244 in liposome, micelle and free drug treatments (chapter 6 (pg. 144)).

5.4 Discussion

5.4.1 Observations on DOPE/DC-cholesterol liposomes

The combination of phospholipids and cholesterol is a common approach in liposome-based drug delivery. The liposomes used in this work were fabricated with a considerably higher content of cholesterol compared to most of the liposomes found in the literature. That decision had two main purposes: 1) to increase the stability of the liposomes as much as possible, and 2) to create a cationic surface to exploit the inherent benefits for cellular internalization derived from the interaction with the anionic cell membrane (Pelaz et al. 2013; Hino et al. 2012; Dokka et al. 2000).

5.4.1.1 *The role of liposome composition on stability and encapsulation*

Liposomes have been used to successfully encapsulate both hydrophilic and hydrophobic molecules. Specifically, DOPE/DC-cholesterol liposomes have been extensively used for nucleic acid delivery (Zhang et al. 2010; Ciani et al. 2004; Rodríguez-Pulido et al. 2008). That was one of the main reasons to select this type of liposome initially, since a combination of a small molecule with interfering RNA was always in consideration (chapter 4 (pg. 82)). As previously mentioned, the positive charge in the polar head of the DC-cholesterol molecule not only allows the interaction with nucleic acids but also with the cell membrane, and this electrostatic interaction works similarly to encapsulate negatively charged gold quantum dots (Figure 5.11).

Contrary to these quantum dots, which served only as a control for a possible hydrophilic molecule encapsulation and for imaging purposes, AZD6244 has a strong hydrophobic character. The encapsulation of AZD6244 in liposomes was proven by HPLC analysis after liposomes went through dialysis, consistently yielding encapsulation efficiencies of approximately 50% of the original drug concentration included during the fabrication. This is relatively high, considering previous reports

on reduced encapsulation efficiencies of hydrophobic molecules after following steps used here such as extrusion, compared to the non-extruded counterparts (Bhardwaj & Burgess 2010). Due to its nature, AZD6244 is expected to be encapsulated in a stable manner inside the membrane bilayer of the liposome, as it has been reported for other hydrophobic small molecules (Daneshpour et al. 2011; Mohammed et al. 2004; Cagdas et al. 2011). The ratio of lipids-to-AZD6244 chosen for liposome fabrication (5mM of each lipid for 2mM of the drug) was loosely based on similar work done with the molecule α -tocopherol (Cagdas et al. 2011), which displays similarities in lipophilicity and molecular weight to AZD6244.

There are different opinions regarding the best phospholipid/cholesterol ratio in liposomes in terms of stability and encapsulation, even among reports using the exact same lipid components: DOPE and DC-cholesterol (Yang et al. 2012; Farhood et al. 1995; Colosimo et al. 1999; Mukherjee et al. 2005). There is no ultimate formula, as the fabrication method and the encapsulated molecules make each case unique, and therefore, we must rely on our specific data. The high encapsulation efficiency achieved by the liposomes described in this chapter could be due to the high amount of cholesterol present in these liposomes, which is known to stabilize the liposomes by inserting itself in between the long chain phospholipids (Gregoriadis & Davis 1979). Moreover, a phospholipid/cholesterol ratio of 1:1 such as the one present in our DOPE/DC-cholesterol liposomes has been suggested as a particularly stable approach with little bilayer permeability (Kirby et al. 1980). While the work by Bhardwaj and Burgess suggests that the addition of cholesterol did in fact hinder the ability of their liposomes to encapsulate dexamethasone, they also suggested that this was caused by the close similarities between the two molecules (Bhardwaj & Burgess 2010). According to Cagdas and colleagues, the stabilization achieved by adding cholesterol to the liposome membrane is more important for hydrophilic compounds, such as the in-house manufactured gold quantum dots, while the interaction of hydrophobic compounds such as AZD6244 with the liposome bilayer remains stable even in a more fluid membrane (Cagdas et al. 2011).

Regarding the phospholipid DOPE, the other compound in the present liposomes, it has a relatively long alkyl chain (18C) with one point of asymmetry (unsaturation) (Figure 5.3). The fact that the presence of asymmetric phospholipids in the liposomal bilayer creates spaces within the membrane has been hypothesized to improve the

encapsulation of hydrophobic molecules. However, Ali and colleagues recently demonstrated that unsaturated alkyl chains had no improvement on encapsulation (Ali et al. 2013). On the other hand, the same work suggests that long alkyl chains such as the 18C chains found in DOPE do indeed improve encapsulation. Combined with the increased stability provided by the high cholesterol content, the long alkyl chains found in DOPE could explain the high encapsulation efficiencies achieved by our DOPE-DC-cholesterol liposomes.

5.4.1.2 The role of liposome fabrication method on size and encapsulation

While the current results are very promising compared to other much lower encapsulation efficiencies found in the literature (Bhardwaj & Burgess 2010; Ali et al. 2013), this parameter varies a lot depending on the molecule and the method of fabrication. More complex techniques, such as the microencapsulation vesicle (MCV) method used to encapsulate ibuprofen and fluribuprofen have achieved encapsulation efficiencies as high as 90% (Nii & Ishii 2005).

The thin layer method (also called dry film method, thin film evaporation method or thin film hydration method) used here for the fabrication of nanoliposomes precursors (large vesicles) has been commonly used over the years and is considered one of the most effective methods (Yang et al. 2012; Cagdas et al. 2011; Bhardwaj & Burgess 2010). For the second phase of fabrication, there were very little differences between DOPE/DC-cholesterol liposomes fabricated through sonication and extrusion methods. Both methods yielded liposomes of approximately 170 nm in diameter (Figure 5.9 and Figure 5.15a), with a similar spherical morphology visible using TEM (Figure 5.8). Once again, the presence of cholesterol could be the reason for these similarities. Cagdas and colleagues studied the differences between extrusion and sonication, as well as, the presence and absence of cholesterol in DMPC and DMPG liposome fabrication. They reported that, while in the absence of cholesterol extruded liposomes had larger sizes than sonicated liposomes, the addition of cholesterol resulted in liposomes closer in size, regardless of the fabrication method. They also suggested that while the encapsulation of a hydrophobic compound like vitamin E was not affected by the fabrication methods,

the encapsulation of a hydrophilic compound like cytochrome C was lower in the sonicated samples. This was due to the fact that sonication disrupts the membrane of the liposomes and this allows the hydrophilic compound to leach out into the outer aqueous environment, while the hydrophobic compound remains stably attached to the bilayer, as mentioned earlier for cholesterol-stabilized liposomes (Cagdas et al. 2011). In general terms, extrusion has shown great results in the past (Kang et al. 2011; Bhardwaj & Burgess 2010; Cagdas et al. 2011). Due to the similar results obtained between these methods in terms of morphology and size and the limitations of sonication, extrusion was chosen for the AZD6244- and Nile Red-bearing nanoparticles and for the control nanoparticles that were used on cell treatments described later in chapter 6 (pg. 144).

It is worth noting that the single liposome diameters observed in the TEM images are often larger than the average diameters shown by DLS analysis. While these liposomes are stable they are not rigid, and there is always a tendency for organic vesicles to be flattened by gravity in contact with a stiff surface. This flattening could have increased the apparent diameter of liposomes during TEM imaging on a carbon grid surface, particularly after the aqueous medium in which they were suspended dried out prior to imaging. DOPE has been suggested to assist the transition of the liposome into a more liquid phase that promotes membrane destabilization (Farhood et al. 1995; Pisani et al. 2011; Wasungu & Hoekstra 2006). The substitution of DOPE for DOPC in control liposomes seemed to have an effect on liposome toxicity, and it is further discussed in chapter 6 (pg.144). This phenomenon could also be related to the seeming less flattening of DOPC/DC-cholesterol liposomes on the carbon grid surface compared to DOPE/DC-cholesterol liposomes (Figure 5.14a/c).

5.4.2 Observations on GCPQ micelles

Contrary to liposomes, which have an aqueous core and a membrane bilayer, polymeric micelles contain a hydrophobic core designed to encapsulate hydrophobic molecules such as Nile Red or AZD6244. GCPQ in particular has shown special promise in the encapsulation of hydrophobic molecules, due to its tendency to create

larger supramicellar structures, while simultaneously being suitable for oral drug delivery (Qu et al. 2006; Siew et al. 2012; Lalatsa et al. 2012).

There is a positive correlation between the degree of hydrophobicity of GCPQ and its ability to solubilize a hydrophobic molecule (Qu et al. 2006; Siew et al. 2012). This derives from the concept of critical micellar concentration (CMC). The lower the CMC is (i.e. the more hydrophobic the polymer is), the lower concentration of GCPQ is needed to form micelles, the larger the micelles (and the multimicellar aggregates) formed and the more hydrophobic drug can be encapsulated. From the different batches of GCPQ fabricated in the laboratory during methodological development, the one used here is highly palmitoylated (18.9% palmitoylation), which increases the polymers hydrophobicity and therefore, reduces its CMC. Similar to the liposomes, the AZD6244 encapsulation efficiency achieved with GCPQ micelles was approximately 50%, which is similar to the 45% reported before for other hydrophobic drugs (Qu et al. 2006). According to Qu and colleagues, this extraordinary encapsulation efficiency is due to the formation of multimicellar aggregates, which was also detected in solution through DLS analysis (Figure 5.15b).

The quaternary ammonium in the polar head of GCPQ gives the micelles a cationic surface. Similar to the liposomes, this positively charged surface facilitates the cellular uptake of GCPQ micelles and creates stable electrostatic interactions with the surrounding aqueous environment. Intuitively, the highly polar head of the amphiphilic molecule polymer GCPQ would create stable micelles that repel each other, but due to the low CMC of the highly palmitoylated polymer, these individual micelles tend to create larger multimicellar aggregates that then act as a stable larger particle and do indeed exhibit repulsive behaviour towards each other (Qu et al. 2006).

5.4.2.1 Formation of AZD6244 crystals and their removal

As a hydrophobic small molecule, the higher the concentration the higher the tendency AZD6244 exhibits to form crystals in aqueous solution. The fabrication of AZD6244-bearing GCPQ micelles involved mixing the polymer GCPQ and the drug AZD6244 in aqueous solution followed by vortexing and sonication. Since the

concentration of this therapeutic agent (2mM) was above its water solubility saturation point during fabrication, the formation of crystals was unavoidable (Figure 5.12). Because the behaviour of these crystals during cell treatments would be extremely difficult to predict (especially in a three-dimensional environment where there is a physical barrier), the unencapsulated drug crystals needed to be removed through filtration and centrifugation steps before characterizing and using the micelles.

5.4.3 The influence of encapsulated molecules on the formation of nanoparticles

According to DLS analysis, DOPE/DC-cholesterol liposomes and GCPQ multimicellar aggregates showed virtually no difference in size whether they bore AZD6244 or Nile Red (Figure 5.15). Both compounds are small molecules of hydrophobic nature, and both of them contain benzene rings and no long aliphatic chains. Furthermore, the molar ratio between the lipid or polymer content and the encapsulated molecule was the same for both. The real difference was observed between the loaded nanoparticles and the control nanoparticles.

The absence of encapsulated molecules seemed to affect liposome size dispersity, making the range of sizes broader in the control liposomes than in the AZD6244- and Nile Red-loaded liposomes. To our knowledge, there is no evidence of this phenomenon in the literature, and we can only speculate. Presumably, it could be that the fluid nature that DOPE confers to the liposome is reduced by the presence of a small hydrophobic molecule that intercalates with the unsaturated alkyl chains, acting in a similar way to cholesterol. This increase in stability could narrow the diameter range during the extrusion phase, although this requires further investigation.

Micelles, on the other hand were extremely affected by the absence of encapsulated molecules. Not only the sizes detected by DLS analysis were much smaller than those for the molecule-bearing micelles, but two distinct peaks were visible, at sizes 9 and 50 nm (Figure 5.17b). Siew and colleagues also reported a possible increase

in the size of GCPQ micelles in the presence of encapsulated hydrophobic drugs, compared with empty GCPQ micelles. In their work, self-assembled GCPQ created micellar aggregates between 40 and 200 nm in size, however, they could only speculate about the sizes of individual micelles within these aggregates, and these micelles were probably smaller than those numbers. On the other hand, the addition of the drug produced defined single micelles between 20 and 50 nm in size and aggregates between 100 and 500 nm in size. Like in our experiments with AZD6244, they also found crystals of unencapsulated drug after micelle formation (Siew et al. 2012). The size of the drug-loaded micelles seems consistent with our data, which shows approximately 30 nm single micelles forming larger aggregates of around 350 nm in size (Figure 5.14b, Figure 5.15b/d).

There seems to be a close correlation between the hydrophobicity of the drug, the hydrophobicity of the polymer, the size of the micellar aggregates and drug encapsulation (Qu et al. 2006). While increasing the hydrophobic volume within the aggregates (i.e. forming supramicellar structures) improves the encapsulation of hydrophobic molecules like AZD6244, the high hydrophobicity of those encapsulated molecules increases the chances of micellar partition. This could be related to the double peak observed in our self-assembled GCPQ micelles. In the absence of AZD6244 to favour equilibrium between micellar partition and the assembly into larger particles, smaller clusters of GCPQ monomers with different characteristics (i.e. different degrees of palmitoylation) might have formed two different populations of self-assembled micelles and subsequent supramicellar aggregates in solution depending on their hydrophobicity, resulting in two different size peaks.

5.4.4 Organic nanoparticles for 2D and 3D experiments

The organic nanocarriers developed in this chapter seemed suitable for cancer cell treatment testing *in vitro*. AZD6244- and Nile Red-bearing liposomes and micelles, as well as their empty control counterparts were thus freshly fabricated and characterized before every treatment shown in chapter 6 (pg. 144). Surprisingly, steps naturally involved in their fabrication, such as filtration, extrusion, centrifugation, or the use of organic solvents and cold storage were enough to keep

these nanocarrier solutions aseptic. While no additional sterilization steps were included, no bacterial or fungal contaminations derived from nanoparticle treatment use were present in the subsequent cell *in vitro* work.

In spite of their high stability, any organic nanocarrier encapsulating a therapeutic or fluorescent agent is susceptible to a small leakage after a certain period of time, particularly at higher temperatures such as at 37°C, (5%CO₂ and 95% humidified air) at which cells were incubated or physiological conditions. For this reason, every fresh batch of nanocarriers fabricated with the purpose of therapeutic testing was immediately characterized and used within 24 h to prevent a loss in efficacy. The amount of drug that could leach out of the nanocarriers during this time was negligible and far within AZD6244s water solubility concentration range, thus preventing the formation of crystals. This, combined with the high reproducibility in the fabrication of these nanocarriers ensures reliable and comparable results.

CHAPTER 6

Nanoparticle *In Vitro* Evaluation

&

Experiments on Tumouroids

6 Nanoparticle *In Vitro* Evaluation and Experiments on Tumouroids

6.1 Introduction

Following the formulation of AZD6244 in nanoparticles, this chapter comprises experiments to test therapeutic efficacy in colorectal cancer cells cultured both as monolayers and in tumouroids. The chapter explains the fabrication of tumouroids, novel *in vitro* three-dimensional models, in detail and presents experimental data from preliminary studies to assess the penetration of nanoparticles, and their uptake by cancer cells to more specific toxicity, therapeutic efficacy and penetration experiments.

6.2 Materials and methods

6.2.1 Cell culture and treatment in monolayers and tumouroids

For conventional *in vitro* experiments, cells were cultured in monolayers following the same methods previously described in chapter 3.2.3. (pg. 44). For the treatments with nanoformulations, the concentration of the therapeutic agent was determined by the overall AZD6244 content, and the same AZD6244 concentration range was used for free drug, micelle and liposome formulations.

Briefly, cells were seeded (30000 HCT116 cells/well or 32000 HT29 cells/well) in 24-well plates (day 1), fed with 500 μ L of McCoy's 5A medium supplemented with FBS and P/S and allowed to grow for 24 h before substituting the culture medium with serum-free medium. Cells were treated 24 h later (day 3) with a range of AZD6244 concentrations (0.01 to 1 μ M) as a free drug or in nanoparticle form) (Table 6.1).

	DAY 1	DAY 2	DAY 3	DAY 4	DAY 5
MONOLAYERS	Seeding	Serum starvation	Treatment	-	Metabolic activity and proliferation assays
TUMOUROIDS	Seeding	-	Medium change	-	Medium change
	DAY 6	DAY 7	DAYS 8, 9 and 10		
TUMOUROIDS	Serum starvation	Treatment	Metabolic activity and proliferation assays		

Table 6.1 Treatment timeline in monolayers and tumouroids.

For toxicity and penetration experiments in 3D, tumouroids were fabricated using the plastic compression method (modified from Brown et al. 2005). At approximately 4°C of temperature, 400 µL of MEM medium (x 10 concentration) with Earle’s Salts, without L-glutamine and without sodium bicarbonate (First Link UK Ltd) were mixed with 3.2 mL of rat tail collagen type I (2.20 mg/mL in 0.6%v/v acetic acid). The mixture was neutralized with 5 M and 1 M sodium hydroxide until a colour change from yellow to pink was observed, and then 6,400,000 HCT116 cells suspended in 400 µL medium were added to the mixture. The resulting solution was placed in a stainless steel mould resting on a sterile glass slide that was placed on a piece of 30nm filter paper and left to gel for 30 min at room temperature. The mould containing the gel was then placed on a nylon mesh resting on a 165 µm stainless steel mesh placed on a piece of 30 nm filter paper. A 176g plunger was placed on

top of the gel allowing compression for 30 sec and the whole compression process was repeated on the other side of the gel (Figure 6.1). The resulting 2.6%w/v collagen dense mass (Nyga et al. 2013) was divided into 4 equal parts (artificial cancer masses, ACMs) with a surgical scalpel. Each of these 4 ACMs (measuring 5.5 x 10 x 10 mm in size and shaped as a prism) was nested in 1 mL of uncompressed acellular collagen per well, in 12-well plates (Figure 6.2). The nested construct (tumouroid) was left for 20 min to gel at 37°C. Fully supplemented medium (1mL) was added and cells were starved with serum-free media on day 6. After 24 h of starvation (day 7), cells were treated with a range of AZD6244 concentrations (0.01 to 1µM) as a free drug or in nanoparticle form (Table 6.1).

The content of AZD6244 in the nanoformulations was determined by HPLC analysis, as described in section 5.2.4.3. (pg. 120). AZD6244 treatment was carried out for 48 h in monolayers and for 24, 48 or 72 h in tumouroids. For control nanoparticle studies, cells were treated with the nanoparticle content equivalent to the AZD6244 concentration of their drug-loaded counterparts.

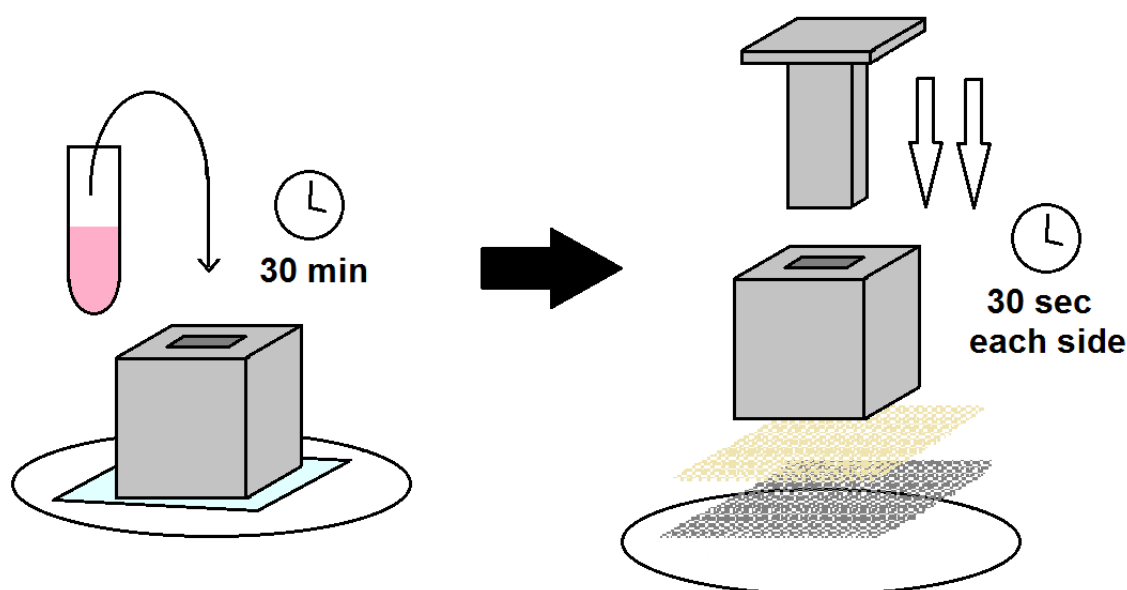


Figure 6.1 Plastic compression to create artificial cancer masses (ACMs). Collagen and MEM medium were mixed at 4°C and neutralized with NaOH until colour change from yellow to pink was observed. 6,400,000 HCT116 cells were added and mixed thoroughly and the mixture was placed in a stainless steel mould to gel for 30 min. A plunger was used to compress the gel on both sides, for 30 sec each.

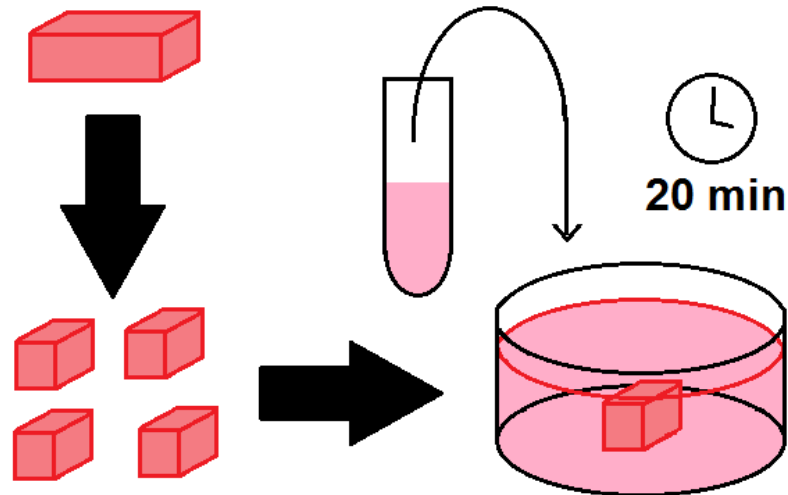


Figure 6.2 Nesting ACMs into hydrogels to form tumouroids. Freshly prepared compressed gels were divided into four equal pieces (ACMs) with a surgical blade and nested into an acellular hydrogel prepared following the neutralization protocol to create tumouroids and placed into a 12-well plate. Plates containing tumouroids were then placed in the incubator for 20 min before 1 mL of fully supplemented medium was added to the tumouroid surface.

For Western blot analysis, 200,000 HCT116 cells were seeded per well in 6-well plates and left to grow until 60% confluence. At that point, cells were treated with a range of AZD6244 concentrations (0.01 to 1 μ M) either free or in nanoparticle formulations for one hour and then 10ng/mL of EGF were added for 10 min to activate the MAPK pathway. Cells were lysed with 250 μ L of RIPA (Radio-Immunoprecipitation Assay) buffer (Sigma-Aldrich) supplemented with protease inhibitors (Roche, Hertfordshire, UK) and samples were stored at -20 $^{\circ}$ C until required.

6.2.2 Protein analysis and proliferation assays

For cells grown in monolayers, drug and nanoparticle efficacy was determined by MTT (metabolic activity) and total DNA (proliferation); while for tumouroids it was determined by Alamar Blue $\text{\textcircled{R}}$ (metabolic activity) and area measurements of aggregates of cancer cells (proliferation). Protein analysis was performed by Western blot. All these techniques are described in detail in chapter 2.3 (pg. 34).

6.2.3 HCT116 metabolic standard curves in monolayers and tumouroid cultures

The metabolic activity of HCT116 cells growing as monolayers and in tumouroids was correlated with cell density to compare drug efficacy results in both models. For monolayers, 50,000, 100,000, 250,000, 500,000 and 1,000,000 cells were seeded in 24-well plates and allowed to attach and start normal metabolism for 24 h before the MTT assay (30 min, 12.5 μ L at 20mg/mL) was performed. For tumouroids, 500,000, 1,500,000, 3,000,000, 5,000,000 and 7,000,000 cells were seeded following the previously described plastic compression protocol, and also left for 24 h before Alamar Blue [®] assay (4 h, 1mL, 1:10 dilution) was performed.

6.2.4 Preliminary penetration and uptake studies

Due to the scarce number of reports on nanocarrier drug delivery in natural 3D scaffolds, a number of preliminary experiments were performed to validate the approach. To determine whether cells take up large nanoparticles, HT29 cells were cultured as monolayers and treated with QD-loaded liposomes for 24 h. At this time, images were taken focusing on top of the cells and inside the cells using a confocal microscope. Free QDs were used for a similar experiment in tumouroids, to minimize size-dependent penetration issues that might be caused by the large size of liposomes or micelles. HCT116 cells were seeded in tumouroids and left to mature for 7 days before being exposed to QDs to test cellular uptake in 3D. Images of cell aggregates at the edge and core of the ACM were taken 24 h after exposure to the nanoparticles.

6.2.5 Confocal microscopy imaging

Confocal microscopy was used for some of the preliminary treatment tests, as well as for penetration studies (described later in this chapter). For preliminary experiments in monolayers (Figure 6.4) and for penetration studies (Figure 6.13), a

single averaged image at 1024x1024 pixel resolution was taken at the most convenient focus plane (i.e. just over the cell membrane and inside the cytoplasm for the monolayer experiments and 300 μm down from the top of the ACM for penetration experiments). For preliminary experiments in tumouroids (Figure 6.5) averaged stacks in the z-plane at the same resolution were taken to create a composite image that emphasizes the three-dimensional quality of cellular aggregates. The excitation wavelength was 488 nm for gold quantum dots and 543 nm for Nile Red, while the emission was detected at a wavelength of 650 for both gold QDs and Nile Red.

6.2.6 Penetration studies

Nile Red liposomes and micelles were fabricated as indicated previously. The fluorescent signal of the solution was normalized for all formulations (liposomes, micelles, GCPQ-dye molecular solution and free dye dissolved in DMSO) before exposing the tumouroids to them. Confocal microscopy was used to focus on an optical plane 300 μm deep from the top of the ACM (approximately the core), using a green laser (543 nm) and a red detector (630 nm). Culture medium was removed and Nile Red formulations were added on top of the construct. Images of the central plane inside the ACM were taken over a period of 24 h to determine the rate of penetration of each formulation. Fluorescent counts were quantified using Image J.

6.3 Results

6.3.1 Standard curves

In order to compare the efficacy of AZD6244 and its nanoformulations in monolayers and tumouroids, the proliferation of HCT116 cells (the cell line chosen for tumouroid culture) was characterized in both models. Known cell densities were seeded as monolayers and in tumouroids, and metabolic activity was measured 24 h later, to allow cells to settle and resume a normal metabolic pattern. Metabolic activity (an indirect method of measuring proliferation) was chosen since MTT (used for monolayer experiments) and Alamar Blue® (used for tumouroid experiments) are equivalent techniques - rather than total DNA and aggregate area measurements, which are the other two techniques used in this body of work to assess proliferation differences. Cells appeared to have a much steeper linear correlation between cell densities and metabolic activity in 2D, with absorbance measurements ranging from 0.3 to 2.5 – roughly 2-fold differences, than in 3D. In the latter, there was a less steep increase in metabolic activity, which appeared to reach a plateau at the greatest concentration of 7,000,000 cells (Figure 6.3), consistent with other reports (Nyga et al. 2013). With cell density and metabolic activity correlated through a standard curve, differences in drug-to-cell ratios between both models can be determined, as will be covered in this chapter's discussion.

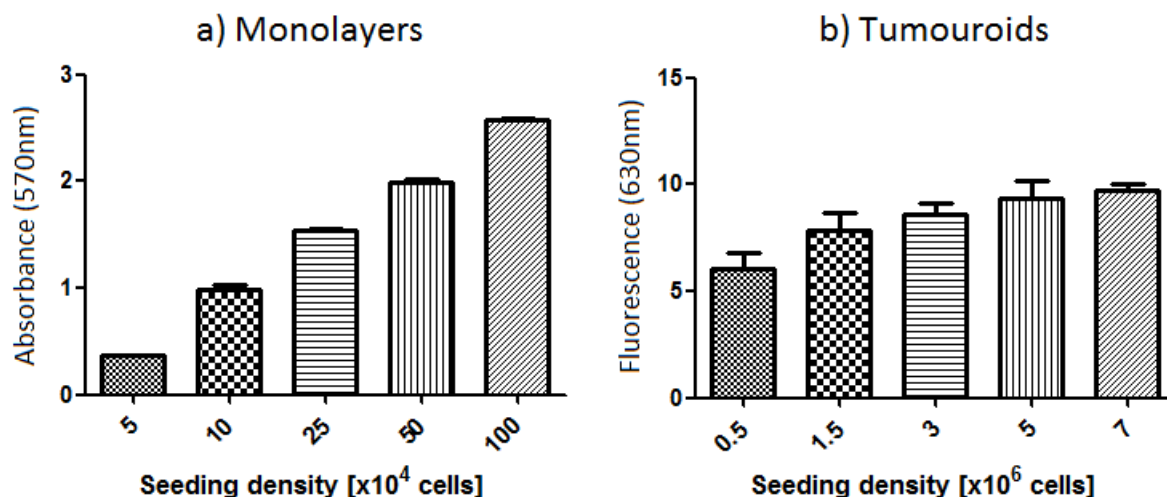


Figure 6.3 HCT116 cells metabolic standard curves as monolayers and in tumouroids. Different concentrations of HCT116 cells were seeded as monolayers (left) and in tumouroids (right), left for 24 h to settle and normalize their metabolism. MTT [a] monolayers] and Alamar Blue ® [b] tumouroids] assays were performed to correlate metabolic activity in both models.

6.3.2 Preliminary penetration and uptake studies

Due to the novel nature of these experiments involving a cancer 3D model and drug nanocarriers, preliminary tests were performed regarding encapsulation and internalization. Highlights of basic methodological development are summarised below.

Once extrusion was established as the preferred method for liposome fabrication, manufacture by double extrusion through 1000 nm followed by a 200 nm polycarbonate membrane was compared to using the later alone. Results showed that there was no significant difference in size between these two methods, so the double extrusion was chosen for further experiments since it facilitates the process, presumably by pre-filtering large impurities. Similarly, QD-loaded liposomes were subject to freeze-thaw cycles to determine whether this technique would improve encapsulation (Xu et al. 2012), but results showed either equal or worse encapsulation efficiency when including this step, so it was not included in the final fabrication protocol. The conjugation of Doxorubicin-loaded DOPE/DC-cholesterol liposomes to a generic anti-EGFR antibody and to the clinically used Cetuximab also

showed no difference in treatment efficacy *in vitro*, so naked nanoparticles were used for these experiments.

To determine the ability of colorectal cancer cell lines to uptake large nanoparticles, HT29 cells were treated with QD-loaded DOPE/DC-cholesterol liposomes for 24 h, and images of the cellular surface and the cytoplasm were taken. As shown in (Figure 6.4), 24 h after exposing the cells to the nanoparticles, most of the latter have been internalized by the cells.

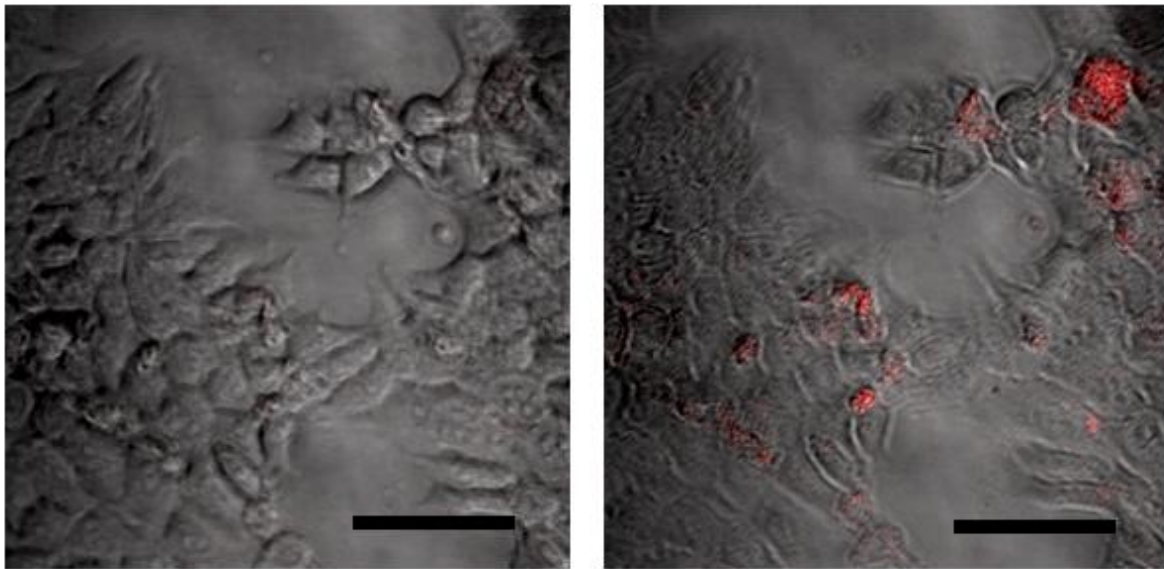


Figure 6.4 Nanoparticle uptake test. HT29 cells were cultured as monolayers and treated with QD-loaded liposomes for 24 h to determine whether cells uptake large nanoparticles. Confocal microscope images were taken focusing at the top surface of the cells (left) and inside the cell (right). Scale bars = 20 μm

A similar experiment was performed in HCT116 tumouroids with free QDs, to determine whether a small nanoparticle would penetrate the mass and be internalized by cells, forming aggregates in the construct. Figure 6.5 shows a very heterogeneous internalization of quantum dots by cell aggregates both at the edge of the ACM and at its core, suggesting irregular diffusion and cell behaviour throughout the cancer mass. Additionally, these images hint at the three-dimensional structure of the aggregates, specially the image from the core (Figure 5, right).

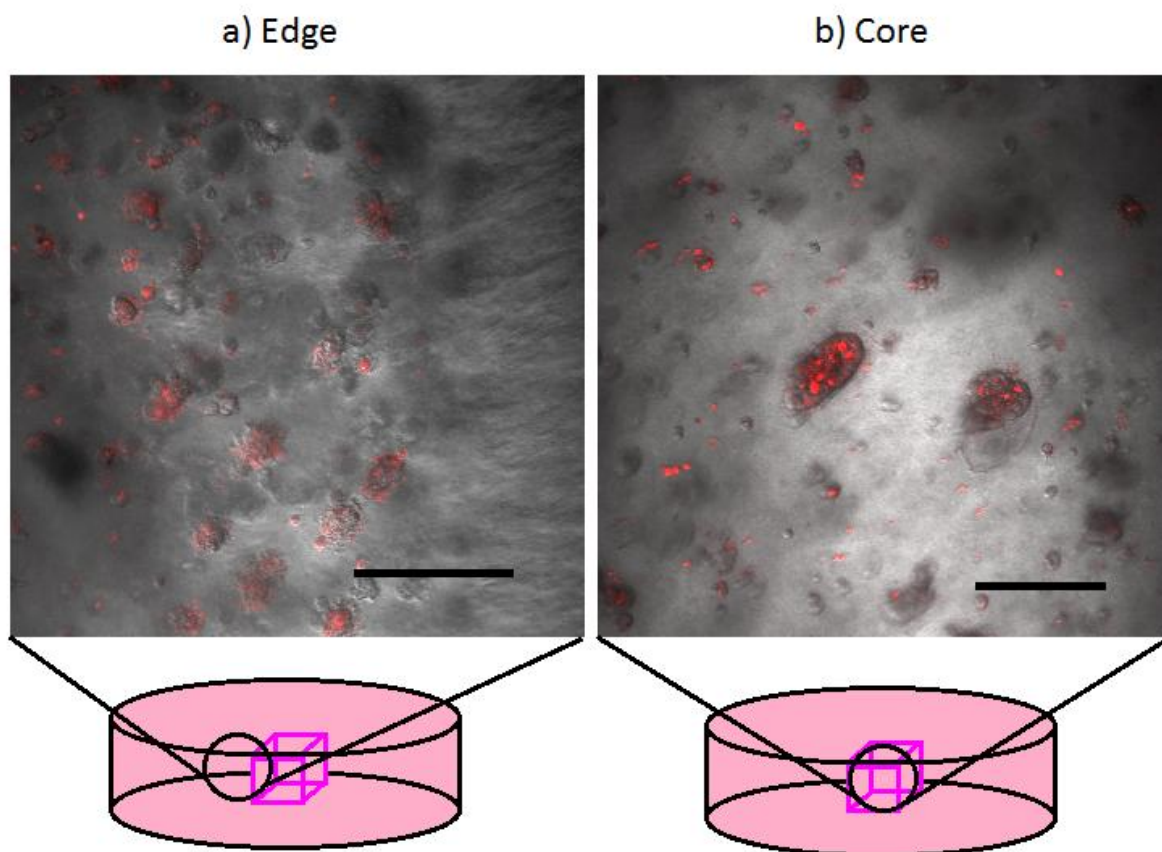


Figure 6.5 Nanoparticle penetration and uptake test in tumouroids. HCT116 tumouroids were exposed to QDs to test nanoparticle penetration and cellular uptake in the ACM. Quantum dots were chosen as the smallest nanoparticle possible (approximately 1 to 2 nm in diameter) to minimize size-dependent penetration issues. Images at the a) edge and b) core of the ACM were taken 24 h after exposure. Scale bar = 100 μm .

6.3.3 Toxicity assessment of control nanoparticles

To establish the intrinsic toxicity of the nanoparticles and to be able to distinguish it from a more efficient delivery of AZD6244 into the cell and its internal processing, similar experiments with water-containing nanoparticles were performed. In these experiments, the concentration of nanoparticles was expressed as “equivalent to AZD6244 concentration”, in reference to the next experiments with drug-bearing nanoparticles. Despite these control nanoparticles being only loaded with water, the amount of polymer or lipid reaching the cells was approximately the same as that of the AZD6244-loaded nanoparticle solution. Also, a third type of nanoparticle (DOPC/DC-cholesterol liposomes) was included in these experiments to further

study the role of ethanolamine in nanoparticle toxicity. For this experiment, one more order of magnitude was tested (10 μ M).

For HCT116 cells, 1 μ M AZD6244-equivalent concentration of nanoparticles elicited 7% and 25% metabolic activity inhibition for liposomes and micelles respectively (Figure 6.6). For HT29 cells, toxicity was much greater, with 50% and 47% metabolic activity inhibition for liposomes and micelles respectively (Figure 6.7). When the concentration of nanoparticles was increased to 10 μ M AZD6244-equivalent the inhibition resulted in 65% and 57% for HCT116 and 54% and 70% for HT29. This suggests a high degree of chemical toxicity caused by the nanoparticle components at sufficiently high concentrations, but a reasonably low toxicity in the case of 1 μ M AZD6244-equivalent for HCT116 cells.

Conversely, DOPC/DC-cholesterol liposomes showed a much lower toxicity even at the highest AZD6244-equivalent concentration (10 μ M), with 32% metabolic activity inhibition for HCT116 cells and 10% for HT29 cells (Figure 6.6, Figure 6.7), suggesting that small changes in the nature of the nanoparticle components can have a huge effect on toxicity.

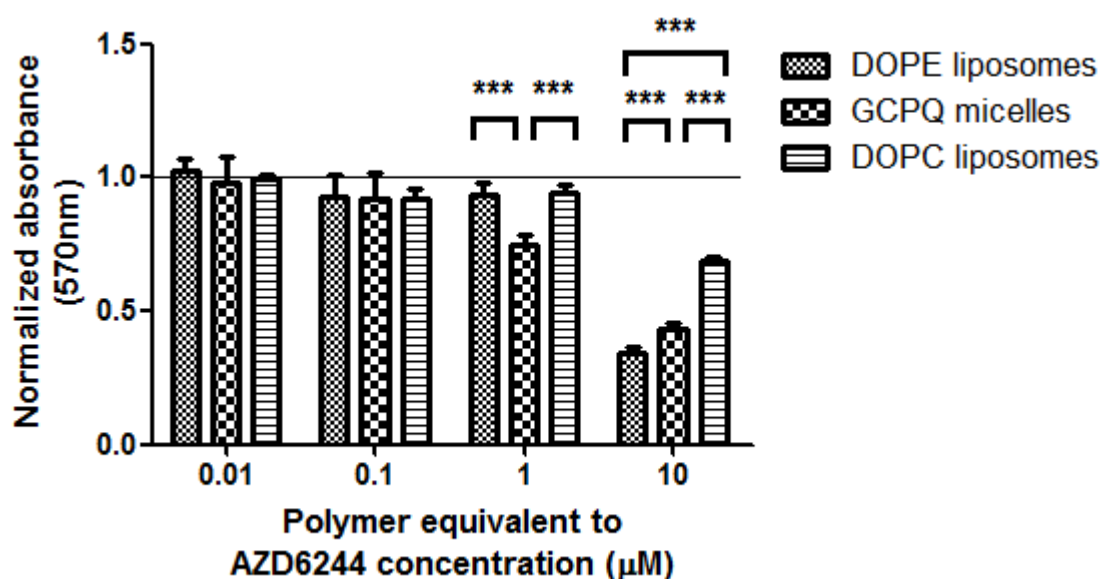


Figure 6.6 Control nanoparticle toxicity on HCT116 cell monolayers. HCT116 cells were treated with control nanoparticles at nanoparticle concentrations equivalent to their AZD6244-loaded nanoparticle counterparts. Treatment was carried out for 48 h before MTT assay was performed. Significance: *** p <0.001. Control: horizontal line.

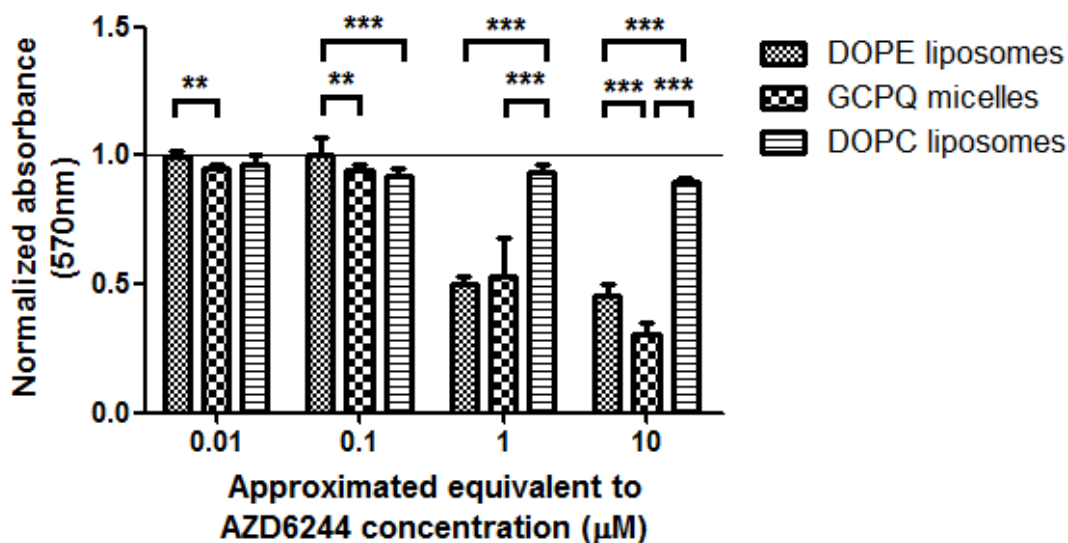


Figure 6.7 Control nanoparticle toxicity on HT29 cell monolayers. HT29 cells were treated with control nanoparticles at nanoparticle concentrations equivalent to their AZD6244-loaded nanoparticle counterparts. Treatment was carried out for 48 h before MTT assay was performed. Significance: ** $p < 0.01$ *** $p < 0.001$. Control: horizontal line.

6.3.4 Drug and nanoparticle efficacy in monolayers

HT29 and HCT116 cells in 2D monolayers were treated with micelles and liposomes containing AZD6244, as well as, free AZD6244 for 48 h before total DNA and MTT assays were performed.

For HCT116, AZD6244 treatment resulted in a 21% decrease in proliferation (determined by total DNA assay) at the highest concentration of the drug (1 µM), whilst liposomes and micelles with the same drug load resulted in 61% and 89% inhibition respectively (Figure 6.8). Results for HT29 cells were quite similar, with 26%, 77% and 96% decreases in proliferation for free drug, liposomes and micelles respectively (Figure 6.9).

Regarding metabolic activity measured by MTT, nanoformulations were clearly more efficient than the free drug, but the differences were slightly less pronounced (18%, 60% and 40% for the free drug, liposomes and micelles, respectively for HCT116

(Figure 6.8), and 14%, 74% and 58% respectively for HT29 cells) (Figure 6.9). This may be due to an increase in metabolic activity by the surviving cells which have less competition for the nutrients in the medium.

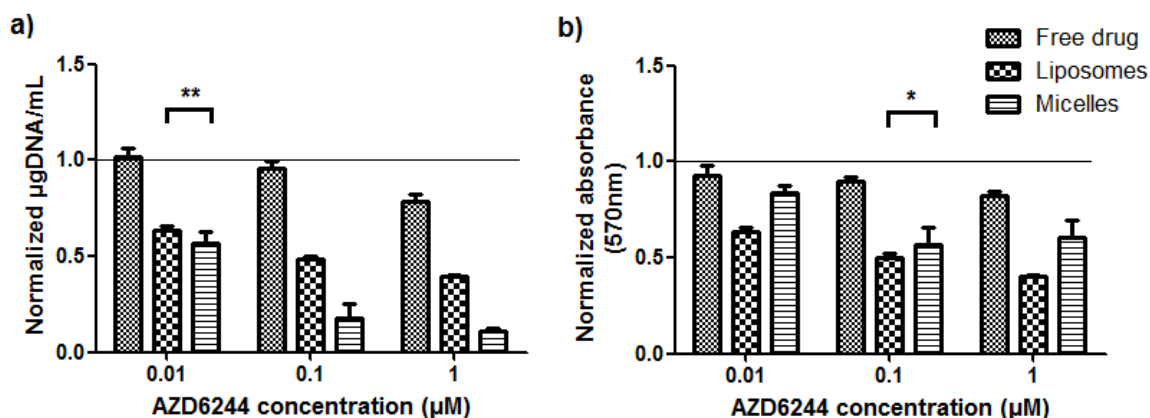


Figure 6.8 Effect of all three formulations of AZD6244 on HCT116 cell monolayers. Cells were treated with different concentrations of the drug in free, liposomal and micellar forms for 48 h before total DNA assay (left) and MTT assay (right) were performed. Significance: all $p < 0.001$, except ** $p < 0.01$ and *no significance. Control: horizontal line.

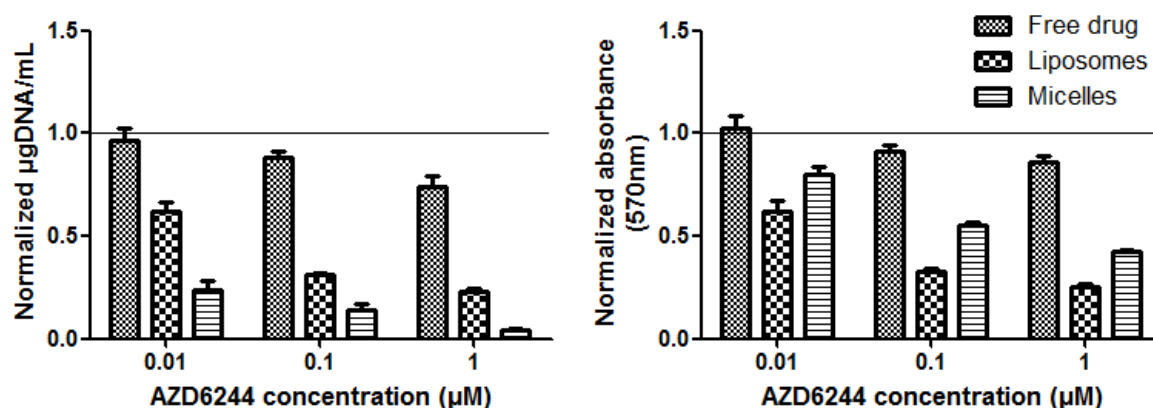


Figure 6.9 Effect of all three formulations of AZD6244 on HT29 cell monolayers. Cells were treated with different concentrations of the drug in free, liposomal and micellar forms for 48 h before total DNA assay (left) and MTT assay (right) were performed. Significance: all $p < 0.001$. Control: horizontal line.

For HCT116 cells, there was a statistically significant difference between micelle and liposomal formulations at every concentration tested, except at 0.01 µM using the DNA proliferation assay and at 0.1 µM when using the MTT assay. In the case of HT29 cells, all treatments at all concentrations resulted in statistically significant

inhibition of proliferation and metabolic activity ($p < 0.001$). Interestingly, in both cell lines micelles appeared more toxic according to the total DNA assay, while MTT assay revealed a higher metabolic activity inhibition in the liposome-treated group, suggesting differences in the delivery and internal processing between these nanoformulations.

6.3.5 Protein analysis of phosphorylated ERK

To further confirm delivery of AZD6244 into the cytoplasm and specific pharmacological action on the target MAPK pathway, Western Blot analysis was performed (Figure 6.10). While it is clear that differences in protein expression between 2D and 3D models are expected, Western blot analysis was only performed in monolayer experiments. This is because it can be assumed that in monolayers the majority of the drug is delivered and the purpose of these experiments is determining the efficacy of the drug reaching the target intracellularly.

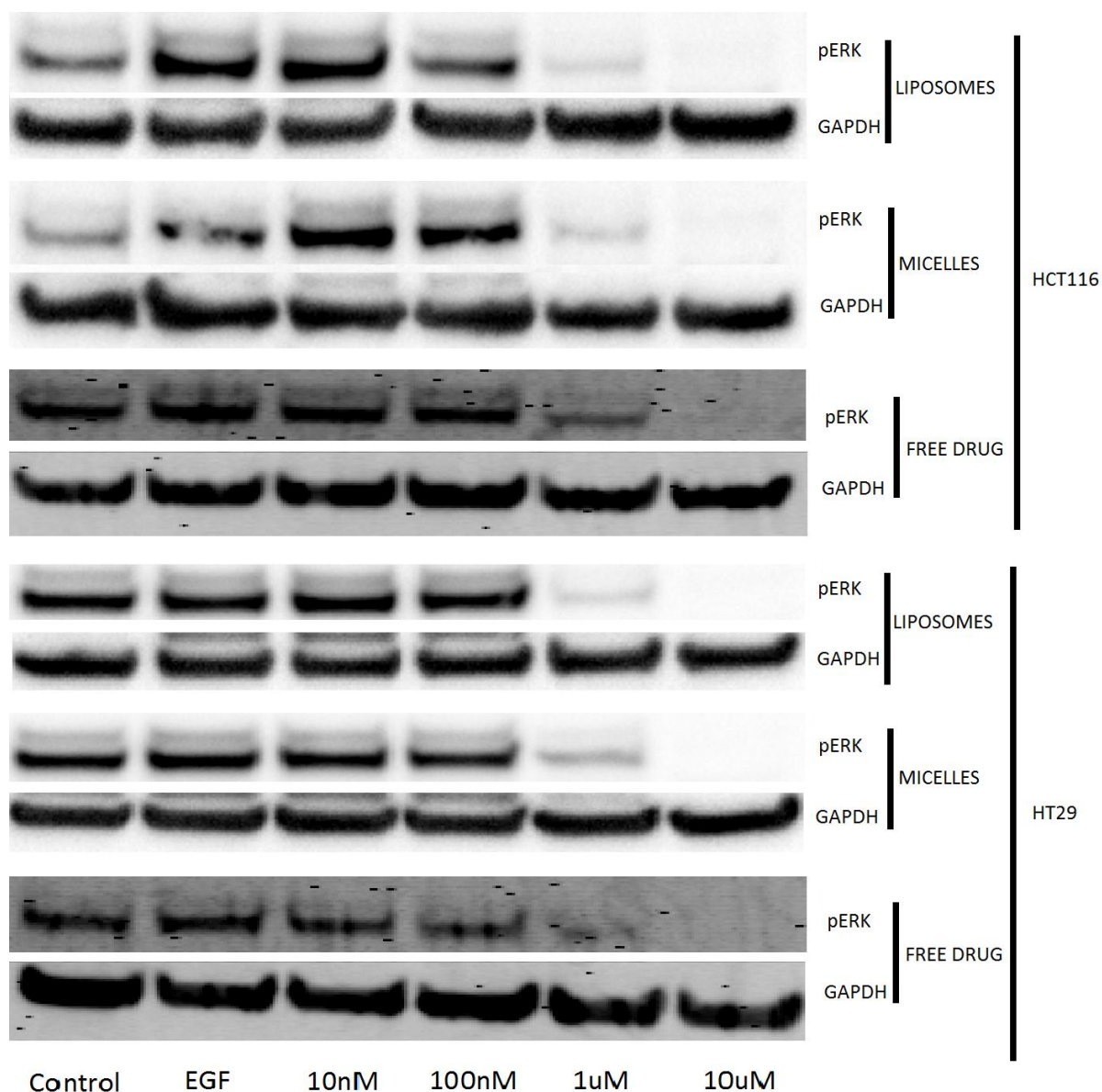


Figure 6.10 Western blot analysis of phosphorylated ERK after treatment with AZD6244 nanoformulations. HCT116 cells were grown in monolayers, serum starved and treated with increasing concentrations of AZD6244-loaded nanoparticles or free AZD6244 for 60 min; then the MAPK pathway was activated with EGF (10ng/mL) for 10 min. Cells were lysed, protein was extracted, quantified and analysed by PAGE and Western Blotting for the presence of the pERK, as an indicator of MAPK activation. Housekeeping protein: GAPDH.

Cells were treated with the two nanoparticle forms carrying the same drug concentrations as well as with the free drug, and proteins were separated by size in a polyacrylamide gel. Phosphorylated ERK, a common indicator of MEK activity, was detected using a mouse monoclonal antibody (9106S, Cell signalling). Densitometry revealed that in all three forms, a dose-dependent reduction in the levels of

phosphorylated ERK occurred; these decreases were 86%, 80% and 53% for liposomes, micelles and free drug respectively (Figure 6.10). This suggests that AZD6244 reached its target and elicited a specific response at the protein level, and that the delivery was much more efficient when the drug was delivered via nanoformulations compared to the free drug. While control GCPQ micelles were significantly more toxic than control DOPE/DC-cholesterol liposomes (Figure 6.6, Figure 6.7), AZD6244-loaded liposomes elicited more inhibition of metabolic activity and MEK1/2 activity than AZD6244-loaded micelles (Figure 6.8, Figure 6.9, Figure), suggesting a more efficient delivery of the drug.

6.3.6 Drug and nanoparticle efficacy in tumouroids

Tumouroids were initially fabricated with both HT29 and HCT116 cells, but some of the results with HT29 seemed to be inconsistent so they are omitted in the present work. All results in tumouroids presented here were performed on HCT116 cells and, consequently, any comparison in cell behaviour between tumouroids and monolayers is also done within HCT116 cultures in both models.

The 3D *in vitro* cancer model used here (tumouroid) consisted of a dense collagen core containing the cancer cells (ACM) surrounded by an uncompressed collagen hydrogel (stromal surround) (Nyga *et al.* 2013). Tumouroids were left to mature for seven days before treatment, allowing cancer cells to form aggregates within the ACM, thereby mimicking *in vivo* avascular micrometastases. Treatment with free AZD6244 and the nanoformulations was performed for 24, 48 and 72 h. It is accepted routine in our laboratories to include extra 24 h incubation when moving from 2D to 3D cultures to optimise the effects of drugs, as more time is needed for the drug to reach the cells in 3D and the metabolism in 3D tumouroids is also slower (Figure 6.3). For that reason, when correlating the data between both models, the 48 hour treatment in 2D was compared to the 72 hour treatment in 3D.

Treatment with free AZD6244 and its nanoformulations showed increasing efficacy with increasing AZD6244 concentrations and treatment times. Inhibition of metabolic activity started to be significant at 0.1 μM .

Drug efficacy in tumouroids was different from monolayers. When comparing the results of metabolic activity assays, whilst the free drug was more effective in 3D than in 2D (38% vs 18% inhibition), the nanoparticle treatments were more effective in 2D (60% vs 26% inhibition for liposomes and 40% vs 34% inhibition for micelles) (Figure 6.11c). Overall, micelles were more toxic in tumouroids than the other formulations (Figure 6.11). Significant differences were observed at 0.1 μM AZD6244 and at 24 h, where micelles were superior to liposomes (Figure 6.11a: $p < 0.01$). Furthermore, at 1 μM and 48 h, micelles were superior to both liposomes ($p < 0.001$) and free drug ($p < 0.01$) (Figure 6.11b), while at 1 μM and 72 h only micelles were only superior to liposomes ($p < 0.05$). In the latter treatment, the free drug also showed more toxicity than the liposomes ($p < 0.01$), making the liposomes the least effective of the three formulations in tumouroids (Figure 6.11c).

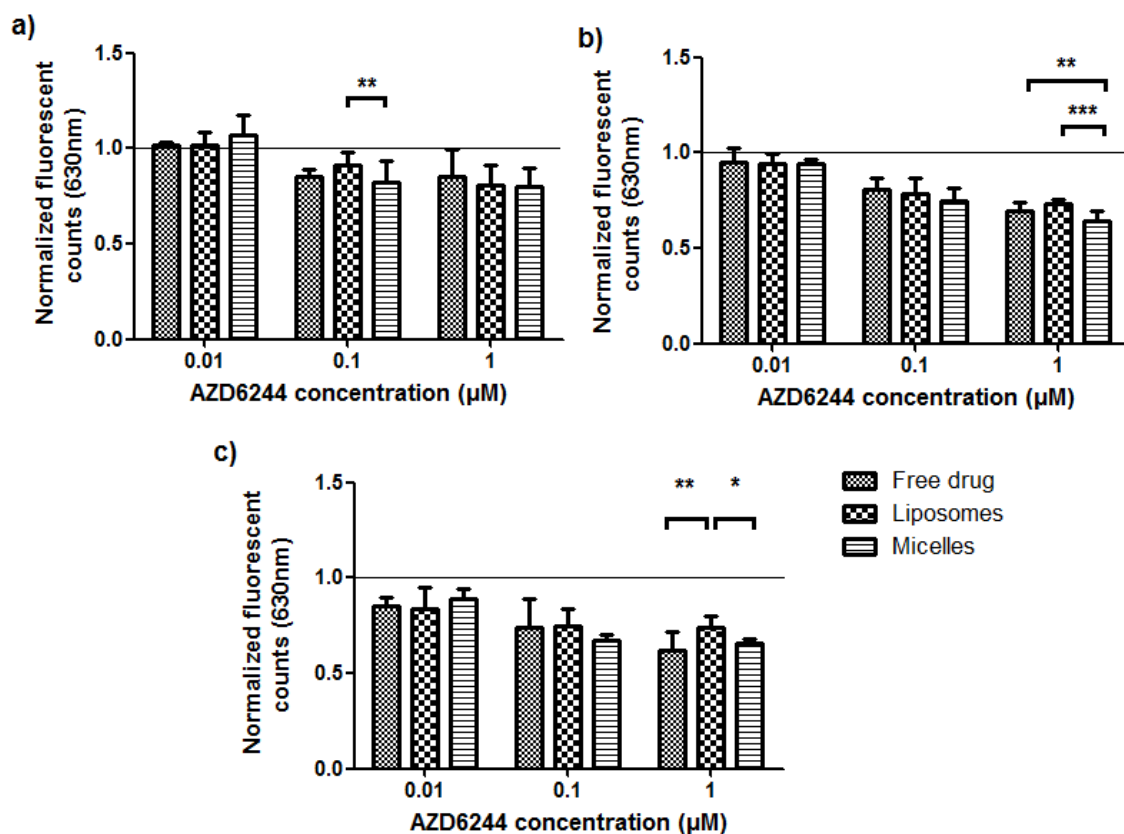


Figure 6.11 Inhibition of metabolic activity of tumouroids by AZD6244 and its nanoformulations. HCT116 tumouroids were manufactured and left to mature for 7 days. Tumouroids were treated with AZD6244 and AZD6244-loaded nanoparticles at a range of concentrations for 24(a), 48(b), and 72(c) h before Alamar blue © assay was performed. Significance: * $p < 0.05$, ** $p < 0.01$, *** $p < 0.001$. Control: horizontal line.

Similar to the experiments in monolayers, a second technique was used to provide a more comprehensive characterization of drug efficacy in tumouroids. Aside from Alamar Blue®, which measures metabolic activity, the areas of cancer cell aggregates at the edge of the ACM were measured as an indicator of cell proliferation within the tumouroid. Aggregates at the edge of solid cancer masses are believed to be metabolically active and migratory, representing actively growing and invasive boundary/potential micrometastases from colorectal tumours. Results from this assay followed a similar pattern to those of metabolic activity tests, except that statistical significance was more prominent in the former. All AZD6244 concentrations showed statistically significant differences between formulations (from $p < 0.05$), with the exception of outcomes using $0.1 \mu\text{M}$ at 48 h, where there was no statistical significance between liposomes and micelles (Figure 6.12).

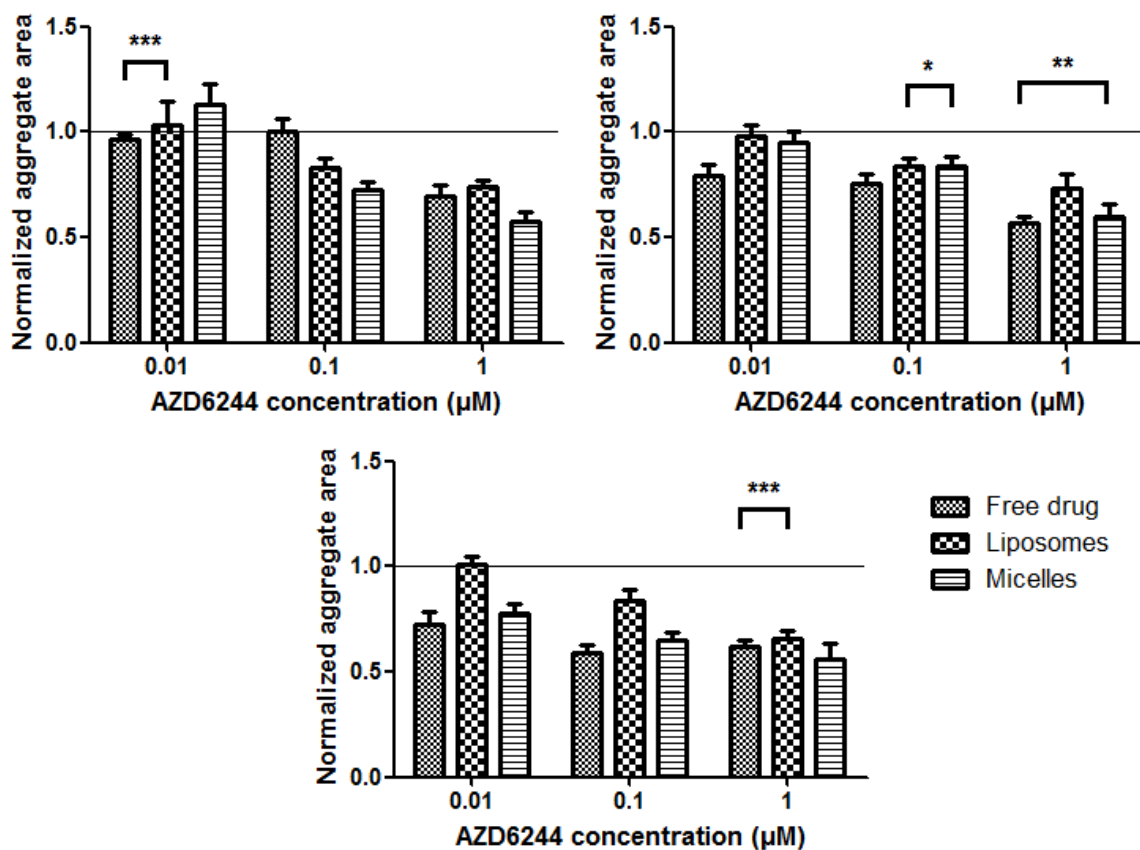


Figure 6.12 Reduction of cancer cell aggregate areas in tumouroids by AZD6244 and its nanoformulations. HCT116 tumouroids were manufactured and left to mature for 7 days. Tumouroids were treated with AZD6244 and AZD6244-loaded nanoparticles at a range of concentrations for 24(a), 48(b), and 72(c) h before fixation. The areas of cancer cell aggregates at ACM periphery were measured. Significance: * $p < 0.05$, ** $p < 0.01$, *** $p < 0.001$. Control: horizontal line.

6.3.7 Drug penetration studies

In order to further explore the differences in the efficacy of nanoparticles for delivery of drug, tumouroids were cultured and matured for seven days and exposed to Nile Red-loaded fluorescent nanoparticles. The focal plane was set at 300 μm into the ACM core, and fluorescence was imaged and measured over time. As in the tumouroid drug efficacy studies, these experiments were performed in HCT116 tumouroids. Two different controls were included: Nile Red dissolved in DMSO and a non-micellar mixture of Nile Red and GCPQ acting as an intermediate point between a molecular solution and nanoparticles of only 1 nm in diameter.

These experiments revealed a clear size-dependent ability of the nanoparticles to penetrate the ACM. The penetration of the free dye control through the ACM core started reaching a plateau before two hours post-incubation (Figure 6.13a/c), with a fluorescent signal ten-fold higher than the one showed by liposomes and micelles after 24 h (Figure 6.13b/c). GPCQ micelles and DOPE /DC-cholesterol liposomes showed a very similar penetration profile, most likely due to the fact that they are both cationic and relatively large nanoparticles.

The non-micellar GCPQ control, which shares the chemical properties with GCPQ micelles but with a much smaller size, exhibited a penetration profile much closer to the nanoparticles than the free dye, but clearly superior to the larger particles, supporting the hypothesis of a size-dependent factor (Figure 6.13b/c).

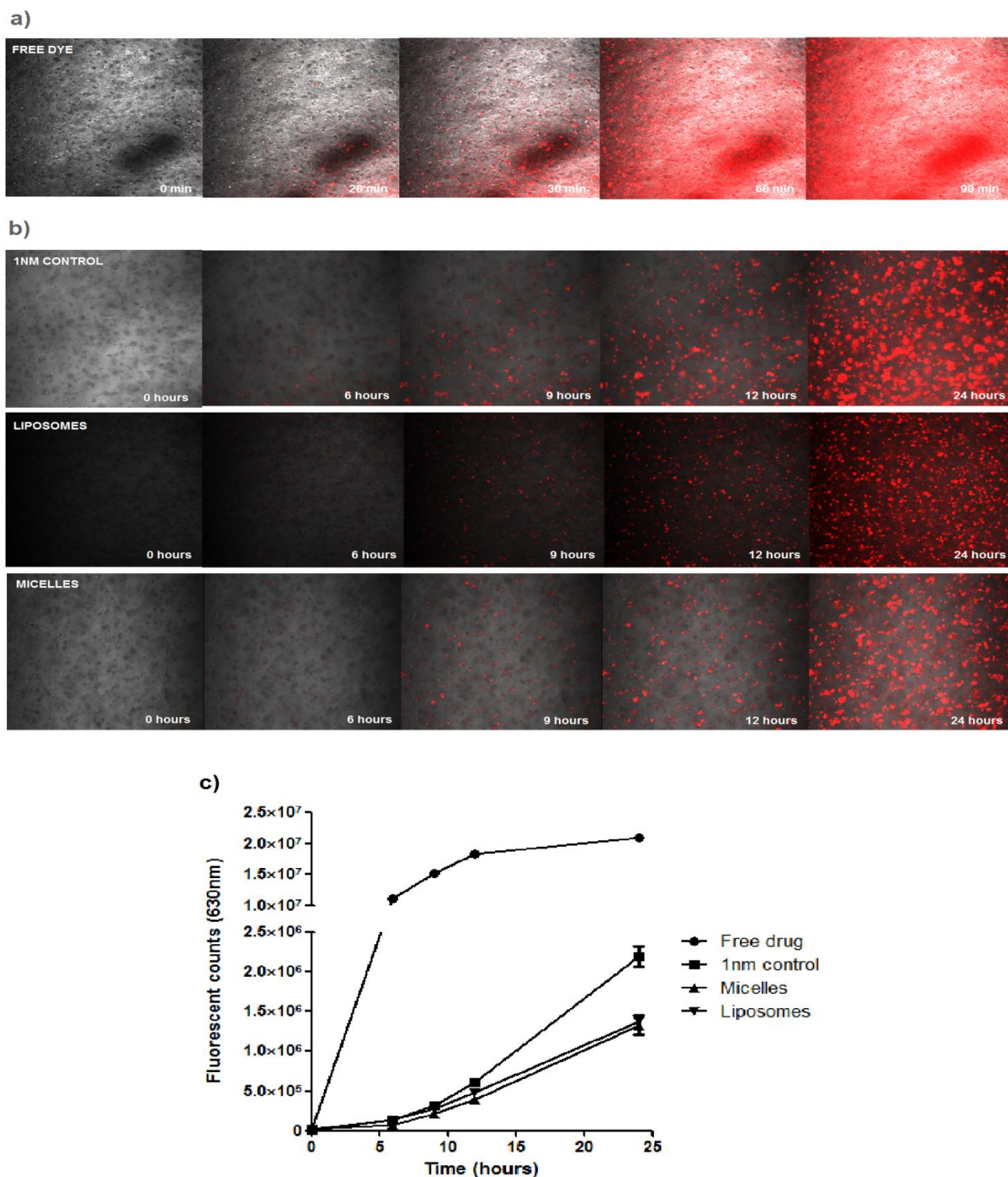


Figure 6.13 Nanoparticle penetration into the tumoroids. HCT116 tumouroids were manufactured and left to mature for 7 days. Tumoroids were treated with a) Free Nile Red dissolved in DMSO and b) GCPQ-Nile Red molecular solution, liposomes and micelles containing Nile Red. Confocal Images of free and encapsulated dye present at the ACM core (300 μm from the surface) were taken over time and c) fluorescence was quantified using the Image J software.

6.4 Discussion

This work explores the effect of cationic organic nanocarriers loaded with AZD6244 on HCT116 colorectal cancer cells cultured both as monolayers and in tumouroids. The use of 3D cancer models aims to mimic the cell microenvironment found *in vivo* while still allowing the control of parameters *in vitro*. AZD6244 was chosen since it has been extensively studied in Phase I, II clinical trials in several cancers, including colorectal, with promising results, alone and in combination with other therapies (Ciombor & Bekaii-Saab 2015).

6.4.1 Previous reports on nanoparticle testing in 3D models and in nanoformulations of MEK inhibitors

MEK inhibitors other than AZD6244 have been encapsulated in nanoformulations. Basu and colleagues demonstrated that PLGA nanoparticles carrying the MEK inhibitor PD98059 successfully induced apoptosis and inhibited proliferation of lung cancer and melanoma *in vitro*, and improved the effect of cisplatin in melanoma cells *in vivo* (Basu et al. 2009). Similarly, a DGL cationic liposome containing a combination of the MEK inhibitor PD0325901 and Mcl I-specific siRNA reduced KB cells survival *in vitro* and induced 79% apoptosis *in vivo* (Kang et al. 2011).

MEK inhibitors have also been tested in 3D cancer models. These include PD98059 for breast cancer cells grown in Matrigel (Polo et al. 2010) and GSK1120212 in combination with BRAF and Aurka inhibitors for melanoma using a skin reconstruction model (Caputo et al. 2014).

As a free drug, the efficacy of AZD6244, the agent evaluated in this thesis, has been previously tested in a 3D model of melanoma grown within a collagen hydrogel, in combination with the SCR inhibitor saracatinib, showing promising results (Ferguson et al. 2012). This work differs significantly from the plastic compression approach adopted in the current studies: cells were cultured in an uncompressed collagen matrix with high water content, while the model I use undergoes plastic compression resulting in a cancer mass with a collagen density of 2.6%w/v. Therefore, to my

knowledge there are no publications that can offer a direct comparison to the present work.

6.4.2 Standard curves and drug to cell ratios

HCT116 cells were grown as monolayers and in tumouroids to correlate the results from MTT and Alamar Blue® assays to cell density and allow for the hypothetical estimation of drug to cell ratio for each model (Figure 6.3). The factors that are needed to be taken into account for the estimation, in addition to the metabolic measurements specific to each cell density, include: the maximum AZD6244 concentration (1 μ M), the total volume of medium per well in 24-well and 12-well plates (500 μ L and 1 mL, respectively), and the fact that the untreated controls in the drug efficacy experiments gave a MTT colorimetric signal of approximately 0.5 and an Alamar Blue® fluorescent signal of approximately 40 for monolayers and tumouroids, respectively.

To calculate the drug to cell ratio in monolayers, the value of 0.5 obtained from the untreated controls was plotted into the standard curve and a cell number of 47766 at the day of treatment (day 5) was extrapolated. Considering a volume of medium of 500 μ L containing 1 μ M AZD6244 (0.5 nmol of AZD6244 in 500 μ L), the approximate drug to cell ratio in monolayers was 10.47 fmol/cell at the day of the assay (day 5). For tumouroids, the untreated controls gave a fluorescence value of 40. This value was plotted into the standard curve and a cell number of 7,250,000 at the day of treatment (day 10) was extrapolated. Considering a volume of medium of 1 mL containing 1 μ M AZD6244 (1 nmol of AZD6244 in 1 mL), the approximate drug to cell ratio in tumouroids was 1.38 amol at the day of the assay (day 10). These calculations suggest a drug to cell ratio over 7500 times higher in monolayers than in tumouroids.

The results from this are only approximated and the conclusions hypothetical, since cells do behave differently between the two models and that includes considerable differences in their metabolic rate. Furthermore, cell density at the day of the assay is not necessarily the same as at the day of treatment, especially for the controls, but

this day was chosen as an approximation for being the endpoint of the experiments. Even considering a large deviation from the real values, the drug-to-cell ratio would still be several orders of magnitude superior for the monolayers, which has great implications when comparing the efficacy of AZD6244 between the two models. As shown in (Figure 6.8 and Figure 6.11), AZD6244 seemed to be more effective in tumouroids than in monolayers in spite of the cells receiving much more drug in the monolayers.

6.4.3 Preliminary uptake and penetration studies

The preliminary tests performed in monolayers and tumouroids demonstrate that cells in both models were capable of internalizing nanoparticles, ranging from 1-2 nm in the case of QDs (Figure 6.4) to over 200 μm in the case of liposomes and micelle aggregates (Figure 6.5). This data indicates only cellular uptake without considering the ability to penetrate the dense collagen mass in the tumouroids. An efficient uptake of large nanoparticles is consistent with the data obtained from drug efficacy experiments, which showed efficient inhibition in proliferation and metabolic activity, as well as, successful delivery of AZD6244 to its target in the MAPK pathway by micelles and liposomes. Specific results are discussed in depth later on in this chapter.

The images in Figure 6.5 clearly showed cellular aggregates in the order of several tens of microns across, present in 7-day matured tumouroids. The irregular distribution of fluorescent nanoparticles within the ACM indicates that drug and nanoparticle diffusion was not homogeneous, and this could have significant implications in the delivery of the drug in the tumouroids, especially in the case of nanoparticles. This is also suggested by the results of the penetration studies (Figure 6.13), which showed great differences in the diffusion of therapeutic agents in line with differences in size and physicochemical properties. Again, this is discussed in more detail later on in this chapter.

6.4.4 Nanoparticle efficacy on monolayers

Results demonstrated that non AZD6244-loaded DOPE/DC-cholesterol cationic liposomes exert very little toxicity (7% inhibition at the highest concentration, Figure 6.6c) which, when considering efficacy of the AZD6244-loaded liposomes (61% for total DNA and 60% for metabolic activity, Figure 6.8a/b), suggests a very successful AZD6244 delivery platform. On the other hand, reports regarding the effect of cationic surfaces on cells could explain the toxicity of non AZD6244-loaded GCPQ nanoparticles (25% inhibition at the highest concentration, Figure 6.6c), which were significantly more toxic than the non-AZD6244 loaded liposomes ($p < 0.001$, Figure 6.6c). However, the drug-loaded GCPQ micelles exerted an even higher toxicity than the control (non AZD6244-loaded) micelles (40% for metabolic activity and 89% for total DNA, Figure 6.8a/b).

Both DOPE/DC-cholesterol liposomes and GCPQ micelles have a positively charged surface. The cationic nature of these nanoparticles not only facilitates nucleic acid loading (as mentioned earlier for the liposomes) but also facilitates the adhesion to the negatively charged cell membrane (through an electrostatic interaction) and internalization (Pelaz et al. 2013; Hino et al. 2012; Dokka et al. 2000), leading to improved delivery and therapeutic effects. The drawback, however, is that a nanoparticle with a surface too rich in positive charges can disrupt the membrane (Lin et al. 2010). Aside from their cationic nature, there have been reports of liposomal toxicities that may be important in the context of their efficacy. For example, hybrid liposomes with no encapsulated molecules have been reported to prolong survival in mice with CRC xenografts by inducing apoptosis (Ichiyama et al. 2012). The adhesion of liposomes also causes mechanical stress and local contraction of the cell membrane (Murrell et al. 2014). Compared to these studies, the liposomes used in our work in the absence of AZD6244 showed relatively little toxicity. The presence of DOPE in this cationic liposomes could have the dual function of reducing their toxicity (Ciani et al. 2004) and potentially eliciting an inverted hexagonal phase transition that facilitates the delivery to the cytoplasm (Pisani et al. 2011). However, substituting DOPE for DOPC in the liposomes reduces their toxicity at high concentrations indicating that the toxicity of these liposomes is somehow related to the ethanolamine group in DOPE. Additionally, both DOPE and

DOPC are zwitterionic in nature, suggesting that the mild toxicity elicited by DOPE/DC-cholesterol liposomes is not necessarily due to the positive charge of DC-cholesterol, common in both liposomes.

Regarding the influence of size and charge in toxicity, it is worth noting that in spite of serum being removed at the time of the treatment, any protein or peptide present in the medium could potentially bind to the charged surface of the nanoparticles. This binding could not only modify the surface charge and therefore modify their ability to bind to the cellular membrane and their uptake, but it could considerably increase the size of the nanoparticles. The adsorption of proteins on the nanoparticle surface could also be responsible for additional nanoparticle aggregation, which is a phenomenon already observed in this formulations. Additionally, cells sense patterns of adsorbed proteins on surfaces and respond accordingly. In order to fully understand the role of surface charge and surface charge to mass ratio in these experiments, a more thorough characterization of the nanoparticle surfaces is needed. This can be achieved by performing experiments such as Zeta potential, secondary ion mass spectrometry (SIMS), or X-ray photoelectron spectroscopy (XPS), which should be included in future work.

On the other hand GCPQ, as a polycation, does have a stronger positive surface charge that might destabilize the cell membrane (Lin et al. 2010) to a certain extent and cause cytotoxicity even in the absence of the drug. While AZD6244-loaded liposomes elicited more proliferation inhibition than AZD6244-loaded micelles in terms of metabolic activity, AZD6244-loaded micelles were more efficient according to the total DNA assay (89% vs 61%, Figure 6.8a). This suggests that genotoxicity, as opposed to direct cytotoxicity, could be an indirect cause of the inhibition of cellular proliferation in this system. In a study by Shah and colleagues, the effect of a number of nanoparticles with different characteristics on DNA was evaluated: neutral and anionic nanoparticles did not exhibit genotoxic properties whilst cationic nanoparticles did, as demonstrated by the formation of micronuclei. The degree of genotoxicity did not correlate to the size or molecular weight of the nanoparticles, rather to the extent of the positive charges on the surface of the nanoparticles (Shah et al. 2013). This results support the findings reported here of greater nanoparticle toxicity elicited by a polycation such as GCPQ. It is worth noting that in the same

work, the overall cytotoxicity of neutral 20 nm diameter micelles was higher than that of 180 nm diameter cationic liposomes, indicating that the toxicity of our 30 nm diameter GCPQ micelles compared with the 165 nm diameter DOPE/DC-cholesterol liposomes even in the absence of AZD6244 could relate to their size.

Similar to this, a fraction of our control micelles (without AZD6244) were smaller compared to the AZD6244-loaded micelles (9 nm vs 30 nm) (chapter 5 (pg. 112)). This could partly explain their toxicity in the absence of AZD6244 compared to the other formulations, since smaller nanoparticles are more easily internalized and can even reach the cell nucleus (Huang et al. 2012). This is supported by the size-dependent cytotoxicity reported by Shah and colleagues mentioned earlier (Shah et al. 2013). However, it is uncertain at what exact nanoparticle size this extra toxicity occurs, since 30 nm diameter GCPQ micelles were small enough to undergo efficient internalization (Andar et al. 2014). For that reason the toxicity of GCPQ control micelles is likely to be due to their positively charged surface.

Aside from the higher toxicity of GCPQ micelles compared to DOPE/DC-cholesterol liposomes, both AZD6244-loaded nanoparticles seemed to be excellent delivery platforms as determined by proliferation (total DNA assay), metabolic activity (MTT assay) and enzyme inhibition (pERK levels). The toxicity of both control nanoparticles was significantly lower than that of the AZD6244-loaded nanoparticles. As determined by Western blot analysis of phosphorylated ERK1/2, all three formulations successfully inhibited the activity of MEK1/2 (Figure 6.10). The most efficient inhibition was elicited by the liposomal formulation. These results, in combination with the much higher cytotoxicity of liposomes and micelles compared to the free drug (61%, 89% and 21% inhibition of proliferation, and 60% 40% and 18% inhibition in metabolic activity, respectively (Figure 6.8 and Figure 6.9)) suggest an efficient internal processing and delivery to the cytoplasm. Specifically, liposomes seem to be the best route of delivery in monolayers, since they inhibit metabolic activity (Figure 6.8) and MEK activity (Figure 6.10) rather more efficiently than both micelles and free drug, even though GCPQ micelles showed higher genotoxicity and chemical toxicity (total DNA for drug-loaded micelles and MTT for control micelles) (Figure 6.6a/c).

6.4.5 Nanoparticle efficacy on tumouroids

In the present work, treatment with free AZD6244 was more effective in tumoroids than in monolayers (18% inhibition at 48 h, 1 μ M in monolayers (Figure 6.8); 38% inhibition at 72 h, 1 μ M in tumoroids (Figure 6.11)). This was especially surprising considering that the cell density in tumoroids is extremely high compared to monolayers, resulting in a drug-to-cell ratio over 7500 times higher in the monolayer experiments, and therefore suggesting very different cell behaviour between the two models. This interpretation must be considered as a hypothesis, since the differences in proliferation inhibition were subtle and the time of treatment differed between the models, but the great difference in drug-to-cell ratio clearly suggests differences in drug delivery or efficacy.

Previous work with spheroids and other 3D models of cancer have shown significant differences in drug response compared to monolayer cultures. However in most cases, unlike AZD6244 being more efficient in tumoroids than monolayers in this work, 3D cultures tend to be more resistant to anti-mitotic drugs than monolayers (Chambers et al. 2014; Mikhail et al. 2013). These differences are not properly understood, but cells in both models are certainly subject to different conditions. Some examples are changes in gene expression and cell behaviour when cells are in contact with each other, drug concentration gradients and differential proliferation patterns in acidic, hypoxic or nutrient deprived regions of the constructs (Nyga *et al.* 2013; Minchinton & Tannock 2006). 3D cancer models mimic these conditions to promote cell behaviour more similar to real tumour tissues (Trédan et al. 2007). However, the differences in drug efficacy between 2D and 3D are unpredictable and that highlights the importance of 3D testing during drug development. For example, although Magdeldin and colleagues reported a 2-fold increase of EGFR expression in HT29 cell tumoroids compared to monolayers, the anti-EGFR monoclonal antibody Cetuximab elicited a weaker inhibitory response in the former (Magdeldin et al. 2014). It is worth noting, however, that the differences in therapeutic efficacy between 2D and 3D could be cell line dependent (Mikhail et al. 2013) and therefore AZD6244 would not necessarily always be superior in tumoroids.

In the present work, the role of the extracellular environment in the tumouroid system was simplified to a compressed collagen matrix, with no additional stromal cells. Therefore, any changes in behaviour of HCT116 cells are exclusively due to the dense collagen microenvironment of the ACM and the cellular three-dimensional conformation encouraged by a protein matrix. There is evidence that these parameters are enough to cause radical changes in cell behaviour (Hickman et al. 2014).

6.4.6 Penetration studies

6.4.6.1 Rationale behind the parameters of the penetration studies

While the preliminary nanoparticle experiments were performed using gold QDs to track uptake, penetration and encapsulation, these experiments were performed using Nile Red as a marker. One of the reasons for this is that QDs could potentially aggregate in solution and create larger structures that would not be removed through dialysis and could give a false positive in penetration experiments. Whilst Nile Red is a hydrophobic dye and tends to form aggregates in an aqueous environment, it only emits a fluorescence signal in the presence of another hydrophobic molecule (such as GCPQ, DC-cholesterol or DOPE), allowing only the nanoparticles to contribute to the fluorescent counts. Additionally, single molecules are small enough to be removed through dialysis, especially after several cycles under agitation, displacing the solute equilibrium to further solubilize Nile Red in every cycle. For penetration studies both the free molecule and the encapsulated molecule needed to be as close as possible to the ones used in the AZD6244 toxicity experiments, and QDs are inorganic hydrophilic nanoparticles. Like AZD6244, Nile Red is a small molecule of hydrophobic nature containing several benzene rings (Figure 6.14). Its molecular weight is 318.37 g/mol, which is relatively close to that of AZD6244, 457.68 g/mol.

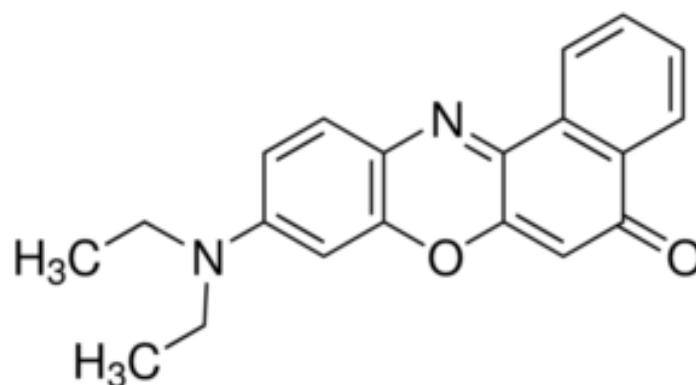


Figure 6.14: Molecular structure of Nile Red

The free dye seemed to start reaching a signal plateau in the ACM core, most likely due to the dye flooding the centre of the ACM and reaching concentration equilibrium throughout the mass rather than saturating the detector, as the curve is gradual. On the other hand the presence of GCPQ micelles and DOPE liposomes in the ACM core was still significantly increasing after 24 h of exposure. While initially these nanoparticles could have been left for a longer time to determine if the majority of them would make it to the core eventually, there are a few reasons why a 24 hour treatment was chosen. Firstly, these penetration experiments were performed outside of an incubator, increasing the probability of the samples drying out or the medium becoming too basic for the cells in the long term. Nanoparticles and dye could not be diluted in a larger volume to make the pH and hydration last longer since the fluorescence would be significantly reduced and a higher dye loading could destabilize or change the nanoparticle structure. Even in the event of cells being viable after a 48 hour period due to their entrapment in a gel that potentially acts as a suitable microenvironment, cells could start behaving differently and this would affect nanoparticle uptake. By day 7 of maturation, which is when these experiments were performed, cells have formed aggregates and start migrating towards the acellular stroma. A way of minimizing how this affects the results is limiting the period of study. To optimize this experiment in future work, a microscope with a built-in incubator would be needed. Similarly, cells are exposed to a high power laser at every image taken, and this could damage cells increasingly the longer the experiment lasts.

Additionally, these dye-loaded nanoparticles are representative of the drug-loaded nanoparticles used for treatment in the previous experiments. Once nanoparticles have been released at room temperature or at 37°C (if it were in an incubator), the drug should be delivered to the cytoplasm as soon as possible, and is likely to lose part of its efficacy after 24 h. That makes the first 24 h of penetration the vital period of time to study. In the long term nanoparticles could have degraded or leaked the drug, or the drug itself could have lost efficacy, and after the drug has reached its target a lapse of time is needed for it to inhibit proliferation, which starts being measured at 24 h.

6.4.6.2 Penetration hinders nanoparticle efficacy

The greater effect of free AZD6244 in tumouroids compared to monolayers, combined with the superior delivery of the drug observed with the nanoparticles in monolayers, suggest that the reduction in efficacy observed in the nanoparticle treatment of the tumoroids (60% for liposomes and 40% for micelles in monolayers (Figure 6.8b) vs 26% inhibition for liposomes and 34% for micelles in tumoroids (Figure 6.11c)) was not caused by the drug itself. The most likely scenario to explain the suboptimal efficacy of these liposomes and micelle aggregates in tumouroids is their localization within the ACM. Their diffusion towards the core could be partly limited by their large size, possible interactions with the collagen matrix and the uptake by cancer cell aggregates at the outer boundary of the ACM. The core of the ACM is representative of cancer cells hundreds of micrometres distant from a blood vessel *in vivo*, to which the drugs have limited access (Minchinton & Tannock 2006). This hypothesis is supported by our penetration studies (Figure 6.13). It is worth noting that further functionalization of the surface such as the addition of antibodies or PEG, would make these nanoparticles even larger. These functionalizations are commonly added to the nanoparticle surface for experiments *in vivo* and for clinical applications, in order to promote active targeting and avoid recognition by the immune system.

The efficacy of micelles (or micelle aggregates) in tumouroids compared to the liposomes is closer to, and in some cases more effective than, the free drug. While

the efficacy of the free drug could be due to a much better penetration, the higher efficacy of micelles could be due to their cationic toxicity, however limited to the periphery. It is also possible that cells in the periphery of the ACM are more metabolically active than those of the core, due to limited diffusion of nutrients across the dense cancer mass. This would favour the toxicity of the nanoparticles that, however remaining in the outer layers of the ACM, have a greater inhibitory effect on metabolic activity.

Molecular weight, solubility, shape and other physicochemical characteristics of a drug influences its diffusion through tissue (Minchinton & Tannock 2006). It has been suggested for large molecules such as antibodies, that size could affect their ability to penetrate 3D models (Magdeldin et al. 2014; Xiang et al. 2011). This is a very common occurrence in spheroids, due to their high density. In the case of antibodies, not only their size but their ability to bind to surface receptors could hinder their penetration by sequestration in the outer layers of cells. Similarly, the very uptake of drugs or nanoparticles in the periphery of the structure could limit the penetration to deeper layers (Minchinton & Tannock 2006). Penetration becomes especially important in the case of nanoparticles, which size far exceeds that of drugs, particularly small molecules. Huang and colleagues demonstrated that different sizes of gold nanoparticles have the ability to penetrate into tumour spheroids in a size-dependent manner. Additionally, the smallest particles (2-6 nm) were able to reach the nucleus while the largest (15 nm) were confined to the cytoplasm of cells (Huang et al. 2012).

According to Andar and colleagues, nanoparticle size affects the way they are internalized. In their work, larger nanoparticles (162.1 nm diameter) tended to be internalized by clathrin-dependent mechanisms whilst the smallest (40.6 nm diameter) were internalized by dynamin-dependent mechanisms (Andar et al. 2014). Smallest particles were internalized 12-fold more efficiently than the largest, and the internalization of intermediate-sized nanoparticles corresponded with a size-dependent pattern. Even though this study was carried out with liposomes exclusively, the differences in size apply to our DOPE/DC-cholesterol liposomes and GCPQ micelles.

A fraction of our control micelles (without AZD6244) were smaller compared to the AZD6244-loaded micelles (9 nm vs 30 nm). This could partly explain their toxicity in the absence of AZD6244, since smaller nanoparticles are more easily internalized and can even reach the cell nucleus (Huang et al. 2012). This is supported by the size-dependent cytotoxicity reported by Shah and colleagues mentioned earlier (Shah et al. 2013). However, since 30 nm diameter GCPQ micelles were small enough to undergo efficient internalization (Andar et al. 2014), the toxicity of GCPQ control micelles is likely to be due to their positively charged surface.

CHAPTER 7

Conclusions

&

Future Directions

7 Conclusions and Future Directions

The field of cancer therapy is one of the most challenging in medicine, and forces the scientific community to find novel and creative ways to overcome the many new hurdles and limitations that constantly arise. Some of the most significant advances in the field merge in this body of work namely targeted therapeutic molecules, nanotechnology-mediated drug delivery and tissue engineering.

Finding a suitable therapeutic candidate for combination treatments and nanoformulations was a difficult task, as a number of molecules widely used at the preclinical and clinical level did not elicit the response that could be expected from them. While PD98059 and U0126, two of the MEK inhibitors used here have been allocated to laboratory work for a number of years now, AZD6244 is still undergoing clinical trials. While all three inhibitors showed promising results in conventional *in vitro* models, their efficacy was not as good as it had been reported before. The reasons for that phenomenon are still unclear; suffice to say inconsistency is not uncommon in the field of pharmacology. The design of combination therapies that involve MEK inhibitors is increasingly popular, and it took a turn in recent years when a combination of dabrafenib and trametinib (Flaherty et al. 2012), a BRAF inhibitor and a MEK inhibitor respectively, got FDA approval for the treatment of melanoma.

Regarding the ETAR axis, previously validated as a promising therapeutic target in this research group, results were inconsistent and very discouraging, driving me to search for a therapeutic alternative. The use of RNA interference as a therapeutic target showed promise, with great ability to reduce target mRNAs and subsequently the expression of target proteins, and a significant therapeutic improvement in combination with AZD6244. Technical difficulties regarding excessive cellular damage together with the complexity of nucleic acid/inhibitor combinations forced me to abandon this option as a combination therapy. However, with the increase of knowledge and technologies available in the field of genetics, the use of RNA interference as a therapeutic approach is exciting and will increase exponentially.

While part of the research developed here has yielded suboptimal results, valuable lessons can be learned regarding the inconsistencies present in the literature.

Special care must be taken in the process of drug development, as great investments often lead to failure at its final stages.

In many cases, it is not the therapeutic potential of a molecule what hinders its efficacy, but the way it is delivered to the target tissue. Improving delivery has been the solution to many limitations such as degradation, solubility and off-target toxicity, and could potentially solve the toxicity issues observed in the use of RNA interference in this work. Nanotechnology has led the efforts regarding novel therapeutic delivery systems. While liposomes have been in the vanguard and are almost exclusively the nanoparticle of choice for anticancer therapy, micelles and protein-based nanoparticles are breaking into the clinic.

The results from micellar and liposomal drug delivery observed in this work support this reality. Both DOPE/DC-cholesterol liposomes and GCPQ micelles significantly improved the efficacy of AZD6244 at the protein, metabolic activity and proliferation levels, whilst exerting little intrinsic toxicity in comparison. While encouraging, conventional *in vitro* approaches such as cell monolayers are often hyper sensitive to treatments and their genetic and proteomic status are far from that of a real tumour. The presence of an ECM and the three-dimensional structure of the cells play major roles in cellular behaviour and gene expression, and have obvious implications in therapy.

Liposomes and micelles containing AZD6244 were less effective in tumouroids than it would be expected from the results obtained in monolayer experiments. Experiments on the tumouroid model suggested that the efficacy of these nanoparticles was hindered by their large size or interactions with cells and dense ECM. These observations are consistent with previous data on spheroid models, where the high density caused by the high cellular concentration and the absence of extracellular matrix tends to limit the penetration of drugs and nutrients. Whether it is the differences in cellular behaviour and gene expression or the physicochemical properties of the matrix itself, the differences between 2D and 3D models are many, and not limited to drug efficacy.

The main difference between the spheroids and the tumouroids is the presence of that ECM, which makes the tumouroids potentially suitable for studies on invasion, metastasis and interactions with stromal cells. Our research group includes a prolific

branch of research in that field, and has produced valuable data regarding the effect of matrix mechanical properties and composition on invasion (unpublished data). Mimicking the tumour environment also provides a suitable platform to culture sensitive cells that would otherwise perish in the harsh laboratory environment. The possibility of growing patient's primary cancer cells in the lab under controlled conditions makes tumouroids a promising route to personalised medicine.

The research described in this thesis sets the basis for further investigation involving nanocarriers for drug delivery and their evaluation in colorectal tumouroids. Specific experiments should be completed to further understand the mechanisms that led to this results. Examples of these are:

- Perform experiments such as XPS, SIMS or Zeta potential on GCPQ micelles and DOPE/DC-cholesterol liposomes to better understand the influence of surface charge and size to surface charge ratio in toxicity.
- Optimize the size of these nanocarriers to 40-80 nm in diameter by modifying parameters in the fabrication protocols (i.e. sonication time, extrusion pore size or cholesterol content), and study the effect of size on penetration, uptake and toxicity.
- Determine the molecular differences between colorectal cancer cells grown as monolayers and in tumouroids by performing thorough analyses at the genetic and protein levels on both models.
- Perform the experiments described in this work on a panel of colorectal cancer cell lines to find common patterns among them and determine the influence of specific mutations on therapeutic response.
- Increase the complexity of the tumouroids by including a stromal component composed of at least two cell types (fibroblasts and endothelial cells) and study their influence on treatment response.
- Combine the nanoformulation treatment on tumouroids with a permeabilisation techniques and study its influence on penetration.
- Utilize caspase assays to determine the effect of nanoformulations on apoptosis and thus discern between cytotoxicity and cytostasis as therapeutic phenomena.

- Modify the surface of nanocarriers with PEG to perform *in vivo* studies and study their relation to the EPR effect.

The work presented in this thesis demonstrates the potential of organic nanoformulations as platforms for anti-cancer therapeutic delivery, and highlights the importance of including 3D models of cancer in the process of drug development. It is imperative that these two technologies evolve together to exploit their potential in cancer therapy.

CHAPTER 8

References

8 References

- Adjei, A.A. et al., 2008. *Phase I pharmacokinetic and pharmacodynamic study of the oral, small-molecule mitogen-activated protein kinase kinase 1/2 inhibitor AZD6244 (ARRY-142886) in patients with advanced cancers.*
- Adjei, A.A. & Hidalgo, M., 2005. Intracellular signal transduction pathway proteins as targets for cancer therapy. *Journal of clinical oncology : official journal of the American Society of Clinical Oncology*, 23(23), pp.5386–5403.
- Ahn, N. et al., 2001. Pharmacologic inhibitors of MKK1 and MKK2. *Methods in enzymology*, 332, pp.417–31.
- Alessi, D.R. et al., 1995. PD 098059 is a specific inhibitor of the activation of mitogen-activated protein kinase in vitro and in vivo. *J Biol Chem*, 270(46), pp.27489–27494.
- Ali, H. et al., 2000. Stimulation of colorectal cancer cell line growth by ET-1 and its inhibition by ET(A) antagonists. *Gut*, 47(5), pp.685–688.
- Ali, M.H. et al., 2013. The role of lipid geometry in designing liposomes for the solubilisation of poorly water soluble drugs. *International Journal of Pharmaceutics*, 453(1), pp.225–232.
- Andar, A.U. et al., 2014. Microfluidic preparation of liposomes to determine particle size influence on cellular uptake mechanisms. *Pharmaceutical Research*, 31(2), pp.401–413.
- Arnault, J.P. et al., 2012. Skin tumors induced by sorafenib; paradoxical RAS-RAF pathway activation and oncogenic mutations of HRAS, TP53, and TGFBR1. *Clinical Cancer Research*, 18(1), pp.263–272.
- Asham, E. et al., 2001. Increased endothelin-1 in colorectal cancer and reduction of tumour growth by ET(A) receptor antagonism. *British journal of cancer*, 85(11), pp.1759–1763.
- Bagnato, A. et al., 1997. Activation of mitogenic signaling by endothelin 1 in ovarian carcinoma cells. *Cancer Research*, 57(7), pp.1306–1311.
- Bagnato, A. et al., 1999. Expression of endothelin 1 and endothelin a receptor in ovarian carcinoma: Evidence for an autocrine role in tumor growth. *Cancer Research*, 59(3), pp.720–727.
- Bagnato, A. & Rosanò, L., 2008. The endothelin axis in cancer. *The international journal of biochemistry & cell biology*, 40(8), pp.1443–51.
- Balmanno, K. et al., 2009. Intrinsic resistance to the MEK1/2 inhibitor AZD6244 (ARRY-142886) is associated with weak ERK1/2 signalling and/or strong PI3K

- signalling in colorectal cancer cell lines. *International Journal of Cancer*, 125(10), pp.2332–2341.
- Bangham, A.D., Standish, M.M. & Watkins, J.C., 1965. Diffusion of univalent ions across the lamellae of swollen phospholipids. *Journal of molecular biology*, 13(1), pp.238–52.
- Basu, S. et al., 2009. Nanoparticle-mediated targeting of MAPK signaling predisposes tumor to chemotherapy. *Proceedings of the National Academy of Sciences of the United States of America*, 106(19), pp.7957–7961.
- Batist, G. et al., 2009. *Safety, pharmacokinetics, and efficacy of CPX-1 liposome injection in patients with advanced solid tumors.*
- Bélanger, L.-F. et al., 2003. Mek2 is dispensable for mouse growth and development. *Molecular and cellular biology*, 23(14), pp.4778–4787.
- Bernstein, E. et al., 2001. Role for a bidentate ribonuclease in the initiation step of RNA interference. *Nature*, 409(6818), pp.363–6.
- Bhardwaj, U. & Burgess, D.J., 2010. Physicochemical properties of extruded and non-extruded liposomes containing the hydrophobic drug dexamethasone. *International Journal of Pharmaceutics*, 388(1-2), pp.181–189.
- Bhat, N.R. & Zhang, P., 1999. Hydrogen peroxide activation of multiple mitogen-activated protein kinases in an oligodendrocyte cell line: role of extracellular signal-regulated kinase in hydrogen peroxide-induced cell death. *Journal of neurochemistry*, 72(1), pp.112–119.
- Bjornsti, M.-A. & Houghton, P.J., 2004. The TOR pathway: a target for cancer therapy. *Nature reviews. Cancer*, 4(5), pp.335–348.
- Blasco, R.B. et al., 2011. C-Raf, but Not B-Raf, Is Essential for Development of K-Ras Oncogene-Driven Non-Small Cell Lung Carcinoma. *Cancer Cell*, 19(5), pp.652–663.
- Blaukat, A. et al., 2000. G protein-coupled receptor-mediated mitogen-activated protein kinase activation through cooperation of Galpha(q) and Galpha(i) signals. *Molecular and cellular biology*, 20(18), pp.6837–6848.
- Board, R.E. et al., 2009. *Detection of BRAF mutations in the tumour and serum of patients enrolled in the AZD6244 (ARRY-142886) advanced melanoma phase II study.*
- Bodmer, W.F. et al., 1987. Localization of the gene for familial adenomatous polyposis on chromosome 5. *Nature*, 328(6131), pp.614–6.
- Bolsover, S. et al., 2004. *Cell Biology: A Short Course* 2nd ed., Hoboken: Wiley-Liss.

- Bradbury, R.H. et al., 1997. New non-peptide endothelin-A receptor antagonists: synthesis, biological properties, and structure-activity relationships of 5-(dimethylamino)-N-pyridyl-, -N-pyrimidinyl-, -N-pyridazinyl-, and -N-pyrazinyl-1-naphthalenesulfonamides. *Journal of medicinal chemistry*, 40(6), pp.996–1004.
- Bromberg-white, J.L., Andersen, N.J. & Duesbery, N.S., 2012. Mek genomics in development and disease. *Briefings in Functional Genomics*, 11(4), pp.300–310.
- Brown, R.A. et al., 2005. Ultrarapid engineering of biomimetic materials and tissues: Fabrication of nano- and microstructures by plastic compression. *Advanced Functional Materials*, 15(11), pp.1762–1770.
- Cagdas, F.M. et al., 2011. Effect of preparation method and cholesterol on drug encapsulation studies by phospholipid liposomes. *Pharmaceutical development and technology*, 16(4), pp.408–414.
- Cagnol, S. & Rivard, N., 2012. Oncogenic KRAS and BRAF activation of the MEK/ERK signaling pathway promotes expression of dual-specificity phosphatase 4 (DUSP4/MKP2) resulting in nuclear ERK1/2 inhibition. *Oncogene*.
- Cancer, T. & Atlas, G., 2012. Comprehensive molecular characterization of human colon and rectal cancer. *Nature*, 487(7407), pp.330–7.
- Caputo, E. et al., 2014. Aurka inhibitors enhance the effects of B-RAF and MEK inhibitors in melanoma treatment. *Journal of translational medicine*, 12(1), p.216.
- Carracedo, A. et al., 2008. Inhibition of mTORC1 leads to MAPK pathway activation through a PI3K-dependent feedback loop in human cancer. *Journal of Clinical Investigation*, 118(9), pp.3065–3074.
- Center, M.M. et al., 2010. Worldwide variations in colorectal cancer. *Diseases of the Colon and Rectum*, 53(7), p.1099.
- Chambers, K.F. et al., 2014. 3D Cultures of Prostate Cancer Cells Cultured in a Novel High-Throughput Culture Platform Are More Resistant to Chemotherapeutics Compared to Cells Cultured in Monolayer . *Plos One*, 9(11).
- Chang, L. & Karin, M., 2001. Mammalian MAP kinase signalling cascades. *Nature*, 410(6824), pp.37–40.
- Chapman, M.S. & Miner, J.N., 2011. Novel mitogen-activated protein kinase kinase inhibitors. *Expert opinion on investigational drugs*, 20(2), pp.209–220.
- Church, D., Midgley, R. & Kerr, D., 2012. Biomarkers in early-stage colorectal cancer: Ready for prime time? In *Digestive Diseases*. pp. 27–33.

- Ciani, L. et al., 2004. DOTAP/DOPE and DC-Chol/DOPE lipoplexes for gene delivery: zeta potential measurements and electron spin resonance spectra. *Biochimica et biophysica acta*, 1664(1), pp.70–79.
- Ciombor, K.K. & Bekaii-Saab, T., 2015. Selumetinib for the treatment of cancer. *Expert Opin. Investig. Drugs*, 24(1).
- Colosimo, A. et al., 1999. Gene transfection efficiency of tracheal epithelial cells by DC-chol-DOPE/DNA complexes. *Biochimica et biophysica acta*, 1419(2), pp.186–194.
- Conlin, A. et al., 2005. The prognostic significance of K-ras, p53, and APC mutations in colorectal carcinoma. *Gut*, 54(9), pp.1283–1286.
- Crews, C.M., Alessandrini, A. & Erikson, R.L., 1992. The primary structure of MEK, a protein kinase that phosphorylates the ERK gene product. *Science (New York, N.Y.)*, 258(5081), pp.478–480.
- Crompton, J.G. et al., 2014. Reprogramming antitumor immunity. *Trends in Immunology*, 35(4), pp.178–185.
- Cuenda, A. & Alessi, D.R., 2000. Use of kinase inhibitors to dissect signaling pathways. *Methods in molecular biology (Clifton, N.J.)*, 99, pp.161–175.
- Cukierman, E. et al., 2001. Taking cell-matrix adhesions to the third dimension. *Science (New York, N.Y.)*, 294(5547), pp.1708–1712.
- Van Cutsem, E. et al., 2009. Cetuximab and chemotherapy as initial treatment for metastatic colorectal cancer. *The New England journal of medicine*, 360(14), pp.1408–17.
- Daneshpour, N. et al., 2011. Targeted delivery of a novel group of site-directed transglutaminase inhibitors to the liver using liposomes: a new approach for the potential treatment of liver fibrosis. *Journal of drug targeting*, 19(8), pp.624–631.
- Dang, Z.C. & Lowik, C.W.G.M., 2004. Differential effects of PD98059 and U0126 on osteogenesis and adipogenesis. *Journal of Cellular Biochemistry*, 92(3), pp.525–533.
- Davenport, A.P., 2002. International Union of Pharmacology. XXIX. Update on endothelin receptor nomenclature. *Pharmacological reviews*, 54(2), pp.219–226.
- Davies, B.R. et al., 2007. AZD6244 (ARRY-142886), a potent inhibitor of mitogen-activated protein kinase/extracellular signal-regulated kinase 1/2 kinases: mechanism of action in vivo, pharmacokinetic/pharmacodynamic relationship, and potential for combination in preclinical. *Molecular cancer therapeutics*, 6(8), pp.2209–2219.
- Davies, H. et al., 2002. Mutations of the BRAF gene in human cancer. *Nature*, 417(6892), pp.949–954.

- Davies, S.P. et al., 2000. Specificity and mechanism of action of some commonly used protein kinase inhibitors. *The Biochemical journal*, 351(Pt 1), pp.95–105.
- Deschner, E.E., Godbold, J. & Lynch, H.T., 1988. Rectal epithelial cell proliferation in a group of young adults. Influence of age and genetic risk for colon cancer. *Cancer*, 61(11), pp.2286–2290.
- Dhanasekaran, D.N. et al., 2007. Scaffold proteins of MAP-kinase modules. *Oncogene*, 26(22), pp.3185–3202.
- Dhillon, A.S. et al., 2007. MAP kinase signalling pathways in cancer. *Oncogene*, 26(22), pp.3279–90.
- Dokka, S. et al., 2000. Oxygen radical-mediated pulmonary toxicity induced by some cationic liposomes. *Pharmaceutical Research*, 17(5), pp.521–525.
- Dokladda, K. et al., 2005. PD98059 and U0126 activate AMP-activated protein kinase by increasing the cellular AMP:ATP ratio and not via inhibition of the MAP kinase pathway. *FEBS Letters*, 579(1), pp.236–240.
- Downward, J., 2003. Targeting RAS signalling pathways in cancer therapy. *Nature reviews. Cancer*, 3(1), pp.11–22.
- Dudley, D.T. et al., 1995. A synthetic inhibitor of the mitogen-activated protein kinase cascade. *Proceedings of the National Academy of Sciences of the United States of America*, 92(17), pp.7686–7689.
- Ebi, H. et al., 2013. PI3K regulates MEK/ERK signaling in breast cancer via the Rac-GEF, P-Rex1. *Proceedings of the National Academy of Sciences of the United States of America*, 110(52), pp.21124–9.
- Engelman, J.A. et al., 2008. Effective use of PI3K and MEK inhibitors to treat mutant Kras G12D and PIK3CA H1047R murine lung cancers. *Nature medicine*, 14(12), pp.1351–1356.
- Faber, A.C. et al., 2009. Differential induction of apoptosis in HER2 and EGFR addicted cancers following PI3K inhibition. *Proceedings of the National Academy of Sciences of the United States of America*, 106(46), pp.19503–19508.
- Fang, J.Y. & Richardson, B.C., 2005. The MAPK signalling pathways and colorectal cancer. *Lancet Oncology*, 6(5), pp.322–327.
- Farhood, H., Serbina, N. & Huang, L., 1995. The role of dioleoyl phosphatidylethanolamine in cationic liposome mediated gene transfer. *Biochimica et biophysica acta*, 1235(2), pp.289–295.
- Farley, J. et al., 2013. Selumetinib in women with recurrent low-grade serous carcinoma of the ovary or peritoneum: An open-label, Single-arm, Phase 2 study. *The Lancet Oncology*, 14(2), pp.134–140.

- Favata, M.F. et al., 1998. Identification of a novel inhibitor of mitogen-activated protein kinase kinase. *The Journal of biological chemistry*, 273(29), pp.18623–18632.
- Ferguson, J. et al., 2012. Combination of MEK and SRC inhibition suppresses melanoma cell growth and invasion. *Oncogene*.
- Fire, A. et al., 1998. Potent and specific genetic interference by double-stranded RNA in *Caenorhabditis elegans*. *Nature*, 391(6669), pp.806–11.
- Fischbach, C. et al., 2007. Engineering tumors with 3D scaffolds. *Nature methods*, 4(10), pp.855–860.
- Flaherty, K.T. et al., 2012. Combined BRAF and MEK Inhibition in Melanoma with BRAF V600 Mutations. *New England Journal of Medicine*, 367(18), pp.1694–1703.
- Fodde, R., Smits, R. & Clevers, H., 2001. APC, signal transduction and genetic instability in colorectal cancer. *Nature reviews. Cancer*, 1(1), pp.55–67.
- Friday, B.B. et al., 2008. BRAF V600E disrupts AZD6244-induced abrogation of negative feedback pathways between extracellular signal-regulated kinase and Raf proteins. *Cancer Research*, 68(15), pp.6145–6153.
- Gailhouste, L. et al., 2010. RNAi-mediated MEK1 knock-down prevents ERK1/2 activation and abolishes human hepatocarcinoma growth in vitro and in vivo. *International journal of cancer. Journal international du cancer*, 126(6), pp.1367–77.
- Gao, J. et al., 2012. EGFR-specific PEGylated immunoliposomes for active siRNA delivery in hepatocellular carcinoma. *Biomaterials*, 33(1), pp.270–82.
- Gao, J. et al., 2011. The promotion of siRNA delivery to breast cancer overexpressing epidermal growth factor receptor through anti-EGFR antibody conjugation by immunoliposomes. *Biomaterials*, 32(13), pp.3459–70.
- Gao, J., Li, J. & Ma, L., 2005. Regulation of EGF-induced ERK/MAPK activation and EGFR internalization by G protein-coupled receptor kinase 2. *Acta Biochimica et Biophysica Sinica*, 37(8), pp.525–531.
- Garnett, M.J. et al., 2005. Wild-type and mutant B-RAF activate C-RAF through distinct mechanisms involving heterodimerization. *Molecular Cell*, 20(6), pp.963–969.
- Gilmartin, A.G. et al., 2011. GSK1120212 (JTP-74057) is an inhibitor of MEK activity and activation with favorable pharmacokinetic properties for sustained in vivo pathway inhibition. *Clinical Cancer Research*, 17(5), pp.989–1000.

- Giroux, S. et al., 1999. Embryonic death of Mek1-deficient mice reveals a role for this kinase in angiogenesis in the labyrinthine region of the placenta. *Current Biology*, 9(7), pp.369–372.
- Grant, K. et al., 2007. Mechanisms of endothelin 1-stimulated proliferation in colorectal cancer cell lines. *British Journal of Surgery*, 94(1), pp.106–112.
- Gregoriadis, G. & Davis, C., 1979. Stability of liposomes in vivo and in vitro is promoted by their cholesterol content in the presence of blood cells. *Biochemical and biophysical research communications*, 90, pp.1287–1293.
- Gröschl, B. et al., 2013. Expression of the MAP kinase phosphatase DUSP4 is associated with microsatellite instability in colorectal cancer (CRC) and causes increased cell proliferation. *International journal of cancer. Journal international du cancer*, 132(7), pp.1537–46.
- Gurski, L.A. et al., 2009. Hyaluronic acid-based hydrogels as 3D matrices for in vitro evaluation of chemotherapeutic drugs using poorly adherent prostate cancer cells. *Biomaterials*, 30(30), pp.6076–6085.
- Hamilton, A.J. & Baulcombe, D.C., 1999. A species of small antisense RNA in posttranscriptional gene silencing in plants. *Science (New York, N. Y.)*, 286(5441), pp.950–2.
- Hammond, S.M. et al., 2000. An RNA-directed nuclease mediates post-transcriptional gene silencing in Drosophila cells. *Nature*, 404(6775), pp.293–6.
- Hanahan, D., 2000. The Hallmarks of Cancer. *Cell*, 100(1), pp.57–70.
- Hanahan, D. & Weinberg, R.A., 2011. Hallmarks of cancer: The next generation. *Cell*, 144(5), pp.646–674.
- Haque, S. et al., 2013. Efficacy of the specific endothelin a receptor antagonist zibotentan (ZD4054) in colorectal cancer: a preclinical study. *Molecular cancer therapeutics*, 12(8), pp.1556–67.
- Harmon, A.W., Paul, D.S. & Patel, Y.M., 2004. MEK inhibitors impair insulin-stimulated glucose uptake in 3T3-L1 adipocytes. *American journal of physiology. Endocrinology and metabolism*, 287(4), pp.E758–E766.
- Hatano, N. et al., 2003. Essential role for ERK2 mitogen-activated protein kinase in placental development. *Genes to Cells*, 8(11), pp.847–856.
- Hatzivassiliou, G. et al., 2013. Mechanism of MEK inhibition determines efficacy in mutant KRAS- versus BRAF-driven cancers. *Nature*, 501(7466), pp.232–6.
- Hay, N. & Sonenberg, N., 2004. Upstream and downstream of mTOR. *Genes and Development*, 18(16), pp.1926–1945.

- Hayes, D.N. et al., 2012. Phase II efficacy and pharmacogenomic study of selumetinib (AZD6244; ARRY-142886) in iodine-131 refractory papillary thyroid carcinoma with or without follicular elements. *Clinical Cancer Research*, 18(7), pp.2056–2065.
- Heidorn, S.J. et al., 2010. Kinase-Dead BRAF and Oncogenic RAS Cooperate to Drive Tumor Progression through CRAF. *Cell*, 140(2), pp.209–221.
- Hickman, J.A. et al., 2014. Three-dimensional models of cancer for pharmacology and cancer cell biology: Capturing tumor complexity in vitro/ex vivo. *Biotechnol. J.*, (9), pp.1115–1128.
- Hino, M. et al., 2012. Anti-tumor Effects of Cationic Hybrid Liposomes against Colon Carcinoma along with Apoptosis in Vitro. *Biological and Pharmaceutical Bulletin*, 35(11), pp.2097–2101.
- Ho, A.L. et al., 2013. Selumetinib-enhanced radioiodine uptake in advanced thyroid cancer. *The New England journal of medicine*, 368(7), pp.623–32.
- Hoeflich, K.P. et al., 2009. In vivo antitumor activity of MEK and phosphatidylinositol 3-kinase inhibitors in basal-like breast cancer models. *Clinical cancer research : an official journal of the American Association for Cancer Research*, 15(14), pp.4649–4664.
- Hoeflich, K.P. et al., 2012. Intermittent administration of MEK inhibitor GDC-0973 plus pi3k inhibitor GDC-0941 triggers robust apoptosis and tumor growth inhibition. *Cancer Research*, 72(1), pp.210–219.
- Holliday, D.L. et al., 2009. Novel multicellular organotypic models of normal and malignant breast: tools for dissecting the role of the microenvironment in breast cancer progression. *Breast cancer research : BCR*, 11(1), p.R3.
- Hoosein, M.M. et al., 2007. Altered endothelin receptor subtypes in colorectal cancer. *European journal of gastroenterology & hepatology*, 19(9), pp.775–782.
- Hoshino, R. et al., 1999. Constitutive activation of the 41-/43-kDa mitogen-activated protein kinase signaling pathway in human tumors. *Oncogene*, 18(3), pp.813–822.
- Huang, K. et al., 2012. Size-dependent localization and penetration of ultrasmall gold nanoparticles in cancer cells, multicellular spheroids, and tumors in vivo. *ACS Nano*, 6(5), pp.4483–4493.
- Huang, T. & Zhang, X., 2013. Host defense against DNA virus infection in shrimp is mediated by the siRNA pathway. *European journal of immunology*, 43(1), pp.137–46.
- Huynh, H. et al., 2007. Targeted inhibition of the extracellular signal-regulated kinase kinase pathway with AZD6244 (ARRY-142886) in the treatment of hepatocellular carcinoma. *Molecular cancer therapeutics*, 6(1), pp.138–146.

- Ichihara, H. et al., 2012. Intravenous injection of hybrid liposomes suppresses the liver metastases in xenograft mouse models of colorectal cancer in vivo. *European Journal of Medicinal Chemistry*, 57, pp.143–148.
- Imamura, Y. et al., 2012. Specific mutations in KRAS codons 12 and 13, and patient prognosis in 1075 BRAF wild-type colorectal cancers. *Clinical Cancer Research*, 18(17), pp.4753–4763.
- Ishimoto, S. et al., 2012. Role of endothelin receptor signalling in squamous cell carcinoma. *International journal of oncology*, 40(4), pp.1011–9.
- James, N. et al., 2009. Safety and efficacy of the specific endothelin-A receptor antagonist ZD4054 in patients with hormone-resistant prostate cancer and bone metastases who were pain free or mildly symptomatic: a double-blind, placebo-controlled, randomised, phase 2 trial. *European Urology*, 55(5), pp.1112–23.
- Jemal, A. et al., 2011. Global Cancer Statistics: 2011. *CA: A Cancer Journal for Clinicians*, 61(2), pp.69–90.
- Jiménez, L.A. et al., 1997. Role of extracellular signal-regulated protein kinases in apoptosis by asbestos and H₂O₂. *The American journal of physiology*, 273(5 Pt 1), pp.L1029–L1035.
- Johannessen, C.M. et al., 2010. COT drives resistance to RAF inhibition through MAP kinase pathway reactivation. *Nature*, 468(7326), pp.968–972.
- Kamakura, S., Moriguchi, T. & Nishida, E., 1999. Activation of the protein kinase ERK5/BMK1 by receptor tyrosine kinases. Identification and characterization of a signaling pathway to the nucleus. *The Journal of biological chemistry*, 274(37), pp.26563–26571.
- Kang, S.H. et al., 2011. Cationic liposomal co-delivery of small interfering RNA and a MEK inhibitor for enhanced anticancer efficacy. *Pharmaceutical Research*, 28(12), pp.3069–3078.
- Keller, A.M. et al., 2004. Randomized phase III trial of pegylated liposomal doxorubicin versus vinorelbine or mitomycin C plus vinblastine in women with taxane-refractory advanced breast cancer. *Journal of Clinical Oncology*, 22(19), pp.3893–3901.
- Kennedy, R., Haynes, W. & Webb, D., 1993. Endothelins as regulators of growth and function in endocrine tissues. *Clinical Endocrinology*, 39(3), pp.259–65.
- Khan, D.R. et al., 2008. Effects of drug hydrophobicity on liposomal stability. *Chemical Biology and Drug Design*, 71(1), pp.3–7.
- Kim, T.H. et al., 2005. beta-Catenin activates the growth factor endothelin-1 in colon cancer cells. *Oncogene*, 24(4), pp.597–604.

- King, R.J.B. & Robins, M.W., 2006. *Cancer Biology* 3rd ed., Pearson Education Limited.
- Kirby, C., Clarke, J. & Gregoriadis, G., 1980. Effect of the cholesterol content of small unilamellar liposomes on their stability in vivo and in vitro. *Biochemical journal*, 186(2), pp.591–598.
- Kirkwood, J.M. et al., 2012. Phase II, open-label, randomized trial of the MEK1/2 inhibitor selumetinib as monotherapy versus temozolomide in patients with advanced melanoma. *Clinical Cancer Research*, 18(2), pp.555–567.
- Knowles, J.P. et al., 2012. Endothelin-1 stimulates colon cancer adjacent fibroblasts. *International journal of cancer. Journal international du cancer*, 130(6), pp.1264–72.
- Koide, H. et al., 2008. Particle size-dependent triggering of accelerated blood clearance phenomenon. *International Journal of Pharmaceutics*, 362(1-2), pp.197–200.
- Kunz-Schughart, L.A., Kreutz, M. & Knuechel, R., 1998. Multicellular spheroids: A three-dimensional in vitro culture system to study tumour biology. *International Journal of Experimental Pathology*, 79(1), pp.1–23.
- Kusuhara, M. et al., 1990. Production of endothelin in human cancer cell lines. *Cancer research*, 50(11), pp.3257–3261.
- Lalatsa, A. et al., 2012. Delivery of peptides to the blood and brain after oral uptake of quaternary ammonium palmitoyl glycol chitosan nanoparticles. *Molecular Pharmaceutics*, 9(6), pp.1764–1774.
- Lammers, T. et al., 2012. Drug targeting to tumors: principles, pitfalls and (pre-) clinical progress. *Journal of controlled release : official journal of the Controlled Release Society*, 161(2), pp.175–87.
- Lee, C.S. et al., 2011. MEK2 is sufficient but not necessary for proliferation and anchorage-independent growth of SK-MEL-28 melanoma cells. *PLoS ONE*, 6(2).
- Lee, G.Y. et al., 2007. Three-dimensional culture models of normal and malignant breast epithelial cells - Nature Methods. *Nature methods*, 4(4), pp.359–365.
- Lefloch, R., Pouysségur, J. & Lenormand, P., 2009. Total ERK1/2 activity regulates cell proliferation. *Cell cycle (Georgetown, Tex.)*, 8(5), pp.705–711.
- Lim, K.H. et al., 2005. Activation of RalA is critical for Ras-induced tumorigenesis of human cells. *Cancer Cell*, 7(6), pp.533–545.
- Lin, J. et al., 2010. Penetration of lipid membranes by gold nanoparticles: Insights into cellular uptake, cytotoxicity, and their relationship. *ACS Nano*, 4(9), pp.5421–5429.

- Little, A.S. et al., 2011. Amplification of the driving oncogene, KRAS or BRAF, underpins acquired resistance to MEK1/2 inhibitors in colorectal cancer cells. *Science signaling*, 4(166), p.ra17.
- Lu, R. et al., 2007. Inhibition of the extracellular signal-regulated kinase/mitogen-activated protein kinase pathway decreases DNA methylation in colon cancer cells. *Journal of Biological Chemistry*, 282(16), pp.12249–12259.
- Magdeldin, T. et al., 2014. The efficacy of cetuximab in a tissue-engineered three-dimensional in vitro model of colorectal cancer. *Journal of Tissue Engineering*, 5(0), p.2041731414544183–.
- Malam, Y., Loizidou, M. & Seifalian, A.M., 2009. Liposomes and nanoparticles: nanosized vehicles for drug delivery in cancer. *Trends in pharmacological sciences*, 30(11), pp.592–9.
- Martin-Liberal, J., Lagares-Tena, L. & Larkin, J., 2014. Prospects for MEK inhibitors for treating cancer. *Expert opinion on drug safety*, 13(4), pp.483–95.
- Mazur, P.K. et al., 2014. SMYD3 links lysine methylation of MAP3K2 to Ras-driven cancer. *Nature*, 510(7504), pp.283–7.
- Mebratu, Y. & Tesfaigzi, Y., 2009. How ERK1/2 activation controls cell proliferation and cell death: Is subcellular localization the answer? *Cell cycle (Georgetown, Tex.)*, 8(8), pp.1168–1175.
- Meloche, S. & Pouyssegur, J., 2007. The ERK1/2 mitogen-activated protein kinase pathway as a master regulator of the G1- to S-phase transition. *Oncogene*, 26(22), pp.3227–3239.
- Mikhail, A.S., Eetezadi, S. & Allen, C., 2013. Multicellular Tumor Spheroids for Evaluation of Cytotoxicity and Tumor Growth Inhibitory Effects of Nanomedicines In Vitro: A Comparison of Docetaxel-Loaded Block Copolymer Micelles and Taxotere®. *PLoS ONE*, 8(4).
- Minchinton, A.I. & Tannock, I.F., 2006. Drug penetration in solid tumours. *Nature reviews. Cancer*, 6(8), pp.583–592.
- Mirzoeva, O.K. et al., 2009. Basal subtype and MAPK/ERK kinase (MEK)-phosphoinositide 3-kinase feedback signaling determine susceptibility of breast cancer cells to MEK inhibition. *Cancer Research*, 69(2), pp.565–572.
- Misale, S. et al., 2014. Blockade of EGFR and MEK intercepts heterogeneous mechanisms of acquired resistance to anti-EGFR therapies in colorectal cancer. *Science translational medicine*, 6(224), p.224ra26.
- Mohammed, A.R. et al., 2004. Liposome formulation of poorly water soluble drugs: Optimisation of drug loading and ESEM analysis of stability. *International Journal of Pharmaceutics*, 285(1-2), pp.23–34.

- Montagut, C. et al., 2008. Elevated CRAF as a potential mechanism of acquired resistance to BRAF inhibition in melanoma. *Cancer Research*, 68(12), pp.4853–4861.
- Mooney, D.J. et al., 2006. Stabilized polyglycolic acid fibre-based tubes for tissue engineering. In *The Biomaterials: Silver Jubilee Compendium*. Elsevier Ltd, pp. 129–138.
- Moribe, K. et al., 1998. Enhanced encapsulation of amphotericin B into liposomes by complex formation with polyethylene glycol derivatives. *Pharmaceutical Research*, 15(11), pp.1737–1742.
- Morris, C.D. et al., 2005. Specific inhibition of the endothelin A receptor with ZD4054: clinical and pre-clinical evidence. *British journal of cancer*, 92(12), pp.2148–2152.
- Mozafari, M.R., 2010. Nanoliposomes: preparation and analysis. *Methods in molecular biology (Clifton, N.J.)*, 605, pp.29–50.
- Mueller, H. et al., 2000. Potential prognostic value of mitogen-activated protein kinase activity for disease-free survival of primary breast cancer patients. *International journal of cancer. Journal international du cancer*, 89(4), pp.384–388.
- Mukherjee, K., Sen, J. & Chaudhuri, A., 2005. Common co-lipids, in synergy, impart high gene transfer properties to transfection-incompetent cationic lipids. *FEBS Letters*, 579(5), pp.1291–1300.
- Muleris, M. et al., 1987. Characteristic chromosomal imbalances in 18 near-diploid colorectal tumors. *Cancer genetics and cytogenetics*, 29(2), pp.289–301.
- Murrell, M.P. et al., 2014. Liposome adhesion generates traction stress. *Nature Physics*, 10(2), pp.163–169.
- Nazarian, R. et al., 2010. Melanomas acquire resistance to B-RAF(V600E) inhibition by RTK or N-RAS upregulation. *Nature*, 468(7326), pp.973–977.
- Nelson, J.B. et al., 1995. Identification of endothelin-1 in the pathophysiology of metastatic adenocarcinoma of the prostate. *Nature medicine*, 1(9), pp.944–949.
- Nii, T. & Ishii, F., 2005. Encapsulation efficiency of water-soluble and insoluble drugs in liposomes prepared by the microencapsulation vesicle method. *International Journal of Pharmaceutics*, 298(1), pp.198–205.
- Normanno, N. et al., 2009. Implications for KRAS status and EGFR-targeted therapies in metastatic CRC. *Nature reviews. Clinical oncology*, 6(9), pp.519–527.
- Nyga, A. et al., 2013. A novel tissue engineered three-dimensional in vitro colorectal cancer model. *Acta biomaterialia*, 9(8), pp.7917–26.

- O'Brien, M.E.R. et al., 2004. Reduced cardiotoxicity and comparable efficacy in a phase III trial of pegylated liposomal doxorubicin HCl (CAELYX/Doxil) versus conventional doxorubicin for first-line treatment of metastatic breast cancer. *Annals of oncology : official journal of the European Society for Medical Oncology / ESMO*, 15(3), pp.440–9.
- O'Connell, J.B., Maggard, M.A. & Ko, C.Y., 2004. Colon cancer survival rates with the new American Joint Committee on Cancer sixth edition staging. *Journal of the National Cancer Institute*, 96(19), pp.1420–1425.
- O'Neil, B.H. et al., 2011. *Phase II study of the mitogen-activated protein kinase 1/2 inhibitor selumetinib in patients with advanced hepatocellular carcinoma.*
- Pagès, G. et al., 1999. Defective thymocyte maturation in p44 MAP kinase (Erk 1) knockout mice. *Science (New York, N. Y.)*, 286(5443), pp.1374–1377.
- Peduto Eberl, L., Bovey, R. & Juillerat-Jeanneret, L., 2003. Endothelin-receptor antagonists are proapoptotic and antiproliferative in human colon cancer cells. *British journal of cancer*, 88(5), pp.788–795.
- Pelaz, B. et al., 2013. Interfacing engineered nanoparticles with biological systems: Anticipating adverse nano-bio interactions. *Small*, 9(9-10), pp.1573–1584.
- Peyssonnaud, C. & Eychène, A., 2001. The Raf/MEK/ERK pathway: new concepts of activation. *Biology of the cell / under the auspices of the European Cell Biology Organization*, 93(1-2), pp.53–62.
- Phipps, a I. et al., 2013. KRAS-mutation status in relation to colorectal cancer survival: the joint impact of correlated tumour markers. *British journal of cancer*, 108(8), pp.1757–64.
- Pickl, M. & Ries, C.H., 2009. Comparison of 3D and 2D tumor models reveals enhanced HER2 activation in 3D associated with an increased response to trastuzumab. *Oncogene*, 28(3), pp.461–468.
- Pisani, M., Mobbili, G. & Bruni, P., 2011. *Neutral Liposomes and DNA Transfection* Prof. Chubo Yuan, ed., Available at: <http://www.intechopen.com/books/non-viral-gene-therapy/neutral-liposomes-and-dna-transfection>.
- Place, E.S. et al., 2009. Synthetic polymer scaffolds for tissue engineering. *Chemical Society reviews*, 38(4), pp.1139–1151.
- Plummer, R. et al., 2011. *A Phase I clinical study of cisplatin-incorporated polymeric micelles (NC-6004) in patients with solid tumours.*
- Polo, M.L. et al., 2010. Responsiveness to PI3K and MEK inhibitors in breast cancer. Use of a 3D culture system to study pathways related to hormone independence in mice. *PLoS ONE*, 5(5).

- Poulikakos, P.I. et al., 2010. RAF inhibitors transactivate RAF dimers and ERK signalling in cells with wild-type BRAF. *Nature*, 464(7287), pp.427–430.
- Pratilas, C.A. et al., 2009. (V600E)BRAF is associated with disabled feedback inhibition of RAF-MEK signaling and elevated transcriptional output of the pathway. *Proceedings of the National Academy of Sciences of the United States of America*, 106(11), pp.4519–4524.
- Qu, X. et al., 2006. Carbohydrate-based micelle clusters which enhance hydrophobic drug bioavailability by up to 1 order of magnitude. *Biomacromolecules*, 7(12), pp.3452–3459.
- Ren, J. et al., 2012. Is K-ras gene mutation a prognostic factor for colorectal cancer: a systematic review and meta-analysis. *Diseases of the colon and rectum*, 55(8), pp.913–23.
- Resnier, P. et al., 2014. Efficient in vitro gene therapy with PEG siRNA lipid nanocapsules for passive targeting strategy in melanoma. *Biotechnology Journal*, 9(11), pp.1389–401.
- Richman, S.D. et al., 2009. KRAS and BRAF mutations in advanced colorectal cancer are associated with poor prognosis but do not preclude benefit from oxaliplatin or irinotecan: results from the MRC FOCUS trial. *Journal of Clinical Oncology*, 27(35), pp.5931–5937.
- Ricketts, K.P.M. et al., 2014. A 3D In Vitro Cancer Model as a Platform for Nanoparticle Uptake and Imaging Investigations. *Small (Weinheim an der Bergstrasse, Germany)*, pp.1–8.
- Roda, E. et al., 2011. Comparative pulmonary toxicity assessment of pristine and functionalized multi-walled carbon nanotubes intratracheally instilled in rats: Morphohistochemical evaluations. *Histology and Histopathology*, 26(3), pp.357–367.
- Rodríguez-Pulido, A. et al., 2008. A physicochemical characterization of the interaction between DC-Chol/DOPE cationic liposomes and DNA. *Journal of Physical Chemistry B*, 112(39), pp.12555–12565.
- Röring, M. et al., 2012. Distinct requirement for an intact dimer interface in wild-type, V600E and kinase-dead B-Raf signalling. *The EMBO Journal*, 31(11), pp.2629–2647.
- Rosanò, L., Di Castro, V., Spinella, F., Tortora, G., et al., 2007b. Combined targeting of endothelin a receptor and epidermal growth factor receptor in ovarian cancer shows enhanced antitumor activity. *Cancer Research*, 67(13), pp.6351–6359.
- Rosanò, L., Di Castro, V., Spinella, F., Nicotra, M.R., et al., 2007a. ZD4054, a specific antagonist of the endothelin A receptor, inhibits tumor growth and enhances paclitaxel activity in human ovarian carcinoma in vitro and in vivo. *Molecular cancer therapeutics*, 6(7), pp.2003–2011.

- Roskoski, R., 2012. MEK1/2 dual-specificity protein kinases: structure and regulation. *Biochemical and biophysical research communications*, 417(1), pp.5–10.
- Roskoski, R., 2010. RAF protein-serine/threonine kinases: Structure and regulation. *Biochemical and Biophysical Research Communications*, 399(3), pp.313–317.
- Roth, A.D. et al., 2010. Prognostic role of KRAS and BRAF in stage II and III resected colon cancer: Results of the translational study on the PETACC-3, EORTC 40993, SAKK 60-00 trial. *Journal of Clinical Oncology*, 28(3), pp.466–474.
- Rubanyi, G. & Polokoff, M., 1994. Endothelins: molecular biology, biochemistry, pharmacology, physiology, and pathophysiology. *Pharmacological Reviews*, 46(3), pp.325–415.
- Ryther, R.C.C. et al., 2005. siRNA therapeutics: big potential from small RNAs. *Gene therapy*, 12(1), pp.5–11.
- Saba-EI-Leil, M.K. et al., 2003. An essential function of the mitogen-activated protein kinase Erk2 in mouse trophoblast development. *EMBO reports*, 4(10), pp.964–968.
- Sakamoto, A. et al., 1991. Cloning and functional expression of human cDNA for the ETB endothelin receptor. *Biochemical and biophysical research communications*, 178(2), pp.656–663.
- Salerno, S. et al., 2002. Specific codon 13 K-ras mutations are predictive of clinical outcome in colorectal cancer patients, whereas codon 12 K-ras mutations are associated with mucinous histotype. *Annals of Oncology*, 13(9), pp.1438–1446.
- Santarpia, L., Lippman, S.M. & El-Naggar, A.K., 2012. Targeting the MAPK-RAS-RAF signaling pathway in cancer therapy. *Expert opinion on therapeutic targets*, 16(1), pp.103–19.
- Santini, M.T., Rainaldi, G. & Indovina, P.L., 1999. Multicellular tumour spheroids in radiation biology. *International journal of radiation biology*, 75(7), pp.787–799.
- Schmitz, K.J. et al., 2007. Activation of extracellular regulated kinases (ERK1/2) but not AKT predicts poor prognosis in colorectal carcinoma and is associated with k-ras mutations. *Virchows Archiv*, 450(2), pp.151–159.
- Scholl, F.A. et al., 2009. Selective role for Mek1 but not Mek2 in the induction of epidermal neoplasia. *Cancer Research*, 69(9), pp.3772–3778.
- Sebolt-Leopold, J.S. et al., 1999. Blockade of the MAP kinase pathway suppresses growth of colon tumors in vivo. *Nature medicine*, 5(7), pp.810–816.

- Sebolt-Leopold, J.S., 2004. MEK inhibitors: a therapeutic approach to targeting the Ras-MAP kinase pathway in tumors. *Current pharmaceutical design*, 10(16), pp.1907–1914.
- Serra, V. et al., 2011. PI3K inhibition results in enhanced HER signaling and acquired ERK dependency in HER2-overexpressing breast cancer. *Oncogene*, 30(22), pp.2547–2557.
- Shah, V. et al., 2013. Genotoxicity of different nanocarriers: possible modifications for the delivery of nucleic acids. *Current drug discovery technologies*, 10(1), pp.8–15.
- Shankar, A. et al., 1998. Raised endothelin 1 levels in patients with colorectal liver metastases. *The British journal of surgery*, 85(4), pp.502–506.
- Shekhar, M.P. V et al., 2001. Breast stroma plays a dominant regulatory role in breast epithelial growth and differentiation: Implications for tumor development and progression. *Cancer Research*, 61(4), pp.1320–1326.
- Shields, J.M. et al., 2000. Understanding Ras: “It ain’t over ‘til it’s over”. *Trends in Cell Biology*, 10(4), pp.147–154.
- Shimizu, T. et al., 2012. The clinical effect of the dual-targeting strategy involving PI3K/AKT/mTOR and RAS/MEK/ERK pathways in patients with advanced cancer. *Clinical Cancer Research*, 18(8), pp.2316–2325.
- Shome, K. et al., 2000. The activation of phospholipase D by endothelin-1, angiotensin II, and platelet-derived growth factor in vascular smooth muscle A10 cells is mediated by small G proteins of the ADP-ribosylation factor family. *Endocrinology*, 141(6), p.220.
- Siew, A. et al., 2012. Enhanced oral absorption of hydrophobic and hydrophilic drugs using quaternary ammonium palmitoyl glycol chitosan nanoparticles. *Molecular Pharmaceutics*, 9(1), pp.14–28.
- Smith, K.J. et al., 1994. Wild-type but not mutant APC associates with the microtubule cytoskeleton. *Cancer Research*, 54(14), pp.3672–3675.
- Solit, D.B. et al., 2006. BRAF mutation predicts sensitivity to MEK inhibition. *Nature*, 439(7074), pp.358–362.
- Sone, M. et al., 2000. Expression of endothelin-1 and endothelin receptors in cultured human glioblastoma cells. *J Cardiovasc Pharmacol*, 36(5 Suppl 1), pp.S390–2.
- Spinella, F. et al., 2002. Endothelin-1 induces vascular endothelial growth factor by increasing hypoxia-inducible factor-1alpha in ovarian carcinoma cells. *J Biol Chem*, 277(31), pp.27850–27855.

- Spinella, F. et al., 2004. Inhibition of cyclooxygenase-1 and -2 expression by targeting the endothelin a receptor in human ovarian carcinoma cells. *Clinical cancer research : an official journal of the American Association for Cancer Research*, 10(14), pp.4670–4679.
- Sturgill, T.W., 2008. MAP kinase: It's been longer than fifteen minutes. *Biochemical and Biophysical Research Communications*, 371(1), pp.1–4.
- Suri, S. & Schmidt, C.E., 2010. Cell-laden hydrogel constructs of hyaluronic acid, collagen, and laminin for neural tissue engineering. *Tissue engineering. Part A*, 16(5), pp.1703–1716.
- Szot, C.S. et al., 2011. Investigation of cancer cell behavior on nanofibrous scaffolds. *Materials Science and Engineering C*, 31(1), pp.37–42.
- Talukdar, S. et al., 2011. Engineered silk fibroin protein 3D matrices for in vitro tumor model. *Biomaterials*, 32(8), pp.2149–2159.
- Tentler, J.J. et al., 2010. Identification of predictive markers of response to the MEK1/2 inhibitor selumetinib (AZD6244) in K-ras-mutated colorectal cancer. *Molecular cancer therapeutics*, 9(12), pp.3351–3362.
- Tentori, L., Lacal, P.M. & Graziani, G., 2013. Challenging resistance mechanisms to therapies for metastatic melanoma. *Trends in Pharmacological Sciences*, 34(12), pp.656–666.
- Torchilin, V.P. et al., 2003. Immunomicelles: targeted pharmaceutical carriers for poorly soluble drugs. *Proceedings of the National Academy of Sciences of the United States of America*, 100(10), pp.6039–6044.
- Trédan, O. et al., 2007. Drug resistance and the solid tumor microenvironment. *Journal of the National Cancer Institute*, 99(19), pp.1441–1454.
- Troiani, T. et al., 2012. Intrinsic resistance to selumetinib, a selective inhibitor of MEK1/2, by cAMP-dependent protein kinase A activation in human lung and colorectal cancer cells. *British journal of cancer*, 106(10), pp.1648–59.
- Turke, A.B. et al., 2012. MEK inhibition leads to PI3K/AKT activation by relieving a negative feedback on ERBB receptors. *Cancer Research*, 72(13), pp.3228–3237.
- Uchegbu, I.F. et al., 2001. Quaternary ammonium palmitoyl glycol chitosan - A new polysoap for drug delivery. *International Journal of Pharmaceutics*, 224(1-2), pp.185–199.
- Ussar, S. & Voss, T., 2004. MEK1 and MEK2, different regulators of the G1/S transition. *Journal of Biological Chemistry*, 279(42), pp.43861–43869.

- Vacca, F. et al., 2000. Transactivation of the epidermal growth factor receptor in endothelin-1-induced mitogenic signaling in human ovarian carcinoma cells. *Cancer research*, 60(18), pp.5310–5317.
- Villanueva, I., Weigel, C.A. & Bryant, S.J., 2009. Cell-matrix interactions and dynamic mechanical loading influence chondrocyte gene expression and bioactivity in PEG-RGD hydrogels. *Acta Biomaterialia*, 5(8), pp.2832–2846.
- Villanueva, J., Vultur, A. & Herlyn, M., 2011. Resistance to BRAF inhibitors: Unraveling mechanisms and future treatment options. *Cancer Research*, 71(23), pp.7137–7140.
- Voisin, L. et al., 2008. Activation of MEK1 or MEK2 isoform is sufficient to fully transform intestinal epithelial cells and induce the formation of metastatic tumors. *BMC cancer*, 8, p.337.
- Wang, X. et al., 2008. Overcoming mTOR inhibition-induced paradoxical activation of survival signaling pathways enhances mTOR inhibitors' anticancer efficacy. *Cancer Biology and Therapy*, 7(12), pp.1952–1958.
- Wang, Y. et al., 2005. A role for K-ras in conferring resistance to the MEK inhibitor, CI-1040. *Neoplasia (New York, N.Y.)*, 7(4), pp.336–347.
- Wasungu, L. & Hoekstra, D., 2006. Cationic lipids, lipoplexes and intracellular delivery of genes. *Journal of Controlled Release*, 116(2 SPEC. ISS.), pp.255–264.
- Weinstein, I.B., 2002. Cancer. Addiction to oncogenes--the Achilles heel of cancer. *Science (New York, N.Y.)*, 297(5578), pp.63–64.
- Weinstein, I.B. & Joe, A., 2008. Oncogene addiction. *Cancer Research*, 68(9), pp.3077–3080.
- Wellbrock, C., Karasarides, M. & Marais, R., 2004. The RAF proteins take centre stage. *Nature reviews. Molecular cell biology*, 5(11), pp.875–885.
- Wilkins, C. et al., 2005. RNA interference is an antiviral defence mechanism in *Caenorhabditis elegans*. *Nature*, 436(7053), pp.1044–7.
- Wilson, T.R. et al., 2012. Widespread potential for growth-factor-driven resistance to anticancer kinase inhibitors. *Nature*, 487(7408), pp.505–509.
- Wood, L.D. et al., 2007. The genomic landscapes of human breast and colorectal cancers. *Science (New York, N.Y.)*, 318(5853), pp.1108–1113.
- Xiang, X. et al., 2011. The Development and Characterization of a Human Mesothelioma In Vitro 3D Model to Investigate Immunotoxin Therapy. *PLoS ONE*, 6(1), p.e14640.

- Xu, R. et al., 2009. Enhancement of paclitaxel-induced apoptosis by inhibition of mitogen-activated protein kinase pathway in colon cancer cells. *Anticancer Research*, 29(1), pp.261–270.
- Xu, S. et al., 1997. Differential regulation of mitogen-activated protein/ERK kinase (MEK)1 and MEK2 and activation by a Ras-independent mechanism. *Molecular endocrinology (Baltimore, Md.)*, 11(11), pp.1618–1625.
- Xu, X., Costa, A. & Burgess, D.J., 2012. Protein encapsulation in unilamellar liposomes: High encapsulation efficiency and a novel technique to assess lipid-protein interaction. *Pharmaceutical Research*, 29(7), pp.1919–1931.
- Yamaguchi, K. et al., 2002. Mitogen-activated protein kinase inhibitor, PD98059, inhibits rat retinal pigment epithelial cell replication by cell cycle arrest. *Jpn J Ophthalmol*, (46), pp.634–639.
- Yang, S. et al., 2012. Comparative study on preparative methods of DC-Chol/DOPE liposomes and formulation optimization by determining encapsulation efficiency. *International Journal of Pharmaceutics*, 434(1-2), pp.155–160.
- Yang, Z., Krasnici, N. & Lüscher, T.F., 1999. Endothelin-1 potentiates human smooth muscle cell growth to PDGF: effects of ETA and ETB receptor blockade. *Circulation*, 100(1), pp.5–8.
- Yeh, J.J. et al., 2009. KRAS/BRAF mutation status and ERK1/2 activation as biomarkers for MEK1/2 inhibitor therapy in colorectal cancer. *Molecular cancer therapeutics*, 8(4), pp.834–843.
- Yeh, T.C. et al., 2007. Biological characterization of ARRY-142886 (AZD6244), a potent, highly selective mitogen-activated protein kinase kinase 1/2 inhibitor. *Clinical Cancer Research*, 13(5), pp.1576–1583.
- Yip-Schneider, M.T. et al., 1999. Lack of elevated MAP kinase (Erk) activity in pancreatic carcinomas despite oncogenic K-ras expression. *International journal of oncology*, 15(2), pp.271–279.
- Yip-Schneider, M.T., Lin, A. & Marshall, M.S., 2001. Pancreatic tumor cells with mutant K-ras suppress ERK activity by MEK-dependent induction of MAP kinase phosphatase-2. *Biochemical and biophysical research communications*, 280(4), pp.992–997.
- Yoon, H.H. et al., 2014. KRAS codon 12 and 13 mutations in relation to disease-free survival in BRAF-wild-type stage III colon cancers from an adjuvant chemotherapy trial (N0147 alliance). *Clinical Cancer Research*, 20(11), pp.3033–3043.
- Yoon, Y.-K. et al., 2009. Combination of EGFR and MEK1/2 inhibitor shows synergistic effects by suppressing EGFR/HER3-dependent AKT activation in human gastric cancer cells. *Molecular cancer therapeutics*, 8(9), pp.2526–2536.

- Yuen, S.T. et al., 2002. Similarity of the phenotypic patterns associated with BRAF and KRAS mutations in colorectal neoplasia. *Cancer Research*, 62(22), pp.6451–6455.
- Zhang, B. et al., 2014. Proteogenomic characterization of human colon and rectal cancer. *Nature*.
- Zhang, Y. et al., 2010. DC-Chol/DOPE cationic liposomes: A comparative study of the influence factors on plasmid pDNA and siRNA gene delivery. *International Journal of Pharmaceutics*, 390(2), pp.198–207.
- Zhang, Y.-J. et al., 2009. Combined inhibition of MEK and mTOR signaling inhibits initiation and progression of colorectal cancer. *Cancer investigation*, 27(3), pp.273–285.